

Design and Synthesis of Novel Dihydroorotate Dehydrogenase Inhibitors

by

Joseph T. Madak

A dissertation submitted in partial fulfillment
of the requirements for the degree of
Doctor of Philosophy
(Medicinal Chemistry)
in the University of Michigan
2018

Doctoral Committee:

Professor Nouri Neamati, Co-Chair
Professor Hollis Showalter, Co-Chair
Professor Zaneta Nikolovska-Coleska
Professor Matthew Soellner

Joseph T. Madak

madakj@umich.edu

ORCID 0000-0003-1079-8151

© Joseph Madak 2018

All Rights Reserved

Acknowledgements

The work described in this thesis would not be possible without a few people. First, I would like to thank Dr. Hollis Showalter and Dr. Nouri Neamati for being my co-mentors. Dr. Showalter is an exceptionally knowledgeable synthetic chemist/scientist and I am very grateful for his advice. Throughout my tenure, he was always willing to help. I am fortunate to be co-mentored by him. The same can be said for Dr. Nouri Neamati. Dr. Neamati gave me an opportunity to research while managing a chemistry lab. I have learned much from my time in his lab and from his advice over the years. I'd like to thank both of my mentors for their time, tolerance, and guidance. Additionally, I'd like to thank my committee members Dr. Matthew Soellner and Dr. Zaneta Nikolovska-Coleska. I am grateful for their time, effort, and thought-provoking questions.

From the Showalter lab, I'd like to thank Rod Sorenson, Yafei Jin, Xinmin Gan, and Dr. Fardokht Abulwerdi for their help. When I first joined this lab, I had very little organic chemistry experience. The listed individuals all took time to answer my questions and teach me new techniques. For that, I am grateful. I have a better understanding of fundamental synthesis techniques because of these lab members.

From the Neamati lab, I'd like to thank Christine Cuthbertson, Dr. Suhui Yang, Dr. Wenmin Chen, Dr. Ding Xue, and Dr. Joyeeta Roy. Christine Cuthbertson generated most of the DHODH assay data and gave considerable time to this project. Her opinion, expertise, and time were greatly appreciated. Additionally, all the chemistry postdoctoral researchers within the Neamati lab have been very helpful throughout the years. I appreciate all that they have taught me. I'd also like to thank Armand Bankhead III for bioinformatics analysis.

From the NMR Core, I'd like to thank Dr. Larisa Yeomans. Dr Yeomans helped me to obtain a GSSA assignment within the NMR room. I have learned a lot about NMR spectroscopy and instrument maintenance from Dr. Yeomans. I appreciate the time she took to teach me how to troubleshoot and how to run advanced NMR studies. I'd also like to thank Elyse Petrunak and Dr. Jeanne Stuckey for their help with the co-crystal structures and structural analysis.

Lastly, I'd like to thank my wife and friends. My wife has proofread all of my writing. She complained significantly but I am still grateful for her efforts. Additionally, my graduate studies would not have been the same without football tailgates/hockey with Will Kaplan, Eric Lachacz, Helen Waldschmidt, Nate Scharf, David Cech, and a few others. I'd also like to thank Dr. Tanpreet Kaur for her chemistry advice. She is very resourceful and eager to help. Finally, I'd like to thank all my friends from the United States Marine Corps including Sergeant Matt Swygart, Sergeant Ryan Clements, and Corporal Nathan Lang. They were always supportive in their own dumb way.

Table of Contents

Acknowledgements.....	ii
List of Figures.....	vi
List of Tables.....	viii
List of Schemes.....	ix
List of Abbreviations.....	x
Abstract.....	xii
Chapter 1: Introduction	
1.1 Background.....	1
1.2 The de novo pyrimidine pathway and DHODH.....	2
1.3 Regulation of DHODH activity in cancer.....	6
1.4 DHODH and cellular differentiation.....	8
1.5 Relevance of DHODH in cancer.....	9
1.6 Select inhibitors of DHODH.....	17
1.7 Combination approaches to increase efficacy of DHODH inhibitors.....	24
1.8 Future of DHODH-targeted therapy.....	28
1.9 Conclusions.....	30
1.10 References.....	30
Chapter 2: Identification of a Novel Dihydroorotate Dehydrogenase Inhibitor from Cell-Based Screening	
2.1 Introduction.....	51
2.2 Phenotypic screen.....	52
2.3 Structural similarity.....	53
2.4 Synthesis.....	54
2.5 Structure activity relationships.....	58
2.6 Expanded cell activity and DHODH overexpression.....	66
2.7 Uridine rescue.....	67
2.8 DHODH activity.....	68

2.8 Conclusion.....	69
2.9 Experimental.....	69
2.10 References.....	91
Chapter 3: Design, Synthesis, and Biological Evaluation of 4-Quinoline Carboxylic Acids as Inhibitors of Dihydroorotate Dehydrogenase	
3.1 Introduction.....	95
3.2 Analogue design.....	96
3.3 Synthesis.....	98
3.4 Structure activity relationships.....	103
3.5 Crystallography.....	115
3.6 Pharmacokinetic evaluation and thermodynamic solubility.....	118
3.7 Conclusions.....	119
3.8 Experimental.....	120
3.9 References.....	173
Chapter 4: Design, Synthesis, and Characterization of Brequinar Conjugates as Probes to Study DHDOH inhibition	
4.1 Introduction.....	178
4.2 Probe design.....	178
4.3 Synthesis.....	180
4.4 Biological evaluation of probes.....	185
4.5 Conclusions.....	188
4.6 Experimental.....	188
4.7 References.....	204
Chapter 5: Summary and Future Directions	
5.1 Summary.....	207
5.2 Significance of the study.....	210
5.3 Future directions.....	211
5.4 References.....	213

List of Figures

Figure 1.1 <i>De novo</i> pyrimidine biosynthesis pathway.....	3
Figure 1.2 DHODH couples mitochondrial respiration with <i>de novo</i> pyrimidine biosynthesis....	4
Figure 1.3 Structural features of DHODH.....	5
Figure 1.4 DHODH knockdown response from the Achilles Project.....	10
Figure 1.5 mRNA levels of DHODH in 1,019 cancer cell lines.....	11
Figure 1.6 Z-score for mRNA expression generated from The Cancer Genome Atlas database.	12
Figure 1.7 Analysis of DHODH in glioma.....	13
Figure 1.8 Common gene sets enriched for genes that are co-expressed with DHODH.....	14
Figure 1.9 DHODH co-expressed genes were identified across multiple TCGA diseases.....	15
Figure 1.10 STRING analysis of interactions with DHODH.....	16
Figure 1.11 Selected inhibitors of the <i>de novo</i> pyrimidine biosynthesis pathway.....	24
Figure 1.12 Proposed compensatory resistance mechanism to DHODH inhibition.....	28
Figure 2.1 Flow diagram and criteria leading to compound 1	53
Figure 2.2 Structurally similar quinolines and their SAR trends.....	54
Figure 2.3 Overexpression and underexpression comparison between normal and cancerous cell lines.....	67
Figure 2.4 Uridine supplementation rescues cells from lead compound 1	68
Figure 3.1 Selected DHODH inhibitors.....	96
Figure 3.2 Co-crystal structure of a brequinar analogue in DHODH with new proposed interactions.....	97
Figure 3.3 Depicted binding cavity of a brequinar analogue.....	111
Figure 3.4 Interactions between DHODH and analogues 76 and 73	116
Figure 4.1 Brequinar binding pocket in DHODH and structures of probes.....	180
Figure 4.2 Biological evaluation of probes 133 , 134 , 150	186
Figure 4.3 Western blot analysis of cells with probes.....	187
Figure 5.1 Summary of anticancer effects induced by DHODH inhibition.....	208
Figure 5.2 Lead compound 1 inhibits DHODH.....	209

Figure 5.3 Lead optimization of DHODH inhibitors forming new electrostatic interactions...	210
Figure 5.4 Novel probes designed to study DHODH inhibition.....	210

List of Tables

Table 1.1 DHODH inhibitors evaluated in clinical trials.....	17
Table 1.2 Selected recently published DHODH inhibitors.....	21
Table 2.1 Biological activity of quinoline analogues with selected aromatic R ₁ substituents.....	59
Table 2.2 Biological activity of quinoline analogues with selected R ₁ substituents.....	61
Table 2.3 Biological activity of quinoline analogues with cyclic R ₁ substituents.....	63
Table 2.4 Biological activity of quinoline analogues with 1,3 biaryl regioisomers.....	64
Table 2.5 Biological activity of quinoline analogues with R ₁ phenyl bioisosteres.....	65
Table 2.6 Biological activity of amide quinoline analogues with modified acid functionality....	66
Table 2.7 Expanded cell activity of lead compound 1.....	67
Table 2.8 Biological data for active compounds in comparison to brequinar.....	69
Table 3.1 Biological activity of quinolines with selected R ₁ substituents.....	104
Table 3.2 Biological activity of quinolines with R ₁ pyridine and pyrimidine moieties.....	106
Table 3.3 Biological activity of quinolines with R ₁ substituted pyridines.....	108
Table 3.4 Biological activity of C3 methyl-substituted quinolines.....	110
Table 3.5 Biological activity of C6 / R ₁ substituted quinolines.....	112
Table 3.6 Biological activity of naphthyridines.....	113
Table 3.7 Biological activity of R ₂ pyridine-substituted naphthyridines.....	115
Table 3.8 Pharmacokinetic parameters of analogue 71.....	118
Table 3.9 Thermodynamic solubility of selected analogues.....	119

List of Schemes

Scheme 2.1 Synthesis of R ₁ substituted quinolines.....	55
Scheme 2.2 Improved synthesis of R ₁ substituted quinolines.....	56
Scheme 2.3 Synthesis of morpholino analogue.....	57
Scheme 2.4 Alternative synthesis of R ₁ substituted quinolines.....	57
Scheme 2.5 Synthesis of quinoline amide analogues.....	58
Scheme 3.1 Synthesis of quinoline analogues without a C3 methyl group.....	99
Scheme 3.2 Synthesis of quinoline analogues with a C3 methyl substituent.....	100
Scheme 3.3 Synthesis of naphthyridine core analogues.....	101
Scheme 3.4 Synthesis of naphthyridine core analogues with terminal diversity.....	102
Scheme 4.1 Synthesis of intermediate 139	181
Scheme 4.2 Synthesis of intermediate 142	181
Scheme 4.3 Synthesis of VHL ligand 147	182
Scheme 4.4 Synthesis of probe 150	183
Scheme 4.5 Synthesis of probe 133	184
Scheme 4.6 Synthesis of mitochondria-directed probe 134	185

List of Abbreviations

AML - Acute myeloid leukemia
BBr₃ - Boron tribromide
CFA - Colony formation assay
CNT - Concentrative nucleoside transporter
DCIP - Dichlorophenolindophenol
DCM - Dichloromethane
DHODH - Dihydroorotate dehydrogenase
DPM - Dipyridamole
ENT - Equilibrative nucleoside transporter
EtOAc - Ethyl acetate
FOLFIRINOX - **FOL**inic acid, **5-F**luorouracil, **IRI**Notecan, and **OX**aliplatin,
Hex - Hexane
IC₅₀ - Half maximal inhibitory concentration
LCMS - Liquid chromatography-mass spectrometry
LipE - Lipophilic ligand efficiency
MeCN - Acetonitrile
MeOH - Methanol
mtDNA - Mitochondria DNA
mTORC1 - Mammalian target of rapamycin complex 1
5-FU - 5-Fluorouracil
PALA - N-(phosphonacetyl)-l-aspartate
PAIN - Pan-interfering
PCC - Pyridinium chlorochromate
PK - Pharmacokinetics
POCl₃ - Phosphorous oxychloride
POBr₃ - Phosphorous oxybromide

PROTAC - Proteolysis targeting chimeras

PTEN - phosphatase and tensin homolog

SAR - Structure activity relationship

TMEDA - Tetramethylethylenediamine

tPSA - Total polar surface area

TRAIL - Tumor necrosis factor-related apoptosis-inducing ligand

Abstract

Rapidly growing cells are dependent on sufficient concentrations of nucleotides to sustain proliferation. One enzyme essential for the *de novo* synthesis of pyrimidine-based nucleotides is dihydroorotate dehydrogenase (DHODH); a known therapeutic target for many diseases. In cancer, inhibition of DHODH depletes intracellular pyrimidine nucleotide concentrations and halts the cell cycle at S-phase. This metabolic enzyme is necessary for rapidly growing cells and DHODH inhibition has been demonstrated to sensitize resistant cells to current chemotherapy options. Therefore, we pursued a drug discovery project towards developing novel inhibitors of DHODH.

A phenotypic screen was utilized to identify hit compounds that may be suitable leads for a drug discovery project. From this, a lead compound was discovered to inhibit cell growth (MIA PaCa-2, BxPC-3) but through an unknown enzyme target. The essential pharmacophore of the lead compound was elucidated via structure activity relationship (SAR) studies and biologically found to be remarkably similar to brequinar, a potent DHODH inhibitor. Cells were rescued from both the lead compound and brequinar by the addition of uridine, a mimic of a downstream byproduct, and both inhibitors have submicromolar IC₅₀ values toward DHODH. For continued optimization, we sought to improve affinity for the DHODH enzyme.

We pursued a structure-guided approach toward the development of improved DHODH inhibitors with the goal of forming new interactions between DHODH and the brequinar class of inhibitors. Two residues, T63 and Y356, suitable for novel H-bonding interactions were identified in the brequinar-binding pocket. Analogues were designed to maintain the essential pharmacophore and form new electrostatic interactions through strategically positioned H-bond accepting groups. This effort led to the discovery of two potent quinoline based analogues with an IC₅₀ against DHODH of 10.6 ± 1.1 nM for one and 32.9 ± 4.6 nM for the other. A co-crystal structure between a quinoline analogue and DHODH depicts a novel water mediated H-bond interaction with T63. Additional optimization led to a third 1,7-naphthyridine analogue with an IC₅₀ = 53.9 ± 1.7 nM, which forms a novel H-bond with Y356. In conclusion, the data from our

SAR investigation supports further preclinical studies of our improved compounds toward selection of a candidate for early stage clinical development.

Finally, to fully understand brequinar-based DHODH inhibition, we developed novel brequinar-based probes. We disclose a 16-step convergent synthesis of the first brequinar-PROTAC and a four-step synthesis to the first mitochondrial-directed brequinar probe. Both of these probes possess cytotoxicity that is superior to brequinar in a colony formation assay and are useful for further pharmacology studies.

The collective work described in this dissertation furthers the understanding of DHODH inhibition in cancer, identifies novel sites for electrostatic interaction between brequinar-class inhibitors and DHODH, and has resulted in the first brequinar-based probes for DHODH study. Additionally, this thesis depicts the limitations and effectiveness of DHODH targeted therapy for cancer and suggests potential solutions that may lead to the clinical efficacy. In general, this work provides an excellent foundation to improve brequinar-class inhibitor design and is of board interest to cancer drug discovery.

Chapter 1

Introduction^a

1.1 Background

Cancer is a disease of dysregulated cell growth and metabolism-related enzymes are important targets for drug development.¹ In fact, targeting enzymes that potentiate a cancer cell's metabolic dependencies presents one of the most successful approaches to halt cell growth. Drugs that target metabolic liabilities, antimetabolites (e.g. 5-fluorouracil, gemcitabine, and methotrexate), make up a significant portion of FDA-approved cancer therapies.² At least 14 different purine- and pyrimidine-based antimetabolites have been FDA-approved for cancer chemotherapy.³ Dihydroorotate dehydrogenase (DHODH) is a druggable enzyme that plays a vital role in the metabolism of cancer cells. DHODH catalyzes the oxidation of dihydroorotate to orotate, which is essential for the production of uridine monophosphate.⁴⁻⁶ Inhibition of DHODH induces pyrimidine depletion, thereby starving the cell of the essential nucleotides required to progress through S-phase.⁷ Extensive efforts have been made to develop inhibitors of DHODH for cancer therapy, however none have gained FDA approval to date.

In this review, we present compelling evidence in support of DHODH as a vital enzyme for cancer cells. DHODH, and its relationship to *de novo* pyrimidine metabolism, will be discussed along with factors that influence its regulation and expression. We will show evidence of DHODH's potential clinical relevance and co-expression network using data from The Cancer Genome Atlas (TCGA) and additional published glioma datasets. Additionally, results using previous DHODH inhibitors in cancer clinical trials and potential improvements for DHODH-targeted therapy will be discussed.

^a **Author contributions:** Joseph Madak was the primary author, Armand Bankhead III generated bioinformatics figures 1.4, 1.6, 1.7, 1.8, and 1.9. Christine Cuthbertson generated data for bioinformatics figures 1.4 and 1.5. Dr. Hollis Showalter and Dr Nouri Neamati are the corresponding authors.

1.2 The *de novo* pyrimidine pathway and DHODH

The therapeutic basis of DHODH targeted therapy primarily derives from inhibition of the *de novo* pyrimidine biosynthetic pathway. Through this pathway, cancer cells generate the required substrates for continual DNA replication and protein synthesis without the limitations of nucleotide salvage pathways. Pharmacological inhibition of this pathway provides a selective approach to targeting cells undergoing rapid cellular growth. Cells growing at normal rates maintain nucleotide concentrations primarily via nucleotide salvage pathways.^{8,9} Alternatively, cells with more rapid proliferation rates, such as cancer and immune cells, depend on *de novo* biosynthesis to fuel nucleotide demands. Hence, enzymes within *de novo* nucleotide pathways are frequently overexpressed in cancer cells to sustain growth.¹⁰ Therefore, enzymes within the *de novo* pyrimidine pathway present attractive targets to suppress cancer cell growth.

In the *de novo* pyrimidine biosynthetic pathway, DHODH catalyzes a committed step and thus presents a desirable target for halting pathway flux. Overall, the *de novo* pyrimidine pathway generates uridine monophosphate (UMP) from glutamine (Figure 1.1). Flux through this pathway begins with a large enzymatic complex known as CAD (an acronym for its domains) that catalyzes the first three steps of the pathway. These separate domains comprise a complex made up of carbamoyl phosphate synthetase, aspartate carbamoyl transferase, and dihydroorotase. The carbamoyl phosphate synthetase domain catalyzes the first reaction and generates carbamoyl phosphate from bicarbonate, ATP, and glutamine or ammonia (Figure 1.1, step 1).⁸ The second step is catalyzed by the aspartate carbamoyl transferase domain, converting carbamoyl phosphate into carbamoyl aspartate (Figure 1.1, step 2).⁸ The dihydroorotase domain hydrolyzes carbamoyl aspartate into dihydroorotate and generates the substrate for DHODH (Figure 1.1, step 3). As previously mentioned, DHODH oxidizes dihydroorotate into orotate (Figure 1.1, step 4) and is the only pathway enzyme located in the mitochondria. The final two steps in the pathway are catalyzed by another large enzyme complex known as uridine monophosphate synthetase. This enzyme is comprised of two domains: orotate phosphoribosyltransferase and orotidine 5'-phosphate decarboxylase. The orotate phosphoribosyltransferase domain catalyzes the transfer of a phosphoribosyl group to orotate (Figure 1.1, step 5). A final decarboxylation by the orotidine 5'-phosphate decarboxylase domain generates the uridine monophosphate nucleotide (Figure 1.1, step 6). Two enzymes that catalyze committed steps primarily control flux through this pathway. These are carbamoyl phosphate

synthase and DHODH.^{8, 11, 12} Inhibition of either enzyme halts flux through the *de novo* pyrimidine pathway, but carbamoyl phosphate synthetase is not expressed in all cancer cells. In fact, carbamoyl phosphate synthase has been observed to have low expression or is completely downregulated in most liver carcinomas.^{13, 14} Therefore, inhibition of DHODH's catalytic activity presents itself as more pharmacologically relevant as an approach to treat cancer.⁴

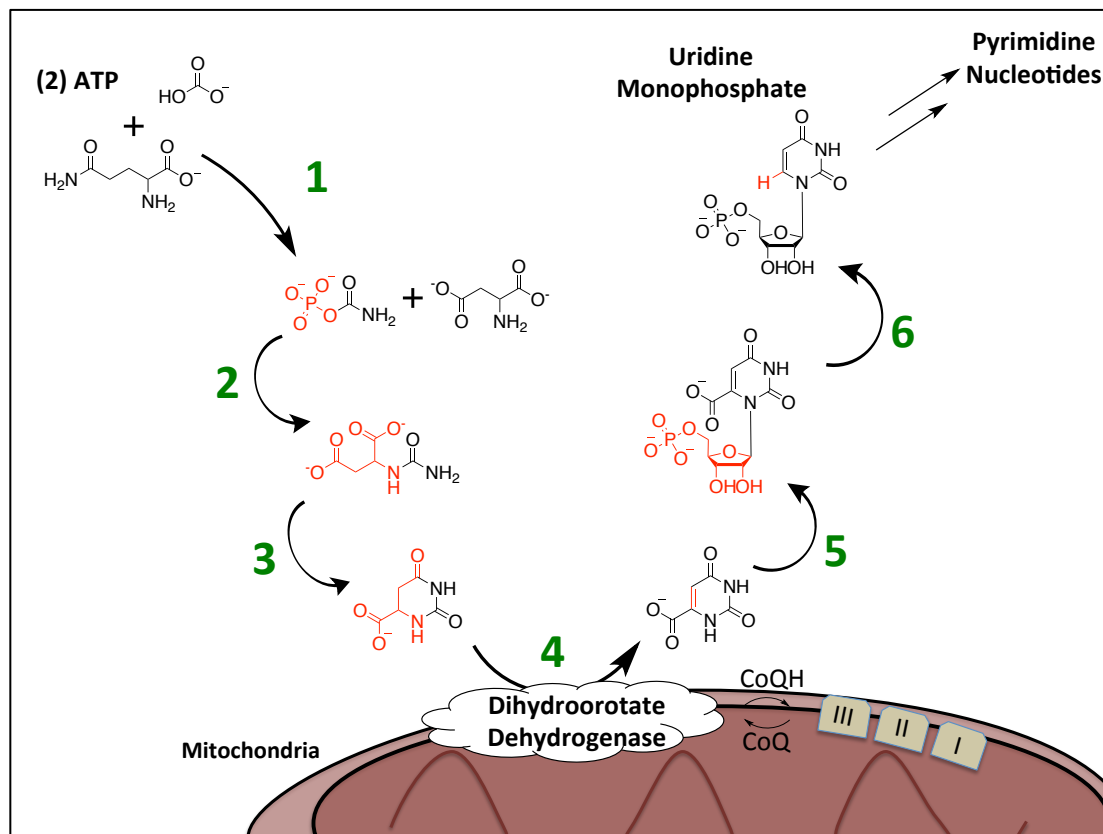


Figure 1.1: *De novo* pyrimidine biosynthesis pathway. Numbered steps represent the following enzymes and their catalyzed transformations: (1) Carbamoyl phosphate synthetase catalyzes the conversion of bicarbonate, ATP, and glutamine into carbamoyl phosphate; (2) aspartate carbamoyl transferase catalyzes the conversion of carbamoyl phosphate to carbamoyl aspartate; (3) dihydroorotase catalyzes the conversion of carbamoyl aspartate to dihydroorotate; (4) dihydroorotate dehydrogenase catalyzes the conversion of dihydroorotate to orotate; (5) orotate phosphoribosyl transferase catalyzes the conversion of orotate to orotidine monophosphate (OMP); (6) OMP decarboxylase catalyzes the conversion of OMP to UMP.

DHODH catalyzes two redox reactions: the oxidation of dihydroorotate to orotate and subsequent flavin mononucleotide (FMN) regeneration (Figure 1.2). The oxidation of dihydroorotate is carried out via a stepwise mechanism with highly conserved residues. This first enzymatic reaction follows a deprotonation of dihydroorotate at the C5 position and a subsequent hydride transfer (from dihydroorotate's C6 position) to the FMN cofactor (Figure 1.2).⁴ The

catalytic base for the initial C5 deprotonation is likely S215 (Figure 1.3). This residue has been reported as the catalytic base for DHODH enzymes in other organisms.^{4, 15, 16} Adjacent residues T218 and F149 are highly conserved as well and may increase the basicity of S215 (Figure 1.3 (C)).¹⁵ However, their precise roles have not been determined. Additional non-catalytic conserved residues contributing to dihydroorotate oxidation are N212, S214, P216, L221, R222, and Q225. These residues are located on a loop region that may be responsible for substrate/product exchange.¹⁵ The second redox reaction, resulting in regeneration of FMN, requires ubiquinone from the mitochondrial electron transport chain (ETC) (Figure 1.2).⁴ FMN is thought to bind with DHODH's G119 and V282, however the catalytic mechanism of FMN regeneration from ubiquinone is not well understood.¹⁵ FMNH₂ is perceived to undergo multiple single-electron transfer but the exact residues that facilitate this oxidation are not known.^{4, 15, 17} Nonetheless, FMN regeneration is necessary for continued DHODH catalysis. Two of the most well-known DHODH inhibitors, leflunomide and brequinar (both discussed later), are proposed to act as competitive inhibitors of ubiquinone.¹⁵ The necessity to regenerate FMN via ubiquinone may correspond to DHODH localization within the inner mitochondrial membrane. This localization increases exposure to ubiquinone from the mitochondrial ETC.

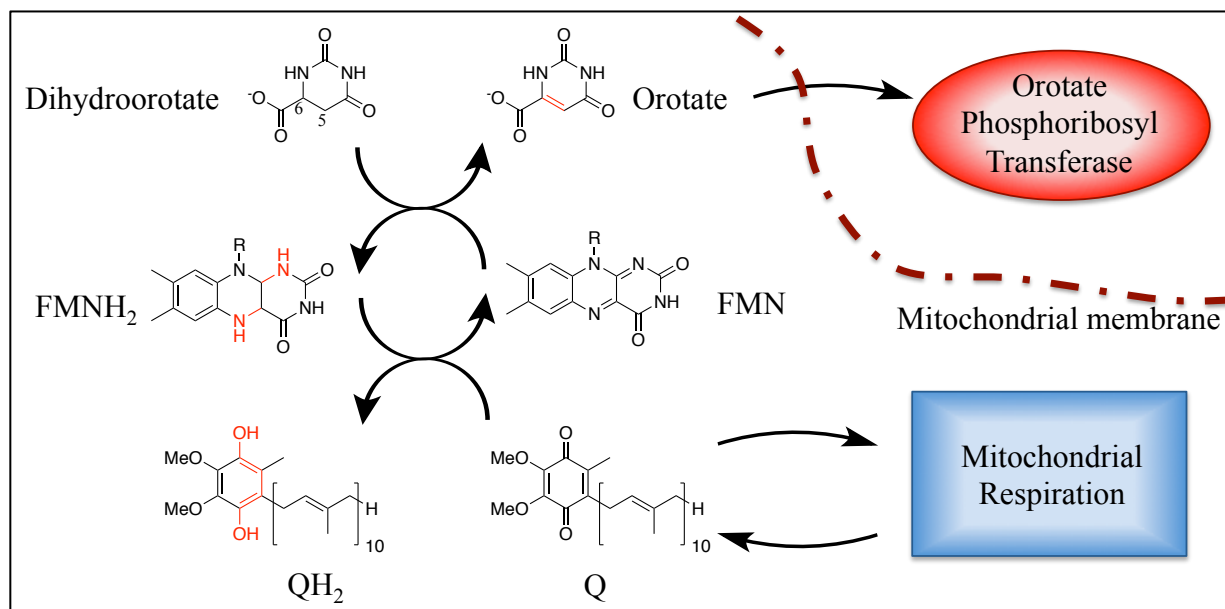


Figure 1.2: DHODH couples mitochondrial respiration with *de novo* pyrimidine biosynthesis. FMN (Flavin-mono-nucleotide, oxidized) FMNH₂ (Flavin-mono-nucleotide, reduced), Q (ubiquinone, oxidized), QH₂ (ubiquinone, reduced).

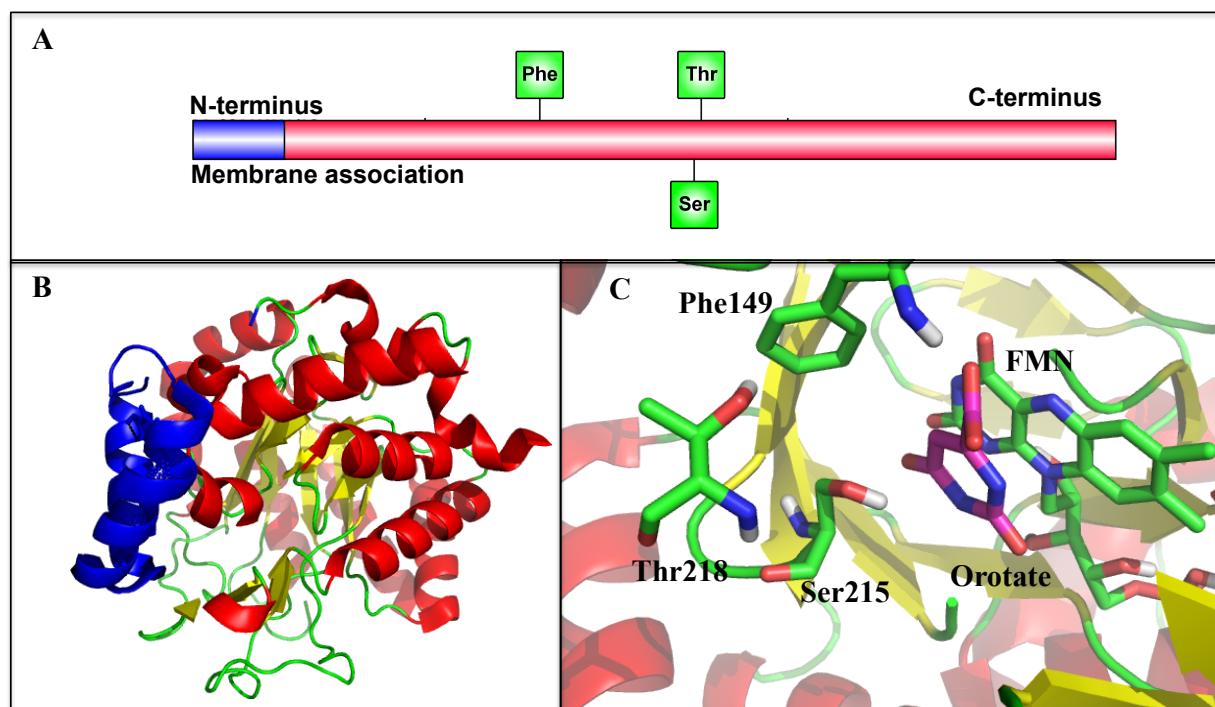


Figure 1.3: Structural features of DHODH. (A) Overall structure of DHODH protein with N and C terminus highlighted. (B) Crystal structure of DHODH generated using PDB (1D3G) and Pymol software. The small N-terminus domain is highlighted in blue. The larger C-terminal domain is color coded by α -helices (red), β -barrels (yellow), and loop regions (green). (C) Key residues within the catalytic site and their orientation towards the product orotate (magenta) are highlighted.

A functional ETC is required for DHODH catalysis (Figure 1.2).¹⁸⁻²⁰ DHODH requires FMN for catalysis and FMN is regenerated via the reduction of ubiquinone. Therefore, DHODH catalysis cannot occur without ubiquinone. This relationship makes DHODH dependent on the mitochondrial ETC to generate adequate concentrations of ubiquinone. In fact, cells lacking a fully functional mitochondrial ETC have an impaired ability to produce uridine monophosphate.^{11, 21, 22} Without a functional mitochondrial ETC, cells must be supplemented with pyruvate and uridine to support proliferation.²¹ This phenomenon is presumed to occur due to limited ubiquinone generation for DHODH catalysis. A cell line containing a dysfunctional mitochondrial ETC has been reported to be transformed with alternative ubiquinone oxidative enzymes. Once transformed, the cell lines were able to sustain cellular growth in uridine- and pyruvate-free media.²³ This result suggests that cells containing a dysfunctional ETC may be indirectly inhibiting DHODH and depleting intracellular pyrimidine nucleotides necessary for growth. Previously, decreased DHODH activity has been observed with small molecule inhibitors of the ETC targeting cytochrome C oxidase.²⁴ Additionally, inhibition of either

DHODH or mitochondrial respiration complexes have resulted in similar cellular responses. For example, inhibition of either target induced p53 up-regulation.²⁵ Collectively, these studies highlight that DHODH catalysis is dependent on a functional ETC or the presence of ubiquinone. This relationship has generated interest around the possible role DHODH may play in reactive oxygen species (ROS) homeostasis.

The connection between DHODH and ROS in cancer is not well understood. Mitochondrial ROS has been shown to be vital to cancer development and DHODH-catalyzed oxidation may affect mitochondrial ROS.^{26, 27} A previous study observed that isolated mitochondria were capable of generating radical species through DHODH and that radical production was diminished by DHODH inhibitors.²⁸ This result implies that DHODH catalysis contributes to elevated ROS levels. However, knockdown of DHODH has been shown to increase the production of ROS and decrease the mitochondria membrane potential.²⁹ These conflicting results complicate the understanding of DHODH's role in ROS generation. It is possible that inhibitors of DHODH alter redox homeostasis in a context-dependent manner. A previous study noted that cell lines most sensitive to DHODH inhibition consistently generated the lowest amount of ROS.⁷ This data implies that an antioxidant dosed with a DHODH inhibitor may be synergistic or at least additive. However, a DHODH inhibitor, teriflunomide, did not abrogate cell growth when the antioxidant pyrrolidine dithiocarbamate was co-administered.³⁰ These studies highlight a correlation between ROS and DHODH catalysis, but the functional consequences appear to be context-dependent.

1.3 Regulation of DHODH activity in cancer

Regulation of DHODH activity occurs primarily through activation of *de novo* pyrimidine biosynthesis via the CAD complex. When cells are not preparing for growth, flux through the *de novo* pyrimidine pathway is slow and functions to generate RNA nucleotides primarily for protein synthesis.^{8, 31, 32} In this state, flux is controlled through product feedback inhibition as high concentrations of uridine inhibit CAD. However, when cells prepare to divide, phosphorylation of CAD alters its affinity for uridine to overcome feedback inhibition.^{33, 34} Selective phosphorylation of CAD at specific residues regulates flux through the *de novo* pyrimidine biosynthesis pathway.³⁵ Flux through the *de novo* pyrimidine pathway is increased when T456 of CAD is phosphorylated by mitogen-activated protein kinase (MAPK) or

mechanistic target of rapamycin 1 complex (mTORC1) via S6 kinase (S6K1).³⁶⁻³⁸ After sufficient concentrations of nucleotides are reached, protein kinase A (PKA) phosphorylates S1406 of CAD to down-regulate nucleotide biosynthesis.³⁹ Overexpression of enzymes controlling CAD phosphorylation, such as MAPK or mTORC1, leads to increased flux through the pathway in cancer. For example, the breast cancer cell line MCF7 has been found to have higher MAPK kinase activation resulting in a nearly 4-fold increase in the rate of *de novo* pyrimidine biosynthesis.⁴⁰ Overexpression of mTORC1 may also increase flux through the pathway, however this has not been confirmed experimentally. In addition to phosphorylation, CAD localization also affects the rate of flux through the *de novo* pyrimidine pathway. Hindrance of CAD nuclear import has been found to decrease the rate of pyrimidine synthesis by 21% and decrease nucleotide concentrations by nearly 60%.⁴¹ However, it is unclear how and why CAD localization affects *de novo* synthesis. Nonetheless, CAD's phosphorylation and localization play a significant role in regulating DHODH activity.

Beyond phosphorylation, cancer cells may alter pyrimidine biosynthesis through the activation of the proto-oncogenic transcription factor MYC. MYC is a master regulator of many different pathways and has significant influence on the expression of nucleotide metabolism genes. Previous studies have shown that overexpression of MYC significantly increased expression of nucleotide metabolism enzymes, including DHODH, which was validated as a direct MYC target gene.⁴² Additionally, shRNA knockdown of MYC decreased the expression of nucleotide metabolism genes and lowered the intracellular concentrations of nucleotides.⁴³ These results demonstrate MYC's control over DHODH expression. Surprisingly, inhibition of DHODH has been observed to affect MYC expression. Two well-known DHODH inhibitors, brequinar and teriflunomide, were shown to decrease the expression of MYC.⁴⁴ However, this may be context-dependent as leflunomide (the pro-drug of teriflunomide), does not affect MYC expression.⁴⁵ It is possible that a sufficient quantity of leflunomide was not converted to teriflunomide and therefore did not affect MYC expression, although this was not evaluated experimentally. Nonetheless, while these conflicting results complicate the understanding of MYC and DHODH's relationship, it is clear that nucleotide biosynthesis is among the many pathways MYC activation influences to facilitate cellular proliferation. This is a unique relationship as other transcription factors, such as those in the E2F family, do not appear to increase expression of DHODH.⁴⁶ It is possible that MYC and DHODH expression are linked

through glutamine metabolism because MYC increases the production of glutamine, the first substrate in *de novo* pyrimidine biosynthesis.⁴⁷

The connection between increased glutamine metabolism and *de novo* pyrimidine synthesis is not well understood. Low glutamine concentrations have been demonstrated to hinder S phase progression, presumably by limiting the starting metabolite for nucleotide production.^{48, 49} Conversely, higher glutamine concentrations may increase the rate of *de novo* nucleotide synthesis. However, it does not appear that cancer cells increase glutamine uptake to solely fuel *de novo* pathways.^{48, 50} In fact, a significant disparity exists between the rates of glutamine uptake and nucleotide biosynthesis, suggesting that glutamine is utilized by far more pathways than nucleotide biosynthesis alone.⁴⁸ Interestingly, glutamine flux may be an indicator of cell sensitivity to DHODH inhibition. Cells containing a mutant PTEN tumor suppressor were observed to have increased glutamine metabolism and were sensitive to DHODH inhibition.⁵¹ While more studies are needed, these results suggest that DHODH inhibitors may be useful in cells with mutant PTEN and possibly increased glutamine metabolism.

1.4 DHODH and cellular differentiation

Beyond directly halting cell growth, DHODH has been implicated as a target to induce cellular differentiation. Previously, DHODH inhibition was shown to induced cell differentiation in neural crest⁵² and leukemic cell lines.⁵³ In leukemic cells, DHODH inhibitors, such as brequinar, were observed to decrease the number of self-renewing cells *in vivo*.⁵³ This finding significantly increased the interest in DHODH targeted therapy for cancer. Theoretically, DHODH inhibitors could induce differentiation of leukemic stem cells and hinder rapid growth of differentiated cancer cells. Further studies are needed to fully evaluate the ability of DHODH inhibitors to induce this effect.

While the mechanism of DHODH-induced differentiation is not fully understood, this phenomenon may be caused by pyrimidine depletion. Inhibitors, such as pyrazofurin, of the *de novo* pyrimidine pathway not targeting DHODH are able to induce differentiation and suggest pyrimidine depletion as a potential mechanism.⁵³ A possible link between pyrimidine depletion and cellular differentiation may be transcriptional elongation. The PHD-finger Phf5a protein is known to modulate transcriptional elongation in pluripotent cells. Through transcriptional elongation, this Phf5a protein is able to influence cellular differentiation.⁵⁴ Transcription

elongation has been induced by pyrimidine depletion previously⁵⁵ with DHODH inhibitors observed to modulate transcriptional elongation in melanoma cells.⁵² This proposed mechanism suggests that DHODH targeted therapy causes pyrimidine depletion that results in cellular transcriptional elongation, thereby inducing cellular differentiation. However, this mechanism has not been confirmed experimentally and the connection between DHODH and cellular differentiation is still not well understood. Despite this, considerable interest exists for DHODH targeted therapy as a potential option to induce cellular differentiation.

1.5 Relevance of DHODH in cancer

DHODH's relevance in cancer was recognized nearly six decades ago when Smith *et al.* noted elevated DHODH activity in leukemic cells.^{56,57} Following that discovery, several cancer projects focused on DHODH studies that culminated in the clinical evaluation of brequinar, a potent human DHODH inhibitor.^{58,59} However, brequinar failed to produce objective responses in clinical trials (discussed in further detail below), leading to questions about the viability of DHODH inhibition as a therapeutic target for cancer. Recent reports have revisited the link between DHODH inhibition and antiproliferative effects on cells. However, no studies have thoroughly evaluated the clinical relevance of DHODH in cancer. Therefore, to address this gap in understanding, we analyzed data from several different *in vitro* and *in vivo* profiling projects to provide an un-biased summary of the potential significance of DHODH in cancer.

Cell growth is suppressed when clinically relevant anticancer targets are knocked down. The Achilles Project⁶⁰⁻⁶² evaluates large-scale cellular responses in the presence of shRNA across a catalogue of cancer cell lines and has been utilized to gauge the importance of DHODH to cancer cells. Changes in shRNA levels (log-fold) were averaged for each cell line and then ranked by essentiality; a negative shRNA score indicates that a cell line responded poorly (i.e., showed growth inhibition) to treatment with shRNA. Achilles' project results (Figure 1.4A) depict a resounding negative response of cancer cell lines to shRNA knockdown of DHODH. The results suggest that DHODH inhibition is cytotoxic to most cancer cell lines. Cell lines that were most sensitive to DHODH knockdown were derived from cancers of the small and large intestines (highlighted in yellow, Figure 1.4A), which had a total of 17 out of 21 cell lines with lower than average shRNA scores (Figure 1.4B). Consistent with this finding, significantly

higher DHODH expression were observed in the Sabetes-Bellver colorectal dataset for adenomas tumor tissue versus normal samples using OncoPrint (Figure 1.4C).⁶³⁻⁶⁶

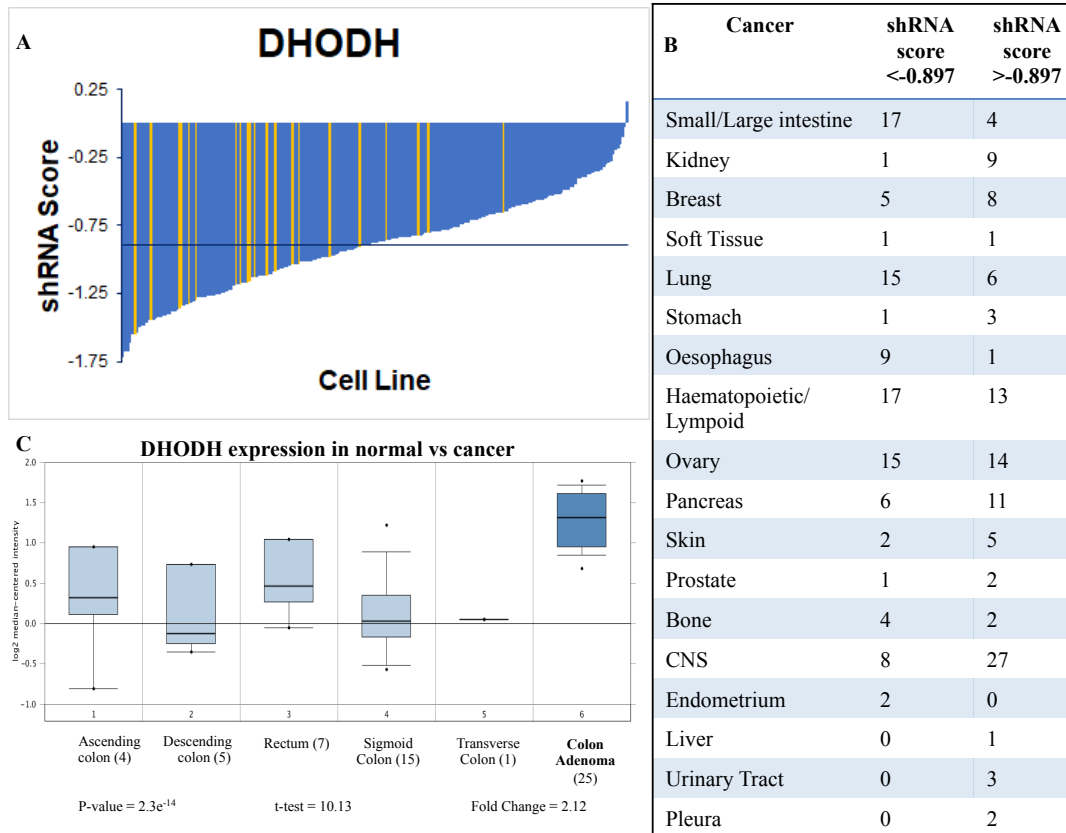


Figure 1.4: DHODH knockdown response from the Achilles Project. (A) Plot depicting shRNA scores in 216 cell lines for shRNA targeting DHODH. Yellow bars indicate intestinal cancer cell lines. The dark blue horizontal line indicates the mean shRNA score (-0.8972). (B) Table depicting the distribution of cell lines with respect to the mean shRNA score. (C) DHODH is overexpressed in colon cancer, generated using the Sabetes-Bellver colorectal database on the OncoPrint platform.

Cells overexpressing DHODH may have higher sensitivity to its inhibition. Using data from the Cancer Cell Line Encyclopedia (CCLE), we evaluated mRNA levels of DHODH in various cancer cell lines (Figure 1.5).⁶⁷ The mRNA expression levels of DHODH in 1,019 cancer cell lines were obtained and converted to Z-scores. The top four highest and lowest expressing cell lines are listed (Figure 1.5). Frequent overexpression of DHODH mRNA occurs in lung (33% of top ten) and haematopoietic/lymphoid (33% of top ten) tissue. Surprisingly, intestinal/colon cancer was not among the top ten tissues with high DHODH mRNA expression. However, this data still correlates well with the Achilles database (Figure 1.4). Both lung and haematopoietic/lymphoid are cell lines that frequently possess higher than average cell growth

inhibition when exposed to DHODH shRNA. Collectively, this data suggests that both lung and haematopoietic/lymphoid cell lines may be more sensitive to DHODH inhibitors.

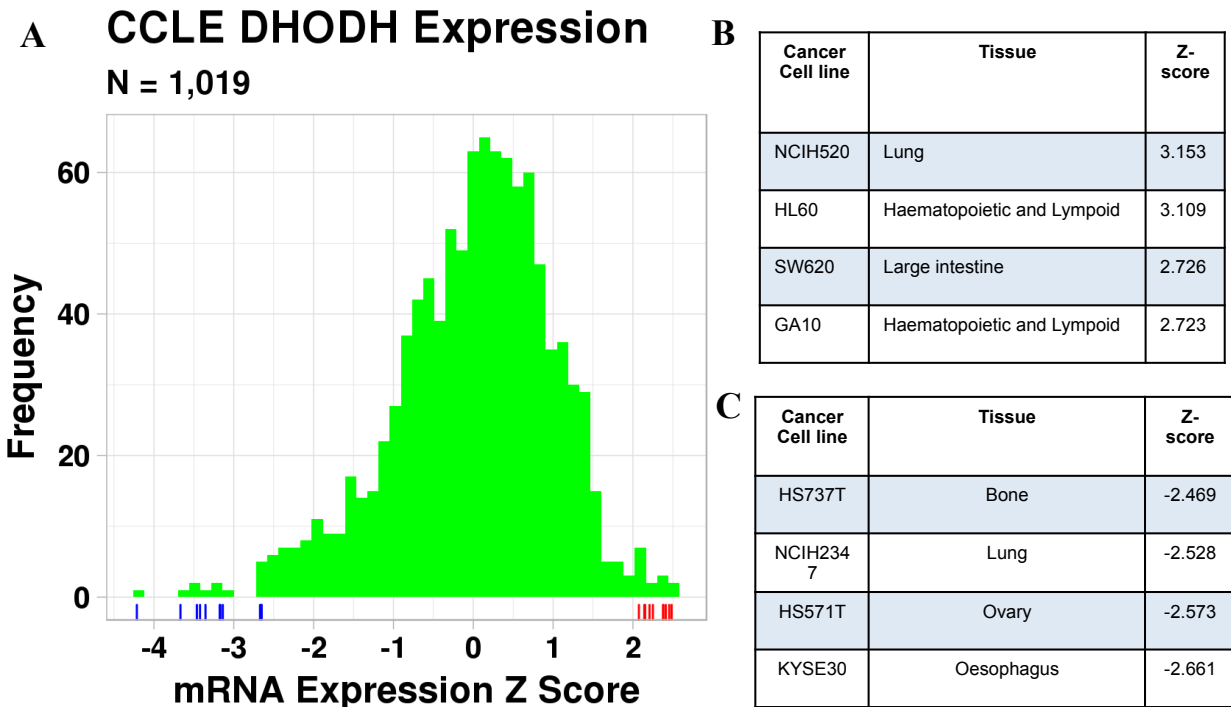


Figure 1.5: mRNA levels of DHODH in 1,019 cancer cell lines. Top four over and under expressing cell lines are depicted. Data generated using the CCLE.

We then evaluated *in vivo* DHODH mRNA expression using data from The Cancer Genome Atlas (TCGA).⁶⁸ To perform a pan-disease comparison of DHODH expression, log₂ TPM expression values were converted to z-scores calculated per patient. Figure 1.6 shows that across all 34 diseases (9,726 unique patient samples) the median DHODH expression is above a Z-score of zero. This indicates that most patients express DHODH more than the average of all other genes measured. Among these diseases, liver hepatocellular carcinoma (LIHC) patients tended to express DHODH the most (Figure 1.6). TCGA disease patient samples were evaluated for reduced survivability by comparing survival outcomes for patients with high DHODH expression to those with low DHODH expression. High DHODH expression was associated with reduced survival in low-grade glioma (LGG) and stomach adenocarcinoma (STAD) patients. High DHODH expression was also found to be associated with increased grade and stage in glioma patients from the TCGA, in the Rembrandt and Gravendeel studies (Figure 1.7).⁶⁹⁻⁷¹ Within glioma, stage III and IV tumors have a higher average mRNA expression of DHODH in

comparison to normal and stage I tumors. Therefore, in general, later stage glioma tumors have a higher DHODH mRNA expression level.

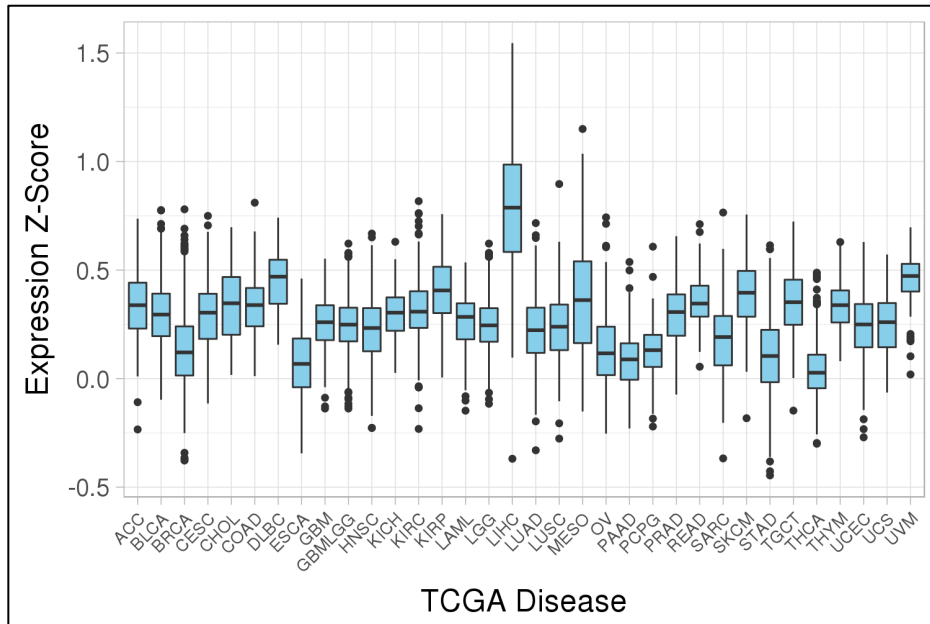


Figure 1.6: Z-score for mRNA expression generated from The Cancer Genome Atlas database. Pan-disease expression of DHODH across 34 TCGA diseases. Z-scores were calculated per patient per disease. The majority of patients across all diseases show higher than average expression (z-score = 0) of DHODH. Adrenocortical carcinoma (ACC), bladder urothelial carcinoma (BLCA), breast invasive carcinoma cohort (BRCA), Cervical squamous cell carcinoma and endocervical adenocarcinoma (CESC), Cholangiocarcinoma (CHOL), colon adenocarcinoma (COAD), lymphoid neoplasm diffuse large B-cell lymphoma (DLBC), esophageal carcinoma (ESCA), glioblastoma multiforme (GBM), glioma (GBMLGG), head and neck squamous cell carcinoma (HNSC), kidney chromophobe (KICH), kidney renal papillary cell carcinoma (KIRP), acute myeloid leukemia (LAML), brain lower grade glioma (LGG), liver hepatocellular carcinoma (LIHC), lung adenocarcinoma (LUAD), lung squamous cell carcinoma (LUSC), mesothelioma (MESO), ovarian serious cystadenocarcinoma (OV), pancreatic adenocarcinoma (PAAD), pheochromocytoma and paraganglioma (PCPG), prostate adenocarcinoma (PRAD), rectum adenocarcinoma (READ), sarcoma (SARC), skin cutaneous melanoma (SKCM), stomach adenocarcinoma (STAD), testicular germ cell tumors (TGCT), thymoma (THYM), uterine corpus endometrial carcinoma (UCEC), uterine carcinosarcoma (UCS), uveal melanoma (UVM).

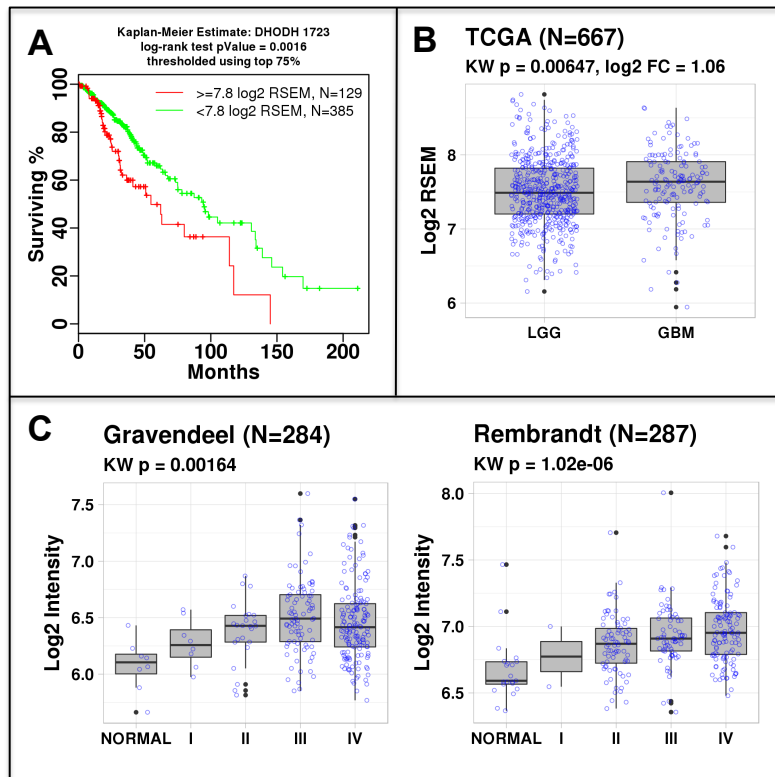


Figure 1.7: Analysis of DHODH in glioma. Kruskal-Wallis and survival analysis statistics were calculated using the R statistical programming language.⁷¹ (A) Kaplan-Meier curves for DHODH in glioma. (B) mRNA expression of DHODH in LGG and GBM. (C) DHODH expression increases with stage in LGG patients. Shown using a Kruskal-Wallis evaluation.^{69, 70}

In an effort to determine genes that are correlated with DHODH expression in the TCGA patient population, gene set enrichment analysis (GSEA) was used to identify pathways that were enriched with genes that co-express with DHODH. Co-expression of DHODH in patients was evaluated in lower grade glioma (LGG), stomach adenocarcinoma (STAD), liver hepatocellular carcinoma (LIHC), colon adenocarcinoma (COAD), rectum adenocarcinoma (READ), and pancreatic adenocarcinoma (PAAD) using a Pearson correlation measure (Figure 1.8).⁷² In each of these patient populations, DHODH is co-expressed with genes involved with mitochondrial translation, mitochondrial respiratory complex, electron transport chain, MYC targets, and translation elongation. These findings are consistent with our description of DHODH function.

We also performed a correlation analysis independent of annotated gene sets to identify potentially novel genes that are co-expressed with DHODH. Using the top 100 DHODH co-expressed genes in COAD, LGG, STAD, and PAAD diseases, we identified four common genes across all four diseases (Figure 1.9). These genes are translation elongation mitochondrial factor

(TUFM), DNA polymerase delta 2 (POLD2), peter pan homolog (PPAN), and ribosomal subunit RNA processing 9 (RRP9). Of these genes, TUFM may be the most relevant in cancer. TUFM has been shown to prevent the epithelial-to-mesenchymal transition (EMT).⁷³ Knockdown of TUFM induces EMT transition in lung cancer cells.⁷³ However, TUFM appears to be considerably overexpressed in colon cancer and may be a potential prognostic biomarker.⁷⁴ Additionally, TUFM may play a role in the transition of normal cells into adenomas for colorectal cancer.⁷⁵ Although co-expression does not prove DHODH is directly interacting with these four targets, one might hypothesize a common functional relationship or transcriptional regulation that is worth investigating.

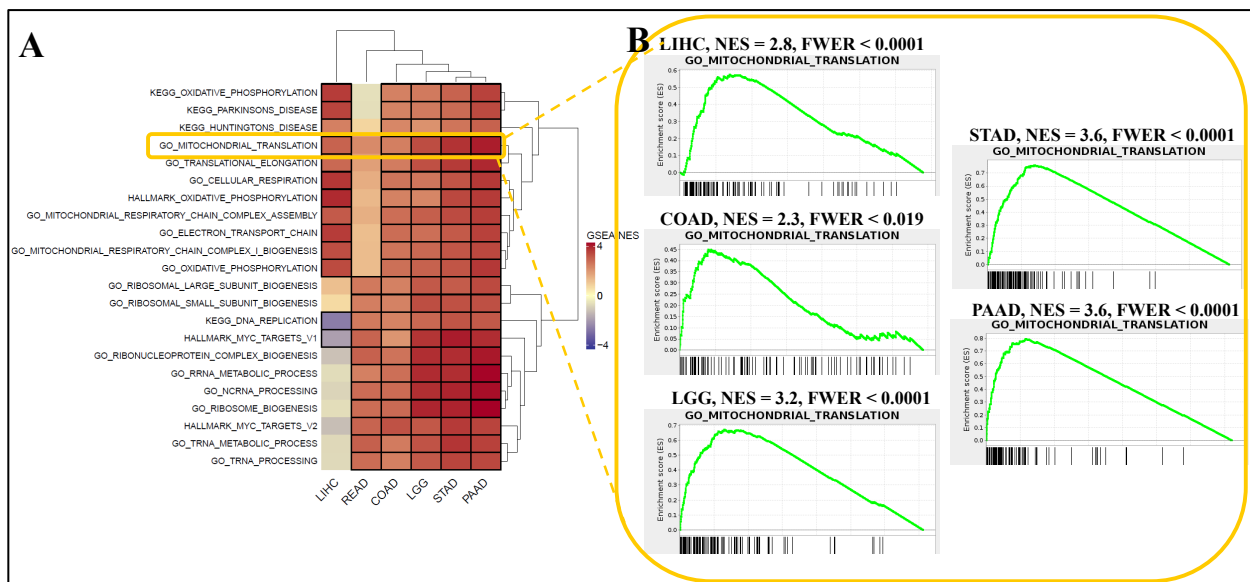


Figure 1.8: Common gene sets enriched for genes that are co-expressed with DHODH. Gene set enrichment analysis (GSEA) was used to identify enriched pathways with genes that are co-expressed with DHODH. GSEAv2.2.3 was used with v6 gene sets sourced from MSigDB. 10,000 gene set permutations were performed using weighted mode scoring and Pearson metric.⁷² Only genes with evidence of expression in > 50% of a disease patient population were considered. Six diseases were evaluated based on association with reduced survivability (LGG, STAD), high expression (LIHC), or experimental evidence (COAD, READ, PAAD). 22 Gene sets were significantly enriched for genes positively correlated with DHODH expression using Gene Set Enrichment Analysis (GSEA) (A). Heatmap coloring indicates the normalized enrichment score (NES) and all gene sets with an FWER adjusted p-value < 0.05 are colored with a black border. GSEA running sum statistic visualizations are shown (B) for the Gene Ontology (GO) category, Mitochondrial Translation that was significantly enriched in LIHC, COAD, LGG, STAD, and PAAD TCGA diseases.

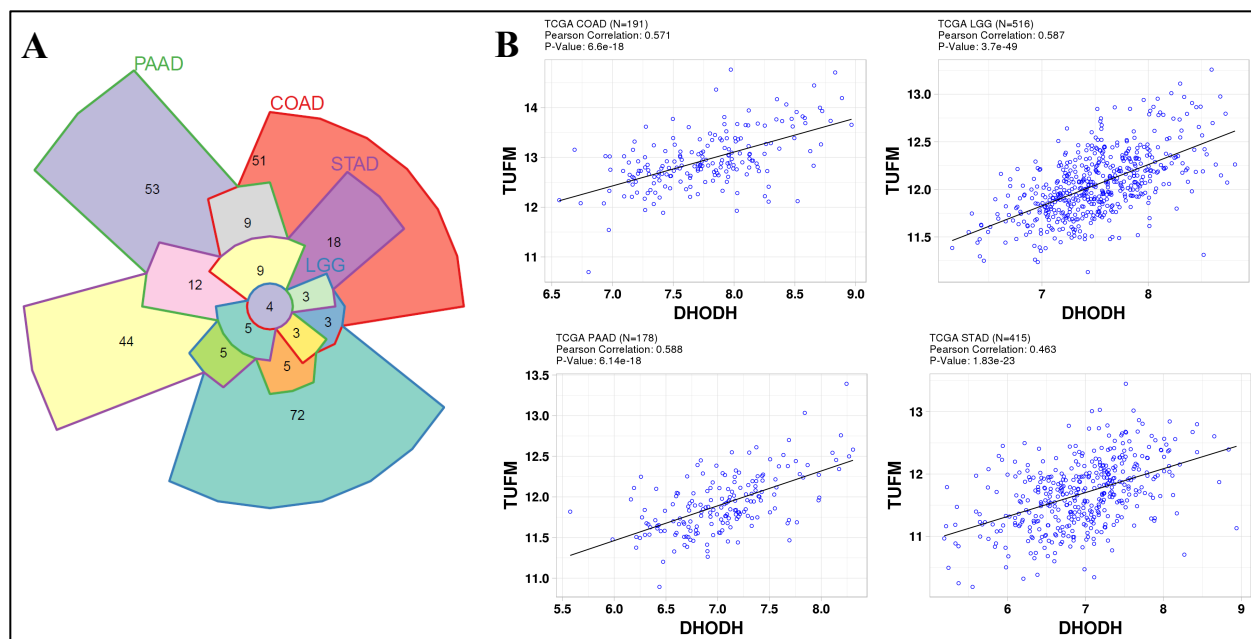


Figure 1.9: DHODH co-expressed genes were identified across multiple TCGA diseases. DHODH gene co-expression was evaluated and compared across multiple diseases. DHODH correlations were clustered using Euclidean distance, agglomerative hierarchical clustering and COAD, LGG, STAD, and PAAD showed the strongest agreement in co-expression. **(A)** A Chow-Ruskey weighted Venn diagram shows overlap of the top 100 genes correlated with DHODH within COAD, LGG, PAAD, and STAD TCGA diseases. **(B)** TUFM was one of the four top co-expressed genes (POLD2, PPNAN, RRP9, TUFM) in common across all four diseases and has been shown to be associated with mitochondrial translation and organelle biogenesis and maintenance.

STRING protein interactions have been used to highlight enzymes associated with DHODH (Figure 1.10).⁷⁶ Using the online database for STRING analysis, all reported/predicted protein-protein interactions with DHODH are depicted. The reported protein-protein associations are primarily within the *de novo* nucleotide synthesis pathways (CAD, carbamoyl phosphate synthase 1, uridine monophosphate synthetase, and phosphoribosylglycinamide formyltransferase (*de novo* purine)).¹¹ These edges, showing connections between proteins, are primarily reported in non-human organisms. Beyond *de novo* pathways, DHODH is reported to associate with the dihydropyrimidinase-like (DPYSL) family. DPYSL is also known as a collapsing response mediator protein (CRMP) family.⁷⁷ CRMP1 has been implicated in metastasis and differentiation⁷⁸ acting as a tumor suppressor in prostate cancer and hindering the epithelial-mesenchymal transition.⁷⁹ Additionally, CRMP may present a potential biomarker for cancers. In neuroblastoma, the activation of MYC selectively decreased the expression of CRMP3, but not CRMP1 or CRMP2. Conversely, siRNA knockdown of MYC increased expression of CRMP3, suggesting a unique role for CRMP3 as a biomarker for aggressive

neuroblastoma.^{77, 80} Beyond neuroblastoma, CRMP5 is reported as a biomarker for poor prognosis in osteosarcoma.⁸¹ However, the complete connection between these proteins, DHODH, and cancer is not fully understood.

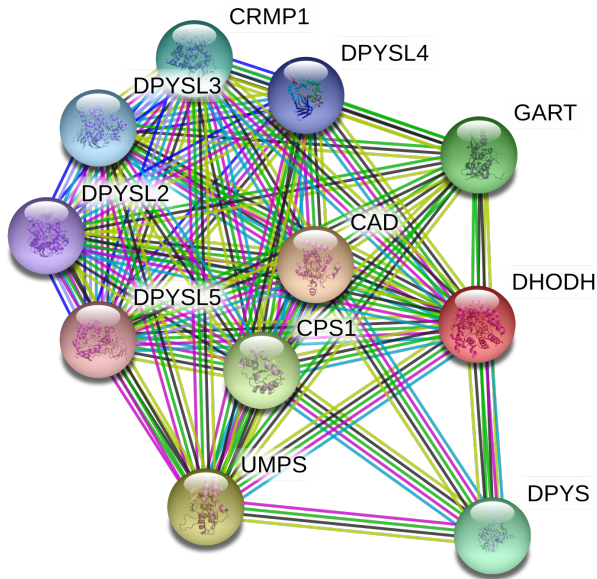


Figure 1.10: STRING analysis of interactions with DHODH. STRING Analysis reports/predicts protein-protein interactions with DHODH using predicted and experimental data from online databases. CAD, carbamoyl phosphate synthetase 2, aspartate transcarbamylase, and dihydroorotase; CPS1 carbamoyl phosphate synthase 1; CRMP1, collapsing response mediator protein 1; DPYS, dihydropyrimidinase; DPYSL2, dihydropyrimidinase-like 2; DPYSL3, dihydropyrimidinase-like 3; DPYSL4, dihydropyrimidinase-like 4; DPYSL5, dihydropyrimidinase-like 5; GART phosphoribosylglycinamide formyltransferase; UMPS, uridine monophosphate synthetase.

Murine knockout studies, performed by the International Mouse Phenotyping Consortium, identified DHODH as homozygous-lethal gene.^{82, 83} At least one functional allele copy is necessary for survival. However, even heterozygous mutations in DHODH may be responsible for health defects, as mutations in DHODH were implicated as a cause of Miller syndrome.⁸⁴ At least 11 different DHODH mutations have been identified.⁸⁴ Some amino acid changes in patients with Miller's syndrome are R346W and G202A.⁸⁴ These mutations do not have an impact on mitochondrial localization but were later observed to decrease protein stability.⁸⁵ It is unclear how other mutations alter DHODH function in patients with Miller's syndrome. However, there is a clear implication that DHODH function is necessary for normal embryonic development. In fact, DHODH inhibitors such as leflunomide are known teratogens and its use is avoided during pregnancy.⁸⁶ In murine studies, leflunomide dosing in pregnant

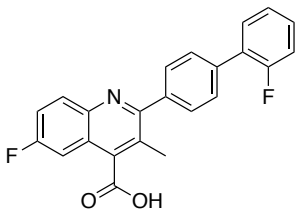
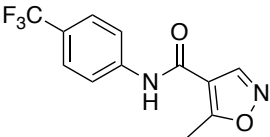
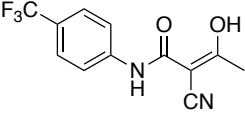
mice caused significant malformations. These malformations did not occur when leflunomide was co-administered with uridine.^{87, 88} For embryonic development, this data suggests that DHODH function is necessary to generate nucleotides for continued growth.

Overall, the results of these bioinformatics studies suggest that DHODH is an important oncology target. The cellular response to DHODH shRNA highlights cancer's dependence on *de novo* pyrimidine biosynthesis. Additionally, increased DHODH expression has been correlated with decreased survival in glioma patients. Collectively, this data strengthens the case to pursue drug discovery campaigns aimed at inhibiting DHODH for cancer therapy.

1.6 Select inhibitors of DHODH

The importance of DHODH to cancer cells has resulted in many drug discovery campaigns. Various DHODH inhibitors belonging to different chemical classes have been reported and recently reviewed.^{5, 6} Only select inhibitors targeting human DHODH, which were not previously reviewed, are discussed with the most notable inhibitors, brequinar and leflunomide/teriflunomide, discussed in detail.

Table 1.1: DHODH inhibitors evaluated in clinical trials.

Name	Structure	Diseases/Status
Brequinar		Cancer ⁵⁹ Did not meet objective response in multiple phase II clinical trials for breast ⁸⁹ , colon ⁹⁰ , head and neck ⁹¹ , gastrointestinal ⁹² , lung ⁹³ , melanoma ⁹⁴ , and ovarian cancer ⁹⁵ .
Leflunomide		Immunomodulatory ^{96, 97} Used in combination with cyclosporine A, observed to alter PK properties of brequinar ⁹⁷ Did not gain FDA approval
Teriflunomide		FDA approved for rheumatoid and psoriatic arthritis ⁹⁸ FDA approved for multiple sclerosis ⁹⁸

Brequinar

Brequinar is a potent DHODH inhibitor (Table 1.1, DHODH assay $K_i = 27.4 \pm 1.6$ nM) with significant anticancer properties.⁹⁹ DuPont Pharmaceuticals developed brequinar from a lead compound discovered in the National Cancer Institute's Developmental Therapeutics Program.⁵⁹ Initial studies with brequinar revealed promising anticancer effects. Dosing at 20-40 mg/kg in murine xenograft models inhibited the growth of breast, lung, stomach, and colon tumors by > 90%.⁵⁹ However, the target was not initially known until a mechanism of action study observed a selective depletion of uridine and cytidine triphosphate.¹⁰⁰ This finding ultimately led to the discovery of DHODH as the target. Further studies of brequinar highlighted a schedule dependency, as cells exposed to brequinar for 1-24 hours could sustain growth once brequinar was removed. However, when exposed for 48 hours, cells were unable to continue growth. Therefore continual inhibition is necessary to maximize DHODH's anticancer effects, which has been demonstrated in multiple cell lines.^{59, 99} Cells with a faster doubling time are more likely to be sensitive to brequinar.⁷ In fact, brequinar's IC_{50} in two breast cancer cell lines with doubling times between 25-45 hours, T-47D and MDA-MD-231, was < 1 μ M whereas in slower growing MDA-MB-436 and W3.006, two breast cancer cell lines with doubling times of 75-85 hours, brequinar's IC_{50} was > 100 μ M.⁷ This data highlights the sensitivity of faster growing cells to DHODH inhibition. The overall impressive preclinical results of brequinar were sufficient to pursue clinical evaluation for treatment of cancer.

Early clinical evaluation of brequinar gave conflicting results. First, high doses were well tolerated by most patients. Doses at 200-250 mg/m² were tolerated with few dose-limiting toxicities (e.g., myelosuppression and nausea).^{58, 101-105} Second, objective responses were not regularly observed¹⁰⁴⁻¹⁰⁶ in multiple studies leading to the recommendation for increasing the dose in phase II studies. However, the results were similar in each study with brequinar failing to produce an objective response in breast,⁸⁹ colon,⁹⁰ head and neck,⁹¹ gastrointestinal,⁹² lung,⁹³ melanoma,⁹⁴ and ovarian cancers.⁹⁵ These results were befuddling considering that patient-derived samples of lymphocytes had undetectable DHODH activity for at least a week after treatment with brequinar had ceased.¹⁰⁷ Furthermore, brequinar at 600 mg/m² induced plasma uridine depletion (40-80%), which ranged from 6 hours to 4 days after dosing. However, a significant rebound of plasma uridine (160-350%) was observed 4-7 days after dosage.¹⁰⁷ These results suggest that despite potent DHODH inhibition, clinically relevant uridine depletion may

not have continually occurred, possibly due to a sub-optimal dosing regimen. Effective brequinar therapy requires continuous inhibition of DHODH. With most patients in these trials dosed weekly at high doses,⁵³ it is likely that alternative sources of plasma uridine overcame DHODH inhibition. Hence, brequinar did not meet its objective response, likely due to poorly chosen dosing regimens.

Recent studies have reported on brequinar's impact beyond cell growth inhibition. Brequinar induced differentiation in acute myeloid leukemia (AML) cells. Differentiation was observed both *in vitro* and *in vivo* suggesting a new utility for brequinar, or other DHODH inhibitors.¹⁰⁸ Additionally, when dosed in neural crest stem cells, both a brequinar analogue and leflunomide (described below) decreased the cell's self-renewing capabilities. This study suggests that DHODH inhibitors halt neural crest cell growth and limit stem cell renewal.⁵² Aside from differentiation, brequinar was also observed to overcome tumor necrosis factor-related apoptosis ligand (TRAIL) resistance. Genomic screening was used to identify potential enzymes that may sensitize cells to TRAIL. In this study, siRNA for DHODH was found to sensitize resistant cells to TRAIL. Dosing cells with brequinar and TRAIL reproduced these results, which validates DHODH as a viable target for these cells.¹⁰⁹ Together these studies highlight a future for brequinar beyond single agent use, potentially in combination with agents that induce apoptosis.

Leflunomide and Teriflunomide

Leflunomide is a potent DHODH inhibitor that has gained FDA approval for the treatment of rheumatoid and psoriatic arthritis (Table 1.1).¹¹⁰ Leflunomide is a prodrug of the active metabolite teriflunomide, itself FDA approved for multiple sclerosis.¹¹¹ The two are used interchangeably for this indication. Besides arthritis, leflunomide has been evaluated in multiple clinical trials for the treatment of ankylosing syndrome,¹¹² Crohn's disease,^{113, 114} rare autoimmune diseases such as Felty syndrome and granulomatosis with polyangiitis,¹¹⁵ Kimura's disease,¹¹⁶ pemphigoid,¹¹⁷ organ transplantation,^{110, 118, 119} sarcoidosis,¹²⁰ Still's disease,¹²¹ systemic lupus,¹²² Takayasu arteritis,¹²³ and uveitis.¹²⁴ Despite being marketed primarily for autoimmune disorders, leflunomide also displays anticancer effects. Several studies report anti-proliferative effects of leflunomide in various cell lines, including those derived from multiple myeloma,¹²⁵ non-small cell lung carcinomas,¹²⁶ neuroblastomas,¹²⁷ neuroendocrine,¹²⁸ and

cancer in medullary thyroids.¹²⁹ However, the off-target effects of leflunomide therapy complicate attributing these responses to DHODH inhibition.

Leflunomide has been reported to target additional enzymes beyond DHODH. One reported off-target effect is due to the aryl hydrocarbon receptor, which may contribute to leflunomide's overall mechanism of action. In fact, melanoma cells were not rescued from leflunomide's antiproliferative effects by uridine supplementation.⁴⁵ DHODH inhibition effects are reversed by uridine supplementation and this result suggests that leflunomide may not be suppressing cell growth solely through DHODH inhibition. Other studies have suggested that leflunomide may inhibit S6 kinase (S6K1), a kinase responsible for ribosomal and CAD phosphorylation,¹³⁰ but this has not been completely verified experimentally. Additionally, leflunomide modestly inhibits the EGF-receptor tyrosine kinase at high concentrations ($IC_{50} \approx 40 \mu M$).¹³¹ As a result, it is difficult to ascribe leflunomide-induced cellular responses to DHODH alone, due to likely contributions from off-target effects.

Leflunomide also affects other signaling pathways beyond antiproliferation. In oral squamous cell carcinoma cells, leflunomide induced an upregulation of cyclin A.¹³² Cyclin A is upregulated in S phase when flux through the *de novo* pyrimidine pathway is abundant and possibly upregulated in response to pyrimidine depletion.¹³³ In murine xenografts of Ehrlich's ascites carcinoma, leflunomide decreased TNF- α and EGF protein levels and this response is associated with immunosuppression.¹³⁴ Leflunomide has been shown to inhibit frizzled-10 (FZD10) gene expression in renal carcinoma cells, which is a receptor protein that can initiate WNT/ β -catenin signaling.¹³⁵ Other cellular studies on leflunomide and teriflunomide have highlighted their chemo-preventative properties for prostate cancer.¹³⁶ In fact, both inhibitors have progressed into clinical trials for prostate cancer.¹³⁷ However, it is difficult to attribute this response to DHODH inhibition, as uridine rescue did not overcome antiproliferative effects in prostate cancer.¹³⁶ Finally, p53 may be a marker of nucleotide depletion as it has been shown that inhibition of *de novo* pyrimidine biosynthesis resulted in a p53 mediated cell cycle arrest.^{25, 138} Leflunomide treatment was found to increase the expression of p53,²⁵ but it is unknown if functional p53 must be present to induce cell death via DHODH inhibition.

Leflunomide and teriflunomide represent the only FDA approved DHODH inhibitors in clinical use. Therefore, they are commonly chosen for studies on DHODH inhibition. However, there are many off-target effects that complicate leflunomide-induced responses and their

relationship to DHODH. Nonetheless, the continued use of these inhibitors highlights the potential of long-term DHODH inhibition as a valid clinical strategy.

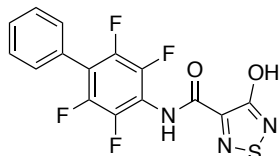
Selected human DHODH inhibitors

In general, DHODH inhibitors possess diverse scaffolds that likely vary mechanistically by different binding sites to the enzyme (Table 1.2). A variety of structurally distinct inhibitors of human DHODH have been developed for cancer,^{5, 6} including biphenyl indoles,¹³⁹ amides like ML390,¹⁴⁰ derivatives of ascochlorin,¹⁴¹ substituted quinolines like brequinar,⁵⁹ and leflunomide.^{45, 52} There are brequinar-like quinoline-based inhibitors such as FA-613,¹⁴² CD44,¹⁴³ and compound 11.¹⁴⁴ Leflunomide-like inhibitors have also been reported, including compound 4.¹⁴⁵ In addition to brequinar and leflunomide-like inhibitors, pyrazole-based analogues 18d¹⁴⁶ and 21q¹⁴⁷ were reported for human DHODH as antivirals. A tri-substituted benzimidazole inhibitor (compound 8d) of DHODH, which is structurally similar to compound A14,¹⁴⁹ was reported with an $IC_{50} = 81 \pm 2$ nM,¹⁴⁸ However, the rest of compounds shown in Table 1.2 represent unique classes of DHODH inhibitors without any obvious structural similarity.

Table 1.2: Selected recently published DHODH inhibitors

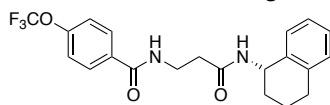
Name	Structure	Diseases/Status
Compound 8d		DHODH $IC_{50} = 81 \pm 2$ nM ¹⁴⁸
DD778		Racemate* Antiviral ¹⁵⁰
BEHI		Anticancer cell data ¹³⁹ $IC_{50} = 20.5$ μ M for A549 $IC_{50} = 18.5$ μ M for 4T ₁
FA-613		Antiviral suggested as DHODH inhibitor ¹⁴²

Compound 4



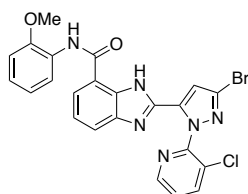
Antiproliferative
 $IC_{50} = 1.04 \pm 0.04 \mu\text{M}$ for Jurkat cells¹⁴⁵

ML390



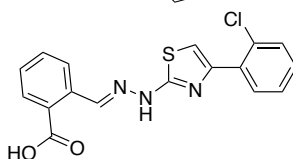
Antiproliferative
 $EC_{50} = 1.8 \pm 0.6 \mu\text{M}$ for ER-HOX-GFP cells¹⁴⁰

Compound A14



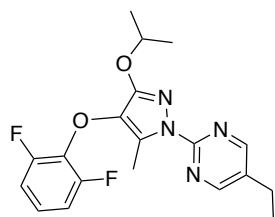
DHODH $IC_{50} = 0.178 \mu\text{M}$ ¹⁴⁹

Compound 19



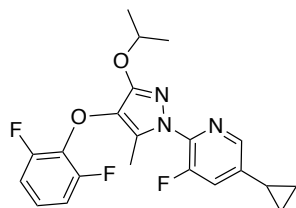
DHODH $IC_{50} = 0.032 \mu\text{M}$ ¹⁵¹

Compound 18d



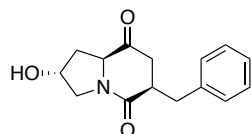
DHODH $IC_{50} = 25 \pm 5 \text{ nM}$
Jurkat $IC_{50} = 0.02 \mu\text{M}$ ¹⁴⁶

Compound 21q



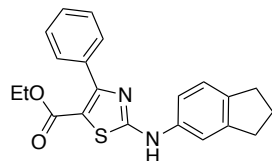
DHODH $pIC_{50} = 5.9 \text{ M}$ ¹⁴⁷

Fr1-4



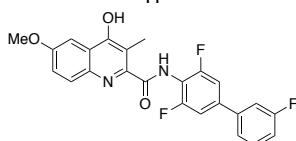
DHODH $IC_{50} = 0.773 \mu\text{M}$ ¹⁵²

Compound 44



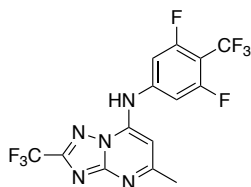
DHODH $IC_{50} = 26 \text{ nM}$ ¹⁵³

Compound 11



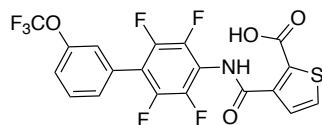
DHODH $IC_{50} = 0.94 \pm 0.06 \mu\text{M}$
 $IC_{50} = 5.03 \mu\text{M}$ A-375 melanoma cells.¹⁴⁴

DSM338



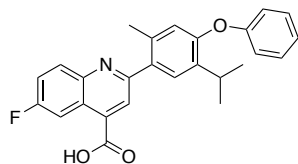
DHODH $IC_{50} = 1.6 \mu M^{154}$

Compound 1



DHODH $IC_{50} = 1.5 \pm 0.2 nM^{155}$

C44



DHODH $IC_{50} = 1 nM^{143}$

Non-DHODH *de novo* pyrimidine biosynthesis inhibitors

Beyond DHODH, multiple inhibitors of the *de novo* pyrimidine biosynthesis pathway have been evaluated for anticancer activity (Figure 1.11). Carbamoyl phosphate synthetase is a reported target for the antitumor agent acivicin.^{156, 157} However, acivicin appears to target most enzymes containing a glutamine binding site, thus studies with this compound were not pursued further due to high toxicity.¹⁵⁸ Aspartate carbamoyl transferase has been targeted by N-phosphoacetyl-L-aspartate (PALA), a potent inhibitor with a $K_i = 26 nM$ for the murine enzyme.^{159, 160} PALA performed well against solid murine tumors, but did not fare well in clinical trials.^{160, 161} In humans, PALA caused a meager decrease in plasma uridine concentrations but only one patient was a reported responder.^{161, 162} A metabolic resistance mechanism was proposed in which PALA-induced inhibition of aspartate carbamoyl transferase led to a significant increase in carbamoyl phosphate, the substrate. Sufficient concentrations may have been reached to displace PALA and continue flux through the *de novo* pathway.^{160, 163} A few inhibitors have been developed for dihydroorotase with the most notable being 4-mecapto-6-oxo-1,4-azaphosphinane-2-carboxylic acid 4-oxide (MOAC). However, these inhibitors have shown minimal anticancer activity.^{160, 164, 165} Additionally, attempts have been made to target orotidine 5'-monophosphate decarboxylase (OMP decarboxylase) by pyrazofurin, which is phosphorylated in the cell to generate an active OMP decarboxylase inhibitor.¹⁶⁶ In clinical trials, pyrazofurin did not fare well as limited objective responses were observed.¹⁶⁷⁻¹⁶⁹ Far more extensive efforts have been made to target dihydroorotase dehydrogenase for cancer.

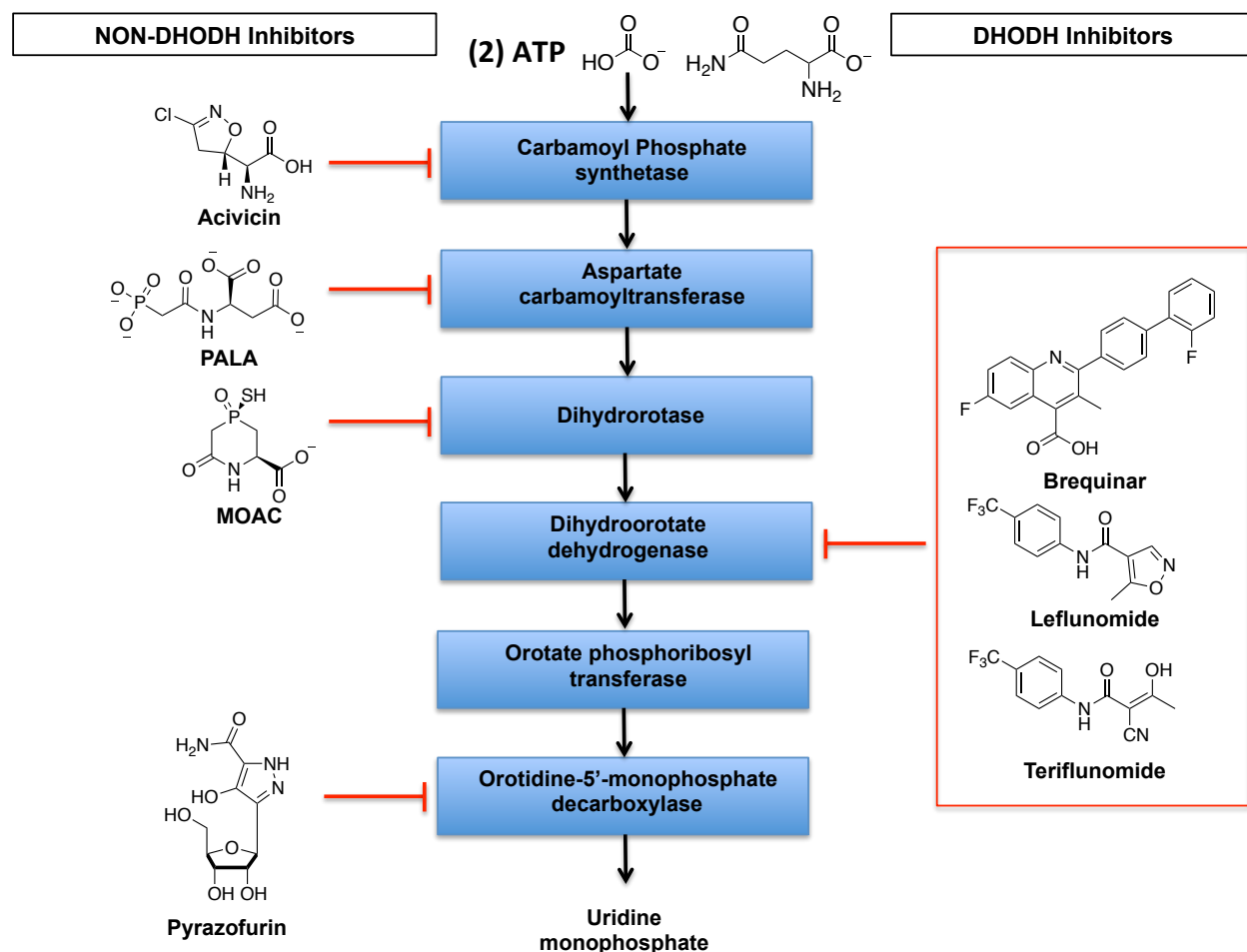


Figure 1.11: Selected inhibitors of the *de novo* pyrimidine biosynthesis pathway.

1.7 Combination approaches to increase efficacy of DHODH inhibitors

Results from the multitude of *de novo* pyrimidine inhibitors in anticancer clinical trials depict a mixed outlook for single agent DHODH inhibition. As previously discussed, brequinar produced minimal objective responses in clinical trials. These results were similar for all inhibitors of the *de novo* pathway evaluated in the clinic (e.g., PALA and pyrazofurin). However, a significant problem with targeting *de novo* pyrimidine biosynthesis is the salvage pathway. Cells can obtain the necessary nucleotides for growth through either pathway. In theory, an inhibitor of DHODH may shut down *de novo* synthesis, but extracellular uridine can enter the intracellular salvage pathway to form the necessary nucleosides/nucleotides. As previously mentioned, supplementation of a treated cell line with uridine or other pyrimidines recapitulates this phenomenon. Uridine rescue has been demonstrated to work exceptionally well in the context of potent DHODH inhibitors such as brequinar.^{58, 170} Results from uridine rescue

experiments have led to the hypothesis that a DHODH inhibitor may require concomitant administration of other agents to be successful.

The combination of brequinar and 5-fluorouracil (5-FU) has been evaluated to assess if brequinar-induced uridine depletion would improve 5-FU activity. In cells, 5-FU is metabolized into FdUMP and inhibits thymidylate synthetase, which catalyzes the formation of thymidine monophosphate from deoxyuridine monophosphate.^{171, 172} A combination of brequinar and 5-FU was proposed to increase generation of FdUMP by decreasing intracellular nucleotide concentrations. Initial evaluation of this combination utilized a low dose of brequinar to assess if pretreatment would improve the activity of 5-FU or 5-FU with leucovorin. The results indicated that brequinar did enhance the potency of 5-FU when pretreated at 24 or 48 hours, and that cells treated with this combination had significantly higher concentrations of FdUMP compared to 5-FU alone.¹⁷³ However, brequinar pretreatment did not significantly improve the 5-FU and leucovorin combination.¹⁷³ A larger study evaluating 5-FU and brequinar *in vivo* suggested the combination provided a synergistic effect in colon cancer cells at low uridine concentrations. However, at higher concentrations, the combination did not perform well. Studies were also conducted in colon 26 (estimated intracellular [uridine] of 10 μ M) and colon 38 (estimated intracellular [uridine] of 50-100 μ M) cell lines.^{174, 175} When applied *in vivo* the 5-FU and brequinar combination significantly decreased tumor weight in colon 26, but the results in colon 38 were not significantly different than for 5-FU alone.¹⁷⁵ A third compound was then added to improve the combination *in vitro*. An equilibrative nucleoside transport inhibitor, dipyridamole (DPM), believed to hinder nucleobase/nucleoside transport across the cell membrane was evaluated. This three inhibitor cocktail combination inhibited cell growth at low concentrations of uridine, but was unable to inhibit cell growth in the presence of 50 μ M uridine.¹⁷⁵ If the salvage pathway rescued the cells, it may have occurred due to additional nucleoside transporters. Additionally, DPM may have limited the influx of 5-fluorouracil across the membrane. Further *in vivo* studies on the combination demonstrated a significant decrease in tumor weight when comparing brequinar as a single agent to brequinar with 5-FU.¹⁷⁶ The combination was tested in a phase I study, where weekly doses as high as 600 mg/m² brequinar and 600 mg/m² of 5-FU were used in patients. However, no objective responses were observed in the 25 patients with refractory solid tumors.¹⁷⁷ Brequinar doses as high as 400 mg/m² were observed to decrease baseline uridine levels by more than 50%.¹⁷⁷ Beyond combinations with 5-

FU, brequinar has also been evaluated in combination with cisplatin. Unfortunately, the results in a phase I study were much the same with no objective responses.⁹⁶

Other combination therapy studies have been pursued with non-DHODH inhibitors of *de novo* biosynthesis. 5-FU and DPM have been evaluated in combinations with other *de novo* pyrimidine biosynthesis inhibitors. PALA and 5-FU were evaluated in multiple anticancer clinical trials, but the combination showed little advantage in comparison to 5-FU alone.^{178, 179} The addition of leucovorin was not much better in a trial against pancreatic ductal adenocarcinoma. From a total of 26 patients, only 3 showed partial responses to a combination of PALA, 5-FU, and leucovorin (12%).¹⁸⁰ Beyond 5-FU, PALA was investigated with DPM. This combination progressed to a phase I clinical trial, but only 4 of 65 patients responded to the therapy.¹⁸¹ An additional phase II study evaluating PALA and DPM for soft tissue sarcoma concluded that the combination was not better than PALA alone, which had previously failed to induce objective responses in clinical trials.¹⁸² Aside from PALA, a combination of acivicin and DPM has been evaluated in cancer patients diagnosed with a various types of tumors. However, this did not result in objective responses despite achieving plasma concentrations of DPM that were sufficient to inhibit nucleoside transport *in vitro*.^{183, 184}

The results from these clinical studies raise an important question. Why have inhibitors of pyrimidine biosynthesis, and in particular DHODH, been unsuccessful in clinical trials? The existence of the salvage pathway may provide an explanation.

Extracellular uridine can be transported across the cell membrane to enter the nucleotide salvage pathway. For brequinar, it was shown that a colon cancer cell line, colon 26, supplemented with 5 μ M uridine was capable of continuing growth in the presence of 1 μ M brequinar.¹⁷⁵ The supplemented uridine may be transported across the cell membrane by either the solute carrier 29 family (equilibrative nucleoside transporter, ENT1-4), solute carrier 28 family (concentrative nucleoside transporters, CNT1-3), or select members of the solute carrier 35 family (Figure 1.12).^{185, 186} Once inside the cell, the uridine may be converted into uridine monophosphate by uridine kinase.¹⁸⁷ This circumvents pyrimidine depletion induced by DHODH inhibition. Thus, an extensive network of salvage enzymes can generate the required nucleotides from extracellular sources of nucleobases/nucleosides to sustain cellular growth. However, it is unclear why combinations of DHODH inhibitors, such as brequinar, with DPM have been unsuccessful. DPM halts flux of nucleobases/nucleosides across the cell membrane by

targeting the ENT isoforms.¹⁸⁵ While other nucleoside transporters are present, the ENT family is thought to be the predominant source of uridine flux across the membrane as most ENT isoforms catalyze facilitative diffusion and have a higher turnover rate in comparison to CNTs (ENT1 200 uridine/sec vs. CNT1 10 uridine/sec).^{185, 188} Despite the slower rate of transport, it is possible that the sodium or proton coupled CNT transport may be able to sustain the required intracellular nucleotide concentrations.¹⁸⁵ The role of nucleoside transporters from the SLC35 family is unknown. Select members of the large family transport UDP analogues across membranes. For example, the SLC35 family member UGT catalyzes the transport of UDP-galactose and UDP-*N*-acetylgalactosamine across the membrane, but requires UMP as an antiport exchange substrate¹⁸⁶ It is unclear if these transporters would be active in cells with low UMP concentrations. For successful combination therapy, inhibitors of both CNT and ENT with DHODH inhibitors might be necessary. To date, this has not been evaluated.

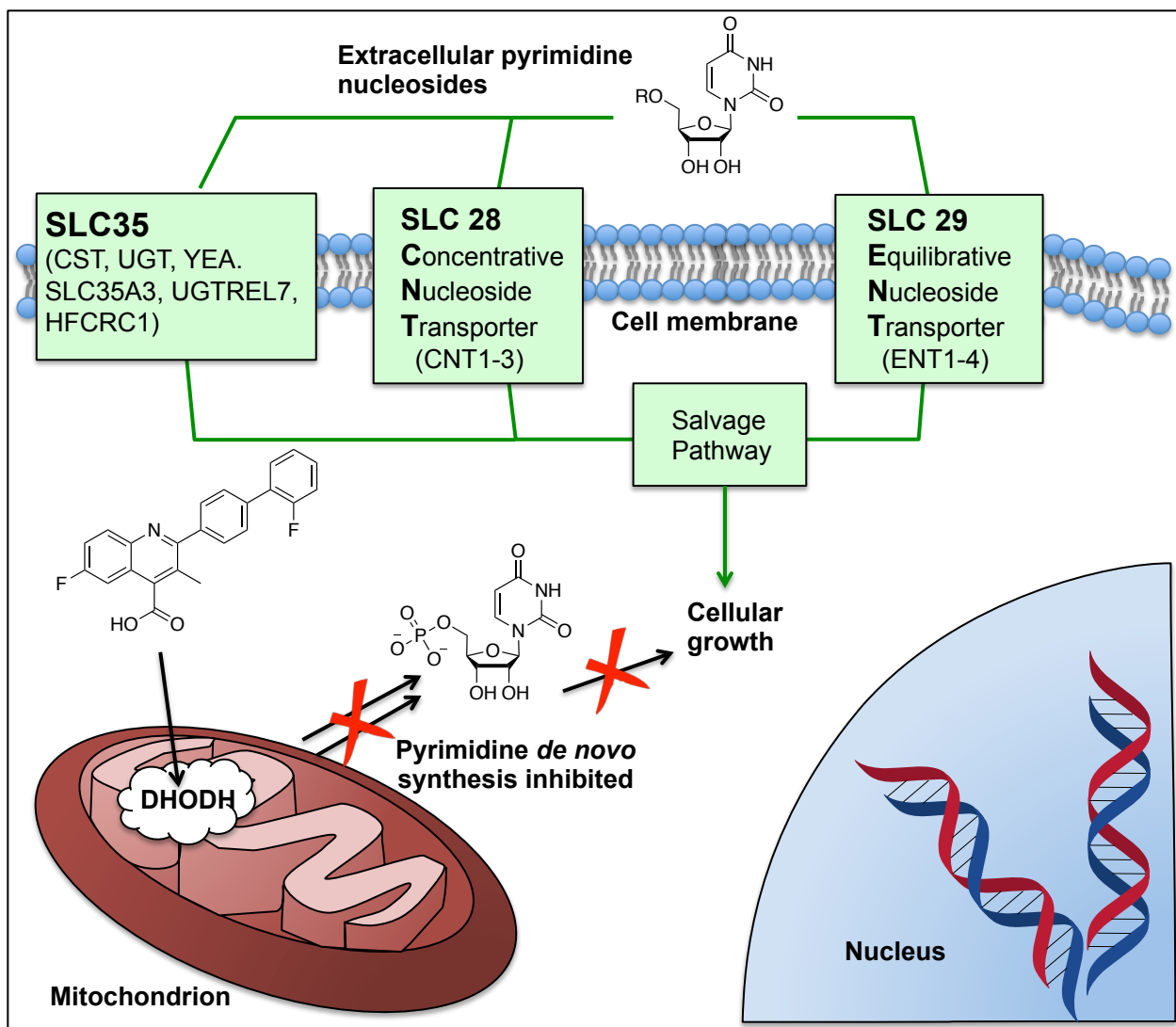


Figure 1.12: Proposed compensatory resistance mechanism to DHODH inhibition.

1.8 Future of DHODH-targeted therapy

The future of DHODH targeted therapy in cancer lies in combination therapy. Despite the setbacks of brequinar in clinical trials, DHODH remains a viable anticancer target. The pyrimidine depletion induced by DHODH inhibition may sensitize cells to better outcomes with current chemotherapy options. In fact, a variety of studies have previously implicated DHODH inhibition as key to overcoming chemotherapy resistance.^{109, 189, 190}

DHODH inhibition sensitizes cancer cells to conventional chemotherapy by targeting their metabolic dependencies. Such inhibition has been demonstrated to overcome resistance mechanisms. A recent publication highlighted leflunomide as a key to overcoming chemotherapy resistance in triple-negative breast cancer cell lines.¹⁹⁰ Triple-negative breast cancer cell lines

exposed to genotoxic agents increased flux through the *de novo* pyrimidine pathway, resulting in increased nucleotide concentrations to facilitate DNA repair. This decreases sensitivity to genotoxic agents. Pretreatment with leflunomide induced pyrimidine depletion in triple-negative breast cancer cells and genotoxic agents such as doxorubicin were able to inhibit cell growth.¹⁹⁰ Additionally, as previously described, brequinar increased cell sensitivity to TRAIL therapy.¹⁰⁹ Beyond doxorubicin and TRAIL, DHODH inhibitors have been shown to sensitize cells to DNA substrate mimics. When leflunomide and gemcitabine were used in combination, it had a more significant effect than single-agent dosing. Similar to combinations of brequinar and 5-FU, leflunomide-induced pyrimidine depletion may have led to a higher incorporation of gemcitabine.¹⁸⁹ Similar combinations were evaluated in resistant cell lines such as teriflunomide with 5-azacytidine in 5-azacytidine-resistant leukemic cells,¹⁹¹ and leflunomide with fludarabine in a fludarabine-resistant chronic lymphocytic leukemia cell line.¹⁹² It is unclear if these combinations would have a similar effect clinically as brequinar and 5-FU. However, preclinical data suggests that DHODH-induced pyrimidine depletion may be used to overcome certain acquired resistance mechanisms.

With the recent expanse of technology to evaluate synthetic lethality, new combinations with DHODH inhibitors may be uncovered.¹⁹³ Synthetic lethality screening with DHODH may soon identify genes corresponding to druggable enzyme targets. For example, a synthetic lethality screening of the nucleotide salvage pathway may be utilized to identify enzymes that are synergistic with DHODH inhibition.

Future DHODH-targeted therapy may be improved by identifying patient populations that are more likely to be sensitive to DHODH inhibition. The recent decrease in the cost of genomic profiling makes effective personalized medicine increasingly feasible and may be used to develop and test biomarkers that predict DHODH sensitivity. A variety of biomarkers have been observed including the mTORC1 enzyme. In fludarabine-resistant cells, mTORC1 is overexpressed, and these cells were surprisingly sensitive to both leflunomide and other inhibitors of the *de novo* pyrimidine pathway (PALA).¹⁹⁴ A similar response was observed with inhibitors of *de novo* purine biosynthesis suggesting a potential dependence of cells expressing mTORC1 on *de novo* nucleotide biosynthesis pathways.¹⁹⁵ An additional biomarker may be PTEN. Cell lines with mutant PTEN, a known hallmark of resistant prostate and breast cancer, were remarkably sensitive to both brequinar and leflunomide.^{51, 196} While the exact mechanism is

not well understood, it appears that PTEN regulates glutamine entry into the *de novo* pathway. The increased flux through the pathway may increase cell sensitivity to DHODH inhibition. While more data is needed, DHODH-targeted therapy may be more effective in cells expressing mTORC1 and/or mutant PTEN.

DHODH-targeted therapy may also be better suited for non-solid tumors. Previous clinical trials focused primarily on solid tumors, which was met with minimal objective responses. Brequinar, for example, was never clinically evaluated in acute myeloid leukemia. As myelosuppression was a common side effect of brequinar therapy, DHODH inhibition may be more efficacious in patients with leukemia.^{101, 102} In fact, the extent of myelosuppression was enough to consider brequinar as a potential immunosuppressant.¹⁹⁷⁻²⁰⁰ DHODH inhibition is well known to suppress the immune system as two FDA-approved DHODH inhibitors, leflunomide/teriflunomide, are for autoimmune diseases, such as rheumatoid arthritis.¹¹⁵ Therefore, DHODH targeted therapy more be more effective in leukemia or other cancers with non-solid tumors.

1.9 Conclusions

DHODH is a promising anticancer target that alters cellular nucleotide concentrations. Inhibition of DHODH is pharmacologically relevant for a variety of diseases, including cancer. However, the impact of DHODH-induced cell inhibition is still not well understood. DHODH inhibition induces pyrimidine depletion and halts cell cycle progression at S-phase. Despite this, brequinar failed to achieve an objective response in multiple cancer clinical trials. Rather than single agent dosing, the future of DHODH inhibitors may lie in combination therapy. Brequinar and leflunomide have been observed to overcome resistance mechanisms for common chemotherapy agents. Additionally, brequinar-induced differentiation in AML and may be used to target cancer stem cells. Collectively, there is considerable optimism surrounding DHODH-targeted therapy for cancer.

1.10 References:

1. Housman, G.; Byler, S.; Heerboth, S.; Lapinska, K.; Longacre, M.; Snyder, N.; Sarkar, S. Drug resistance in cancer: an overview. *Cancers (Basel)* **2014**, *6*, 1769-92.

2. Kaye, S. B. New antimetabolites in cancer chemotherapy and their clinical impact. *Br J Cancer* **1998**, 78 Suppl 3, 1-7.
3. Parker, W. B. Enzymology of purine and pyrimidine antimetabolites used in the treatment of cancer. *Chem Rev* **2009**, 109, 2880-93.
4. Reis, R. A. G.; Calil, F. A.; Feliciano, P. R.; Pinheiro, M. P.; Nonato, M. C. The dihydroorotate dehydrogenases: Past and present. *Arch Biochem Biophys* **2017**, 632, 175-191.
5. Munier-Lehmann, H.; Vidalain, P.-O.; Tangy, F.; Janin, Y. L. On Dihydroorotate Dehydrogenases and Their Inhibitors and Uses. *J Med Chem* **2013**, 56, 3148-3167.
6. Vyas, V. K.; Ghate, M. Recent developments in the medicinal chemistry and therapeutic potential of dihydroorotate dehydrogenase (DHODH) inhibitors. *Mini Rev Med Chem* **2011**, 11, 1039-55.
7. Mohamad Fairus, A. K.; Choudhary, B.; Hosahalli, S.; Kavitha, N.; Shatrah, O. Dihydroorotate dehydrogenase (DHODH) inhibitors affect ATP depletion, endogenous ROS and mediate S-phase arrest in breast cancer cells. *Biochimie* **2017**, 135, 154-163.
8. Evans, D. R.; Guy, H. I. Mammalian pyrimidine biosynthesis: fresh insights into an ancient pathway. *J Biol Chem* **2004**, 279, 33035-8.
9. Fairbanks, L. D.; Bofill, M.; Ruckemann, K.; Simmonds, H. A. Importance of ribonucleotide availability to proliferating T-lymphocytes from healthy humans. Disproportionate expansion of pyrimidine pools and contrasting effects of de novo synthesis inhibitors. *J Biol Chem* **1995**, 270, 29682-9.
10. Weber, G. Ordered biochemical program of gene expression in cancer cells. *Biochemistry (Mosc)* **2001**, 66, 1164-73.
11. Lane, A. N.; Fan, T. W. Regulation of mammalian nucleotide metabolism and biosynthesis. *Nucleic Acids Res* **2015**, 43, 2466-85.
12. Baumgartner, R.; Walloschek, M.; Kralik, M.; Gotschlich, A.; Tasler, S.; Mies, J.; Leban, J. Dual binding mode of a novel series of DHODH inhibitors. *J Med Chem* **2006**, 49, 1239-47.
13. Liu, H.; Dong, H.; Robertson, K.; Liu, C. DNA methylation suppresses expression of the urea cycle enzyme carbamoyl phosphate synthetase 1 (CPS1) in human hepatocellular carcinoma. *Am J Pathol* **2011**, 178, 652-61.

14. Siddiqui, M. T.; Saboorian, M. H.; Gokaslan, S. T.; Ashfaq, R. Diagnostic utility of the HepPar1 antibody to differentiate hepatocellular carcinoma from metastatic carcinoma in fine-needle aspiration samples. *Cancer* **2002**, 96, 49-52.
15. Liu, S.; Neidhardt, E. A.; Grossman, T. H.; Ocain, T.; Clardy, J. Structures of human dihydroorotate dehydrogenase in complex with antiproliferative agents. *Structure* **2000**, 8, 25-33.
16. Bjornberg, O.; Gruner, A. C.; Roepstorff, P.; Jensen, K. F. The activity of Escherichia coli dihydroorotate dehydrogenase is dependent on a conserved loop identified by sequence homology, mutagenesis, and limited proteolysis. *Biochemistry* **1999**, 38, 2899-908.
17. Palfey, B. A.; Bjornberg, O.; Jensen, K. F. Insight into the chemistry of flavin reduction and oxidation in Escherichia coli dihydroorotate dehydrogenase obtained by rapid reaction studies. *Biochemistry* **2001**, 40, 4381-90.
18. Zameitat, E.; Freymark, G.; Dietz, C. D.; Loffler, M.; Bolker, M. Functional expression of human dihydroorotate dehydrogenase (DHODH) in pyr4 mutants of *Ustilago maydis* allows target validation of DHODH inhibitors in vivo. *Appl Environ Microbiol* **2007**, 73, 3371-9.
19. Rawls, J.; Knecht, W.; Diekert, K.; Lill, R.; Loffler, M. Requirements for the mitochondrial import and localization of dihydroorotate dehydrogenase. *Eur J Biochem* **2000**, 267, 2079-87.
20. Loffler, M.; Jockel, J.; Schuster, G.; Becker, C. Dihydroorotat-ubiquinone oxidoreductase links mitochondria in the biosynthesis of pyrimidine nucleotides. *Mol Cell Biochem* **1997**, 174, 125-9.
21. King, M. P.; Attardi, G. Human cells lacking mtDNA: repopulation with exogenous mitochondria by complementation. *Science* **1989**, 246, 500-3.
22. Morais, R.; Desjardins, P.; Turmel, C.; Zinkewich-Peotti, K. Development and characterization of continuous avian cell lines depleted of mitochondrial DNA. *In Vitro Cell Dev Biol* **1988**, 24, 649-58.
23. Perales-Clemente, E.; Bayona-Bafaluy, M. P.; Perez-Martos, A.; Barrientos, A.; Fernandez-Silva, P.; Enriquez, J. A. Restoration of electron transport without proton pumping in mammalian mitochondria. *Proc Natl Acad Sci U S A* **2008**, 105, 18735-9.
24. Beuneu, C.; Auger, R.; Loffler, M.; Guissani, A.; Lemaire, G.; Lepoivre, M. Indirect inhibition of mitochondrial dihydroorotate dehydrogenase activity by nitric oxide. *Free Radic Biol Med* **2000**, 28, 1206-13.

25. Khutornenko, A. A.; Roudko, V. V.; Chernyak, B. V.; Vartapetian, A. B.; Chumakov, P. M.; Evstafieva, A. G. Pyrimidine biosynthesis links mitochondrial respiration to the p53 pathway. *Proc Natl Acad Sci U S A* **2010**, 107, 12828-33.
26. Idelchik, M.; Begley, U.; Begley, T. J.; Melendez, J. A. Mitochondrial ROS control of cancer. *Semin Cancer Biol* **2017**, 47, 57-66.
27. Diebold, L.; Chandel, N. S. Mitochondrial ROS regulation of proliferating cells. *Free Radic Biol Med* **2016**, 100, 86-93.
28. Hey-Mogensen, M.; Goncalves, R. L.; Orr, A. L.; Brand, M. D. Production of superoxide/H₂O₂ by dihydroorotate dehydrogenase in rat skeletal muscle mitochondria. *Free Radic Biol Med* **2014**, 72, 149-55.
29. Fang, J.; Uchiyama, T.; Yagi, M.; Matsumoto, S.; Amamoto, R.; Takazaki, S.; Yamaza, H.; Nonaka, K.; Kang, D. Dihydro-orotate dehydrogenase is physically associated with the respiratory complex and its loss leads to mitochondrial dysfunction. *Biosci Rep* **2013**, 33, e00021.
30. Hail, N., Jr.; Chen, P.; Kepa, J. J.; Bushman, L. R. Evidence supporting a role for dihydroorotate dehydrogenase, bioenergetics, and p53 in selective teriflunomide-induced apoptosis in transformed versus normal human keratinocytes. *Apoptosis* **2012**, 17, 258-68.
31. Coleman, P. F.; Suttle, D. P.; Stark, G. R. Purification from hamster cells of the multifunctional protein that initiates de novo synthesis of pyrimidine nucleotides. *J Biol Chem* **1977**, 252, 6379-85.
32. Jones, M. E. Pyrimidine nucleotide biosynthesis in animals: genes, enzymes, and regulation of UMP biosynthesis. *Annu Rev Biochem* **1980**, 49, 253-79.
33. Carrey, E. A.; Campbell, D. G.; Hardie, D. G. Phosphorylation and activation of hamster carbamyl phosphate synthetase II by cAMP-dependent protein kinase. A novel mechanism for regulation of pyrimidine nucleotide biosynthesis. *EMBO J* **1985**, 4, 3735-42.
34. Sahay, N.; Guy, H. I.; Liu, X.; Evans, D. R. Regulation of an Escherichia coli/mammalian chimeric carbamoyl-phosphate synthetase. *J Biol Chem* **1998**, 273, 31195-202.
35. Huang, M.; Graves, L. M. De novo synthesis of pyrimidine nucleotides; emerging interfaces with signal transduction pathways. *Cell Mol Life Sci* **2003**, 60, 321-36.
36. Sigoillot, F. D.; Berkowski, J. A.; Sigoillot, S. M.; Kotsis, D. H.; Guy, H. I. Cell cycle-dependent regulation of pyrimidine biosynthesis. *J Biol Chem* **2003**, 278, 3403-9.

37. Ben-Sahra, I.; Howell, J. J.; Asara, J. M.; Manning, B. D. Stimulation of de novo pyrimidine synthesis by growth signaling through mTOR and S6K1. *Science* **2013**, 339, 1323-8.
38. Robitaille, A. M.; Christen, S.; Shimobayashi, M.; Cornu, M.; Fava, L. L.; Moes, S.; Prescianotto-Baschong, C.; Sauer, U.; Jenoe, P.; Hall, M. N. Quantitative phosphoproteomics reveal mTORC1 activates de novo pyrimidine synthesis. *Science* **2013**, 339, 1320-3.
39. Kotsis, D. H.; Masko, E. M.; Sigoillot, F. D.; Di Gregorio, R.; Guy-Evans, H. I.; Evans, D. R. Protein kinase A phosphorylation of the multifunctional protein CAD antagonizes activation by the MAP kinase cascade. *Mol Cell Biochem* **2007**, 301, 69-81.
40. Sigoillot, F. D.; Sigoillot, S. M.; Guy, H. I. Breakdown of the regulatory control of pyrimidine biosynthesis in human breast cancer cells. *Int J Cancer* **2004**, 109, 491-8.
41. Sigoillot, F. D.; Kotsis, D. H.; Serre, V.; Sigoillot, S. M.; Evans, D. R.; Guy, H. I. Nuclear localization and mitogen-activated protein kinase phosphorylation of the multifunctional protein CAD. *J Biol Chem* **2005**, 280, 25611-20.
42. Liu, Y. C.; Li, F.; Handler, J.; Huang, C. R.; Xiang, Y.; Neretti, N.; Sedivy, J. M.; Zeller, K. I.; Dang, C. V. Global regulation of nucleotide biosynthetic genes by c-Myc. *PLoS One* **2008**, 3, e2722.
43. Mannava, S.; Grachtchouk, V.; Wheeler, L. J.; Im, M.; Zhuang, D.; Slavina, E. G.; Mathews, C. K.; Shewach, D. S.; Nikiforov, M. A. Direct role of nucleotide metabolism in C-MYC-dependent proliferation of melanoma cells. *Cell Cycle* **2008**, 7, 2392-400.
44. Dorasamy, M. S.; Choudhary, B.; Nellore, K.; Subramanya, H.; Wong, P. F. Dihydroorotate dehydrogenase Inhibitors Target c-Myc and Arrest Melanoma, Myeloma and Lymphoma cells at S-phase. *J Cancer* **2017**, 8, 3086-3098.
45. O'Donnell, E. F.; Kopparapu, P. R.; Koch, D. C.; Jang, H. S.; Phillips, J. L.; Tanguay, R. L.; Kerkvliet, N. I.; Kolluri, S. K. The aryl hydrocarbon receptor mediates leflunomide-induced growth inhibition of melanoma cells. *PLoS One* **2012**, 7, e40926.
46. Bester, A. C.; Roniger, M.; Oren, Y. S.; Im, M. M.; Sarni, D.; Chaoat, M.; Bensimon, A.; Zamir, G.; Shewach, D. S.; Kerem, B. Nucleotide deficiency promotes genomic instability in early stages of cancer development. *Cell* **2011**, 145, 435-46.
47. Hsieh, A. L.; Walton, Z. E.; Altman, B. J.; Stine, Z. E.; Dang, C. V. MYC and metabolism on the path to cancer. *Seminars in Cell & Developmental Biology* **2015**, 43, 11-21.
48. DeBerardinis, R. J.; Cheng, T. Q's next: the diverse functions of glutamine in metabolism, cell biology and cancer. *Oncogene* **2010**, 29, 313-24.

49. Gaglio, D.; Soldati, C.; Vanoni, M.; Alberghina, L.; Chiaradonna, F. Glutamine deprivation induces abortive s-phase rescued by deoxyribonucleotides in k-ras transformed fibroblasts. *PLoS One* **2009**, *4*, e4715.
50. Wise, D. R.; Thompson, C. B. Glutamine addiction: a new therapeutic target in cancer. *Trends Biochem Sci* **2010**, *35*, 427-33.
51. Mathur, D.; Stratikopoulos, E.; Ozturk, S.; Steinbach, N.; Pegno, S.; Schoenfeld, S.; Yong, R.; Murty, V. V.; Asara, J. M.; Cantley, L. C.; Parsons, R. PTEN Regulates Glutamine Flux to Pyrimidine Synthesis and Sensitivity to Dihydroorotate Dehydrogenase Inhibition. *Cancer Discov* **2017**, *7*, 380-390.
52. White, R. M.; Cech, J.; Ratanasirintrawoot, S.; Lin, C. Y.; Rahl, P. B.; Burke, C. J.; Langdon, E.; Tomlinson, M. L.; Mosher, J.; Kaufman, C.; Chen, F.; Long, H. K.; Kramer, M.; Datta, S.; Neuberg, D.; Granter, S.; Young, R. A.; Morrison, S.; Wheeler, G. N.; Zon, L. I. DHODH modulates transcriptional elongation in the neural crest and melanoma. *Nature* **2011**, *471*, 518-22.
53. Sykes, D. B.; Kfoury, Y. S.; Mercier, F. E.; Wawer, M. J.; Law, J. M.; Haynes, M. K.; Lewis, T. A.; Schajnovitz, A.; Jain, E.; Lee, D.; Meyer, H.; Pierce, K. A.; Tolliday, N. J.; Waller, A.; Ferrara, S. J.; Eheim, A. L.; Stoekigt, D.; Maxcy, K. L.; Cobert, J. M.; Bachand, J.; Szekely, B. A.; Mukherjee, S.; Sklar, L. A.; Kotz, J. D.; Clish, C. B.; Sadreyev, R. I.; Clemons, P. A.; Janzer, A.; Schreiber, S. L.; Scadden, D. T. Inhibition of Dihydroorotate Dehydrogenase Overcomes Differentiation Blockade in Acute Myeloid Leukemia. *Cell* **2016**, *167*, 171-186 e15.
54. Strikoudis, A.; Lazaris, C.; Trimarchi, T.; Galvao Neto, A. L.; Yang, Y.; Ntziachristos, P.; Rothbart, S.; Buckley, S.; Dolgalev, I.; Stadtfeld, M.; Strahl, B. D.; Dynlacht, B. D.; Tsirigos, A.; Aifantis, I. Regulation of transcriptional elongation in pluripotency and cell differentiation by the PHD-finger protein Phf5a. *Nature Cell Biology* **2016**, *18*, 1127.
55. Tan, J. L.; Fogley, R. D.; Flynn, R. A.; Ablain, J.; Yang, S.; Saint-Andre, V.; Fan, Z. P.; Do, B. T.; Laga, A. C.; Fujinaga, K.; Santoriello, C.; Greer, C. B.; Kim, Y. J.; Clohessy, J. G.; Bothmer, A.; Pandell, N.; Avagyan, S.; Brogie, J. E.; van Rooijen, E.; Hagedorn, E. J.; Shyh-Chang, N.; White, R. M.; Price, D. H.; Pandolfi, P. P.; Peterlin, B. M.; Zhou, Y.; Kim, T. H.; Asara, J. M.; Chang, H. Y.; Young, R. A.; Zon, L. I. Stress from Nucleotide Depletion Activates the Transcriptional Regulator HEXIM1 to Suppress Melanoma. *Mol Cell* **2016**, *62*, 34-46.
56. SMITH, L. H.; BAKER, F. A.; SULLIVAN, M. Pyrimidine Metabolism in Man. II. Studies of Leukemic Cells. *Blood* **1960**, *15*, 360-369.
57. Smith, L. H., Jr.; Baker, F. A. Pyrimidine metabolism in man. I. The biosynthesis of orotic acid. *J Clin Invest* **1959**, *38*, 798-809.

58. Schwartzmann, G.; Peters, G. J.; Laurensse, E.; de Waal, F. C.; Loonen, A. H.; Leyva, A.; Pinedo, H. M. DUP 785 (NSC 368390): schedule-dependency of growth-inhibitory and antiprimidine effects. *Biochem Pharmacol* **1988**, *37*, 3257-66.
59. Dexter, D. L.; Hesson, D. P.; Ardecky, R. J.; Rao, G. V.; Tippett, D. L.; Dusak, B. A.; Paull, K. D.; Plowman, J.; DeLarco, B. M.; Narayanan, V. L.; et al. Activity of a novel 4-quinolinecarboxylic acid, NSC 368390 [6-fluoro-2-(2'-fluoro-1,1'-biphenyl-4-yl)-3-methyl-4-quinolinecarb oxylic acid sodium salt], against experimental tumors. *Cancer Res* **1985**, *45*, 5563-8.
60. Tsherniak, A.; Vazquez, F.; Montgomery, P. G.; Weir, B. A.; Kryukov, G.; Cowley, G. S.; Gill, S.; Harrington, W. F.; Pantel, S.; Krill-Burger, J. M.; Meyers, R. M.; Ali, L.; Goodale, A.; Lee, Y.; Jiang, G.; Hsiao, J.; Gerath, W. F. J.; Howell, S.; Merkel, E.; Ghandi, M.; Garraway, L. A.; Root, D. E.; Golub, T. R.; Boehm, J. S.; Hahn, W. C. Defining a Cancer Dependency Map. *Cell* **2017**, *170*, 564-576 e16.
61. Aguirre, A. J.; Meyers, R. M.; Weir, B. A.; Vazquez, F.; Zhang, C. Z.; Ben-David, U.; Cook, A.; Ha, G.; Harrington, W. F.; Doshi, M. B.; Kost-Alimova, M.; Gill, S.; Xu, H.; Ali, L. D.; Jiang, G.; Pantel, S.; Lee, Y.; Goodale, A.; Cherniack, A. D.; Oh, C.; Kryukov, G.; Cowley, G. S.; Garraway, L. A.; Stegmaier, K.; Roberts, C. W.; Golub, T. R.; Meyerson, M.; Root, D. E.; Tsherniak, A.; Hahn, W. C. Genomic Copy Number Dictates a Gene-Independent Cell Response to CRISPR/Cas9 Targeting. *Cancer Discov* **2016**, *6*, 914-29.
62. Cowley, G. S.; Weir, B. A.; Vazquez, F.; Tamayo, P.; Scott, J. A.; Rusin, S.; East-Seletsky, A.; Ali, L. D.; Gerath, W. F.; Pantel, S. E.; Lizotte, P. H.; Jiang, G.; Hsiao, J.; Tsherniak, A.; Dwinell, E.; Aoyama, S.; Okamoto, M.; Harrington, W.; Gelfand, E.; Green, T. M.; Tomko, M. J.; Gopal, S.; Wong, T. C.; Li, H.; Howell, S.; Stransky, N.; Liefeld, T.; Jang, D.; Bistline, J.; Hill Meyers, B.; Armstrong, S. A.; Anderson, K. C.; Stegmaier, K.; Reich, M.; Pellman, D.; Boehm, J. S.; Mesirov, J. P.; Golub, T. R.; Root, D. E.; Hahn, W. C. Parallel genome-scale loss of function screens in 216 cancer cell lines for the identification of context-specific genetic dependencies. *Sci Data* **2014**, *1*, 140035.
63. The OncoPrint™ Platform (Thermo. Fisher, Ann Arbor, MI) was used for analysis and visualization for further information, refer to the terms of use. OncoPrint Source: <https://www.oncoPrint.com/resource/main.html> - dso:geneOverex;ec:[2];epv:150001.151078,3508;g:1723;pg:1;pvf:10222;scr:summary;v:18
64. Rhodes, D. R.; Yu, J.; Shanker, K.; Deshpande, N.; Varambally, R.; Ghosh, D.; Barrette, T.; Pandey, A.; Chinnaiyan, A. M. ONCOMINE: a cancer microarray database and integrated data-mining platform. *Neoplasia* **2004**, *6*, 1-6.
65. Rhodes, D. R.; Kalyana-Sundaram, S.; Mahavisno, V.; Varambally, R.; Yu, J.; Briggs, B. B.; Barrette, T. R.; Anstet, M. J.; Kincaid-Beal, C.; Kulkarni, P.; Varambally, S.; Ghosh, D.;

Chinnaiyan, A. M. OncoPrint 3.0: genes, pathways, and networks in a collection of 18,000 cancer gene expression profiles. *Neoplasia* **2007**, *9*, 166-80.

66. Sabates-Bellver, J.; Van der Flier, L. G.; de Palo, M.; Cattaneo, E.; Maake, C.; Rehrauer, H.; Laczko, E.; Kurowski, M. A.; Bujnicki, J. M.; Menigatti, M.; Luz, J.; Ranalli, T. V.; Gomes, V.; Pastorelli, A.; Faggiani, R.; Anti, M.; Jiricny, J.; Clevers, H.; Marra, G. Transcriptome profile of human colorectal adenomas. *Mol Cancer Res* **2007**, *5*, 1263-75.

67. Barretina, J.; Caponigro, G.; Stransky, N.; Venkatesan, K.; Margolin, A. A.; Kim, S.; Wilson, C. J.; Lehar, J.; Kryukov, G. V.; Sonkin, D.; Reddy, A.; Liu, M.; Murray, L.; Berger, M. F.; Monahan, J. E.; Morais, P.; Meltzer, J.; Korejwa, A.; Jane-Valbuena, J.; Mapa, F. A.; Thibault, J.; Bric-Furlong, E.; Raman, P.; Shipway, A.; Engels, I. H.; Cheng, J.; Yu, G. K.; Yu, J.; Aspesi, P., Jr.; de Silva, M.; Jagtap, K.; Jones, M. D.; Wang, L.; Hatton, C.; Palesscandolo, E.; Gupta, S.; Mahan, S.; Sougnez, C.; Onofrio, R. C.; Liefeld, T.; MacConaill, L.; Winckler, W.; Reich, M.; Li, N.; Mesirov, J. P.; Gabriel, S. B.; Getz, G.; Ardlie, K.; Chan, V.; Myer, V. E.; Weber, B. L.; Porter, J.; Warmuth, M.; Finan, P.; Harris, J. L.; Meyerson, M.; Golub, T. R.; Morrissey, M. P.; Sellers, W. R.; Schlegel, R.; Garraway, L. A. The Cancer Cell Line Encyclopedia enables predictive modelling of anticancer drug sensitivity. *Nature* **2012**, *483*, 603-7.

68. Lee, H.; Palm, J.; Grimes, S. M.; Ji, H. P. The Cancer Genome Atlas Clinical Explorer: a web and mobile interface for identifying clinical-genomic driver associations. *Genome Med* **2015**, *7*, 112.

69. Madhavan, S.; Zenklusen, J. C.; Kotliarov, Y.; Sahni, H.; Fine, H. A.; Buetow, K. Rembrandt: helping personalized medicine become a reality through integrative translational research. *Mol Cancer Res* **2009**, *7*, 157-67.

70. Gravendeel, L. A.; Kouwenhoven, M. C.; Gevaert, O.; de Rooij, J. J.; Stubbs, A. P.; Duijm, J. E.; Daemen, A.; Bleeker, F. E.; Bralten, L. B.; Kloosterhof, N. K.; De Moor, B.; Eilers, P. H.; van der Spek, P. J.; Kros, J. M.; Sillevius Smitt, P. A.; van den Bent, M. J.; French, P. J. Intrinsic gene expression profiles of gliomas are a better predictor of survival than histology. *Cancer Res* **2009**, *69*, 9065-72.

71. Team, R. C. A language and environment for statistical computing. <http://www.R-project.org/>.

72. Subramanian, A.; Tamayo, P.; Mootha, V. K.; Mukherjee, S.; Ebert, B. L.; Gillette, M. A.; Paulovich, A.; Pomeroy, S. L.; Golub, T. R.; Lander, E. S.; Mesirov, J. P. Gene set enrichment analysis: a knowledge-based approach for interpreting genome-wide expression profiles. *Proc Natl Acad Sci U S A* **2005**, *102*, 15545-50.

73. He, K.; Guo, X.; Liu, Y.; Li, J.; Hu, Y.; Wang, D.; Song, J. TUFM downregulation induces epithelial-mesenchymal transition and invasion in lung cancer cells via a mechanism involving AMPK-GSK3beta signaling. *Cell Mol Life Sci* **2016**, *73*, 2105-21.
74. Shi, H.; Hayes, M.; Kirana, C.; Miller, R.; Keating, J.; Macartney-Coxson, D.; Stubbs, R. TUFM is a potential new prognostic indicator for colorectal carcinoma. *Pathology* **2012**, *44*, 506-12.
75. Xi, H. Q.; Zhang, K. C.; Li, J. Y.; Cui, J. X.; Zhao, P.; Chen, L. Expression and clinicopathologic significance of TUFM and p53 for the normal-adenoma-carcinoma sequence in colorectal epithelia. *World J Surg Oncol* **2017**, *15*, 90.
76. Szklarczyk, D.; Franceschini, A.; Wyder, S.; Forslund, K.; Heller, D.; Huerta-Cepas, J.; Simonovic, M.; Roth, A.; Santos, A.; Tsafou, K. P.; Kuhn, M.; Bork, P.; Jensen, L. J.; von Mering, C. STRING v10: protein-protein interaction networks, integrated over the tree of life. *Nucleic Acids Res* **2015**, *43*, D447-52.
77. Tan, F.; Wahdan-Alaswad, R.; Yan, S.; Thiele, C. J.; Li, Z. Dihydropyrimidinase-like protein 3 expression is negatively regulated by MYCN and associated with clinical outcome in neuroblastoma. *Cancer Sci* **2013**, *104*, 1586-92.
78. Tan, F.; Thiele, C. J.; Li, Z. Collapsin response mediator proteins: Potential diagnostic and prognostic biomarkers in cancers (Review). *Oncol Lett* **2014**, *7*, 1333-1340.
79. Cai, G.; Wu, D.; Wang, Z.; Xu, Z.; Wong, K. B.; Ng, C. F.; Chan, F. L.; Yu, S. Collapsin response mediator protein-1 (CRMP1) acts as an invasion and metastasis suppressor of prostate cancer via its suppression of epithelial-mesenchymal transition and remodeling of actin cytoskeleton organization. *Oncogene* **2016**, *36*, 546.
80. Gaetano, C.; Matsuo, T.; Thiele, C. J. Identification and characterization of a retinoic acid-regulated human homologue of the unc-33-like phosphoprotein gene (hUlip) from neuroblastoma cells. *J Biol Chem* **1997**, *272*, 12195-201.
81. Wang, L.; Liu, W.; Tang, H.; Xie, X.; Zou, C.; Wang, Y.; Gao, Z.; Yin, J. DRP5 is involved in cancer cell growth and predicts poor prognosis in human osteosarcoma. *Cancer Med* **2017**, *6*, 982-993.
82. Brown, S. D.; Moore, M. W. The International Mouse Phenotyping Consortium: past and future perspectives on mouse phenotyping. *Mamm Genome* **2012**, *23*, 632-40.
83. Meehan, T. F.; Conte, N.; West, D. B.; Jacobsen, J. O.; Mason, J.; Warren, J.; Chen, C. K.; Tudose, I.; Relac, M.; Matthews, P.; Karp, N.; Santos, L.; Fiegel, T.; Ring, N.; Westerberg, H.; Greenaway, S.; Sneddon, D.; Morgan, H.; Codner, G. F.; Stewart, M. E.; Brown, J.; Horner,

N.; International Mouse Phenotyping, C.; Haendel, M.; Washington, N.; Mungall, C. J.; Reynolds, C. L.; Gallegos, J.; Gailus-Durner, V.; Sorg, T.; Pavlovic, G.; Bower, L. R.; Moore, M.; Morse, I.; Gao, X.; Tocchini-Valentini, G. P.; Obata, Y.; Cho, S. Y.; Seong, J. K.; Seavitt, J.; Beaudet, A. L.; Dickinson, M. E.; Herculat, Y.; Wurst, W.; de Angelis, M. H.; Lloyd, K. C. K.; Flenniken, A. M.; Nutter, L. M. J.; Newbigging, S.; McKerlie, C.; Justice, M. J.; Murray, S. A.; Svenson, K. L.; Braun, R. E.; White, J. K.; Bradley, A.; Flicek, P.; Wells, S.; Skarnes, W. C.; Adams, D. J.; Parkinson, H.; Mallon, A. M.; Brown, S. D. M.; Smedley, D. Disease model discovery from 3,328 gene knockouts by The International Mouse Phenotyping Consortium. *Nat Genet* **2017**, 49, 1231-1238.

84. Ng, S. B.; Buckingham, K. J.; Lee, C.; Bigham, A. W.; Tabor, H. K.; Dent, K. M.; Huff, C. D.; Shannon, P. T.; Jabs, E. W.; Nickerson, D. A.; Shendure, J.; Bamshad, M. J. Exome sequencing identifies the cause of a mendelian disorder. *Nat Genet* **2010**, 42, 30-5.

85. Fang, J.; Uchiumi, T.; Yagi, M.; Matsumoto, S.; Amamoto, R.; Saito, T.; Takazaki, S.; Kanki, T.; Yamaza, H.; Nonaka, K.; Kang, D. Protein instability and functional defects caused by mutations of dihydro-orotate dehydrogenase in Miller syndrome patients. *Biosci Rep* **2012**, 32, 631-9.

86. Hajdyla-Banas, I.; Banas, T.; Rydz-Stryszowska, I.; Batko, B.; Skura, A.; Gornisiewicz, T.; Pitynska-Korab, E. Pregnancy course and neonatal outcome after exposure to leflunomide--2 cases report and review of literature. *Przegl Lek* **2009**, 66, 1069-71.

87. Fukushima, R.; Kanamori, S.; Hirashiba, M.; Hishikawa, A.; Muranaka, R.; Kaneto, M.; Kitagawa, H. Inhibiting the teratogenicity of the immunosuppressant leflunomide in mice by supplementation of exogenous uridine. *Toxicol Sci* **2009**, 108, 419-26.

88. Fukushima, R.; Kanamori, S.; Hirashiba, M.; Hishikawa, A.; Muranaka, R. I.; Kaneto, M.; Nakamura, K.; Kato, I. Teratogenicity study of the dihydroorotate-dehydrogenase inhibitor and protein tyrosine kinase inhibitor Leflunomide in mice. *Reprod Toxicol* **2007**, 24, 310-6.

89. Cody, R.; Stewart, D.; DeForni, M.; Moore, M.; Dallaire, B.; Azarnia, N.; Gyves, J. Multicenter phase II study of brequinar sodium in patients with advanced breast cancer. *Am J Clin Oncol* **1993**, 16, 526-8.

90. Dodion, P. F.; Wagener, T.; Stoter, G.; Drozd, A.; Lev, L. M.; Skovsgaard, T.; Renard, J.; Cavalli, F. Phase II trial with Brequinar (DUP-785, NSC 368390) in patients with metastatic colorectal cancer: a study of the Early Clinical Trials Group of the EORTC. *Ann Oncol* **1990**, 1, 79-80.

91. Urba, S.; Doroshow, J.; Cripps, C.; Robert, F.; Velez-Garcia, E.; Dallaire, B.; Adams, D.; Carlson, R.; Grillo-Lopez, A.; Gyves, J. Multicenter phase II trial of brequinar sodium in patients with advanced squamous-cell carcinoma of the head and neck. *Cancer Chemother Pharmacol* **1992**, 31, 167-9.

92. Moore, M.; Maroun, J.; Robert, F.; Natale, R.; Neidhart, J.; Dallaire, B.; Sisk, R.; Gyves, J. Multicenter phase II study of brequinar sodium in patients with advanced gastrointestinal cancer. *Invest New Drugs* **1993**, *11*, 61-5.
93. Maroun, J.; Ruckdeschel, J.; Natale, R.; Morgan, R.; Dallaire, B.; Sisk, R.; Gyves, J. Multicenter phase II study of brequinar sodium in patients with advanced lung cancer. *Cancer Chemother Pharmacol* **1993**, *32*, 64-6.
94. Natale, R.; Wheeler, R.; Moore, M.; Dallaire, B.; Lynch, W.; Carlson, R.; Grillo-Lopez, A.; Gyves, J. Multicenter phase II trial of brequinar sodium in patients with advanced melanoma. *Ann Oncol* **1992**, *3*, 659-60.
95. Boven, E.; Winograd, B.; Berger, D. P.; Dumont, M. P.; Braakhuis, B. J.; Fodstad, O.; Langdon, S.; Fiebig, H. H. Phase II preclinical drug screening in human tumor xenografts: a first European multicenter collaborative study. *Cancer Res* **1992**, *52*, 5940-7.
96. Burris, H. A., 3rd; Raymond, E.; Awada, A.; Kuhn, J. G.; O'Rourke, T. J.; Brentzel, J.; Lynch, W.; King, S. Y.; Brown, T. D.; Von Hoff, D. D. Pharmacokinetic and phase I studies of brequinar (DUP 785; NSC 368390) in combination with cisplatin in patients with advanced malignancies. *Invest New Drugs* **1998**, *16*, 19-27.
97. Joshi, A. S.; King, S. Y.; Zajac, B. A.; Makowka, L.; Sher, L. S.; Kahan, B. D.; Menkis, A. H.; Stiller, C. R.; Schaeffle, B.; Kornhauser, D. M. Phase I safety and pharmacokinetic studies of brequinar sodium after single ascending oral doses in stable renal, hepatic, and cardiac allograft recipients. *J Clin Pharmacol* **1997**, *37*, 1121-8.
98. Fragoso, Y. D.; Brooks, J. B. Leflunomide and teriflunomide: altering the metabolism of pyrimidines for the treatment of autoimmune diseases. *Expert Rev Clin Pharmacol* **2015**, *8*, 315-20.
99. Chen, S. F.; Papp, L. M.; Ardecky, R. J.; Rao, G. V.; Hesson, D. P.; Forbes, M.; Dexter, D. L. Structure-activity relationship of quinoline carboxylic acids. A new class of inhibitors of dihydroorotate dehydrogenase. *Biochem Pharmacol* **1990**, *40*, 709-14.
100. Chen, S. F.; Ruben, R. L.; Dexter, D. L. Mechanism of action of the novel anticancer agent 6-fluoro-2-(2'-fluoro-1,1'-biphenyl-4-yl)-3-methyl-4-quinolinecarboxylic acid sodium salt (NSC 368390): inhibition of de novo pyrimidine nucleotide biosynthesis. *Cancer Res* **1986**, *46*, 5014-9.
101. de Forni, M.; Chabot, G. G.; Armand, J. P.; Fontana, X.; Recondo, G.; Domenge, C.; Carde, P.; Barbu, M.; Gouyette, A. Phase I and pharmacokinetic study of brequinar (DUP 785; NSC 368390) in cancer patients. *Eur J Cancer* **1993**, *29A*, 983-8.

102. Schwartzmann, G.; Dodion, P.; Vermorken, J. B.; ten Bokkel Huinink, W. W.; Joggi, J.; Winograd, B.; Gall, H.; Simonetti, G.; van der Vijgh, W. J.; van Hennik, M. B.; et al. Phase I study of Brequinar sodium (NSC 368390) in patients with solid malignancies. *Cancer Chemother Pharmacol* **1990**, *25*, 345-51.
103. Schwartzmann, G.; van der Vijgh, W. J.; van Hennik, M. B.; Klein, I.; Vermorken, J. B.; Dodion, P.; ten Bokkel Huinink, W. W.; Joggi, G.; Gall, H.; Crespeigne, N.; et al. Pharmacokinetics of Brequinar sodium (NSC 368390) in patients with solid tumors during a phase I study. *Eur J Cancer Clin Oncol* **1989**, *25*, 1675-81.
104. Bork, E.; Vest, S.; Hansen, H. H. A phase I clinical and pharmacokinetic study of Brequinar sodium, DUP 785 (NSC 368390), using a weekly and a biweekly schedule. *Eur J Cancer Clin Oncol* **1989**, *25*, 1403-11.
105. Arteaga, C. L.; Brown, T. D.; Kuhn, J. G.; Shen, H. S.; O'Rourke, T. J.; Beougher, K.; Brentzel, H. J.; Von Hoff, D. D.; Weiss, G. R. Phase I clinical and pharmacokinetic trial of Brequinar sodium (DuP 785; NSC 368390). *Cancer Res* **1989**, *49*, 4648-53.
106. Braakhuis, B. J.; van Dongen, G. A.; Bagnay, M.; van Walsum, M.; Snow, G. B. Preclinical chemotherapy on human head and neck cancer xenografts grown in athymic nude mice. *Head Neck* **1989**, *11*, 511-5.
107. Peters, G. J.; Schwartzmann, G.; Nadal, J. C.; Laurensse, E. J.; van Groeningen, C. J.; van der Vijgh, W. J.; Pinedo, H. M. In vivo inhibition of the pyrimidine de novo enzyme dihydroorotic acid dehydrogenase by brequinar sodium (DUP-785; NSC 368390) in mice and patients. *Cancer Res* **1990**, *50*, 4644-9.
108. Sykes, D. B.; Kfoury, Y. S.; Mercier, F. E.; Wawer, M. J.; Law, J. M.; Haynes, M. K.; Lewis, T. A.; Schajnovitz, A.; Jain, E.; Lee, D.; Meyer, H.; Pierce, K. A.; Tolliday, N. J.; Waller, A.; Ferrara, S. J.; Eheim, A. L.; Stoeckigt, D.; Maxcy, K. L.; Cobert, J. M.; Bachand, J.; Szekely, B. A.; Mukherjee, S.; Sklar, L. A.; Kotz, J. D.; Clish, C. B.; Sadreyev, R. I.; Clemons, P. A.; Janzer, A.; Schreiber, S. L.; Scadden, D. T. Inhibition of Dihydroorotate Dehydrogenase Overcomes Differentiation Blockade in Acute Myeloid Leukemia. *Cell* **2016**, *167*, 171-186.e15.
109. He, T.; Haapa-Paananen, S.; Kaminsky, V. O.; Kohonen, P.; Fey, V.; Zhivotovsky, B.; Kallioniemi, O.; Perala, M. Inhibition of the mitochondrial pyrimidine biosynthesis enzyme dihydroorotate dehydrogenase by doxorubicin and brequinar sensitizes cancer cells to TRAIL-induced apoptosis. *Oncogene* **2014**, *33*, 3538-49.
110. Teschner, S.; Burst, V. Leflunomide: a drug with a potential beyond rheumatology. *Immunotherapy* **2010**, *2*, 637-50.
111. Oh, J.; O'Connor, P. W. Teriflunomide in the treatment of multiple sclerosis: current evidence and future prospects. *Ther Adv Neurol Disord* **2014**, *7*, 239-52.

112. Haibel, H.; Rudwaleit, M.; Braun, J.; Sieper, J. Six months open label trial of leflunomide in active ankylosing spondylitis. *Ann Rheum Dis* **2005**, *64*, 124-6.
113. Holtmann, M. H.; Gerts, A. L.; Weinman, A.; Galle, P. R.; Neurath, M. F. Treatment of Crohn's disease with leflunomide as second-line immunosuppression : a phase 1 open-label trial on efficacy, tolerability and safety. *Dig Dis Sci* **2008**, *53*, 1025-32.
114. Prajapati, D. N.; Knox, J. F.; Emmons, J.; Saeian, K.; Csuka, M. E.; Binion, D. G. Leflunomide treatment of Crohn's disease patients intolerant to standard immunomodulator therapy. *J Clin Gastroenterol* **2003**, *37*, 125-8.
115. Sanders, S.; Harisdangkul, V. Leflunomide for the treatment of rheumatoid arthritis and autoimmunity. *Am J Med Sci* **2002**, *323*, 190-3.
116. Dai, L.; Wei, X. N.; Zheng, D. H.; Mo, Y. Q.; Pessler, F.; Zhang, B. Y. Effective treatment of Kimura's disease with leflunomide in combination with glucocorticoids. *Clin Rheumatol* **2011**, *30*, 859-65.
117. Leflunomide Associated With Topical Corticosteroids for Bullous Pemphigoid (ARABUL). <https://clinicaltrials.gov/ct2/show/NCT00802243> (November 2017).
118. Hardinger, K. L.; Wang, C. D.; Schnitzler, M. A.; Miller, B. W.; Jendrisak, M. D.; Shenoy, S.; Lowell, J. A.; Brennan, D. C. Prospective, pilot, open-label, short-term study of conversion to leflunomide reverses chronic renal allograft dysfunction. *Am J Transplant* **2002**, *2*, 867-71.
119. Williams, J. W.; Mital, D.; Chong, A.; Kottayil, A.; Millis, M.; Longstreth, J.; Huang, W.; Brady, L.; Jensik, S. Experiences with leflunomide in solid organ transplantation. *Transplantation* **2002**, *73*, 358-66.
120. Bohelay, G.; Bouaziz, J. D.; Nunes, H.; Rybojad, M.; Bagot, M.; Petit, A.; Laroche, L. Striking leflunomide efficacy against refractory cutaneous sarcoidosis. *J Am Acad Dermatol* **2014**, *70*, e111-3.
121. Pirildar, T. Treatment of adult-onset Still's disease with leflunomide and chloroquine combination in two patients. *Clin Rheumatol* **2003**, *22*, 157.
122. Wu, G. C.; Xu, X. D.; Huang, Q.; Wu, H. Leflunomide: friend or foe for systemic lupus erythematosus? *Rheumatol Int* **2013**, *33*, 273-6.
123. Unizony, S.; Stone, J. H.; Stone, J. R. New treatment strategies in large-vessel vasculitis. *Curr Opin Rheumatol* **2013**, *25*, 3-9.

124. Roy, M. Early clinical experience with leflunomide in uveitis. *Can J Ophthalmol* **2007**, 42, 634.
125. Baumann, P.; Mandl-Weber, S.; Volkl, A.; Adam, C.; Bumeder, I.; Oduncu, F.; Schmidmaier, R. Dihydroorotate dehydrogenase inhibitor A771726 (leflunomide) induces apoptosis and diminishes proliferation of multiple myeloma cells. *Mol Cancer Ther* **2009**, 8, 366-75.
126. Jiang, L.; Zhang, W.; Li, W.; Ling, C.; Jiang, M. Anti-inflammatory drug, leflunomide and its metabolite teriflunomide inhibit NSCLC proliferation in vivo and in vitro. *Toxicol Lett* **2017**.
127. Zhu, S.; Yan, X.; Xiang, Z.; Ding, H. F.; Cui, H. Leflunomide reduces proliferation and induces apoptosis in neuroblastoma cells in vitro and in vivo. *PLoS One* **2013**, 8, e71555.
128. Cook, M. R.; Pinchot, S. N.; Jaskula-Sztul, R.; Luo, J.; Kunnimalaiyaan, M.; Chen, H. Identification of a novel Raf-1 pathway activator that inhibits gastrointestinal carcinoid cell growth. *Mol Cancer Ther* **2010**, 9, 429-37.
129. Alhefdhi, A.; Burke, J. F.; Redlich, A.; Kunnimalaiyaan, M.; Chen, H. Leflunomide suppresses growth in human medullary thyroid cancer cells. *J Surg Res* **2013**, 185, 212-6.
130. Doscas, M. E.; Williamson, A. J.; Usha, L.; Bogachkov, Y.; Rao, G. S.; Xiao, F.; Wang, Y.; Ruby, C.; Kaufman, H.; Zhou, J.; Williams, J. W.; Li, Y.; Xu, X. Inhibition of p70 S6 kinase (S6K1) activity by A77 1726 and its effect on cell proliferation and cell cycle progress. *Neoplasia* **2014**, 16, 824-34.
131. Mattar, T.; Kochhar, K.; Bartlett, R.; Bremer, E. G.; Finnegan, A. Inhibition of the epidermal growth factor receptor tyrosine kinase activity by leflunomide. *FEBS Letters* **1993**, 334, 161-164.
132. Ren, A.; Fu, G.; Qiu, Y.; Cui, H. Leflunomide inhibits proliferation and tumorigenesis of oral squamous cell carcinoma. *Mol Med Rep* **2017**.
133. Yam, C. H.; Fung, T. K.; Poon, R. Y. Cyclin A in cell cycle control and cancer. *Cell Mol Life Sci* **2002**, 59, 1317-26.
134. Bahr, H. I.; Toraih, E. A.; Mohammed, E. A.; Mohammad, H. M.; Ali, E. A.; Zaitone, S. A. Chemopreventive effect of leflunomide against Ehrlich's solid tumor grown in mice: Effect on EGF and EGFR expression and tumor proliferation. *Life Sci* **2015**, 141, 193-201.

135. Chen, Y.; Huang, Q.; Zhou, H.; Wang, Y.; Hu, X.; Li, T. Inhibition of canonical WNT/beta-catenin signaling is involved in leflunomide (LEF)-mediated cytotoxic effects on renal carcinoma cells. *Oncotarget* **2016**, *7*, 50401-50416.
136. Hail, N., Jr.; Chen, P.; Bushman, L. R. Teriflunomide (leflunomide) promotes cytostatic, antioxidant, and apoptotic effects in transformed prostate epithelial cells: evidence supporting a role for teriflunomide in prostate cancer chemoprevention. *Neoplasia* **2010**, *12*, 464-75.
137. Mitoxantrone and Prednisone With or Without Leflunomide in Treating Patients With Stage IV Prostate Cancer. <https://clinicaltrials.gov/ct2/show/NCT00004071> (November 2017).
138. Linke, S. P.; Clarkin, K. C.; Di Leonardo, A.; Tsou, A.; Wahl, G. M. A reversible, p53-dependent G0/G1 cell cycle arrest induced by ribonucleotide depletion in the absence of detectable DNA damage. *Genes Dev* **1996**, *10*, 934-47.
139. Bu, F. Z.; Tan, X. J.; Xing, D. X.; Wang, C. Design, synthesis, crystal structure and in vitro cytotoxic properties of a novel Schiff base derived from indole and biphenyl. *Acta Crystallogr C Struct Chem* **2017**, *73*, 546-555.
140. Lewis, T. A.; Sykes, D. B.; Law, J. M.; Munoz, B.; Rustiguel, J. K.; Nonato, M. C.; Scadden, D. T.; Schreiber, S. L. Development of ML390: A Human DHODH Inhibitor That Induces Differentiation in Acute Myeloid Leukemia. *ACS Med Chem Lett* **2016**, *7*, 1112-1117.
141. Shen, W.; Ren, X.; Zhu, J.; Xu, Y.; Lin, J.; Li, Y.; Zhao, F.; Zheng, H.; Li, R.; Cui, X.; Zhang, X.; Lu, X.; Zheng, Z. Discovery of a new structural class of competitive hDHODH inhibitors with in vitro and in vivo anti-inflammatory, immunosuppressive effects. *Eur J Pharmacol* **2016**, *791*, 205-212.
142. Cheung, N. N.; Lai, K. K.; Dai, J.; Kok, K. H.; Chen, H.; Chan, K. H.; Yuen, K. Y.; Kao, R. Y. T. Broad-spectrum inhibition of common respiratory RNA viruses by a pyrimidine synthesis inhibitor with involvement of the host antiviral response. *J Gen Virol* **2017**, *98*, 946-954.
143. Das, P.; Deng, X.; Zhang, L.; Roth, M. G.; Fontoura, B. M.; Phillips, M. A.; De Brabander, J. K. SAR Based Optimization of a 4-Quinoline Carboxylic Acid Analog with Potent Anti-Viral Activity. *ACS Med Chem Lett* **2013**, *4*, 517-521.
144. Vyas, V. K.; Variya, B.; Ghate, M. D. Design, synthesis and pharmacological evaluation of novel substituted quinoline-2-carboxamide derivatives as human dihydroorotate dehydrogenase (hDHODH) inhibitors and anticancer agents. *Eur J Med Chem* **2014**, *82*, 385-93.
145. Sainas, S.; Pippione, A. C.; Giorgis, M.; Lupino, E.; Goyal, P.; Ramondetti, C.; Buccinna, B.; Piccinini, M.; Braga, R. C.; Andrade, C. H.; Andersson, M.; Moritzer, A. C.;

Friemann, R.; Mensa, S.; Al-Kadaraghi, S.; Boschi, D.; Lolli, M. L. Design, synthesis, biological evaluation and X-ray structural studies of potent human dihydroorotate dehydrogenase inhibitors based on hydroxylated azole scaffolds. *Eur J Med Chem* **2017**, *129*, 287-302.

146. Lucas-Hourani, M.; Munier-Lehmann, H.; El Mazouni, F.; Malmquist, N. A.; Harpon, J.; Coutant, E. P.; Guillou, S.; Helynck, O.; Noel, A.; Scherf, A.; Phillips, M. A.; Tangy, F.; Vidalain, P. O.; Janin, Y. L. Original 2-(3-Alkoxy-1H-pyrazol-1-yl)azines Inhibitors of Human Dihydroorotate Dehydrogenase (DHODH). *J Med Chem* **2015**, *58*, 5579-98.

147. Munier-Lehmann, H.; Lucas-Hourani, M.; Guillou, S.; Helynck, O.; Zanghi, G.; Noel, A.; Tangy, F.; Vidalain, P. O.; Janin, Y. L. Original 2-(3-alkoxy-1H-pyrazol-1-yl)pyrimidine derivatives as inhibitors of human dihydroorotate dehydrogenase (DHODH). *J Med Chem* **2015**, *58*, 860-77.

148. Sitwala, N. D.; Vyas, V. K.; Variya, B. C.; Patel, S. S.; Mehta, C. C.; Rana, D. N.; Ghate, M. D. Liquid phase combinatorial synthesis of 1,2,5-trisubstituted benzimidazole derivatives as human DHODH inhibitors. *Bioorg Chem* **2017**, *75*, 118-126.

149. Li, J.; Wu, D.; Xu, X.; Huang, J.; Shao, X.; Li, Z. Design, synthesis and inhibitory activity against human dihydroorotate dehydrogenase (hDHODH) of 1,3-benzazole derivatives bearing amide units. *Bioorg Med Chem Lett* **2016**, *26*, 3064-3066.

150. Lucas-Hourani, M.; Dauzonne, D.; Munier-Lehmann, H.; Khier, S.; Nisole, S.; Dairou, J.; Helynck, O.; Afonso, P. V.; Tangy, F.; Vidalain, P. O. Original Chemical Series of Pyrimidine Biosynthesis Inhibitors That Boost the Antiviral Interferon Response. *Antimicrob Agents Chemother* **2017**, *61*.

151. Li, S.; Luan, G.; Ren, X.; Song, W.; Xu, L.; Xu, M.; Zhu, J.; Dong, D.; Diao, Y.; Liu, X.; Zhu, L.; Wang, R.; Zhao, Z.; Xu, Y.; Li, H. Rational Design of Benzylidenehydrazinyl-Substituted Thiazole Derivatives as Potent Inhibitors of Human Dihydroorotate Dehydrogenase with in Vivo Anti-arthritis Activity. *Sci Rep* **2015**, *5*, 14836.

152. Jiang, L.; Wen, H.; Shao, Y.; Yu, R.; Liu, Z.; Wang, S.; Wang, Q.; Zhao, X.; Zhang, P.; Tao, Y.; Mei, L. Novel Diketopiperazine Dihydroorotate Dehydrogenase Inhibitors Purified from Traditional Tibetan Animal Medicine *Osteon Myospalacem Baileyi*. *Chem Biol Drug Des* **2015**, *86*, 626-36.

153. Zhu, J.; Han, L.; Diao, Y.; Ren, X.; Xu, M.; Xu, L.; Li, S.; Li, Q.; Dong, D.; Huang, J.; Liu, X.; Zhao, Z.; Wang, R.; Zhu, L.; Xu, Y.; Qian, X.; Li, H. Design, synthesis, X-ray crystallographic analysis, and biological evaluation of thiazole derivatives as potent and selective inhibitors of human dihydroorotate dehydrogenase. *J Med Chem* **2015**, *58*, 1123-39.

154. Deng, X.; Kokkonda, S.; El Mazouni, F.; White, J.; Burrows, J. N.; Kaminsky, W.; Charman, S. A.; Matthews, D.; Rathod, P. K.; Phillips, M. A. Fluorine modulates species

selectivity in the triazolopyrimidine class of Plasmodium falciparum dihydroorotate dehydrogenase inhibitors. *J Med Chem* **2014**, *57*, 5381-94.

155. Marschall, M.; Niemann, I.; Kosulin, K.; Bootz, A.; Wagner, S.; Dobner, T.; Herz, T.; Kramer, B.; Leban, J.; Vitt, D.; Stamminger, T.; Hutterer, C.; Strobl, S. Assessment of drug candidates for broad-spectrum antiviral therapy targeting cellular pyrimidine biosynthesis. *Antiviral Res* **2013**, *100*, 640-8.

156. Aoki, T.; Sebolt, J.; Weber, G. In vivo inactivation by acivicin of carbamoyl-phosphate synthetase II in rat hepatoma. *Biochem Pharmacol* **1982**, *31*, 927-32.

157. Sebolt, J. S.; Aoki, T.; Eble, J. N.; Glover, J. L.; Weber, G. Inactivation by acivicin of carbamoyl-phosphate synthetase II of human colon carcinoma. *Biochem Pharmacol* **1985**, *34*, 97-100.

158. Kreuzer, J.; Bach, N. C.; Forler, D.; Sieber, S. A. Target discovery of acivicin in cancer cells elucidates its mechanism of growth inhibition. Electronic supplementary information (ESI) available: Synthesis, cloning, protein expression, purification and biochemical assays. See DOI: 10.1039/c4sc02339k. *Chem Sci* **2014**, *6*, 237-245.

159. Collins, K. D.; Stark, G. R. Aspartate transcarbamylase. Interaction with the transition state analogue N-(phosphonacetyl)-L-aspartate. *J Biol Chem* **1971**, *246*, 6599-605.

160. Christopherson, R. I.; Lyons, S. D.; Wilson, P. K. Inhibitors of de novo nucleotide biosynthesis as drugs. *Acc Chem Res* **2002**, *35*, 961-71.

161. Grem, J. L.; King, S. A.; O'Dwyer, P. J.; Leyland-Jones, B. Biochemistry and clinical activity of N-(phosphonacetyl)-L-aspartate: a review. *Cancer Res* **1988**, *48*, 4441-54.

162. Karle, J. M.; Anderson, L. W.; Erlichman, C.; Cysyk, R. L. Serum uridine levels in patients receiving N-(phosphonacetyl)-L-aspartate. *Cancer Res* **1980**, *40*, 2938-40.

163. Christopherson, R. I.; Duggleby, R. G. Metabolic resistance: the protection of enzymes against drugs which are tight-binding inhibitors by the accumulation of substrate. *Eur J Biochem* **1983**, *134*, 331-5.

164. Manthey, M. K.; Huang, D. T.; Bubb, W. A.; Christopherson, R. I. Synthesis and enzymic evaluation of 4-mercapto-6-oxo-1, 4-azaphosphinane-2-carboxylic acid 4-oxide as an inhibitor of mammalian dihydroorotase. *J Med Chem* **1998**, *41*, 4550-5.

165. Adams, J. L.; Meek, T. D.; Mong, S. M.; Johnson, R. K.; Metcalf, B. W. cis-4-Carboxy-6-(mercaptomethyl)-3,4,5,6-tetrahydropyrimidin-2(1 H)-one, a potent inhibitor of mammalian dihydroorotase. *J Med Chem* **1988**, *31*, 1355-9.

166. Dix, D. E.; Lehman, C. P.; Jakubowski, A.; Moyer, J. D.; Handschumacher, R. E. Pyrazofurin metabolism, enzyme inhibition, and resistance in L5178Y cells. *Cancer Res* **1979**, *39*, 4485-90.
167. Gutowski, G. E.; Sweeney, M. J.; DeLong, D. C.; Hamill, R. L.; Gerzon, K.; Dyke, R. W. Biochemistry and Biological Effects of the Pyrazofurins* (Pyrazomycins): Initial Clinical Trial. *Ann NY Acad Sci* **1975**, *255*, 544-551.
168. Ohnuma, T.; Roboz, J.; Shapiro, M. L.; Holland, J. F. Pharmacological and biochemical effects of pyrazofurin in humans. *Cancer Res* **1977**, *37*, 2043-9.
169. Cadman, E. C.; Dix, D. E.; Handschumacher, R. E. Clinical, biological, and biochemical effect of pyrazofurin. *Cancer Res* **1978**, *38*, 682-8.
170. Peters, G. J.; Sharma, S. L.; Laurensse, E.; Pinedo, H. M. Inhibition of pyrimidine de novo synthesis by DUP-785 (NSC 368390). *Invest New Drugs* **1987**, *5*, 235-44.
171. Wilson, P. M.; Danenberg, P. V.; Johnston, P. G.; Lenz, H. J.; Ladner, R. D. Standing the test of time: targeting thymidylate biosynthesis in cancer therapy. *Nat Rev Clin Oncol* **2014**, *11*, 282-98.
172. Longley, D. B.; Harkin, D. P.; Johnston, P. G. 5-fluorouracil: mechanisms of action and clinical strategies. *Nat Rev Cancer* **2003**, *3*, 330-8.
173. Chen, T. L.; Erlichman, C. Biochemical modulation of 5-fluorouracil with or without leucovorin by a low dose of brequinar in MGH-U1 cells. *Cancer Chemother Pharmacol* **1992**, *30*, 370-6.
174. Peters, G. J.; van Groeningen, C. J.; Laurensse, E. J.; Lankelma, J.; Leyva, A.; Pinedo, H. M. Uridine-induced hypothermia in mice and rats in relation to plasma and tissue levels of uridine and its metabolites. *Cancer Chemother Pharmacol* **1987**, *20*, 101-8.
175. Peters, G. J.; Kraal, I.; Pinedo, H. M. In vitro and in vivo studies on the combination of Brequinar sodium (DUP-785; NSC 368390) with 5-fluorouracil; effects of uridine. *Br J Cancer* **1992**, *65*, 229-33.
176. Pizzorno, G.; Wiegand, R. A.; Lentz, S. K.; Handschumacher, R. E. Brequinar potentiates 5-fluorouracil antitumor activity in a murine model colon 38 tumor by tissue-specific modulation of uridine nucleotide pools. *Cancer Res* **1992**, *52*, 1660-5.
177. Buzaid, A. C.; Pizzorno, G.; Marsh, J. C.; Ravikumar, T. S.; Murren, J. R.; Todd, M.; Strair, R. K.; Poo, W. J.; Hait, W. N. Biochemical modulation of 5-fluorouracil with brequinar: results of a phase I study. *Cancer Chemother Pharmacol* **1995**, *36*, 373-8.

178. Weiss, G. R.; Ervin, T. J.; Meshad, M. W.; Kufe, D. W. Phase II trial of combination therapy with continuous-infusion PALA and bolus-injection 5-FU. *Cancer Treat Rep* **1982**, 66, 299-303.
179. Ardalan, B.; Jamin, D.; Jayaram, H. N.; Presant, C. A. Phase I study of continuous-infusion PALA and 5-FU. *Cancer Treat Rep* **1984**, 68, 531-4.
180. Whitehead, R. P.; Benedetti, J. K.; Abbruzzese, J. L.; Ardalan, B.; Goodwin, J. W.; Balcerzak, S. P.; Samlowski, W. E.; Lenz, H. J.; Macdonald, J. S. A phase II study of high-dose 24 hour continuous infusion 5-FU and leucovorin and low-dose PALA for patients with advanced pancreatic adenocarcinoma: a Southwest Oncology Group Study. *Invest New Drugs* **2004**, 22, 335-41.
181. Markman, M.; Chan, T. C.; Cleary, S.; Howell, S. B. Phase I trial of combination therapy of cancer with N-phosphonacetyl-L-aspartic acid and dipyridamole. *Cancer Chemother Pharmacol* **1987**, 19, 80-3.
182. Casper, E. S.; Baselga, J.; Smart, T. B.; Magill, G. B.; Markman, M.; Ranhosky, A. A phase II trial of PALA + dipyridamole in patients with advanced soft-tissue sarcoma. *Cancer Chemother Pharmacol* **1991**, 28, 51-4.
183. Fischer, P. H.; Pamukcu, R.; Bittner, G.; Willson, J. K. Enhancement of the sensitivity of human colon cancer cells to growth inhibition by acivicin achieved through inhibition of nucleic acid precursor salvage by dipyridamole. *Cancer Res* **1984**, 44, 3355-9.
184. Willson, J. K.; Fischer, P. H.; Tutsch, K.; Alberti, D.; Simon, K.; Hamilton, R. D.; Bruggink, J.; Koeller, J. M.; Tormey, D. C.; Earhart, R. H.; et al. Phase I clinical trial of a combination of dipyridamole and acivicin based upon inhibition of nucleoside salvage. *Cancer Res* **1988**, 48, 5585-90.
185. Young, J. D.; Yao, S. Y.; Baldwin, J. M.; Cass, C. E.; Baldwin, S. A. The human concentrative and equilibrative nucleoside transporter families, SLC28 and SLC29. *Mol Aspects Med* **2013**, 34, 529-47.
186. Song, Z. Roles of the nucleotide sugar transporters (SLC35 family) in health and disease. *Mol Aspects Med* **2013**, 34, 590-600.
187. Greenberg, N.; Schumm, D. E.; Webb, T. E. Uridine kinase activities and pyrimidine nucleoside phosphorylation in fluoropyrimidine-sensitive and -resistant cell lines of the Novikoff hepatoma. *Biochem J* **1977**, 164, 379-87.
188. Smith, K. M.; Ng, A. M.; Yao, S. Y.; Labeledz, K. A.; Knaus, E. E.; Wiebe, L. I.; Cass, C. E.; Baldwin, S. A.; Chen, X. Z.; Karpinski, E.; Young, J. D. Electrophysiological

characterization of a recombinant human Na⁺-coupled nucleoside transporter (hCNT1) produced in *Xenopus* oocytes. *J Physiol* **2004**, 558, 807-23.

189. Shukla, S. K.; Purohit, V.; Mehla, K.; Gunda, V.; Chaika, N. V.; Vernucci, E.; King, R. J.; Abrego, J.; Goode, G. D.; Dasgupta, A.; Illies, A. L.; Gebregiworgis, T.; Dai, B.; Augustine, J. J.; Murthy, D.; Attri, K. S.; Mashadova, O.; Grandgenett, P. M.; Powers, R.; Ly, Q. P.; Lazenby, A. J.; Grem, J. L.; Yu, F.; Mates, J. M.; Asara, J. M.; Kim, J. W.; Hankins, J. H.; Weekes, C.; Hollingsworth, M. A.; Serkova, N. J.; Sasson, A. R.; Fleming, J. B.; Oliveto, J. M.; Lyssiotis, C. A.; Cantley, L. C.; Berim, L.; Singh, P. K. MUC1 and HIF-1 α Signaling Crosstalk Induces Anabolic Glucose Metabolism to Impart Gemcitabine Resistance to Pancreatic Cancer. *Cancer Cell* **2017**, 32, 71-87 e7.

190. Brown, K. K.; Spinelli, J. B.; Asara, J. M.; Toker, A. Adaptive Reprogramming of De Novo Pyrimidine Synthesis Is a Metabolic Vulnerability in Triple-Negative Breast Cancer. *Cancer Discov* **2017**, 7, 391-399.

191. Imanishi, S.; Takahashi, R.; Katagiri, S.; Kobayashi, C.; Umezu, T.; Ohyashiki, K.; Ohyashiki, J. H. Teriflunomide restores 5-azacytidine sensitivity via activation of pyrimidine salvage in 5-azacytidine-resistant leukemia cells. *Oncotarget* **2017**, 8, 69906-69915.

192. Dietrich, S.; Kramer, O. H.; Hahn, E.; Schafer, C.; Giese, T.; Hess, M.; Tretter, T.; Rieger, M.; Hullein, J.; Zenz, T.; Ho, A. D.; Dreger, P.; Luft, T. Leflunomide induces apoptosis in fludarabine-resistant and clinically refractory CLL cells. *Clin Cancer Res* **2012**, 18, 417-31.

193. O'Neil, N. J.; Bailey, M. L.; Hieter, P. Synthetic lethality and cancer. *Nat Rev Genet* **2017**, 18, 613.

194. Sharma, A.; Janocha, A. J.; Hill, B. T.; Smith, M. R.; Erzurum, S. C.; Almasan, A. Targeting mTORC1-mediated metabolic addiction overcomes fludarabine resistance in malignant B cells. *Mol Cancer Res* **2014**, 12, 1205-15.

195. Valvezan, A. J.; Turner, M.; Belaid, A.; Lam, H. C.; Miller, S. K.; McNamara, M. C.; Baglini, C.; Housden, B. E.; Perrimon, N.; Kwiatkowski, D. J.; Asara, J. M.; Henske, E. P.; Manning, B. D. mTORC1 Couples Nucleotide Synthesis to Nucleotide Demand Resulting in a Targetable Metabolic Vulnerability. *Cancer Cell* **2017**, 32, 624-638 e5.

196. Keniry, M.; Parsons, R. The role of PTEN signaling perturbations in cancer and in targeted therapy. *Oncogene* **2008**, 27, 5477-85.

197. Chastanet, S.; Cursio, R.; Gugenheim, J.; Baldini, E.; Chevallier, A.; Damais, A.; Charpentier, B.; Mouiel, J. Brequinar sodium and liver hemoperfusion in xenotransplantation. *Transplant Proc* **1998**, 30, 2244-5.

198. Wang, M.; Qu, X.; Stepkowski, S. M.; Chou, T. C.; Kahan, B. D. Beneficial effect of graft perfusion with anti-T cell receptor monoclonal antibodies on survival of small bowel allografts in rat recipients treated with brequinar alone or in combination with cyclosporine and sirolimus. *Transplantation* **1996**, 61, 458-64.
199. D'Silva, M.; Antoniou, E.; DeRoover, A.; Nishimura, Y.; Howie, A.; McMaster, P. Immunosuppressive effect of brequinar on rat cardiac allograft survival in combination with leflunomide or FK 506. *Transplant Proc* **1996**, 28, 950-1.
200. Makowka, L.; Sher, L. S.; Cramer, D. V. The development of Brequinar as an immunosuppressive drug for transplantation. *Immunol Rev* **1993**, 136, 51-70.

Chapter 2

Identification of a Novel Dihydroorotate Dehydrogenase Inhibitor From Cell-Based Screening^b

2.1 Introduction

There is a perpetually unmet medical need for new and effective anticancer therapeutics, especially for pancreatic cancer. Due to poor diagnosis, pancreatic tumors are discovered in late stages and therapy regimes are centered around chemotherapy.¹ Chemotherapy options for patients with metastatic pancreatic cancer are gemcitabine or combinations such as FOLFIRINOX (folinic acid, 5-fluorouracil, irinotecan, and oxaliplatin).¹⁻⁵ However, drug resistance and low response rates to these treatments limit patient survival.⁶⁻⁸ In fact, the 5-year survival rate of patients diagnosed with stage IV endocrine pancreatic cancer is 1%.⁹ To improve patient survival, new therapeutics must be developed, preferably with a novel mechanism of action.

Our efforts towards developing a new anticancer drug focused on utilizing phenotypic screening. It is well known that drug discovery projects have high attrition rates and low probability of achieving FDA approval. A variety of factors have been suggested as a cause, including the use of target-based screening.^{10, 11} Target-based screening focuses on enzymatic inhibition or affinity to a recombinant protein rather than eliciting a desired cellular response. Often this approach identifies potent ligands for protein inhibition but the ligands may not elicit the desired cellular response. In contrast, the alternative phenotypic screening evaluates the ability of hit compounds to induce a desired cellular phenotype. A comparison between the two screening methods shows that phenotypic screening has led to a higher percentage of FDA approved drugs with a novel mechanism of action.¹¹ In our program to identify novel scaffolds eliciting a desirable response against transformed cell lines, we utilized a phenotypic screen to identify lead compound **1** (Figure 2.1), which is structurally similar to brequinar (**2**, Figure 2.2)

^b **Author contributions:** Joseph Madak designed, synthesized, and characterized all compounds. Shuzo Tamura and Christine Cuthbertson evaluated compounds in biochemical and cellular assays. Dr. Hollis Showalter and Dr. Nouri Neamati are corresponding authors.

Compound **1** elicits its cell growth inhibition through an unknown cellular target. To reach our ultimate goal of developing an anticancer clinical candidate, **1** must be optimized to display better drug-like properties. In particular, the potency and solubility must be improved (BxPC-3 $IC_{50} = 13.9 \pm 5.8 \mu\text{M}$, MIA PaCA-2 $IC_{50} = 18.8 \pm 12 \mu\text{M}$, cLogP = 6.49). However, cell-based evaluations present significant challenges to lead optimization campaigns. For example, the multitude of enzymatic targets makes structure-activity-relationship (SAR) studies difficult to attribute a cellular response to one enzyme. Furthermore, analogues with poor cell permeability may generate false negatives despite potent inhibition of an enzymatic target. To minimize these possibilities and expedite an optimization campaign, we sought to identify the enzymatic target of **1**.

We postulated that lead compound **1** targets the same enzymatic target as brequinar (**2**), a structurally similar compound that inhibits dihydroorotate dehydrogenase (Figure 2.2). To validate this hypothesis, we sought to establish the essential pharmacophore of **1** and compare it directly to brequinar's SAR. Furthermore, we sought to identify if compound **1** is susceptible to the same resistance mechanisms as DHODH inhibitors. Finally, we evaluated compound **1** for activity in a DHODH assay.

2.2 Phenotypic screen

A phenotypic screen was utilized to identify compound **1**. Nearly 2 million compounds from commercial sources were filtered based on their adherence to “drug-like” properties to generate the Neamati library.^{12, 13} Compounds in the Neamati library were evaluated for physiochemical properties, which included cLogP < 7, the presence of pan-interfering structures (PAINS), and adherence to a modified version of Lipinski's rules.^{12, 13} Compounds (20,000) from the Neamati library were selected at random and evaluated for their ability to inhibit cancer cell growth in a panel of three cell lines: MIA PaCa-2 (pancreatic), BxPC-3 (pancreatic), and HFF-1 (non-transformed) (Figure 2.1). Initial analysis focused on cell growth inhibition in the MTT (3-(4,5-dimethylthiazol-2-yl)-2,5-diphenyltetrazolium bromide) assay and active compounds were further tested in a colony formation assay (CFA). Compounds with consistent activity in both the MTT and CFA assay were progressed further for evaluation of purity and the presence of structural alerts (primarily metabolic liabilities).^{14, 15} Only compound **1** met the

selection criteria. Due to the use of phenotypic screening, the enzymatic target of **1** was unknown and thus SAR studies had to be conducted to elucidate its primary pharmacophore.

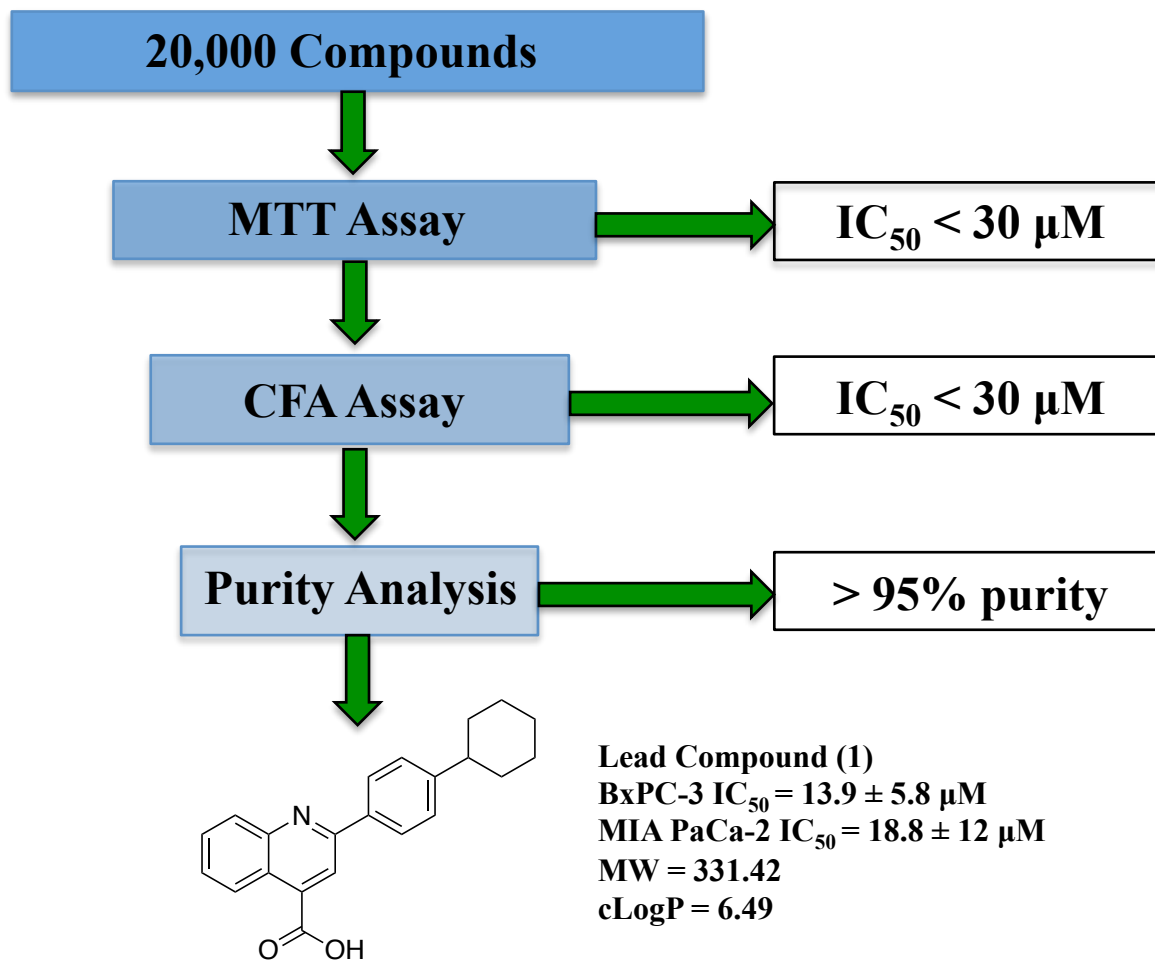


Figure 2.1: Flow diagram and criteria leading to compound **1**

2.3 Structural similarity

Compound **1** contains a quinoline ring with an aryl-lipophilic attachment at the C2 position and a carboxylic acid at the C4 position (Figure 2.2). Other known inhibitors with potential anticancer properties incorporate this core including brequinar (**2**)¹⁶, a P-selectin inhibitor (**3**)¹⁷, and a geminin-CDT complex inhibitor (**4**) (unpublished ChEMBL result).¹⁸

These quinoline inhibitors possess distinct SAR trends that were previously published and may be useful toward assessing target similarity with **1** (Figure 2.2). The potent dihydroorotate dehydrogenase (DHODH) inhibitor, brequinar (DHODH assay $K_i = 27.4 \pm 1.6$ nM), has a strict requirement for the C4 carboxylic acid to form an interaction with Arg136.^{19,20} In fact, the ethyl ester analogue is significantly less potent than brequinar (DHODH assay $K_i =$

74,800 ± 10,800 μM).¹⁹ Additionally, only large lipophilic functional groups were tolerated at the C2 position, primarily 1,4 biaryl attachments. In contrast, the P-selectin inhibitor **3** (Cell-flow assay IC₅₀ = 4.5 μM, DHODH assay IC₅₀ = 26 μM) does not tolerate large biaryl attachments at the C2 position.¹⁷ However, a dependence upon the carboxylic acid was also observed. While the authors did not evaluate anticancer activity for **3**, we were aware of previous studies that suggest P-selectin as an anticancer target.²¹ Additionally, an unpublished ChEMBL finding reported **4** as an inhibitor of the geminin-CDT complex. Compound **4** possesses a quinoline core similar to **1** but incorporates an amide moiety. While SAR trends were not disclosed, geminin is a known anticancer target.²² A collective comparison of the SAR trends for compound **1** and these related scaffolds may reveal if **1** targets any of these enzymes.

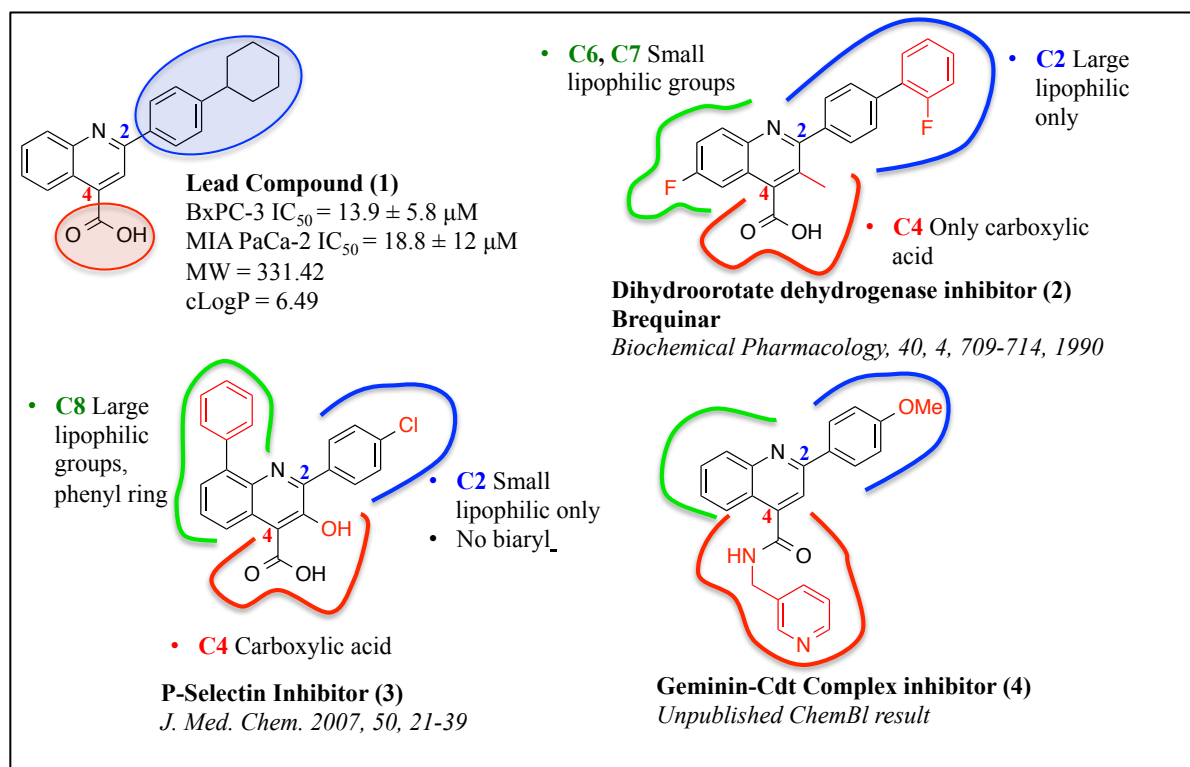
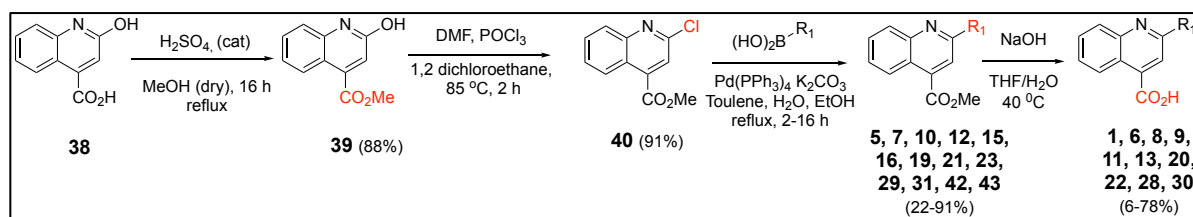


Figure 2.2: Structurally similar quinolines and their SAR trends. Molecular weight and cLogP predicted using Chemdraw Professional 16.0 software.

2.4 Synthesis

To explore the basic pharmacophore of **1** through robust SAR, it was necessary to develop a novel synthetic route to access a library of derivatives. As compound **1** is primarily aromatic and contains few heteroatoms, palladium catalysis was utilized to introduce diversity

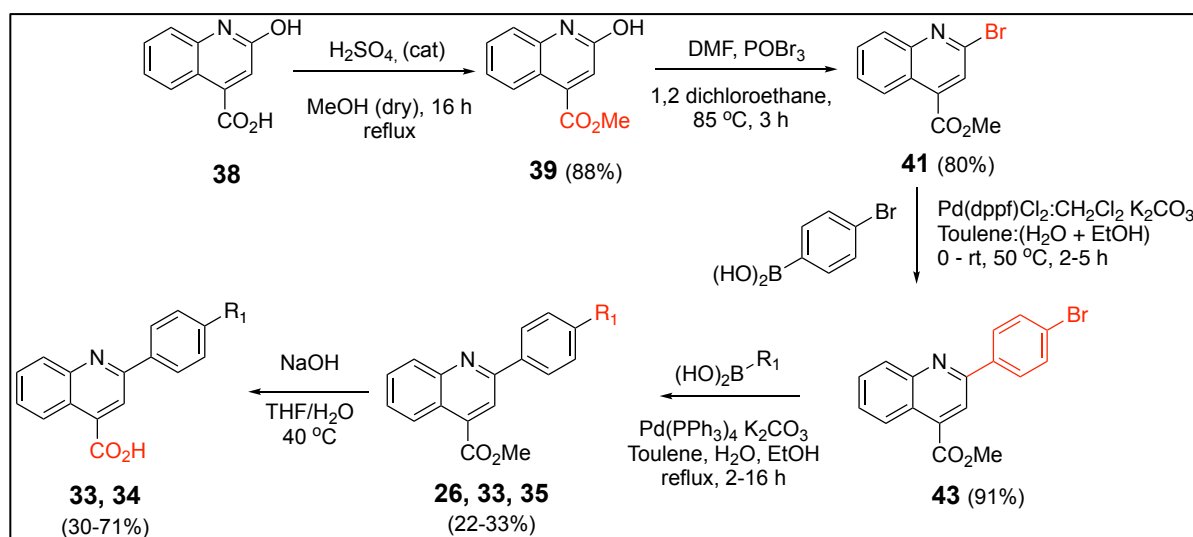
through carbon-carbon bond coupling. Towards this aim, a halogenated starting material must be synthesized in large quantities as a suitable coupling partner. Initial efforts focused on chlorination of the 2-hydroxyl of commercially available 2-hydroxyquinoline-4-carboxylic acid (**38**, Scheme 2.1), which would provide a suitable starting material for Suzuki coupling to quickly introduce diversity. However, initial approaches to generate the halogenated C2 position resulted in low yields, presumably due to the presence of the carboxylic acid. A Fischer esterification protocol, similar to Yang *et al.*, was utilized to install a methyl ester-protecting group at the C4 position, giving **39** in 88%.²³ With the ester in hand, a modified version of Donohoe *et al.*'s Vilsmeier chlorination protocol was utilized to generate the chlorinated intermediate **40** in a 91% yield.²⁴ The adjacent nitrogen improved the reactivity of the C2 chlorine for Suzuki coupling, which was accomplished in yields ranging from 22-91%. Once the diverse substituents had been installed, the methyl ester was readily hydrolyzed with NaOH (6-78%). While this synthetic scheme worked well, the limited commercial availability of phenyl substituted boronic acids diminished its usefulness toward installing diverse chemical moieties. To explore a greater range of chemical diversity, a new protocol was developed.



Scheme 2.1: Synthesis of R₁ substituted quinolines.

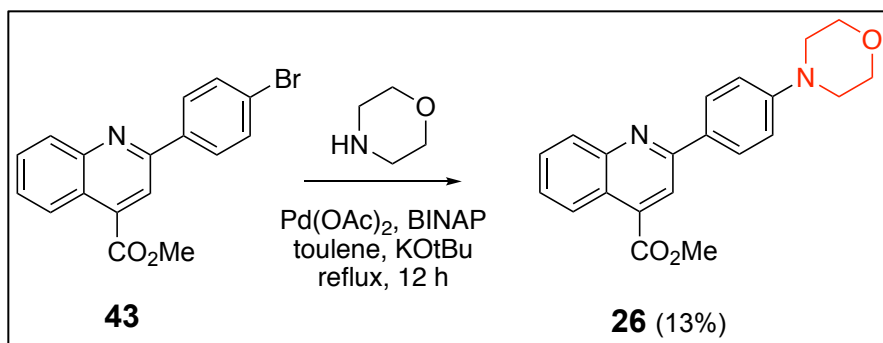
To cover additional chemical space, a new synthetic route was pursued that focused on the generation of a quinoline scaffold (**43**) with a *p*-bromo phenyl substituent off the C2 position (Scheme 2.2). This allows for a Suzuki coupling with a variety of commercially available boronic acids (Scheme 2.2, i.e. **26**, **33**, **35**). This route incorporates the phenyl ring early on and expands the possible chemical space around its *para*-position. However, working out full details of the route presented significant challenges. Direct Suzuki coupling between chloroquinoline **40** and 4-bromobenzene boronic acid was unsuccessful and produced many side products. The hypothesized problem was deemed to be the order of reactivity, as palladium inserts better into carbon-bromide bonds than carbon-chloride bonds.²⁵ The lower chloro reactivity of **40** presented a significant hurdle that a variety of palladium catalysts, bases, and solvent conditions could not

overcome. An alternate solution to this problem focused on generating a C2 triflate of **39** for direct Suzuki coupling with 4-bromobenzene boronic acid. This was unsuccessful, directing our attention towards utilizing a Vilsmeier-bromination protocol. With this, intermediate **41** was reproducibly generated in high yields (80%). The nitrogen adjacent to the C2-bromine bond on **41** decreases the activation energy for palladium insertion and presents a better coupling partner for selective reaction onto the boron-bearing carbon of 4-bromobenzene boronic acid. Under precise temperature control **43** was generated in high yields. With this in hand, a variety of commercially available boronic acids were coupled to yield ester intermediates, which were readily hydrolyzed to generate acid analogues.

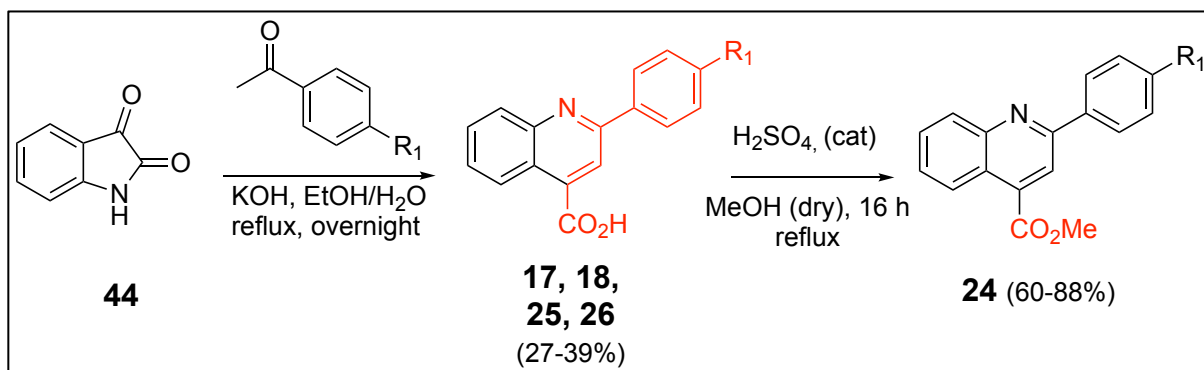


Scheme 2.2: Improved synthesis of R_1 substituted quinolines.

In addition to analogues derived from Suzuki couplings, analogues derived via Buchwald-Hartwig coupling were evaluated. Such an attempt to make **26** was unsuccessful (Scheme 2.3). An alternative approach to derive amine-substituted analogues focused on first generating the quinoline ring using the Pfitzinger reactions in which the desired R_1 substituent would be incorporated into the acetophenone coupling partner (Scheme 2.4). This route yielded carboxylic acid analogues directly and eliminated the need for ester hydrolysis. However, this approach is limited to reagents that can tolerate the harsh basic conditions and high temperatures. Furthermore, our carboxylic acid analogues presented significant purification difficulties, as they were not amenable to silica gel chromatography.

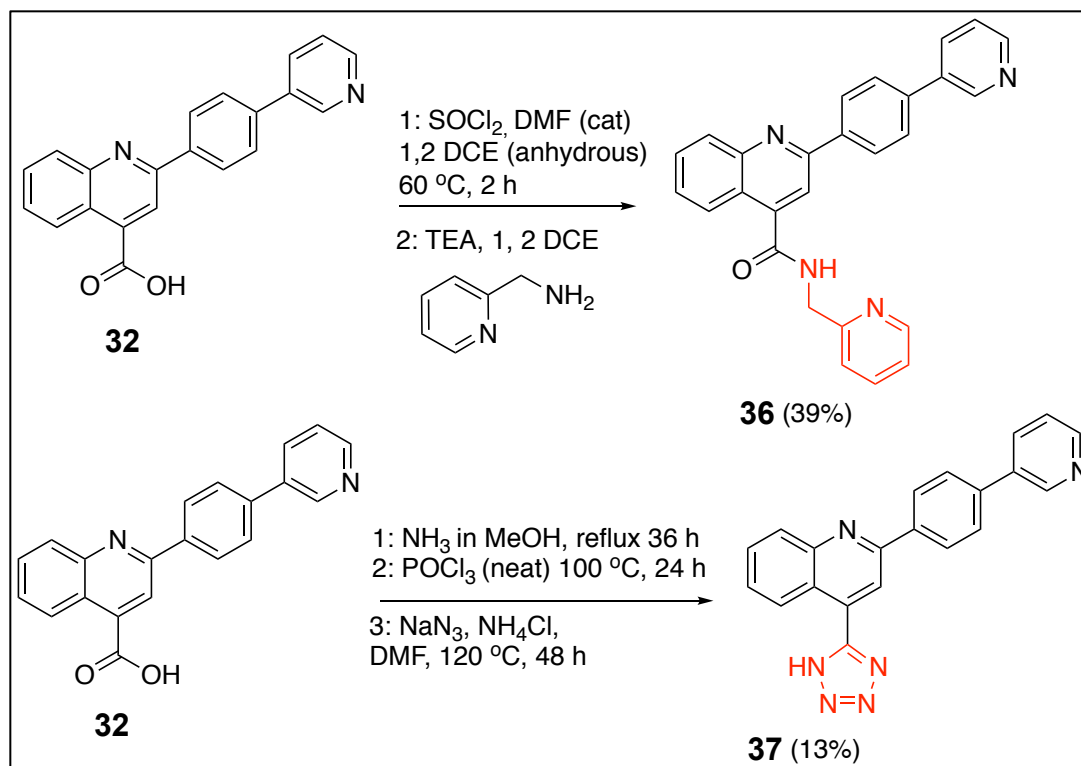


Scheme 2.3: Synthesis of morpholino analogue.



Scheme 2.4: Alternative synthesis of R₁ substituted quinolines.

Additional efforts were made to evaluate amine-containing analogues at the C4 position (Scheme 2.5). An analogue (**36**) containing the same amide functional group as **4** was generated from **32** using a modified acid chloride protocol.²⁶ A tetrazole analogue (**37**) was made using a single pot 3-step reaction protocol. Refluxing **32** in methanolic ammonia generated the corresponding amide, which was converted to a nitrile with neat POCl₃ utilizing a modified protocol of Borkin *et al.*²⁷ Tetrazole formation followed upon exposure of the nitrile intermediate to sodium azide at high temperatures in DMF, which was a modified protocol of Lassig *et al.*²⁸ and successfully generated **37** in a 13% overall yield.



Scheme 2.5: Synthesis of quinoline amide analogues

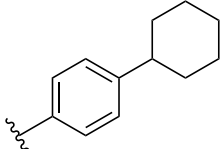
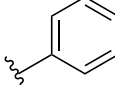
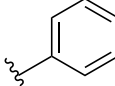
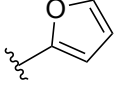
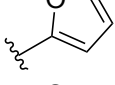
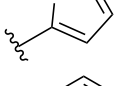
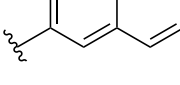
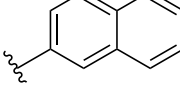
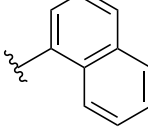
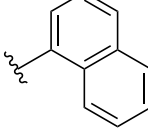
2.5 Structure activity relationships

To assess the essential pharmacophore required for activity, a cell-based SAR campaign was pursued. Cellular activity was measured using MTT assays in BxPC-3 and MiaPaca-2 pancreatic cancer cell lines. BxPC-3 contains wild-type KRAS (define KRAS) whereas MiaPaca-2 contains mutant KRAS. A comparison between the two cell lines may indicate if the lead compound targets an enzyme associated with the KRAS pathway. Evaluation of toxicity in the "non-cancerous" HFF-1 cell line provided selectivity assessment and helped to ascertain an analogue's toxicity. We were aware that these compounds contained a relatively planar structure and possessed a high cLogP. Both of these properties may lead to non-specific molecular aggregation, so we sought to minimize that risk by limiting the maximum dose evaluated in cells to 30 μM .

Removal of the cyclohexyl ring of **1** to give analogue **6** did not cause a significant reduction in potency in HCT-116 (Table 2.1). However, in MIA PaCa-2 **6** did not inhibit cell growth within our screening limits. It is possible that despite their structural similarity, **1** and **6** may target different enzymes. The methyl ester analogue of **6** did not have activity in any cell

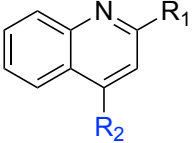
line (5, Table 2.1). When R₁ was replaced with furans (7, 8), thiophene (9), or naphthylenes (10-13) no cell growth inhibition was observed at the screening limit (30 μM). Collectively these trends suggest that the phenyl ring is the best tolerated at the C2 position.

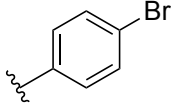
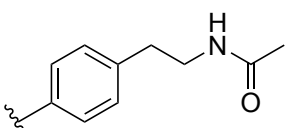
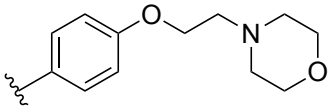
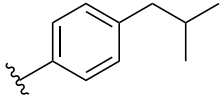
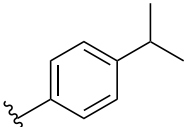
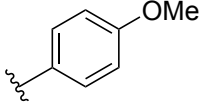
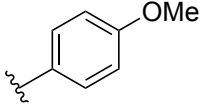
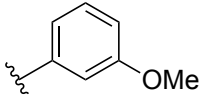
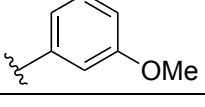
Table 2.1 Biological activity of quinoline analogues with selected aromatic R₁ substituents.

#	R ₁	R ₂	MTT Assay		
			BxPC-3 IC ₅₀ (μM)	MIA PaCa-2 IC ₅₀ (μM)	HFF-1 IC ₅₀ (μM)
1		CO ₂ H	13.9 ± 5.8	18.8 ± 12	>30
5		CO ₂ Me	>30	>30	>30
6		CO ₂ H	12.1 ± 13.9	>30	>30
7		CO ₂ Me	>30	>30	>30
8		CO ₂ H	>30	>30	>30
9		CO ₂ H	>30	>30	>30
10		CO ₂ Me	>30	>30	>30
11		CO ₂ H	>30	>30	>30
12		CO ₂ Me	>30	>30	>30
13		CO ₂ H	>30	>30	>30

Our focus shifted towards substituents on the phenyl ring to further probe the binding site. Small attachments on the phenyl ring did not induce cell growth inhibition at or below our defined detection limit. Single substituents like Br (**14**), methoxy (**19-22**), isobutyl (**17**), and isopropyl (**18**) were not well tolerated (Table 2.2). There were no observed differences between *meta* (**21, 22**) or *para* (**19, 20**) methoxy substituents. Furthermore, due to our screening concentrations, no significant difference was observed between these ester and acid analogues. However, higher concentrations were not evaluated as they increase the likelihood of false positives from aggregation. The biological results of analogues **5-22** suggest that larger lipophilic groups similar to those of **1** may be required at the C2 position of the quinoline ring. The SAR study on the P-selectin inhibitor (**3**) found that large lipophilic groups are not well tolerated at this position.¹⁷ This differs from brequinar's (**2**) SAR that favors biaryl attachments at the C2 of the quinoline ring.¹⁹ Thus, our efforts shifted towards incorporating large lipophilic groups similar to brequinar.

Table 2.2 Biological activity of quinoline analogues with selected R₁ substituents.

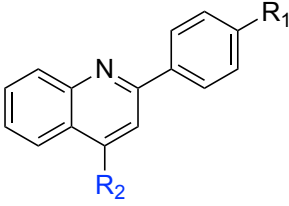


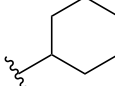
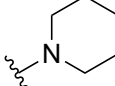
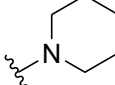
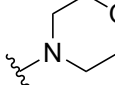
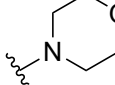
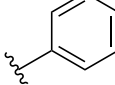
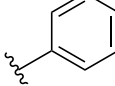
#	R ₁	R ₂	MTT Assay		
			BxPC-3 IC ₅₀ (μM)	MIA PaCa-2 IC ₅₀ (μM)	HFF-1 IC ₅₀ (μM)
14		CO ₂ H	>30	>30	>30
15		CO ₂ Me	>30	>30	>30
16		CO ₂ Me	>30	>30	>30
17		CO ₂ H	>30	>30	>30
18		CO ₂ H	>30	>30	>30
19		CO ₂ Me	>30	>30	>30
20		CO ₂ H	>30	>30	>30
21		CO ₂ Me	>30	>30	>30
22		CO ₂ H	>30	>30	>30

The incorporation of select large substituents off the C2 position of the quinoline ring resulted in analogues more potent than lead compound **1**. In the case of **1**, the methyl ester analogue (**23**) did not inhibit cell growth in any cell line (Table 2.3). This comparison suggests

the carboxylic acid is essential for activity. Replacement of the cyclohexyl group with similar bioisosteres were not tolerated. Methyl ester and carboxylic acid derivatives incorporating piperidine (**24**, **25**) and morpholino (**26**, **27**) groups in place of the cyclohexyl were inactive. However, potency was improved by replacing the cyclohexyl with a phenyl group. Both the carboxylic acid (**28**) and methyl ester (**29**) biphenyl analogues were potent. In fact, **28** had a lower IC_{50} than the lead compound. The comparison between **28** and **1** suggests that a terminal phenyl ring may occupy the binding pocket of its enzymatic target better than the cyclohexyl ring. Additionally, the results from **28** and **29** suggest that the carboxylic acid may be necessary to maintain interactions in the binding pocket. The potency observed for **29** can be rationalized by assuming an esterase within the cell hydrolyzes **29** to **28**. However, more studies are needed to support this hypothesis. While biphenyl analogue **28** appears to be more potent than **1**, we were concerned about non-specific aggregation giving a false positive readout. A highly conjugated system of aromatic rings, similar to **28**, may have a flat 3D structure and be more susceptible to forming self-association interactions in aqueous solution.²⁹ This molecular aggregation may cause non-specific cell growth inhibition. To explore this possibility, we focused on the generation of biaryl regioisomers, which would have similar physiochemical properties (Table 2.4).

Table 2.3 Biological activity of quinoline analogues with cyclic R₁ substituents.

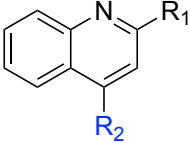


#	R ₁	R ₂	MTT Assay		
			BxPC-3 IC ₅₀ (μM)	MIA PaCa-2 IC ₅₀ (μM)	HFF-1 IC ₅₀ (μM)
23		CO ₂ Me	>30	>30	>30
24		CO ₂ Me	>30	>30	>30
25		CO ₂ H	>30	>30	>30
26		CO ₂ Me	>30	>30	>30
27		CO ₂ H	>30	>30	>30
28		CO ₂ H	5.4 ± 7.4	16.2 ± 14	>30
29		CO ₂ Me	18.2 ± 3.2	27.9 ± 15	>30

The potency of analogues with a biaryl substituent appears to be dependent upon the connectivity pattern with 1,4 being optimal. Table 2.4 highlights a biaryl isomer of **28** and **29** with 1,3 connectivity (**30**, **31**). The inactivity of both the biaryl ester (**31**) and acid (**30**) suggests that the potential enzyme interaction seen for **28** and **29** is real and not an aggregation effect.

Furthermore, these results suggest a biaryl attachment is well suited for this compound series, which is similar to the SAR trends observed for brequinar. Further observations from the brequinar SAR suggest that the C2 position occupies a very hydrophobic pocket and does not tolerate hydrophilic groups. Analogues **24-27** correlate well with this trend. Additional analogues containing heteroatom bioisosteres were evaluated. Incorporation of a pyridine ring (Table 2.5) was not well tolerated (**32, 34, 35**). Analogue **33** did have some activity in MIA PaCa-2 cell lines but not in BxPC-3 and thus may indicate a different enzyme target than for lead compound **1**.

Table 2.4: Biological activity of quinolines analogues with 1,3 biaryl regioisomers.



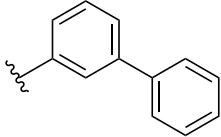
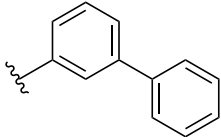
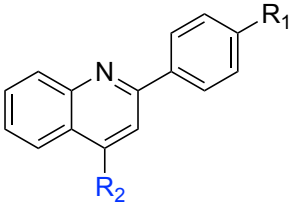
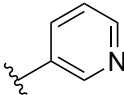
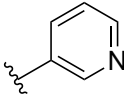
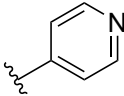
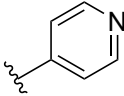
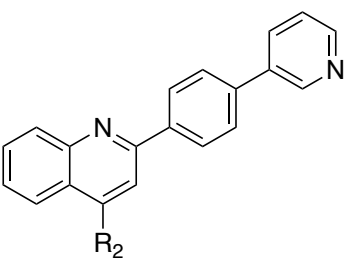
#	R ₁	R ₂	MTT Assay		
			BxPC-3 IC ₅₀ (μM)	MiaPaca-2 IC ₅₀ (μM)	HFF-1 IC ₅₀ (μM)
30		CO ₂ H	>30	>30	>30
31		CO ₂ Me	>30	>30	>30

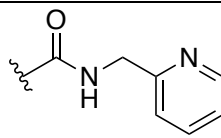
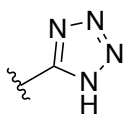
Table 2.5 Biological activity of quinolines analogues with R₁ phenyl bioisosteres



#	R ₁	R ₂	MTT Assay		
			BxPC-3 IC ₅₀ (μM)	MIA PaCa-2 IC ₅₀ (μM)	HFF-1 IC ₅₀ (μM)
32		CO ₂ H	>30	>30	>30
33		CO ₂ Me	>30	8.10 ± 4.0	>30
34		CO ₂ H	>30	>30	>30
35		CO ₂ Me	>30	>30	>30

Additionally, to assess potential similarity with the geminin-CDT inhibitor (**4**), we incorporated its amide moiety into **32**. The goal was to determine if an amide containing compound similar to **4** would be more potent than **1**. Table 2.6 shows that the amide congener of the geminin inhibitor (**36**) possessed some cytotoxicity in BxPC-3. However, the margin of error was significant and not consistently below our cutoff concentration. A tetrazole bioisostere congener of **36** did not inhibit cell growth inhibition in MIA PaCa-2 cell lines. These limited results highlight the necessity of the carboxylic acid substituent for activity.

Table 2.6: Biological activity of amide quinoline analogues with modified acid functionality

#	R ₂	MTT Assay		
		BxPC-3 IC ₅₀ (μM)	MIA PaCa-2 IC ₅₀ (μM)	HFF-1 IC ₅₀ (μM)
36		23.0 ± 13.6	>30	>30
37		-	>30	-

Collectively, the pharmacophore study highlighted the type of substituents necessary at the C2 and C4 positions of the quinoline ring. At the C2 position, large biaryl substituents with the 1,4 connectivity contributed most to potency. C4 carboxylic acids were the most potent but the amide congener of **4** was not tolerated. These SAR trends matched those observed for brequinar and suggested that DHODH may be a potential enzymatic target of compound **1**. Beyond further pharmacophore studies, our efforts shifted towards evaluating compound **1** in additional cell lines.

2.6 Expanded cell activity and DHODH overexpression

Our attention turned to evaluating cell growth inhibition of compound **1** in additional cancer cell lines. Despite initial evaluation in pancreatic cancer cell lines, we were interested in testing our inhibitors for efficacy in additional cell lines. Gratifyingly, **1** was observed to possess an IC₅₀ = 7.4 ± 1.5 μM in HCT-116 (colon cancer) which is more potent than that observed in the pancreatic BxPC-3 cell line (IC₅₀ = 13.9 ± 5.8 μM) (Table 2.7). This is a similar pattern to brequinar, which was more potent in HCT-116 (IC₅₀ = 0.98 ± 0.52 μM) vs MiaPaca-2 (IC₅₀ = 7.4 ± 2.3 μM). The expression levels of DHODH in these cell lines may provide a rationale for this phenomenon. HCT-116 is a colon cancer cell line and data from the Oncomine database suggest that DHODH is significantly overexpressed in colon cancer (Figure 2.3).³⁰ In fact, colon cancer

appears to have a higher expression of DHODH than pancreatic cancer. The protein expression of DHODH accounts for brequinar's improved potency in HCT-116 and may explain lead compound 1's potency improvement. This further links lead compound 1 with DHODH inhibition. Thus, we postulated that if 1 inhibits DHODH, it should be susceptible to the same resistance mechanisms as brequinar.

Table 2.7: Expanded cell activity of lead compound 1, green => 50% inhibition, red =<50% inhibition

Compound 1	BxPC-3	MIAPaCa-2	OVCAR8	NCI/ADR-Res	HCT-116 p53 +/+	HCT-116 p53 -/-	NU04	U87Mg	HT29
30 μM									
10 μM									

Analysis Type by Cancer	Cancer vs. Normal	Cancer vs. Cancer		Cancer Subtype Analysis										Cancer vs. Baseline (DNA only)	Pathway and Drug		Outlier			
		Cancer Histology	Multi-Cancer	Clinical Outcome	Metastasis vs. Primary	Molecular Subtype Biomarker	Molecular Subtype Mutation	Pathology (e.g., Grade)	Pathology Subtype Stage	Patient Treatment Response	Recurrence vs. Primary	Other	Drug Sensitivity		Perturbation					
Bladder Cancer																		2	2	
Brain and CNS Cancer																			2	7
Breast Cancer																			6	8
Cervical Cancer																				
Colorectal Cancer	1																		5	6
Esophageal Cancer																				1
Gastric Cancer																			4	2
Head and Neck Cancer																			2	4
Kidney Cancer	1	1	1														1		3	4
Leukemia																			5	14
Liver Cancer	6	1	1																4	6
Lung Cancer																			2	4
Lymphoma	1																		4	7
Melanoma																			4	5
Myeloma																				9
Other Cancer																			4	10
Ovarian Cancer																			3	1
Pancreatic Cancer																			2	1
Prostate Cancer																			1	14
Sarcoma																			5	8
Significant Unique Analyses	3	6	2	2															51	101
Total Unique Analyses	464	743	255	622	50	254	634	211	462	100	27	118	243	942	291			964		

Figure 2.3: Overexpression (red) and underexpression (blue) comparison between normal and cancerous cell lines. Data generated from the OncoPrint platform using all databases.³⁰

2.7 Uridine rescue

Supplementation of cells with uridine overcomes growth inhibition induced by DHODH inhibitors.³¹⁻³³ Brequinar depletes intracellular pyrimidine-based nucleotide concentrations by halting flux through *de novo* pyrimidine biosynthesis. Cellular salvage pathways utilize extracellular sources of uridine to restore nucleotide concentrations. If compound 1 is an inhibitor of DHODH, uridine should rescue cells from its induced cell growth inhibition.

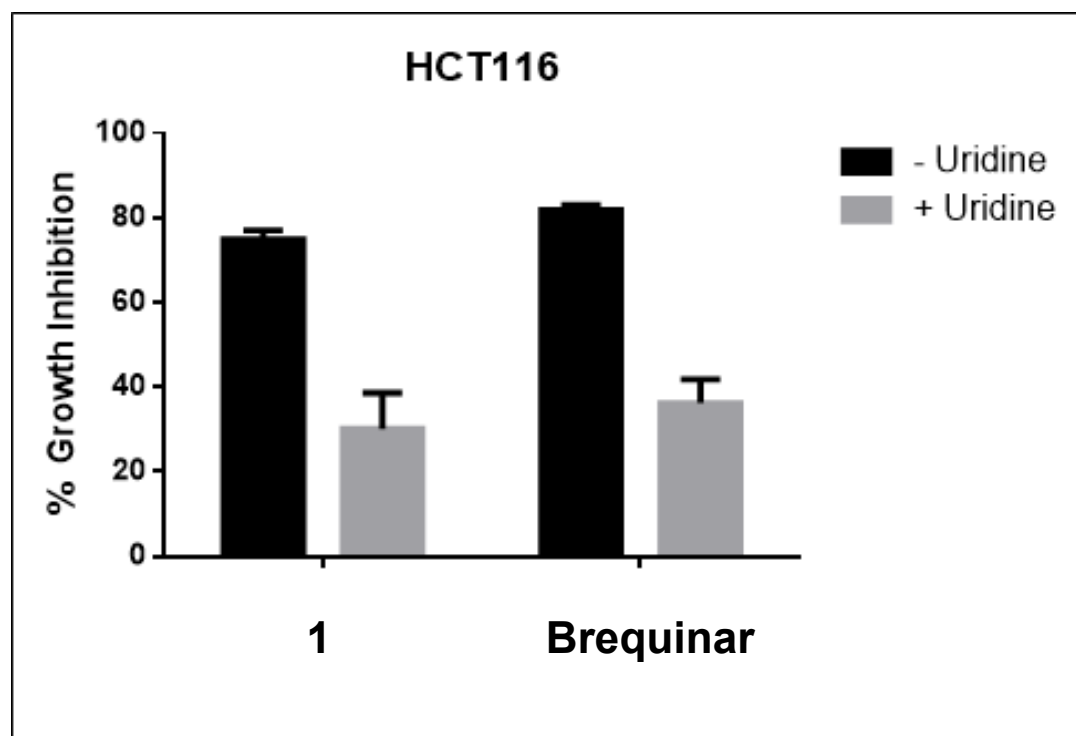


Figure 2.4: Uridine supplementation rescues cells from lead compound 1. HCT-116 cells, 3,000 c/w, 72 hours MTT assay. 10 μ M of compounds used for dosing.

Uridine rescues HCT-116 cells from growth inhibition by brequinar and compound **1** (Figure 2.4). In HCT-116, both compound **1** and brequinar induced a greater than 50% cell growth inhibition at 10 μ M. However, this response was not observed for cells supplemented with uridine. In fact, neither **1** nor brequinar was able to generate >50% cell growth inhibition in the presence of uridine. These results were consistent with previous uridine rescue experiments performed on brequinar.^{33, 34} Furthermore, these results implicate that lead compound **1** may target an enzyme within the *de novo* pyrimidine pathway as its ability to induce cell growth inhibition is sensitive to uridine supplementation. Considering the structural similarity of **1** to brequinar, it is likely that lead compound **1** is an inhibitor of DHODH. To augment this argument, we evaluated our most potent compounds in a known DHODH absorbance based assay.³⁵

2.8 DHODH Activity

To determine if lead compound **1** directly inhibits DHODH, an absorbance-based DHODH assay was utilized. DHODH catalyzes the oxidation of dihydroorotate to orotate, which is coupled to the reduction/oxidation of flavin mononucleotide and ubiquinone.^{36, 37} During

DHODH catalysis, the flavin mononucleotide cofactor is reduced by dihydroorotate. This cofactor is re-oxidized by ubiquinone, and the oxidation state of ubiquinone can be monitored using the 2,6-dichlorophenolindophenol (DCIP) redox dye.³⁶ Using this assay, the IC₅₀ values of both compounds **1** and **28** were determined to be below 1 μM for DHODH (Table 2.8). In fact, both compounds **1** (IC₅₀ = 0.35 ± 0.07 μM) and **28** (IC₅₀ = 0.16 ± 0.09 μM) are quite potent for inhibition of DHODH. These results strengthen our claim of DHODH inhibition as a primary mechanism of action.

Table 2.8: Biological data for active compounds in comparison to brequinar.

Compound	DHODH IC ₅₀ (μM)	HCT-116 IC ₅₀ (μM)	MiaPaca-2 (μM)
1	0.35 ± 0.07	7.4 ± 1.50	18.8 ± 12
28	0.16 ± 0.09	1.10 ± 1.0	16.2 ± 14
Brequinar	0.02 ± 0.02	0.98 ± 0.52	7.4 ± 2.3

2.9 Conclusion

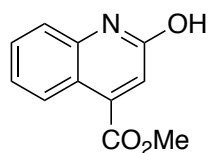
Collectively, the data suggests that compound **1** is a potent DHODH inhibitor. Pharmacophore studies on **1** showed SAR trends similar to brequinar's. Furthermore, compounds **1** and **28** are most potent in cell lines overexpressing DHODH and uridine supplementation was able to rescue cells from **1** and brequinar's cytotoxicity. Finally, compound **1** was discovered to be a potent inhibitor of DHODH (IC₅₀ = 0.35 ± 0.07 μM). These results will significantly expedite lead optimization studies with future studies will focused on developing a more potent DHODH inhibitor.

2.10 Experimental

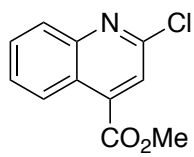
General methods. Reactions were performed in oven dried glassware under an inert atmosphere, under nitrogen or argon. Reagents and solvents were purchased from commercial sources and used without further purification. Reaction progress was monitored using analytical thin-layer chromatography (TLC) on aluminum-backed pre-coated silica plates (Silicycle, SiliaPlate 200 μM thickness, F₂₅₄) and visualized by UV absorbance. Silica chromatography purifications were performed using Siliashow® P60 (40 – 63 μM, 230 – 400 mesh). ¹H NMR spectra were obtained using a Bruker (300 or 400 MHz) or a Varian (400 or 500 MHz). Chemical shifts are reported in ppm and calibrated based on known solvent peaks (¹H using CDCl₃ = 7.26 ppm, MeOD =

3.31 ppm, DMSO, 2.50 ppm; ^{13}C using $\text{CDCl}_3 = 77.16$ ppm, MeOD = 49.00 ppm, DMSO, 39.52 ppm).³⁸ Spectral data was reported using the following abbreviations: (s = singlet, d = doublet, t = triplet, q = quartet, m = multiplet, dd = doublet of doublets), coupling constants are reported in Hz, followed by integration. ^{13}C NMR spectra were obtained at 126 MHz on a Varian 500 MHz instrument with a proton decoupled probe. Data from MS spectrometry and HPLC traces were obtained using a Shimadzu LCMS 20-20 system, which was equipped with a photo diode UV detector and a Kinetex® 2.6 μm , XB-C18 100 Å, 75 x 4.6 mm column. HPLC traces were obtained at room temperature using a gradient method from 1% to 90% MeCN in H_2O with 0.01% formic acid over 20 minutes. The flow rate was 0.50 mL/min.³⁹ Reverse phase preparatory chromatography was performed on a Shimadzu HPLC LC-20 system. The Shimadzu HPLC utilized a PDA detector and was equipped with a Kinetex® 5 μm XB-C18 100 Å, 150 x 21.2 mm column. The gradient method utilized was 10% to 90% MeCN with 0.05% trifluoroacetic acid over a 25 minute time period.

Synthesis.

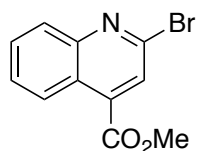


Methyl 2-hydroxyquinoline-4-carboxylate (39): 2-Hydroxyquinoline-4-carboxylic acid (1.0 g, 5.3 mmol) was dissolved in 18 mL of anhydrous MeOH. A catalytic amount of H_2SO_4 (≈ 16 drops) was added to the solution and the mixture was heated at reflux for 18 hours. Upon completion, the mixture was cooled to room temperature for 20 minutes, filtered over a fritted funnel, and triturated with deionized H_2O and cold MeOH. The precipitant was dried overnight in a vacuum oven to yield methyl 2-hydroxyquinoline-4-carboxylate (955 mg, 4.7 mmol, 88% yield). ^1H NMR (300 MHz, $\text{DMSO}-d_6$) δ 8.11 – 8.00 (m, 1H), 7.64 – 7.53 (m, 1H), 7.38 (d, $J = 8.2$ Hz, 1H), 7.32 – 7.18 (m, 1H), 6.91 (s, 1H), 3.93 (s, 3H). MS (ESI) 204.0 $[\text{M}+\text{H}]^+$.



Methyl 2-chloroquinoline-4-carboxylate (40): Dimethylformamide (1.67 mL, 21.35 mmol) was added to a round bottom flask containing 8 mL of 1,2 dichloroethane at 0 °C.

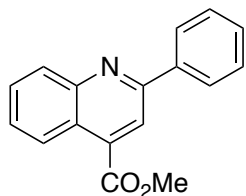
POCl₃ (2 mL, 21.35 mmol) was added dropwise to the chilled solution and the mixture was stirred at 0 °C for 15 minutes before warming to room temperature. After 15 minutes at room temperature, methyl 2-hydroxyquinoline-4-carboxylate (955 mg, 4.70 mmol) was added and the mixture was heated to reflux for 2 hours, until starting material was no longer observed. Upon completion, the solution was cooled to room temperature, poured into a solution of DCM, and washed 6x with brine. The organic layer was dried with MgSO₄, concentrated, and purified using silica chromatography (Hex/EtOAc gradient towards 1:1) to yield methyl 2-chloroquinoline-4-carboxylate (951 mg, 4.30 mmol, 91% yield). ¹H NMR (300 MHz, Chloroform-*d*) δ 8.75 (dd, *J* = 8.6, 1.3 Hz, 1H), 8.10 (dd, *J* = 8.5, 1.3 Hz, 1H), 7.93 (s, 1H), 7.81 (t, *J* = 7.7 Hz, 1H), 7.74 – 7.63 (m, 1H), 4.07 (d, *J* = 0.7 Hz, 3H). MS (ESI) 222.0 [M+H]⁺.



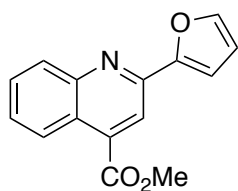
Methyl 2-bromoquinoline-4-carboxylate (41): Dimethylformamide (0.5 mL, 5.91 mmol) was added to a round bottom flask containing 4 mL of 1,2 dichloroethane at 0 °C. POBr₃ (1.33 g, 4.92 mmol) was added slowly to the chilled solution and the mixture was stirred at 0 °C for 15 minutes before warming to room temperature. After 15 minutes at room temperature, methyl 2-hydroxyquinoline-4-carboxylate (400 mg, 1.97 mmol) was added and the mixture was heated to reflux for 2 hours, until starting material was no longer observed. Upon completion, the solution was cooled to room temperature, poured into a solution of DCM, and washed 6x with brine. The organic layer was dried, concentrated, and purified using silica chromatography (Hex/EtOAc gradient towards 1:1) to yield methyl 2-bromoquinoline-4-carboxylate (417 mg, 1.57 mmol, 80% yield). ¹H NMR (300 MHz, Chloroform-*d*) δ 8.73 – 8.65 (m, 1H), 8.07 – 7.96 (m, 1H), 7.86 (s, 1H), 7.80 – 7.71 (m, 1H), 7.67 – 7.56 (m, 1H), 4.02 (s, 3H). MS (ESI) 265.7 [M+H]⁺.

General Procedure for Suzuki couplings: A round bottom flask containing halogenated starting material (1 eq) and boronic acid (1.6 eq) was dissolved in a 2:1:1 degassed solution of toluene:EtOH:H₂O (≈0.1 M of halogenated starting material). K₂CO₃ (5 eq) and Pd(PPh₃)₄ (5% mol) were added to the solution and the mixture was heated to reflux overnight. Upon completion, the mixture was cooled to room temperature, added to a solution of ethyl acetate,

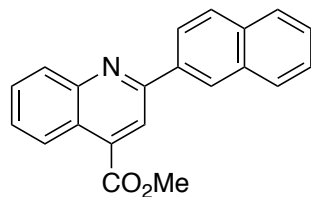
and washed with H₂O (1x) and brine (2x). The organic layer was dried with MgSO₄, filtered, and purified via silica chromatography using a variety of gradients of Hex/EtOAc.



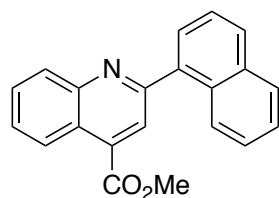
Methyl 2-phenylquinoline-4-carboxylate (5): Methyl 2-chloroquinoline-4-carboxylate (50 mg, 0.23 mmol), phenyl-boronic acid (33 mg, 0.27 mmol), Pd(PPh₃)₄ (10 mg), and K₂CO₃ (163 mg, 1.18 mmol) were combined in a round bottom flask and subjected to the conditions described in the general Suzuki coupling protocol. Methyl 2-phenylquinoline-4-carboxylate (56 mg, 0.21 mmol, 91% yield) was recovered following purification from silica chromatography (Hex/EtOAc 2:1 gradient). **¹H NMR** (300 MHz, Chloroform-*d*) δ 8.82 – 8.74 (m, 1H), 8.43 (s, 1H), 8.29 – 8.19 (m, 3H), 7.84 – 7.74 (m, 1H), 7.69 – 7.62 (m, 1H), 7.61 – 7.47 (m, 3H), 4.10 (s, 3H); **LCMS** (ESI) 264.8 [M+H]⁺; **HPLC** Purity at 254 nm, 98.4%



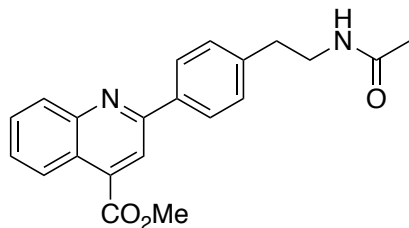
Methyl 2-(furan-2-yl)quinoline-4-carboxylate (7): Methyl 2-chloroquinoline-4-carboxylate (95 mg, 0.43 mmol), furan-2-ylboronic acid (58 mg, 0.52 mmol), Pd(PPh₃)₄ (34 mg), and K₂CO₃ (297 mg, 2.15 mmol) were combined in a round bottom flask and subjected to the conditions described in the general Suzuki coupling protocol. Methyl 2-(furan-2-yl)quinoline-4-carboxylate (27 mg, 0.11 mmol, 26% yield) was recovered following purification from silica chromatography (Hex/EtOAc 9:1 gradient). **¹H NMR** (300 MHz, Chloroform-*d*) δ 8.75 – 8.69 (m, 1H), 8.34 (s, 1H), 8.22 – 8.15 (m, 1H), 7.76 (ddd, *J* = 8.4, 6.8, 1.4 Hz, 1H), 7.68 – 7.57 (m, 3H), 6.62 (dd, *J* = 3.5, 1.8 Hz, 1H), 4.08 (s, 3H); **LCMS** [ESI] 254.0 [M+H]⁺; **HPLC** Purity at 254 nm, 99.1%



Methyl 2-(naphthalen-2-yl)quinoline-4-carboxylate (10): Methyl 2-chloroquinoline-4-carboxylate (95 mg, 0.43 mmol), naphthalen-2-ylboronic acid (118 mg, 0.69 mmol), Pd(PPh₃)₄ (15 mg), and K₂CO₃ (297 mg, 2.15 mmol) were combined in a round bottom flask and subjected to the conditions described in the general Suzuki coupling protocol. Methyl 2-(naphthalen-2-yl)quinoline-4-carboxylate (91 mg, 0.29 mmol, 67% yield) was recovered following purification from silica chromatography (Hex/EtOAc 9:1 gradient). ¹H NMR (300 MHz, Chloroform-*d*) δ 8.79 (d, *J* = 8.6 Hz, 1H), 8.69 (s, 1H), 8.60 (s, 1H), 8.47 – 8.40 (m, 1H), 8.31 (d, *J* = 8.5 Hz, 1H), 8.08 – 8.01 (m, 2H), 7.95 – 7.89 (m, 1H), 7.83 (t, *J* = 7.7 Hz, 1H), 7.67 (t, *J* = 7.7 Hz, 1H), 7.61 – 7.53 (m, 2H), 4.14 (s, 3H); LCMS (ESI) 314.1 [M+H]⁺; HPLC Purity at 254 nm, 95.0%

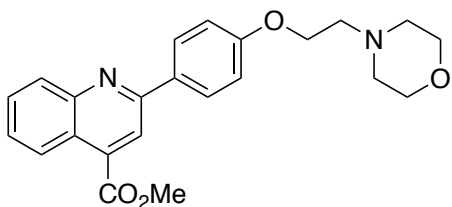


Methyl 2-(naphthalen-1-yl)quinoline-4-carboxylate (12): Methyl 2-chloroquinoline-4-carboxylate (95 mg, 0.43 mmol), naphthalen-1-ylboronic acid (118 mg, 0.69 mmol), Pd(PPh₃)₄ (15 mg), and K₂CO₃ (297 mg, 2.15 mmol) were combined in a round bottom flask and subjected to the conditions described in the general Suzuki coupling protocol. Methyl 2-(naphthalen-1-yl)quinoline-4-carboxylate (81 mg, 0.26 mmol, 60% yield) was recovered following purification from silica chromatography (Hex/EtOAc 9:1 gradient). ¹H NMR (300 MHz, Chloroform-*d*) δ 8.91 – 8.84 (m, 1H), 8.32 (d, *J* = 8.4 Hz, 1H), 8.27 (s, 1H), 8.18 – 8.10 (m, 1H), 8.04 – 7.95 (m, 2H), 7.89 – 7.82 (m, 1H), 7.80 – 7.71 (m, 2H), 7.68 – 7.60 (m, 1H), 7.61 – 7.49 (m, 2H), 4.07 (s, 3H); LCMS (ESI) 314.1 [M+H]⁺; HPLC Purity at 254 nm, 97.8%



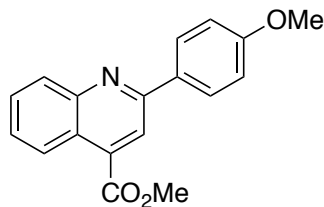
Methyl 2-(4-(2-acetamidoethyl)phenyl)quinoline-4-

carboxylate (15): Methyl 2-chloroquinoline-4-carboxylate (44 mg, 0.20 mmol), (4-(2-acetamidoethyl)phenyl)boronic acid (50 mg, 0.24 mmol), Pd(PPh₃)₄ (10 mg), and K₂CO₃ (163 mg, 1.18 mmol) were combined in a round bottom flask and subjected to the conditions described in the general Suzuki coupling protocol. Methyl 2-(4-(2-acetamidoethyl)phenyl)quinoline-4-carboxylate (49 mg, 0.14 mmol, 70% yield) was recovered following purification from silica chromatography (Hex/EtOAc 9:1 gradient). ¹H NMR (300 MHz, Chloroform-*d*) δ 8.77 (d, *J* = 8.5 Hz, 1H), 8.41 (s, 1H), 8.26 (d, *J* = 8.5 Hz, 1H), 8.17 (d, *J* = 8.0 Hz, 2H), 7.81 (t, *J* = 7.6 Hz, 1H), 7.72 – 7.62 (m, 1H), 7.40 (d, *J* = 7.9 Hz, 2H), 4.11 (s, 3H), 3.66 – 3.54 (m, 2H), 2.94 (t, *J* = 6.8 Hz, 2H), 1.99 (s, 3H); LCMS (ESI) 349.2 [M+H]⁺; HPLC Purity at 254 nm, 96.9%.

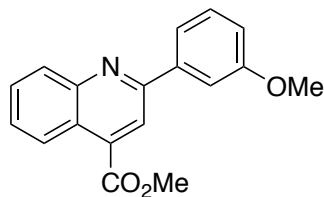


Methyl 2-(4-(2-morpholinoethoxy)phenyl)quinoline-4-

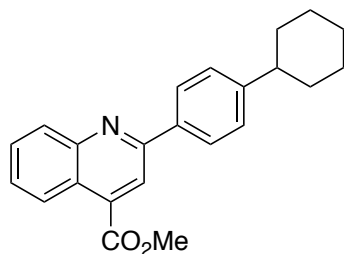
carboxylate (16): Methyl 2-chloroquinoline-4-carboxylate (52 mg, 0.24 mmol), (4-(2-morpholinoethoxy)phenyl)boronic acid (75 mg, 0.26 mmol), Pd(PPh₃)₄ (10 mg), and K₂CO₃ (164 mg, 1.19 mmol) were combined in a round bottom flask and subjected to the conditions described in the general Suzuki coupling protocol. Methyl 2-(4-(2-morpholinoethoxy)phenyl)quinoline-4-carboxylate (74 mg, 0.18 mmol, 75% yield) was recovered following purification from silica chromatography (Hex/EtOAc 9:1 gradient). ¹H NMR (300 MHz, Chloroform-*d*) δ 8.78 – 8.70 (m, 1H), 8.36 (s, 1H), 8.26 (d, *J* = 8.4 Hz, 1H), 8.18 (d, *J* = 8.6 Hz, 2H), 7.86 – 7.77 (m, 1H), 7.70 – 7.60 (m, 1H), 7.05 (d, *J* = 8.6 Hz, 2H), 4.54 – 4.47 (m, 2H), 4.10 (s, 3H), 4.03 (t, *J* = 4.8 Hz, 4H), 3.78 – 3.60 (m, 2H), 3.59 – 3.52 (m, 2H), 3.19 – 3.01 (m, 2H); LCMS (ESI) 393.2 [M+H]⁺; HPLC Purity at 254 nm, 98.8%.



Methyl 2-(4-methoxyphenyl)quinoline-4-carboxylate (19): Methyl 2-(3-methoxyphenyl)quinoline-4-carboxylate (32 mg, 0.15 mmol), (4-methoxyphenyl)boronic acid (26 mg, 0.17 mmol), Pd(PPh₃)₄ (9 mg), and K₂CO₃ (100 mg, 0.73 mmol) were combined in a round bottom flask and subjected to the conditions described in the general Suzuki coupling protocol. Methyl 2-(4-methoxyphenyl)quinoline-4-carboxylate (10 mg, 0.03 mmol, 23% yield) was recovered following purification from silica chromatography (Hex/EtOAc 9:1 gradient). ¹H NMR (300 MHz, Chloroform-*d*) δ 8.73 (d, *J* = 8.5 Hz, 1H), 8.37 (s, 1H), 8.25 – 8.14 (m, 3H), 7.84 – 7.73 (m, 1H), 7.65 – 7.55 (m, 1H), 7.12 – 7.02 (m, 2H), 4.08 (s, 3H), 3.90 (s, 3H); LCMS (ESI) 294.0 [M+H]⁺; HPLC Purity at 254 nm, 99.2%.

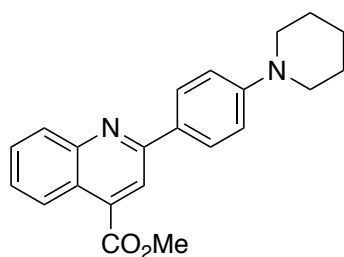


Methyl 2-(3-methoxyphenyl)quinoline-4-carboxylate (21): Methyl 2-chloroquinoline-4-carboxylate (67 mg, 0.30 mmol), (3-methoxyphenyl)boronic acid (50 mg, 0.33 mmol), Pd(PPh₃)₄ (15 mg), and K₂CO₃ (207 mg, 1.5 mmol) were combined in a round bottom flask and subjected to the conditions described in the general Suzuki coupling protocol. Methyl 2-(3-methoxyphenyl)quinoline-4-carboxylate (23 mg, 0.08 mmol, 27% yield) was recovered following purification from silica chromatography (Hex/EtOAc 9:1 gradient). ¹H NMR (300 MHz, Chloroform-*d*) δ 8.81 – 8.73 (m, 1H), 8.40 (s, 1H), 8.30 – 8.21 (m, 1H), 7.86 – 7.74 (m, 3H), 7.68 – 7.60 (m, 1H), 7.46 (t, *J* = 7.9 Hz, 1H), 7.09 – 7.01 (m, 1H), 4.08 (s, 3H), 3.95 (s, 3H); LCMS (ESI) 294.2 [M+H]⁺; HPLC Purity at 254 nm, 98.4%



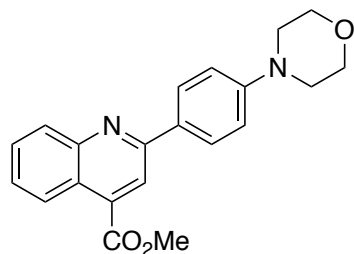
Methyl 2-(4-cyclohexylphenyl)quinoline-4-carboxylate (23):

Methyl 2-chloroquinoline-4-carboxylate (62 mg, 0.28 mmol), (3-cyclohexylphenyl)boronic acid (62 mg, 0.31 mmol), Pd(PPh₃)₄ (12 mg), and K₂CO₃ (193 mg, 1.4 mmol) were combined in a round bottom flask and subjected to the conditions described in the general Suzuki coupling protocol. Methyl 2-(4-cyclohexylphenyl)quinoline-4-carboxylate (27 mg, 0.08 mmol, 29% yield) was recovered following purification from silica chromatography (Hex/EtOAc 9:1 gradient). ¹H NMR (300 MHz, Chloroform-*d*) δ 8.76 (d, *J* = 8.5 Hz, 1H), 8.41 (s, 1H), 8.24 (d, *J* = 8.4 Hz, 1H), 8.15 (d, *J* = 8.0 Hz, 2H), 7.86 – 7.71 (m, 1H), 7.69 – 7.59 (m, 1H), 7.41 (d, *J* = 8.0 Hz, 2H), 4.09 (s, 3H), 2.70 – 2.57 (m, 1H), 2.03 – 1.85 (m, 4H), 1.84 – 1.67 (m, 1H), 1.61 – 1.21 (m, 5H); LCMS (ESI) 346.2 [M+H]⁺; HPLC Purity at 254 nm, 98.7%



Methyl 2-(4-(piperidin-1-yl)phenyl)quinoline-4-carboxylate (24):

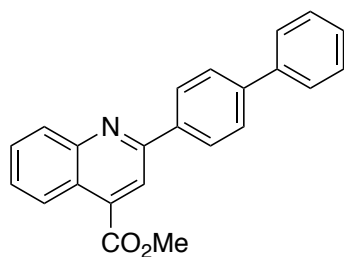
2-(4-(Piperidin-1-yl)phenyl)quinoline-4-carboxylic acid (30 mg, 0.09 mmol) was dissolved in 2 mL MeOH and a catalytic amount of H₂SO₄ (4 drops). The mixture was heated to reflux overnight, concentrated, and dried with MgSO₄. Upon filtration, the organic layer was concentrated and product was purified using silica chromatography (DCM/MeOH 9:1 gradient) to yield methyl 2-(4-(piperidin-1-yl)phenyl)quinoline-4-carboxylate as a dark red solid (29 mg, 0.08 mmol, 88%). ¹H NMR (400 MHz, Chloroform-*d*) δ 8.71 (dd, *J* = 8.5, 1.4 Hz, 1H), 8.38 (s, 1H), 8.21 – 8.12 (m, 3H), 7.80 – 7.70 (m, 1H), 7.63 – 7.53 (m, 1H), 7.13 – 7.00 (m, 2H), 4.08 (d, *J* = 1.0 Hz, 3H), 3.39 – 3.28 (m, 4H), 1.80 – 1.71 (m, 4H), 1.70 – 1.60 (m, 2H); LCMS (ESI) 347.2 [M+H]⁺; HPLC Purity at 254 nm, 97.3%



Methyl 2-(4-morpholinophenyl)quinoline-4-carboxylate (26):

Methyl 2-(4-bromophenyl)quinoline-4-carboxylate (80 mg, 0.23 mmol), morpholine (0.23 mL, 0.28 mmol), Pd₂dba₃ (11 mg), BINAP (21 mg, 0.04 mmol), and KO^tBu (37 mg, 0.33 mmol) were combined in a degassed solution of 2.5 mL toluene. The mixture was heated to reflux overnight, before addition of water, and extraction with dichloromethane. The organic layer was dried with MgSO₄, filtered, concentrated and purified via silica chromatography (DCM/MeOH 9:1 gradient). Methyl 2-(4-morpholinophenyl)quinoline-4-carboxylate was collected as a thick yellow oil (11 mg, 0.03 mmol, 13%).

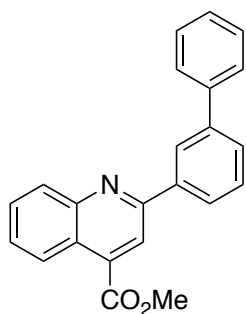
Alternate route using esterification: 2-(4-morpholinophenyl)quinoline-4-carboxylic acid (31 mg, 0.09 mmol) was dissolved in 2 mL MeOH with catalytic H₂SO₄ (16 drops) and the mixture was refluxed overnight. The mixture was concentrated and partitioned between 1M KOH and EtOAc. The organic layer was dried with MgSO₄, filtered, concentrated, and purified via silica chromatography. Methyl 2-(4-morpholinophenyl)quinoline-4-carboxylate was recovered as a red solid (28 mg, 0.08 mmol, 88%). ¹H NMR (300 MHz, Chloroform-*d*) δ 8.80 – 8.66 (m, 2H), 8.43 (s, 1H), 8.18 (d, *J* = 8.5 Hz, 2H), 8.01 (t, *J* = 7.9 Hz, 1H), 7.81 (t, *J* = 7.8 Hz, 1H), 7.03 (d, *J* = 8.4 Hz, 2H), 4.17 (s, 3H), 3.90 (t, *J* = 4.9 Hz, 4H), 3.45 (t, *J* = 5.0 Hz, 4H); LCMS (ESI) 349.2 [M+H]⁺; HPLC Purity at 254 nm, 98.0%



Methyl 2-([1,1'-biphenyl]-4-yl)quinoline-4-carboxylate (29):

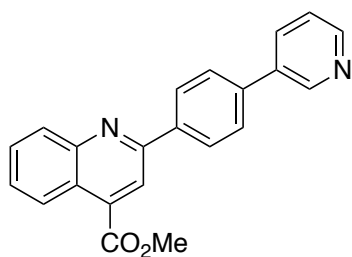
Methyl 2-chloroquinoline-4-carboxylate (95 mg, 0.43 mmol), [1,1'-biphenyl]-4-ylboronic acid (136 mg, 0.69 mmol), Pd(PPh₃)₄ (15 mg), and K₂CO₃ (297 mg, 2.15 mmol) were combined in a round bottom flask and subjected to the conditions described in the general Suzuki coupling

protocol. Methyl 2-([1,1'-biphenyl]-4-yl)quinoline-4-carboxylate (91 mg, 0.27 mmol, 63%) was recovered following purification from silica chromatography (Hex/EtOAc 9:1 gradient). ¹H NMR (300 MHz, Chloroform-*d*) δ 8.76 (dd, *J* = 8.6, 1.3 Hz, 1H), 8.46 (s, 1H), 8.35 – 8.20 (m, 3H), 7.85 – 7.73 (m, 3H), 7.74 – 7.58 (m, 3H), 7.49 (t, *J* = 7.4 Hz, 2H), 4.09 (s, 3H); LCMS (ESI) 340.10 [M+H]⁺; HPLC Purity at 254 nm, 99.5%.



Methyl 2-([1,1'-biphenyl]-3-yl)quinoline-4-carboxylate (31): Methyl 2-

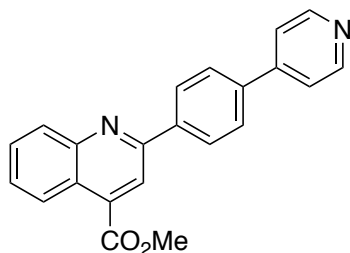
chloroquinoline-4-carboxylate (95 mg, 0.43 mmol), [1,1'-biphenyl]-3-ylboronic acid (137 mg, 0.69 mmol), Pd(PPh₃)₄ (22 mg), and K₂CO₃ (297 mg, 2.15 mmol) were combined in a round bottom flask and subjected to the conditions described in the general Suzuki coupling protocol. Methyl 2-([1,1'-biphenyl]-3-yl)quinoline-4-carboxylate (83 mg, 0.24 mmol, 56% yield) was recovered following purification from silica chromatography (Hex/EtOAc 9:1 gradient). ¹H NMR (400 MHz, Chloroform-*d*) δ 8.80 (m, 1H), 8.49 (s, 1H), 8.46 (m, 1H), 8.29 (m, 1H), 8.21 (m, 1H), 7.82 (m, 1H), 7.75 (m, 3H), 7.71 – 7.60 (m, 2H), 7.58 – 7.50 (m, 2H), 7.47 – 7.40 (m, 1H), 4.11 (s, 3H); LCMS (ESI) 340.1 [M+H]⁺; HPLC purity at 254 nm, 96.2%



Methyl 2-(4-(pyridin-3-yl)phenyl)quinoline-4-carboxylate (33):

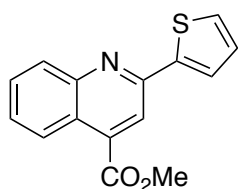
Methyl 2-(4-bromophenyl)quinoline-4-carboxylate (60 mg, 0.18 mmol), pyridin-3-ylboronic acid (23 mg, 0.19 mmol), Pd(PPh₃)₄ (10 mg), and K₂CO₃ (72 mg, 0.53 mmol) were combined in a round bottom flask and subjected the conditions described in the general Suzuki coupling protocol. Methyl 2-(4-(pyridin-3-yl)phenyl)quinoline-4-carboxylate (20 mg, 0.06 mmol, 33%) was recovered following purification from silica chromatography (Hex/EtOAc 9:1 gradient). ¹H

NMR (300 MHz, Chloroform-*d*) δ 8.92 (s, 1H), 8.74 (d, J = 8.5 Hz, 1H), 8.62 (d, J = 4.8 Hz, 1H), 8.40 (s, 1H), 8.29 (d, J = 8.2 Hz, 2H), 8.21 (d, J = 8.4 Hz, 1H), 7.91 (dd, J = 8.0, 2.0 Hz, 1H), 7.82 – 7.68 (m, 3H), 7.66 – 7.57 (m, 1H), 7.37 (dd, J = 7.9, 4.8 Hz, 1H), 4.23 – 3.94 (m, 3H); **LCMS** (ESI) 341.10 [M+H]⁺; **HPLC** Chromatogram purity at 254 nm, 99.6%.



Methyl 2-(4-(pyridin-4-yl)phenyl)quinoline-4-carboxylate (35):

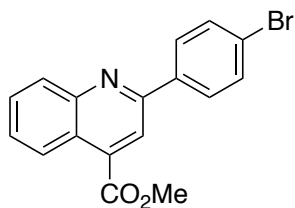
Methyl 2-(4-bromophenyl)quinoline-4-carboxylate (60 mg, 0.18 mmol), pyridin-4-ylboronic acid (23 mg, 0.19 mmol), Pd(PPh₃)₄ (20 mg), and K₂CO₃ (72 mg, 0.53 mmol) were combined in a round bottom flask and subjected to the conditions described in the general Suzuki coupling protocol. Methyl 2-(4-(pyridin-4-yl)phenyl)quinoline-4-carboxylate (7 mg, 0.02 mmol, 11%) was recovered following purification from silica chromatography (Hex/EtOAc 9:1 gradient), recrystallization using 2-propanol and diethyl ether. **¹H NMR** (300 MHz, Chloroform-*d*) δ 8.80 – 8.67 (m, 3H), 8.44 (s, 1H), 8.39 – 8.30 (m, 2H), 8.28 – 8.20 (m, 1H), 7.79 (dd, J = 8.8, 6.7 Hz, 3H), 7.70 – 7.55 (m, 3H), 4.09 (s, 3H); **LCMS** (ESI) 341.1 [M+H]⁺; **HPLC** Purity at 254 nm, 99.6%



Methyl 2-(thiophen-2-yl)quinoline-4-carboxylate (42):

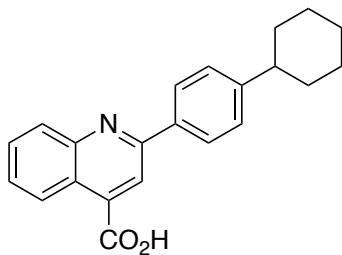
Methyl 2-chloroquinoline-4-carboxylate (100 mg, 0.45 mmol), thiophen-2-ylboronic acid (81 mg, 0.63 mmol), Pd(PPh₃)₄ (78 mg), and K₂CO₃ (310 mg, 2.25 mmol) were combined in a round bottom flask and subjected to the conditions described in the general Suzuki coupling protocol. Methyl 2-(thiophen-2-yl)quinoline-4-carboxylate (70 mg, 0.26 mmol, 58% yield) was recovered following purification from silica chromatography (Hex/EtOAc 9:1 gradient). **¹H NMR** (300 MHz, Chloroform-*d*) δ 8.74 – 8.66 (m, 1H), 8.31 (s, 1H), 8.20 – 8.09 (m, 1H), 7.84 – 7.70 (m,

2H), 7.64 – 7.56 (m, 1H), 7.51 (dd, $J = 5.0, 1.1$ Hz, 1H), 7.22 – 7.13 (m, 1H), 4.08 (s, 3H); **MS** (ESI) 270.0 $[M+H]^+$.



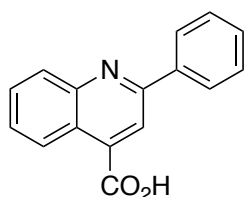
Methyl 2-(4-bromophenyl)quinoline-4-carboxylate (43): Methyl 2-bromoquinoline-4-carboxylate (358 mg, 1.35 mmol), (4-bromophenyl)boronic acid (298 mg, 1.48 mmol), Pd(dppf)Cl₂:CH₂Cl₂ (65 mg), and K₂CO₃ (650 mg, 4.71 mmol) were combined in a round bottom flask at 0 °C. The mixture was slowly warmed to room temperature over 1 hour, heated to 50 °C for 30 minutes, then followed the general Suzuki coupling workup conditions. Methyl 2-(4-bromophenyl)quinoline-4-carboxylate (417 mg, 1.22 mmol, 91% yield) was recovered following purification from silica chromatography (Hex/EtOAc 9:1 gradient). **¹H NMR** (300 MHz, Chloroform-*d*) δ 8.79 – 8.71 (m, 1H), 8.36 (s, 1H), 8.25 – 8.17 (m, 1H), 8.14 – 8.06 (m, 2H), 7.83 – 7.74 (m, 1H), 7.71 – 7.61 (m, 3H), 4.09 (s, 3H); **MS** (ESI) 342.0 $[M+H]^+$.

General conditions for ester hydrolysis: A round bottom flask containing the ester starting material (1 eq) and a large excess of NaOH (5-10 eq) was dissolved in a 1:1 mixture of THF:H₂O (≈0.1 - 0.5 M of ester). The solution was heated to 40 °C until starting material was no longer detectable by TLC. Upon completion, the mixture was cooled to room temperature, concentrated under reduced pressure, redissolved in 1 M KOH, and washed with EtOAc (3x). The basic aqueous layer was acidified with HCl until a pH ≈ 2-3 was obtained; formed precipitant was filtered over a fritted funnel, washed with cold deionized H₂O, and dried overnight in a vacuum oven.



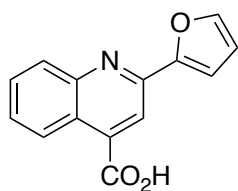
2-(4-Cyclohexylphenyl)quinoline-4-carboxylic acid (1): Methyl 2-(4-cyclohexylphenyl)quinoline-4-carboxylate (15 mg, 0.04 mmol) and NaOH (40 mg, 1.05 mmol) was dissolved in a 1:1 mixture of THF/H₂O and followed the general ester hydrolysis

conditions. A white solid was collected from the vacuum oven to yield 2-(4-cyclohexylphenyl)quinoline-4-carboxylic acid (7 mg, 0.02 mmol, 50%). **¹H NMR** (500 MHz, DMSO-*d*₆) δ 8.64 (d, *J* = 8.6 Hz, 1H), 8.41 (d, *J* = 1.8 Hz, 1H), 8.21 – 8.15 (m, 2H), 8.14 – 8.08 (m, 1H), 7.85 – 7.79 (m, 1H), 7.71 – 7.61 (m, 1H), 7.40 – 7.34 (m, 2H), 2.59 – 2.50 (m, 1H), 1.83 – 1.73 (m, 4H), 1.72 – 1.65 (m, 1H), 1.49 – 1.27 (m, 4H), 1.27 – 1.10 (m, 1H). **¹³C NMR** (126 MHz, DMSO-*d*₆) δ 168.09, 156.23, 150.06, 148.86, 138.00, 136.02, 130.55, 130.14, 127.97, 127.72 (2H), 127.64 (2H), 125.85, 123.81, 119.42, 44.03, 34.22 (2H), 26.73 (2H), 26.00; **LCMS** (ESI) 332.20 [M+H]⁺ 330.20 [M-H]⁻; **HPLC** Purity at 254 nm, 98.6%



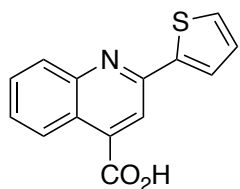
2-Phenylquinoline-4-carboxylic acid (6): Methyl 2-phenylquinoline-4-

carboxylate (25 mg, 0.10 mmol) was dissolved in a 1:1 mixture of THF/H₂O and followed the general ester hydrolysis conditions. A yellow solid was collected from the vacuum oven to yield 2-phenylquinoline-4-carboxylic acid (9 mg, 0.04 mmol, 40%). **¹H NMR** (300 MHz, DMSO-*d*₆) δ 8.72 – 8.62 (m, 1H), 8.47 (s, 1H), 8.35 – 8.27 (m, 2H), 8.23 – 8.13 (m, 1H), 7.91 – 7.79 (m, 1H), 7.76 – 7.66 (m, 1H), 7.63 – 7.49 (m, 3H); **LCMS** (ESI) 250.1 [M+H]⁺; **HPLC** Purity at 254 nm, 96.4%

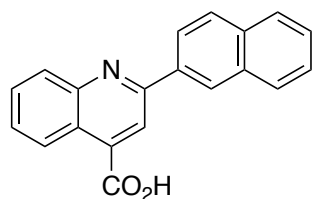


2-(Furan-2-yl)quinoline-4-carboxylic acid (8): Methyl 2-(furan-2-

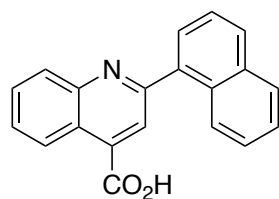
yl)quinoline-4-carboxylate (15 mg, 0.06 mmol) and NaOH (59 mg, 1.48 mmol) was dissolved in a 1:1 mixture of THF/H₂O and followed the general ester hydrolysis conditions. A brown/tan solid was collected from the vacuum oven to yield 2-(furan-2-yl)quinoline-4-carboxylic acid (8 mg, 0.03 mmol, 50%). **¹H NMR** (300 MHz, DMSO-*d*₆) δ 8.68 – 8.61 (m, 1H), 8.30 (s, 1H), 8.08 (d, *J* = 8.4 Hz, 1H), 8.01 – 7.96 (m, 1H), 7.86 – 7.78 (m, 1H), 7.72 – 7.62 (m, 1H), 7.46 (d, *J* = 3.5 Hz, 1H), 6.78 – 6.72 (m, 1H); **LCMS** (ESI) 240.2 [M+H]⁺; **HPLC** Purity at 254 nm, 97.1%



2-(Thiophen-2-yl)quinoline-4-carboxylic acid (9): Methyl 2-(thiophen-2-yl)quinoline-4-carboxylate (20 mg, 0.07 mmol) and NaOH (46 mg, 1.15 mmol) was dissolved in a 1:1 mixture of THF/H₂O and followed the general ester hydrolysis conditions. A yellow solid was collected from the vacuum oven to yield methyl 2-(thiophen-2-yl)quinoline-4-carboxylate (3 mg, 0.004 mmol, 6%). ¹H NMR (300 MHz, DMSO-*d*₆) δ 8.63 – 8.54 (m, 1H), 8.43 (s, 1H), 8.13 – 8.02 (m, 2H), 7.87 – 7.74 (m, 2H), 7.70 – 7.59 (m, 1H), 7.29 – 7.20 (m, 1H); LCMS (ESI) 256.0 [M+H]⁺; HPLC Purity at 254 nm, 96.8%

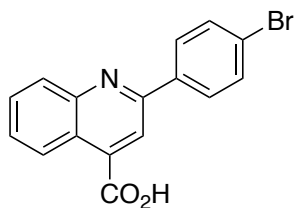


2-(Naphthalen-2-yl)quinoline-4-carboxylic acid (11): Methyl 2-(naphthalen-2-yl)quinoline-4-carboxylate (40 mg, 0.13 mmol) was dissolved in a 1:1 mixture of THF/H₂O and followed the general ester hydrolysis protocol. A yellow solid was collected from the vacuum oven to yield 2-(naphthalen-2-yl)quinoline-4-carboxylic acid (17 mg, 0.06 mmol, 46%). ¹H NMR (300 MHz, DMSO-*d*₆) δ 8.79 (s, 1H), 8.73 (d, *J* = 8.4 Hz, 1H), 8.48 (d, *J* = 8.6 Hz, 1H), 8.24 (s, 1H), 8.18 – 8.10 (m, 1H), 8.07 (t, *J* = 7.5 Hz, 2H), 7.99 (m, 1H), 7.70 (t, *J* = 7.5 Hz, 1H), 7.58 (m, 2H), 7.51 (t, *J* = 7.7 Hz, 1H); LCMS (ESI) 300.1 [M+H]⁺; HPLC purity at 254 nm, 98.8%

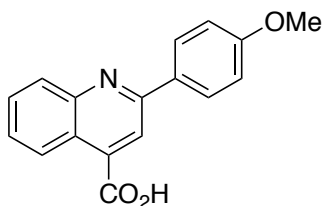


2-(Naphthalen-1-yl)quinoline-4-carboxylic acid (13): Methyl 2-(naphthalen-1-yl)quinoline-4-carboxylate (22 mg, 0.07 mmol) and LiOH (71 mg, 3.08 mmol) were dissolved in a 1:1 THF/H₂O solution and followed the general ester hydrolysis protocol. A white solid was collected from the vacuum oven to yield 2-(naphthalen-1-yl)quinoline-4-carboxylic acid (13 mg, 0.04 mmol, 57%). ¹H NMR (300 MHz, DMSO-*d*₆) δ 8.75 (d, *J* = 8.4

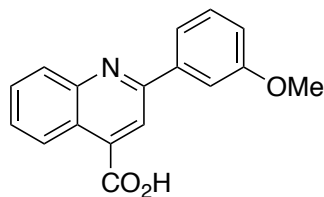
Hz, 1H), 8.12 (d, $J = 8.2$ Hz, 1H), 8.09 – 8.01 (m, 3H), 7.84 – 7.48 (m, 7H); **LCMS** (ESI) 300.1 [M+H]⁺; **HPLC** purity at 254 nm, 96.2%



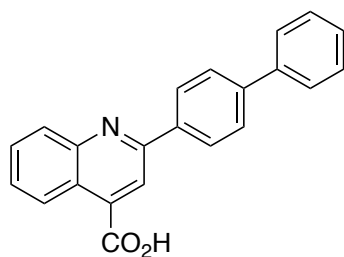
2-(4-Bromophenyl)quinoline-4-carboxylic acid (14): Methyl 2-(4-bromophenyl)quinoline-4-carboxylate (25 mg, 0.07 mmol) and NaOH (42 mg, 1.05 mmol) was dissolved in a 1:1 mixture of THF/H₂O and followed the general ester hydrolysis protocol. A off-white solid was collected from the vacuum oven to yield 2-(4-bromophenyl)quinoline-4-carboxylic acid (17 mg, 0.05 mmol, 71%). **¹H NMR** (300 MHz, DMSO-*d*₆) δ 8.68 (d, $J = 8.3$ Hz, 1H), 8.20 (d, $J = 8.5$ Hz, 2H), 8.08 (s, 1H), 8.02 (d, $J = 8.4$ Hz, 1H), 7.72 (dd, $J = 12.5, 8.1$ Hz, 3H), 7.53 (t, $J = 7.6$ Hz, 1H); **LCMS** (ESI) 328.0 [M+H]⁺; **HPLC** Purity at 254 nm, 98.2%



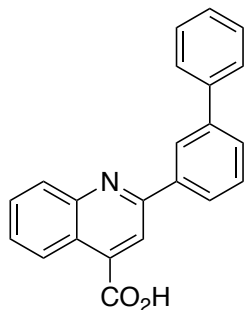
2-(4-Methoxyphenyl)quinoline-4-carboxylic acid (20): Methyl 2-(4-methoxyphenyl)quinoline-4-carboxylate (3 mg, 0.01 mmol) and NaOH (42 mg, 1.05 mmol) were dissolved in a 1:1 mixture of THF/H₂O and followed the general ester hydrolysis conditions. A cakey brown solid was collected from the vacuum oven to yield 2-(4-methoxyphenyl)quinoline-4-carboxylic acid (1 mg, 0.004 mmol, 40%). **¹H NMR** (300 MHz, DMSO-*d*₆) δ 8.64 (d, $J = 8.5$ Hz, 1H), 8.42 (s, 1H), 8.26 (d, $J = 8.4$ Hz, 2H), 8.12 (d, $J = 8.4$ Hz, 1H), 7.81 (t, $J = 7.7$ Hz, 1H), 7.66 (t, $J = 7.7$ Hz, 1H), 7.10 (d, $J = 8.4$ Hz, 2H), 3.84 (s, 3H); **LCMS** (ESI) 280.1 [M+H]⁺; **HPLC** Purity at 254 nm, 99.9%



2-(3-Methoxyphenyl)quinoline-4-carboxylic acid (22): Methyl 2-(3-methoxyphenyl)quinoline-4-carboxylate (20 mg, 0.07 mmol) and NaOH (73 mg, 1.83 mmol) was dissolved in a 1:1 mixture of THF/H₂O and followed the general ester hydrolysis conditions. A tan solid was collected from the vacuum oven to yield 2-(3-methoxyphenyl)quinoline-4-carboxylic acid (12 mg, 0.04 mmol, 57%). ¹H NMR (300 MHz, DMSO-*d*₆) δ 8.64 (d, *J* = 8.4 Hz, 1H), 8.46 (s, 1H), 8.20 (d, *J* = 8.4 Hz, 1H), 7.86 (d, *J* = 8.3 Hz, 3H), 7.72 (t, *J* = 7.7 Hz, 1H), 7.50 (t, *J* = 7.9 Hz, 1H), 7.12 (dd, *J* = 8.3, 2.4 Hz, 1H), 3.89 (s, 3H); LCMS (ESI) 280.0 [M+H]⁺, 278.1 [M-H]⁻; HPLC Purity at 254 nm, 99.9%

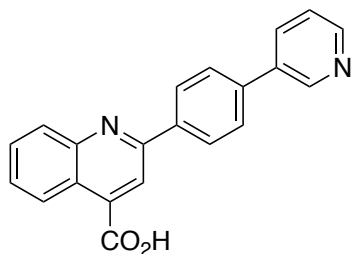


2-([1,1'-Biphenyl]-4-yl)quinoline-4-carboxylic acid (28): Methyl 2-([1,1'-biphenyl]-4-yl)quinoline-4-carboxylate (50 mg, 0.15 mmol) and NaOH (29 mg, 0.74 mmol) was dissolved in a 1:1 mixture of THF/H₂O and followed the general ester hydrolysis conditions. A white solid was collected from the vacuum oven to yield 2-([1,1'-biphenyl]-4-yl)quinoline-4-carboxylic acid (36 mg, 0.11 mmol, 78%). ¹H NMR (300 MHz, Methanol-*d*₄) δ 8.46 – 8.36 (m, 1H), 8.19 (d, *J* = 8.4 Hz, 2H), 8.14 – 8.02 (m, 2H), 7.83 – 7.63 (m, 5H), 7.56 (ddd, *J* = 8.2, 6.8, 1.2 Hz, 1H), 7.44 (t, *J* = 7.4 Hz, 2H), 7.40 – 7.28 (m, 1H); LCMS (ESI) 326.15 [M+H]⁺, 324.10 [M-H]⁻; HPLC Purity at 254 nm, 98.9%.



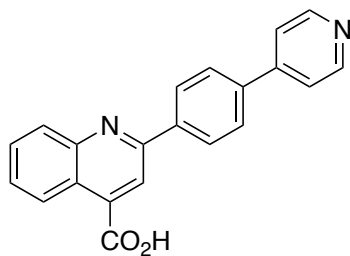
2-([1,1'-Biphenyl]-3-yl)quinoline-4-carboxylic acid (30):

Methyl 2-([1,1'-biphenyl]-3-yl)quinoline-4-carboxylate (31 mg, 0.09 mmol) and NaOH (153 mg, 3.83 mmol) was dissolved in a 1:1 mixture of THF/H₂O and followed the general ester hydrolysis conditions. A white solid was collected from the vacuum oven to yield 2-([1,1'-biphenyl]-3-yl)quinoline-4-carboxylic acid (21 mg, 0.06 mmol, 67%). ¹H NMR (300 MHz, DMSO-*d*₆) δ 8.68 (d, *J* = 8.5 Hz, 1H), 8.46 (s, 1H), 8.22 (d, *J* = 7.7 Hz, 1H), 8.15 (s, 1H), 8.05 (d, *J* = 8.4 Hz, 1H), 7.80 (d, *J* = 7.7 Hz, 3H), 7.74 – 7.61 (m, 2H), 7.53 (t, *J* = 7.4 Hz, 3H), 7.42 (t, *J* = 7.6 Hz, 1H); LCMS (ESI) 326.1 [M+H]⁺; HPLC Purity at 254 nm, 99.9%



2-(4-(Pyridin-3-yl)phenyl)quinoline-4-carboxylic acid (32):

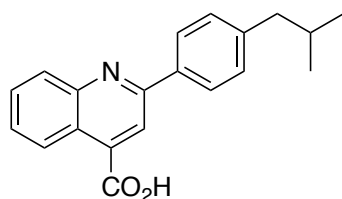
Methyl 2-(4-(pyridin-3-yl)phenyl)quinoline-4-carboxylate (8 mg, 0.02 mmol) and NaOH (45 mg, 1.13 mmol) was dissolved in a 1:1 mixture of THF/H₂O and followed the general ester hydrolysis conditions. A white solid was collected from the vacuum oven to yield 2-(4-(pyridin-3-yl)phenyl)quinoline-4-carboxylic acid (2 mg, 0.006 mmol, 30%). ¹H NMR (400 MHz, DMSO-*d*₆) δ 9.24 – 9.20 (m, 1H), 8.82 – 8.78 (m, 1H), 8.67 (d, *J* = 8.5, 1.5, 0.6 Hz, 1H), 8.64 – 8.61 (m, 1H), 8.56 (s, 1H), 8.50 (d, *J* = 8.5 Hz, 2H), 8.21 (d, 1H), 8.05 (d, *J* = 8.5 Hz, 2H), 7.93 – 7.85 (m, 2H), 7.78 – 7.71 (m, 1H); LCMS (ESI) 326.90 [M+H]⁺, 324.85 [M-H]⁻; HPLC Purity at 254 nm, 95.2%.



2-(4-(Pyridin-4-yl)phenyl)quinoline-4-carboxylic acid (34):

Methyl 2-(4-(pyridin-4-yl)phenyl)quinoline-4-carboxylate (14 mg, 0.04 mmol) and NaOH (62 mg, 1.59 mmol) was dissolved in a 1:1 mixture of THF/H₂O and followed the general ester hydrolysis protocol. A white solid was collected from the vacuum oven to yield 2-(4-(Pyridin-4-yl)phenyl)quinoline-4-carboxylic acid (2 mg, 0.006 mmol, 15%). ¹H NMR (400 MHz, DMSO-*d*₆) δ 8.72 – 8.66 (m, 3H), 8.39 (d, *J* = 8.3 Hz, 2H), 8.08 (s, 1H), 8.04 – 7.99 (m, 3H), 7.85 – 7.80 (m, 2H), 7.73 – 7.66 (m, 1H), 7.53 – 7.47 (m, 1H); LCMS (ESI) 326.85 [M+H]⁺ 324.80 [M-H]⁻; HPLC Chromatogram purity at 254 nm, 95.1%

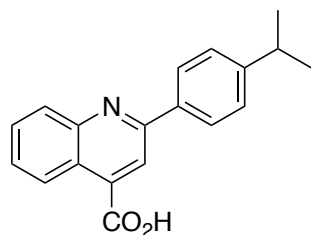
General conditions for Pfitzinger reaction: A round bottom flask containing isatin (1 eq), the corresponding acetophenone (1 eq), and KOH (3-6 eq) were dissolved in mixture of EtOH and H₂O. The mixture was heated to reflux overnight and EtOH was removed under reduced pressure upon completion. The residue was re-dissolved in 1 M KOH and washed with EtOAc (3x). The aqueous layer was acidified using HCl to pH 2-3, the solution was chilled overnight at 2-8 °C, and precipitant was collected upon filtration. Precipitant was washed with de-ionized water and used without further purification unless otherwise noted.



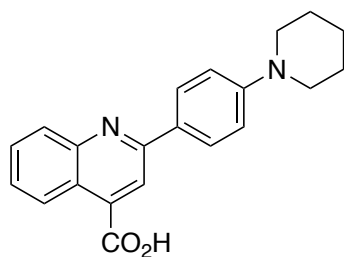
2-(4-Isobutylphenyl)quinoline-4-carboxylic acid (17):

Isatin (500 mg, 3.40 mmol), 1-(4-isobutylphenyl)ethan-1-one (0.57 mL, 3.08 mmol), and KOH (1.14 g, 20.4 mmol). were dissolved in 12 mL EtOH + 2 mL H₂O. Following the general Pfitzinger purification protocol, 2-(4-isobutylphenyl)quinoline-4-carboxylic acid was recovered as a pink solid after recrystallization from EtOH (101 mg, 0.33 mmol, 10% yield). ¹H NMR (300 MHz, DMSO-*d*₆) δ 8.68 (d, *J* = 8.4 Hz, 1H), 8.14 (d, *J* = 7.9 Hz, 2H), 8.03 – 7.94 (m, 2H), 7.66 (t, *J* =

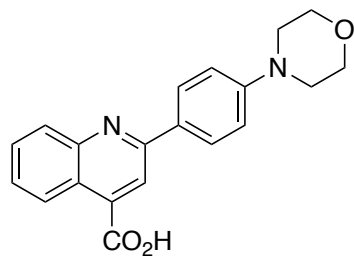
7.6 Hz, 1H), 7.46 (t, $J = 7.6$ Hz, 1H), 7.33 (d, $J = 7.9$ Hz, 2H), 2.59 – 2.52 (m, 2H), 2.00 – 1.85 (m, 1H), 0.91 (d, $J = 6.6$ Hz, 6H); **LCMS** (ESI) 306.10 $[M+H]^+$, 304.20 $[M-H]^-$; **HPLC** Purity at 254 nm, 99.9%.



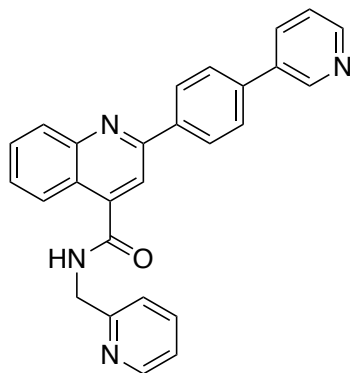
2-(4-Isopropylphenyl)quinoline-4-carboxylic acid (18): Isatin (264 mg, 1.8 mmol), 1-(4-isopropylphenyl)ethan-1-one (0.27 mL, 1.6 mmol), and KOH (275 mg, 4.92 mmol) were dissolved in 7 mL EtOH. Following the general Pfitzinger protocol, 2-(4-isopropylphenyl)quinoline-4-carboxylic acid was recovered as a tan solid (130 mg, 0.44 mmol, 28%) after recrystallization from diethyl ether and EtOH. $^1\text{H NMR}$ (400 MHz, DMSO- d_6) δ 8.65 (d, $J = 8.5, 1.3$ Hz, 1H), 8.44 (s, 1H), 8.23 (d, $J = 8.3$ Hz, 2H), 8.16 (d, $J = 8.5, 1.2$ Hz, 1H), 7.89 – 7.81 (m, 1H), 7.75 – 7.67 (m, 1H), 7.46 (d, $J = 8.3$ Hz, 2H), 3.09 – 2.94 (m, 1H), 1.28 (d, $J = 6.9$ Hz, 6H); **LCMS** (ESI) 292.20 $[M+H]^+$, 290.15 $[M-H]^-$; **HPLC** Chromatogram purity: 95.8%



2-(4-(Piperidin-1-yl)phenyl)quinoline-4-carboxylic acid (25): Isatin (247 mg, 1.7 mmol), 1-(4-(piperidin-1-yl)phenyl)ethan-1-one (200 mg, 1.0 mmol), and KOH (336 mg, 6.0 mmol) were dissolved in 7 mL EtOH and 1 mL H₂O. Following the general Pfitzinger protocol, 2-(4-(piperidin-1-yl)phenyl)quinoline-4-carboxylic acid was recovered as a red solid (88 mg, 0.27 mmol, 27%). $^1\text{H NMR}$ (400 MHz, DMSO- d_6) δ 8.59 (d, $J = 8.4$ Hz, 1H), 8.37 (s, 1H), 8.18 (d, $J = 8.6$ Hz, 2H), 8.09 (d, $J = 8.4$ Hz, 1H), 7.85 – 7.76 (m, 1H), 7.68 – 7.58 (m, 1H), 7.16 – 7.04 (m, 2H), 3.34 – 3.27 (m, 4H), 1.71 – 1.54 (m, 6H). **LCMS** (ESI) 333.25 $[M+H]^+$, 331.15 $[M-H]^-$; **HPLC** Chromatogram purity: 99.7%

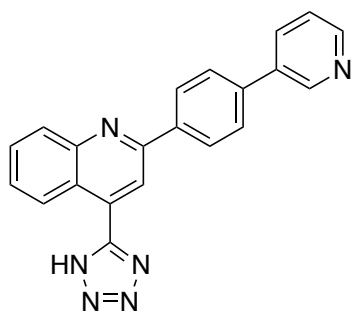


2-(4-Morpholinophenyl)quinoline-4-carboxylic acid (27): Isatin (247 mg, 1.7 mmol), 1-(4-morpholinophenyl)ethan-1-one (200 mg, 1.0 mmol), and KOH (336 mg, 6.0 mmol) were dissolved in 7 mL EtOH and 1 mL H₂O. Following the general Pfitzinger protocol, 2-(4-morpholinophenyl)quinoline-4-carboxylic acid as a bright red solid after recrystallization from EtOH (132 mg, 0.39 mmol, 39%). ¹H NMR (400 MHz, DMSO-*d*₆) δ 8.60 (d, *J* = 8.5 Hz, 1H), 8.39 (s, 1H), 8.21 (d, *J* = 8.7 Hz, 2H), 8.10 (d, *J* = 8.4 Hz, 1H), 7.85 – 7.76 (m, 1H), 7.68 – 7.59 (m, 1H), 7.11 (d, *J* = 8.7 Hz, 2H), 3.77 (t, *J* = 4.8 Hz, 4H), 3.26 (t, *J* = 4.9 Hz, 4H); LCMS (ESI) 335.90 [M+H]⁺, 333.15 [M-H]⁻; HPLC Chromatogram purity: 98.8%



N-(pyridin-2-ylmethyl)-2-(4-(pyridin-3-yl)phenyl)quinoline-4-carboxamide (36): 2-(4-(Pyridin-3-yl)phenyl)quinoline-4-carboxylic acid (50 mg, 0.15 mmol) was dissolved in 2 mL 1,2 dichloroethane and 2 drops of anhydrous DMF. SOCl₂ (0.06 mL, 0.83 mmol) was added slowly and the mixture was heated to 60 °C for 2 hours. Acid chloride formation was monitored by esterifying reaction aliquots with MeOH and TEA for TLC. After 2 hours, the mixture was concentrated under reduced pressure, dissolved in 1,2 dichloroethane, and re-concentrated (3x). The mixture was redissolved again in 2 mL 1,2 dichloroethane and added dropwise to a 0 °C stirring solution of 3-picolylamine (0.03 mL, 0.33 mmol) and triethylamine (0.17 mL, 1.22 mmol) in 1,2 dichloroethane. The mixture was stirred overnight and allowed to warm to room temperature. Upon completion, the solution was concentrated, redissolved in EtOAc and washed with brine (3x). The product was then extracted from the EtOAc through subsequent washing with 6 M HCl (3x). The acidified layer was neutralized with NaHCO₃, and

product was extracted using EtOAc (3x). The organic layer was dried with MgSO₄, filtered, concentrated, and recrystallized in 2-propanol to yield *N*-(pyridin-2-ylmethyl)-2-(4-(pyridin-3-yl)phenyl)quinoline-4-carboxamide as a beige solid (23 mg, 0.06 mmol, 39%). ¹H NMR (400 MHz, Chloroform-*d*) δ 8.98 – 8.92 (m, 1H), 8.67 – 8.63 (m, 1H), 8.59 – 8.55 (m, 1H), 8.36 – 8.30 (m, 3H), 8.28 – 8.21 (m, 1H), 8.11 (s, 1H), 8.02 – 7.95 (m, 1H), 7.84 – 7.70 (m, 4H), 7.64 – 7.58 (m, 1H), 7.47 – 7.37 (m, 2H), 7.28 – 7.26 (m, 0H), 4.94 (d, *J* = 4.8 Hz, 2H); LCMS (ESI) 417.2 [M+H]⁺; HPLC Purity at 254 nm, 98.7%



2-(4-(Pyridin-3-yl)phenyl)-4-(1*H*-tetrazol-5-yl)quinoline (37): 2-

(4-(Pyridin-3-yl)phenyl)quinoline-4-carboxylic acid (25 mg, 0.08 mmol) was dissolved in 2 mL of 7 N NH₃ in MeOH. The mixture was refluxed for 36 hours. Upon completion, the mixture was concentrated and product was used without further purification. Following a modification protocol from Borkin *et al.*²⁷, the residue was re-dissolved in 3 mL of POCl₃ and heated to 100 °C for 24 hours. The mixture was concentrated and used without further purification. A modified protocol of Lassig's *et al.*²⁸ was followed for the next step and the residue was re-dissolved in anhydrous DMF with NaN₃ (3 mg, 0.05 mmol) and NH₄Cl (3 mg, 0.05 mmol) and heated to 120 °C for 24 hours. Upon completion, the mixture was concentrated and product was purified by reverse phase preparatory chromatography. 2-(4-(Pyridin-3-yl)phenyl)-4-(1*H*-tetrazol-5-yl)quinoline was recovered as an amorphous solid (3 mg, 0.01 mmol, 13% yield over 3 steps). ¹H NMR (300 MHz, Methanol-*d*₄) δ 9.01 – 8.95 (m, 1H), 8.84 (d, *J* = 8.7 Hz, 1H), 8.60 (s, 1H), 8.55 (s, 1H), 8.43 (d, *J* = 8.3 Hz, 2H), 8.31 – 8.21 (m, 2H), 7.94 (d, *J* = 8.4 Hz, 2H), 7.92 – 7.84 (m, 1H), 7.74 – 7.59 (m, 2H); LCMS (ESI) 351.2 [M+H]⁺, 349.2 [M-H]⁻; HPLC Purity at 254 nm, 96.2%.

hDHODH expression and purification. DHODH expression and purification followed the protocol published by Madak *et al.*³⁹ The *h*DHODH construct was provided by the De Brabander lab at UT Southwestern.³⁷ *h*DHODH was expressed in *E. coli* Rosetta 2 (DE3) in LB medium with ampicillin (100 µg/mL) and 0.1 mM FMN. Cells were grown at 37 °C to OD₆₀₀ = 0.6, then induced with 1 mM IPTG for 3 hours. Cells were harvested by centrifugation at 4,000 x g for 15 min at 4 °C. The pellet was re-suspended in lysis buffer (50 mM Tris-HCl, pH 8.5, 300 mM NaCl, 10% glycerol, 5 mM β-mercaptoethanol, 10 mM imidazole, 2% Triton X-100, 0.5 mM FMN, 200 µM PMSF, 1 mg/mL lysozyme). The cell suspension was incubated on ice for 2 hours, followed by sonication. The lysate was clarified by centrifugation at 35,000 x g for 20 min at 4 °C. After the supernatant was incubated with Ni-NTA resin for 1 h at 4 °C, the resin was loaded onto a column. The column was washed with wash buffer (50 mM Tris-HCl, pH 8.5, 300 mM NaCl, 10% glycerol, 5 mM β-mercaptoethanol, 25 mM imidazole, 0.1 mM FMN) and *h*DHODH was eluted with elution buffer (wash buffer containing 300 mM imidazole). Buffer exchange was carried out using an Amicon concentrator into storage buffer (100 mM HEPES, pH 8.0, 150 mM NaCl, 10% glycerol) and *h*DHODH was stored at -80 °C.

DHODH activity assay. DHODH activity was monitored using the same protocol published by Madak *et al.*³⁹ DHODH activity was monitored as previously described with modifications.³⁵ First, 1 µL of test compound (50x) or DMSO, 60 nM DHODH, 100 µM DCIP, and 20 µM CoQ₁₀ (final concentrations for 50 µL) in the assay buffer (100 mM HEPES pH 8.0, 150 mM NaCl, 10% glycerol, 0.1% Triton X-100) in a total of 40 µL were incubated together for 30 min. The assay began with the addition of 10 µL of dihydroorotate to a final concentration of 200 µM. The reduction of DCIP was measured by monitoring the absorbance at 600 nm over 1 hr at room temperature using a microplate reader (BMG Labtech). Data were exported to Microsoft Excel for analysis and IC₅₀ values were determined using Prism 6 software.

Cell culture. Cells were cultured following the protocol described by Madak *et al.*³⁹ HCT116 P53 +/+ and MiaPaca-2 cells were maintained in RPMI-1640 (Gibco) supplemented with 10% heat-inactivated FBS (Gibco). Cells were grown at 37 °C in a humidified atmosphere of 5% CO₂. For subculture and counting, cells were washed with DPBS (Gibco) without calcium or magnesium, incubated with 0.25% trypsin-EDTA solution (Gibco) for 5 min, neutralized with full medium, centrifuged, re-suspended with culture medium and counted by Countess II FL. All

experiments were performed using cells in exponential growth. Cells were checked for Mycoplasma contamination.

Growth inhibition assay. Growth inhibition assay followed the same protocol published by Madak *et al.*³⁹ HCT116 p53+/+ cells or MiaPaCa-2 cells were seeded 2500-3000 cells per well in 96-well microtiter plates, and allowed to attach overnight before the addition of the serial dilution of compounds (10X). After 72h, cells were incubated with 0.3 mg/mL 3-(4,5-dimethylthiazol-2-yl)-2,5-diphenyltetrazolium bromide (VWR) for an additional 3h at 37 °C. After removal of the supernatant, DMSO was added to the wells, and the absorbance was read at 570 nm. All assays were performed in triplicate. Percentage of cell growth inhibition was expressed as $(1 - A/C) \times 100\%$ (A and C were the absorbance values from experimental and control cells, respectively). IC₅₀ values were determined for each drug from nonlinear regression analysis of log (drug concentration) vs. percentage of cell growth inhibition using Prism 7.0. SD or SEM was calculated based on the IC₅₀ values obtained from at least three independent experiment.

2.11 References

1. Garrido-Laguna, I.; Hidalgo, M. Pancreatic cancer: from state-of-the-art treatments to promising novel therapies. *Nature Reviews Clinical Oncology* **2015**, *12*, 319.
2. Steeg, P. S. Targeting metastasis. *Nat Rev Cancer* **2016**, *16*, 201-18.
3. Coghlin, C.; Murray, G. I. Current and emerging concepts in tumour metastasis. *J Pathol* **2010**, *222*, 1-15.
4. Shewach, D. S.; Kuchta, R. D. Introduction to cancer chemotherapeutics. *Chem Rev* **2009**, *109*, 2859-61.
5. Rebelo, A.; Molpeceres, J.; Rijo, P.; Reis, C. P. Pancreatic Cancer Therapy Review: From Classic Therapeutic Agents to Modern Nanotechnologies. *Curr Drug Metab* **2017**, *18*, 346-359.
6. Housman, G.; Byler, S.; Heerboth, S.; Lapinska, K.; Longacre, M.; Snyder, N.; Sarkar, S. Drug resistance in cancer: an overview. *Cancers (Basel)* **2014**, *6*, 1769-92.

7. Shanafelt, T. D.; Loprinzi, C.; Marks, R.; Novotny, P.; Sloan, J. Are Chemotherapy Response Rates Related to Treatment-Induced Survival Prolongations in Patients With Advanced Cancer? *Journal of Clinical Oncology* **2004**, *22*, 1966-1974.
8. Holohan, C.; Van Schaeybroeck, S.; Longley, D. B.; Johnston, P. G. Cancer drug resistance: an evolving paradigm. *Nature Reviews Cancer* **2013**, *13*, 714.
9. Society, A. C. Pancreatic Cancer Survival Rates, by Stage. <https://www.cancer.org/cancer/pancreatic-cancer/detection-diagnosis-staging/survival-rates.html> (27 November).
10. Hutchinson, L.; Kirk, R. High drug attrition rates—where are we going wrong? *Nature Reviews Clinical Oncology* **2011**, *8*, 189.
11. Swinney, D. C.; Anthony, J. How were new medicines discovered? *Nature Reviews Drug Discovery* **2011**, *10*, 507.
12. Lipinski, C. A. Lead- and drug-like compounds: the rule-of-five revolution. *Drug Discov Today Technol* **2004**, *1*, 337-41.
13. Baell, J.; Walters, M. A. Chemistry: Chemical con artists foil drug discovery. *Nature* **2014**, *513*, 481-3.
14. Shu, Y. Z.; Johnson, B. M.; Yang, T. J. Role of biotransformation studies in minimizing metabolism-related liabilities in drug discovery. *AAPS J* **2008**, *10*, 178-92.
15. Kumar, G. N.; Surapaneni, S. Role of drug metabolism in drug discovery and development. *Med Res Rev* **2001**, *21*, 397-411.
16. Dexter, D. L.; Hesson, D. P.; Ardecky, R. J.; Rao, G. V.; Tippett, D. L.; Dusak, B. A.; Paull, K. D.; Plowman, J.; DeLarco, B. M.; Narayanan, V. L.; et al. Activity of a novel 4-quinolinecarboxylic acid, NSC 368390 [6-fluoro-2-(2'-fluoro-1,1'-biphenyl-4-yl)-3-methyl-4-quinolinecarb oxylic acid sodium salt], against experimental tumors. *Cancer Res* **1985**, *45*, 5563-8.
17. Kaila, N.; Janz, K.; DeBernardo, S.; Bedard, P. W.; Camphausen, R. T.; Tam, S.; Tsao, D. H.; Keith, J. C., Jr.; Nickerson-Nutter, C.; Shilling, A.; Young-Sciame, R.; Wang, Q. Synthesis and biological evaluation of quinoline salicylic acids as P-selectin antagonists. *J Med Chem* **2007**, *50*, 21-39.
18. Bento, A. P.; Gaulton, A.; Hersey, A.; Bellis, L. J.; Chambers, J.; Davies, M.; Krüger, F. A.; Light, Y.; Mak, L.; McGlinchey, S.; Nowotka, M.; Papadatos, G.; Santos, R.; Overington, J.

- P. The ChEMBL bioactivity database: an update. *Nucleic Acids Research* **2014**, 42, D1083-D1090.
19. Chen, S. F.; Papp, L. M.; Ardecky, R. J.; Rao, G. V.; Hesson, D. P.; Forbes, M.; Dexter, D. L. Structure-activity relationship of quinoline carboxylic acids. A new class of inhibitors of dihydroorotate dehydrogenase. *Biochem Pharmacol* **1990**, 40, 709-14.
20. Liu, S.; Neidhardt, E. A.; Grossman, T. H.; Ocain, T.; Clardy, J. Structures of human dihydroorotate dehydrogenase in complex with antiproliferative agents. *Structure* **2000**, 8, 25-33.
21. Kim, Y. J.; Borsig, L.; Varki, N. M.; Varki, A. P-selectin deficiency attenuates tumor growth and metastasis. *Proc Natl Acad Sci U S A* **1998**, 95, 9325-30.
22. Zhu, W.; Depamphilis, M. L. Selective killing of cancer cells by suppression of geminin activity. *Cancer Res* **2009**, 69, 4870-7.
23. Yang, J.; Liu, S.; Zheng, J.-F.; Zhou, J. Room-Temperature Suzuki–Miyaura Coupling of Heteroaryl Chlorides and Tosylates. *European Journal of Organic Chemistry* **2012**, 2012, 6248-6259.
24. Donohoe, T. J.; Jones, C. R.; Barbosa, L. C. Total synthesis of (+/-)-streptonigrin: de novo construction of a pentasubstituted pyridine using ring-closing metathesis. *J Am Chem Soc* **2011**, 133, 16418-21.
25. Miyaura, N.; Suzuki, A. Palladium-Catalyzed Cross-Coupling Reactions of Organoboron Compounds. *Chemical Reviews* **1995**, 95, 2457-2483.
26. Motoshima, K.; Hiwasa, Y.; Yoshikawa, M.; Fujimoto, K.; Tai, A.; Kakuta, H.; Sasaki, K. Antimalarial Cation-dimers Synthesized in Two Steps from an Inexpensive Starting Material, Isonicotinic Acid. *ChemMedChem* **2007**, 2, 1527-1532.
27. Borkin, D.; Pollock, J.; Kempinska, K.; Purohit, T.; Li, X.; Wen, B.; Zhao, T.; Miao, H.; Shukla, S.; He, M.; Sun, D.; Cierpicki, T.; Grembecka, J. Property Focused Structure-Based Optimization of Small Molecule Inhibitors of the Protein-Protein Interaction between Menin and Mixed Lineage Leukemia (MLL). *J Med Chem* **2016**, 59, 892-913.
28. Lassig, D.; Lincke, J.; Moellmer, J.; Reichenbach, C.; Moeller, A.; Glaser, R.; Kalies, G.; Cychosz, K. A.; Thommes, M.; Staudt, R.; Krautscheid, H. A microporous copper metal-organic framework with high H₂ and CO₂ adsorption capacity at ambient pressure. *Angew Chem Int Ed Engl* **2011**, 50, 10344-8.
29. King, S. Y.; Basista, A. M.; Torosian, G. Self-association and solubility behaviors of a novel anticancer agent, brequinar sodium. *J Pharm Sci* **1989**, 78, 95-100.

30. The Oncomine™ Platform (Thermo. FFisher, Ann Arbor, MI) was used for analysis and visualization or further information, refer to the terms of use. Oncomine Source: <https://www.oncomine.com/resource/main.html> - [dsogeneOverex;ec:\[2\];epv:150001.151078,3508;g:1723;pg:1;pvf:10222;scr:summary;v:18](https://www.oncomine.com/resource/main.html?dsogeneOverex;ec:[2];epv:150001.151078,3508;g:1723;pg:1;pvf:10222;scr:summary;v:18)
31. Schwartzmann, G.; Peters, G. J.; Laurensse, E.; de Waal, F. C.; Loonen, A. H.; Leyva, A.; Pinedo, H. M. DUP 785 (NSC 368390): schedule-dependency of growth-inhibitory and antiprimidine effects. *Biochem Pharmacol* **1988**, 37, 3257-66.
32. Peters, G. J.; Sharma, S. L.; Laurensse, E.; Pinedo, H. M. Inhibition of pyrimidine de novo synthesis by DUP-785 (NSC 368390). *Invest New Drugs* **1987**, 5, 235-44.
33. Chen, S. F.; Ruben, R. L.; Dexter, D. L. Mechanism of action of the novel anticancer agent 6-fluoro-2-(2'-fluoro-1,1'-biphenyl-4-yl)-3-methyl-4-quinolinecarboxylic acid sodium salt (NSC 368390): inhibition of de novo pyrimidine nucleotide biosynthesis. *Cancer Res* **1986**, 46, 5014-9.
34. Peters, G. J.; Kraal, I.; Pinedo, H. M. In vitro and in vivo studies on the combination of Brequinar sodium (DUP-785; NSC 368390) with 5-fluorouracil; effects of uridine. *Br J Cancer* **1992**, 65, 229-33.
35. Baldwin, J.; Michnoff, C. H.; Malmquist, N. A.; White, J.; Roth, M. G.; Rathod, P. K.; Phillips, M. A. High-throughput screening for potent and selective inhibitors of Plasmodium falciparum dihydroorotate dehydrogenase. *J Biol Chem* **2005**, 280, 21847-53.
36. Reis, R. A. G.; Calil, F. A.; Feliciano, P. R.; Pinheiro, M. P.; Nonato, M. C. The dihydroorotate dehydrogenases: Past and present. *Arch Biochem Biophys* **2017**, 632, 175-191.
37. Das, P.; Deng, X.; Zhang, L.; Roth, M. G.; Fontoura, B. M.; Phillips, M. A.; De Brabander, J. K. SAR Based Optimization of a 4-Quinoline Carboxylic Acid Analog with Potent Anti-Viral Activity. *ACS Med Chem Lett* **2013**, 4, 517-521.
38. Gottlieb, H. E.; Kotlyar, V.; Nudelman, A. NMR Chemical Shifts of Common Laboratory Solvents as Trace Impurities. *J Org Chem* **1997**, 62, 7512-7515.
39. Madak, J. T.; Cuthbertson, C. R.; Chen, W.; Showalter, H. D.; Neamati, N. Design, Synthesis, and Characterization of Brequinar Conjugates as Probes to Study DHODH Inhibition. *Chemistry* **2017**, 23, 13875-13878.

Chapter 3

Design, Synthesis, and Biological Evaluation of 4-Quinoline Carboxylic Acids as Inhibitors of Dihydroorotate Dehydrogenase^c

3.1 Introduction

Dihydroorotate dehydrogenase (DHODH) catalyzes the oxidation of dihydroorotate to orotate, which represents a committed step in the *de novo* pyrimidine biosynthesis pathway.^{1,2} Inhibitors of DHODH induce pyrimidine depletion and halt cell cycle progression at S-phase, where a sufficient concentration of nucleotides is required for continued growth.³ Beyond directly halting cell growth, DHODH inhibitors sensitize cells to doxorubicin⁴, fludarabine,^{5,6} and TRAIL therapy.⁷ Additionally, PTEN-deficient cancer cells are significantly sensitive to DHODH inhibition.⁸ DHODH inhibitors have also been shown to induce differentiation and to thwart self-renewal capacity of different cell types.^{9,10} Collectively, these studies bolster interest for DHODH as an anticancer target.

Previous DHODH inhibitors have failed in clinical trials as single agents and in selected drug combinations for the treatment of various cancers. This includes the well-known DHODH inhibitors, brequinar (**2**) and leflunomide (**45**, Figure 3.1), which have not demonstrated widespread success in anticancer clinical trials. Despite promising preclinical data, brequinar failed to generate an objective response in multiple phase II clinical trials for breast,¹¹ colon,¹² head and neck,¹³ gastrointestinal,¹⁴ lung,¹⁵ and skin¹⁶ cancers. Brequinar sodium has poor water solubility (< 0.10 mg/mL in room temperature water at pH 7.4) and molecular aggregation occurs at high concentrations.¹⁷ In addition, common serum electrolytes, such as sodium chloride have been demonstrated to reduce aqueous solubility by over 200-fold.¹⁷ As such, a previous attempt to utilize brequinar in combination with cyclosporine A changed brequinar's pharmacokinetic profile in which its terminal half-life was extended and oral clearance rate was lowered.¹⁸ Altered pharmacokinetic properties such as this present a significant liability for safe

^c **Author contributions:** Joseph Madak designed, synthesized, and characterized all compounds. Christine Cuthbertson and Yoshinari Miyata evaluated compounds in biochemical and cellular assays. Elyse Petrunak and Dr. Jeanne Stuckey generated and solved co-crystal structures. Dr. Duxin Sun, Yanyan Han, and Miao He evaluated the compounds pharmacokinetic properties. Dr. Hollis Showalter and Dr. Nouri Neamati are corresponding authors.

dosing, thus limiting the selection of potential patient populations for combination therapy. Leflunomide, an FDA approved drug for rheumatoid and psoriatic arthritis,¹⁹ is currently being evaluated as a single agent in clinical trials for multiple myeloma (ClinicalTrials.gov, NCT02509052)²⁰ but is no longer being evaluated in combination with vemurafenib for melanoma (ClinicalTrials.gov, NCT01611675).²¹ Leflunomide is a reported agonist for the aryl-hydrocarbon receptor, which controls expression of drug metabolizing enzymes.^{22, 23} Despite the disappointing results of both these agents in clinical trials, we feel that DHODH remains a promising anticancer target awaiting the discovery of a small molecule inhibitors with better drug-like properties. Additionally, we believe that DHODH presents a vital anticancer target for combination therapy. In this chapter, we report the design and synthesis of novel class of brequinar-like inhibitors toward the discovery of agents with improved physicochemical properties, principally better aqueous solubility that we hypothesized would translate into improved enzyme and cellular potency.

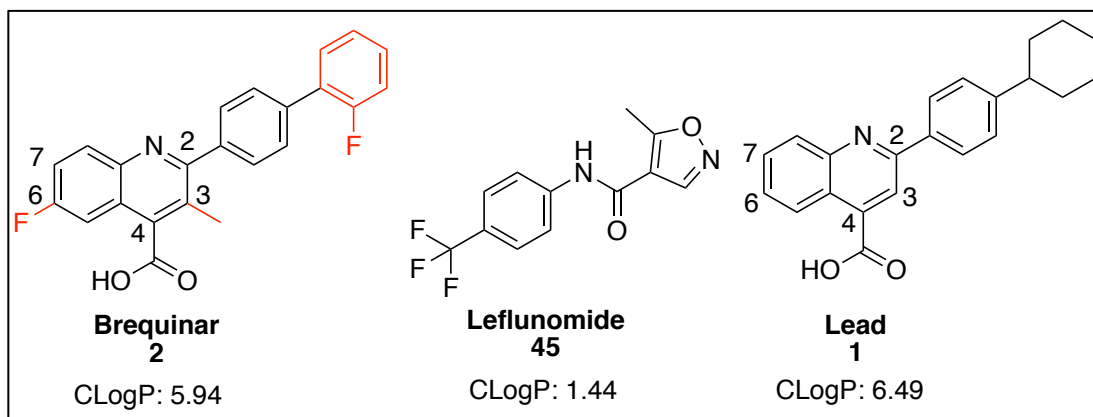


Figure 3.1. Selected DHODH inhibitors

3.2 Analogue Design

Our project was guided by the basic pharmacophore interactions between brequinar and DHODH. Initially, we began with an unbiased cell-based screening approach to identify new small molecule hits possessing antiproliferative properties. This led to lead compound (**1**) that showed potent DHODH activity ($IC_{50} = 0.347 \pm 0.072 \mu M$) (Figure 3.1). We postulated that **1** occupies a similar binding site as brequinar based on its structural similarity. The brequinar binding pocket of DHODH is primarily filled with nonpolar residues, therefore requiring lipophilic moieties. A high-resolution co-crystal structure of DHODH with a brequinar analogue (PDB: 1D3G) provided insight into the essential pharmacophore.²⁴ The carboxylate of brequinar

forms a salt bridge with R136 and a potential hydrogen bond interaction with Q47, exemplifying the importance of the carboxylic acid.^{24, 25} The remaining interactions between brequinar and DHODH occur in a hydrophobic channel with the biphenyl group or the quinoline core.²⁶ To develop a DHODH inhibitor with a lower cLogP, we identified sites where ring heteroatom replacements could be tolerated toward enhancing binding without disrupting the essential pharmacophore.

Two potential regions were identified for the formation of new electrostatic interactions. The first region, located within a hydrophobic channel has two hydroxyls, one on Y38 and another on T63. Each region is in close proximity to form an interaction with the *meta* position of the distal phenyl of a brequinar analogue (Figure 3.2).²⁴ The distance is suitable for an H-bonding interaction and, if achieved, may provide an inhibitor with improved enthalpy-driven potency and a lower cLogP.²⁷ Additionally, the hydroxyl of Y356 is nearly 2.5 Å away from C7 on the quinoline ring (Figure 3.2) and presents another opportunity to form an electrostatic interaction. With these residues in mind, we postulated that strategically positioned H-bond acceptors on the brequinar pharmacophore would improve potency while lowering the cLogP. The overall decrease in cLogP should significantly improve the aqueous solubility leading to inhibitors with better drug-like properties.

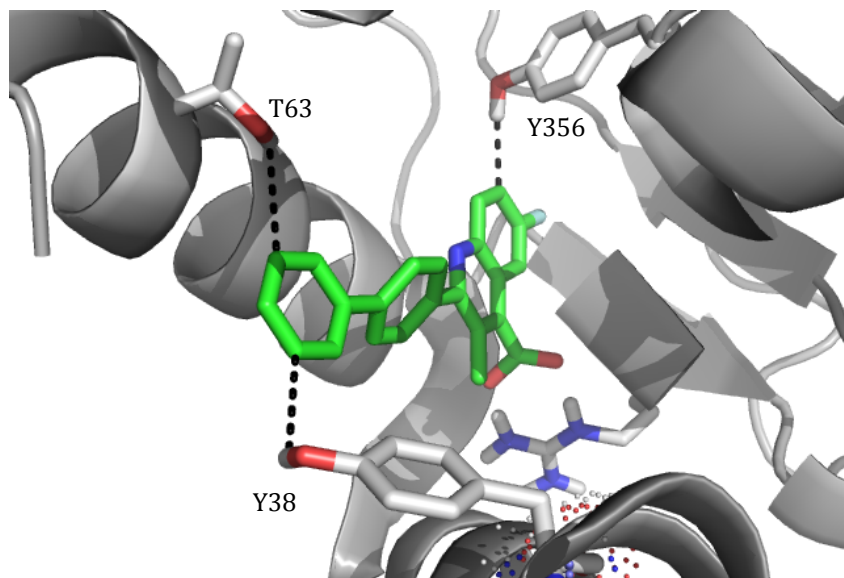


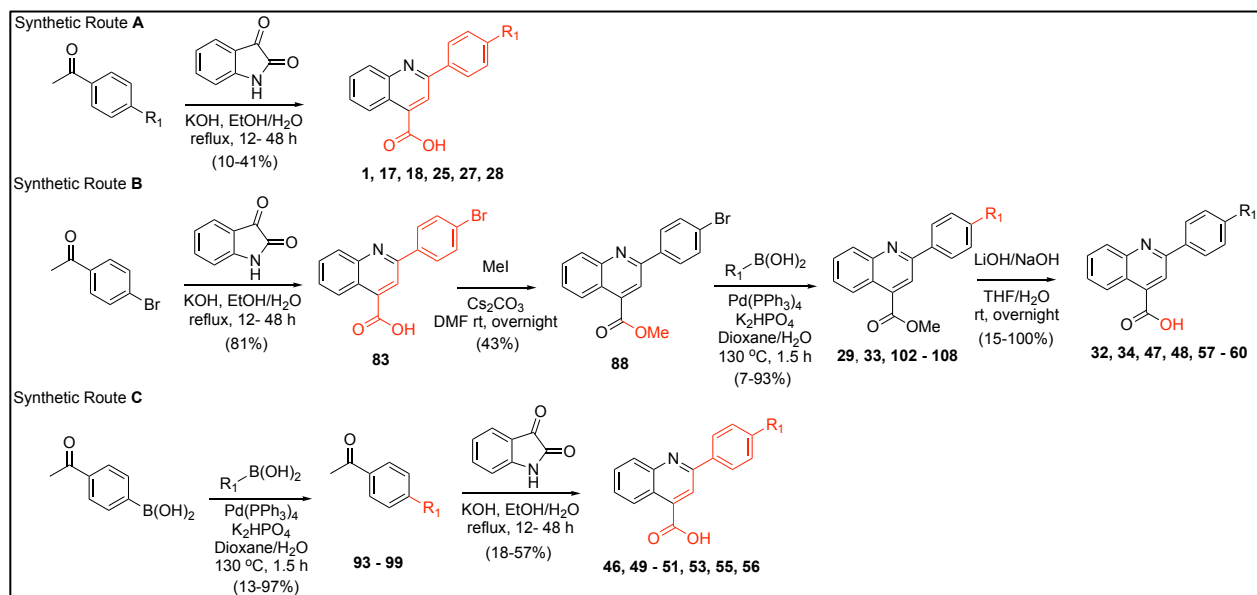
Figure 3.2. Co-crystal structure of a brequinar analogue in DHODH with new proposed interactions. Proposed interactions are depicted. Y356 is 2.5 Å from C7 of the quinoline ring; Y38 and T63 are 3.7 Å, 3.9 Å respectively from the meta position of the second phenyl ring.

Measurements were calculated from the hydrogen of side chain hydroxyl groups. Figure generated using PDB file 1D3G, resolution 1.6 Å.

To optimize our screening lead, designed analogues were evaluated in the DHODH enzyme assay and MTT assay. We sought to develop analogues with a lower cLogP that may interact with T63 and Y356. Obviously, reducing the cLogP with analogues containing an ionizable acid could significantly reduce cellular permeability. However, we rationalized that, if necessary, an improved DHODH inhibitor could utilize a pro-drug strategy to address this issue.²⁹ Therefore, our optimization process was primarily informed by a DHODH enzyme assay. Cellular activity was evaluated in HCT-116, a colon cancer cell line, and MIA PaCa-2, a pancreatic cancer cell line. Colon cancer has a high expression of DHODH and HCT-116 is sensitive to DHODH inhibition (Figure 2.4). DHODH is not overexpressed in pancreatic cancer and should be less sensitive to DHODH inhibitors. Collectively, these two cell lines may help distinguish between DHODH induced growth inhibition and potential off-target effects. Additionally, cLogP and LipE calculators were utilized to approximate aqueous solubility.²⁸

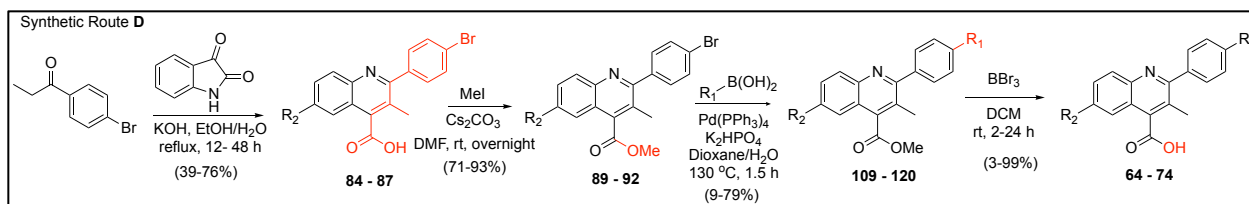
3.3 Synthesis

The synthesis of analogues containing the quinoline core utilized the classic Pfitzinger condensation.³⁰ 2,4-Substituted quinoline analogues were generated using synthetic routes **A-C** (Scheme 3.1). Route **A** generates analogues in one step. However, this approach was limited primarily to commercially available 4'-substituted acetophenones. To expand our SAR beyond these limitations, we developed routes **B** and **C**, which introduce diversity through carbon-carbon bond coupling via the Suzuki reaction on suitable precursors. These routes differ principally when such couplings take place with a phenyl-R₁ moiety generated at a late and early stage, respectively. The advantage of Route **B** (Scheme 3.1) is that R₁ moieties sensitive to the harsh Pfitzinger reaction conditions can be successfully installed, whereas Route **C** (Scheme 3.1) is less tolerant to such moieties.



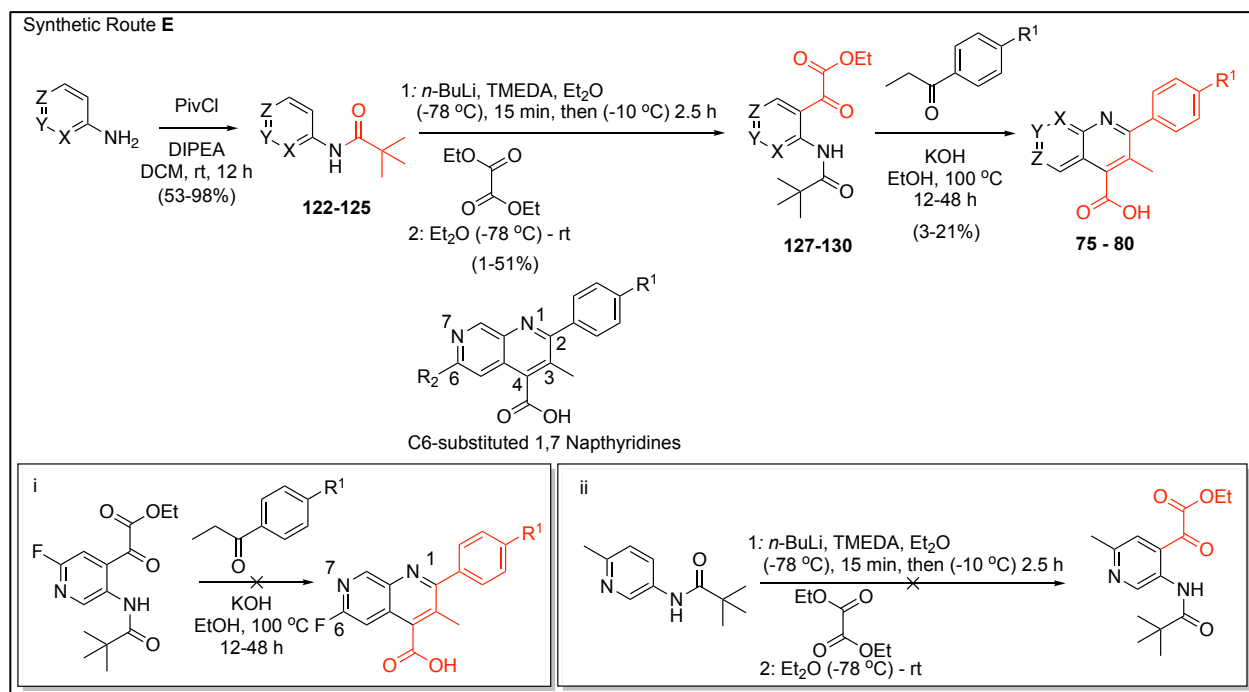
Scheme 3.1. Synthesis of quinoline analogues without a C3 methyl group.

Analogues containing a C3 methyl were incorporated through the Pfitzinger reaction with the appropriate 4'-bromopropiophenone (**84-87**, Scheme 3.2). Surprisingly, Fischer-Speier esterification conditions were low-yielding on carboxylic acid analogues containing the C3 methyl. Alternatively, methyl ester analogues (**89-92**) were obtained through generation of the cesium salt of the carboxylic acid followed by exposure to iodomethane. Subsequent Suzuki coupling was used for installation of the terminal R_1 substituent (**109-120**). However, the C3 methyl thwarted mild ester hydrolysis, therefore harsher conditions with strong base ($> 60^\circ\text{C}$ with NaOH) were required for the reaction to occur. Unfortunately, this favored side product formation with little to no generation of acid, thus alternative deprotection methods were evaluated. Gratifyingly, the carboxylic acid could be unveiled upon exposure to BBr_3 in dichloromethane at room temperature with minimal side product formation (**64-74**, Scheme 3.2).



Scheme 3.2. Synthesis of quinoline analogues with a C3 methyl substituent.

Additional analogues were generated to evaluate a scaffold hop from the quinoline series to the synthetically challenging naphthyridines. As previously noted, we postulated that Y356 is close enough to potentially form an H-bond interaction with the 7'-nitrogen of a 1,7-naphthyridine (Figure 3.2, Scheme 3.3). Initial attempts to generate the naphthyridine core focused on oxidation of aza-indoles to yield the corresponding aza-isatin for subsequent Pfitzinger condensation. However, reactions involving PCC oxidation³¹ or a reusable poly-aniline catalyst³² on 1,6-aza-indoles did not provide the desired 1,6-aza-isatin. Inspired by the work of Stockmann *et al.*³³ and Zong *et al.*,³⁴ we sought to generate our naphthyridine series by installing an α -keto ester on an aminopyridine amide precursor,³⁴ which would provide an intermediate for a subsequent Pfitzinger condensation. Drawing on the work of Turner *et al.*,³⁵ Meanwell *et al.*,³⁶ and Zong *et al.*,³⁴ we generated our desired intermediate through directed metalation to control regioselectivity as shown in Scheme 3.3. A pivaloyl amide (**122-125**) was utilized to direct ortho-lithiation. Exposure of the intermediate to *n*-BuLi/TMEDA complex under strict temperature control provided the anion, which was then quenched with diethyl oxalate to give the key α -keto-ester (**127-130**). This intermediate was then used to generate the naphthyridine (**75-80**) through base-catalyzed cyclization under Pfitzinger-type reaction conditions.

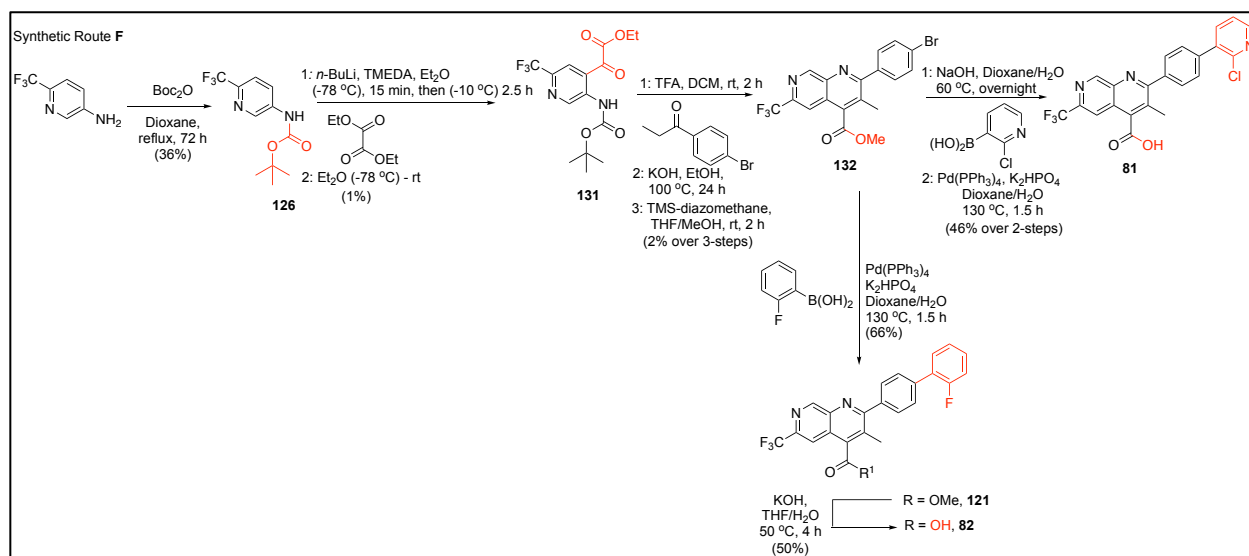


Scheme 3.3. Synthesis of naphthyridine core analogues.

The synthesis of C6 substituted 1,7-naphthyridines presented an obstacle for SAR evaluation. Attempts to generate the C6-fluoro substituted 1,7-naphthyridine were foiled by the harsh reaction conditions necessary for the Pfitzinger cyclization (Scheme 3.3, Box i). The high temperatures and basic conditions favor fluorine displacement through an S_NAr mechanism, which would likely proceed at a faster rate than the cyclization reaction. LCMS studies indicated that when the reaction temperature was above 50 °C, the fluorine was displaced under basic conditions within a few hours. Attempts to generate the C6 substituted methyl analogue were foiled during the ortho-lithiation protocol, as the excess of *n*-BuLi favored kinetic deprotonation of the methyl group and led to a variety of unwanted side products (Scheme 3.3, Box ii). To overcome this difficulty, we focused on generation of the C6 trifluoromethyl analogue and were gratified to generate the product through ortho-lithiation (Scheme 3.3), despite low yields.

The overall low yield of our synthetic route to 1,7-naphthyridines presented an obstacle to expanding the SAR around this core. Efforts to improve the ortho-lithiation/acylation step initially focused on improving the electrophile's reactivity. The diethyl oxalate electrophile was replaced with asymmetric electrophiles such as ethyl chlorooxoacetate or ethyl 2-(methoxy(methyl)amino)-2-oxoacetate (Weinreb amide derivative), but without any yield enhancement. We then shifted our efforts to improving the Pfitzinger cyclization reactions

(Scheme 3.3, (c)). LCMS traces indicated that ester hydrolysis was followed by decarboxylation, which occurred at a faster rate than hydrolysis of the pivaloyl amide, resulting in low yields of cyclization product. To avoid the unwanted decarboxylation, we decided to swap the ortho-lithiating pivaloyl amide group with a Boc carbamate. Formation of the oxalate ester followed by mild Boc acid hydrolysis could then unmask the amine needed for intramolecular cyclization onto an α -keto acid. The reduction of this to practice is shown in Scheme 3.4. With the α -keto ester intermediate **131** in hand, acid hydrolysis unveiled the amine, followed by condensation with the 4'-bromopropionone and cyclization to provide the key 1,7-naphthyridine intermediate. Methyl esterification via a cesium salt/methyl iodide failed, but was successful using TMS-diazomethane to give **132**. Suzuki coupling resulting in installation of the terminal 2-fluorophenyl substituent was followed by methyl ester hydrolysis to yield the final product (Scheme 3.4, **82**). Alternatively, initial ester hydrolysis followed by Suzuki coupling on the resultant carboxylic acid successfully yielded final product **81** (Scheme 3.4). With the improved reaction conditions, we were able to incorporate the C6 CF₃ substituent into the 1,7-naphthyridine scaffold. This methodology should be readily amenable to the synthesis of additional naphthyridine analogues.

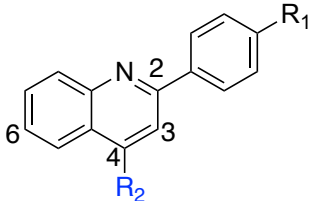


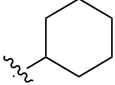
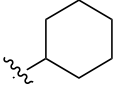
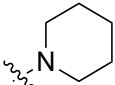
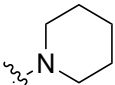
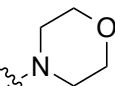
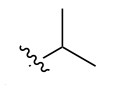
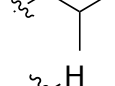
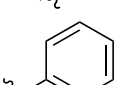
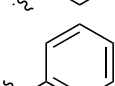
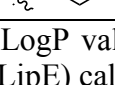
Scheme 3.4. Synthesis of naphthyridine core analogues with terminal diversity.

3.4 Structure activity relationships

Our initial goal was to validate that our synthesized analogues followed the same SAR trends (Table 3.1) as observed previously for the brequinar series.²⁵ With screen lead **1** and subsequent analogues, we noted an immediate decrease in potency for analogues containing a methyl ester substituent (e.g., compare **1** to **23**, Table 3.1). Attempts to lower cLogP by incorporating piperidine (**25**) or morpholine (**27**) moieties were not well tolerated and resulted in a marked potency decrease in comparison to **1**. Replacement of the cyclohexyl group with branched aliphatic groups (**17**, **18**) maintained modest potency in the DHODH assay, but were far less potent than **3**. As expected, replacement of the cyclohexyl ring with a phenyl ring resulted in potency enhancement (**28**). This analogue has a lower cLogP than **1** but substitution of the conformationally flexible cyclohexyl with the planar phenyl allows for formation of stacking interactions at high concentrations in aqueous solutions. In cells, there is a strong correlation with DHODH inhibition and HCT-116 growth inhibition. Inhibitors with a lower DHODH IC₅₀ were generally more potent in HCT-116 cells than MIA PaCa-2 cells (e.g. **1**, **28**). Overall, these SAR trends are consistent with those observed for established DHODH inhibitors and suggest that our inhibitors bind in a similar pocket as brequinar.²⁵ To further confirm that DHODH is the primary target for cell growth inhibition, we evaluated screen lead **1** in the presence of excess uridine, a nucleoside capable of entering the pyrimidine salvage pathway which overcomes DHODH inhibition.^{37, 38} In the absence of uridine, cells are susceptible to growth inhibition by **1** and brequinar (Chapter 2, Figure 2.5). However, uridine supplementation (5 μM) significantly decreased cell growth inhibition (below 50%), suggesting **1** inhibits an enzyme upstream of uridine nucleotide production. This data strengthened our initial postulation that **1** has a similar mechanism of action as brequinar, which shifted our attention towards incorporation of H-bond acceptors into our next set of analogues.

Table 3.1. Biological activity of quinolines with selected R₁ substituents.^a



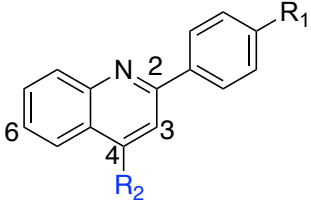
#	R ₁	R ₂	DHODH Assay		LipE	MTT Assay	
			IC ₅₀ (μM)	cLogP		HCT-116 IC ₅₀ (μM)	MIA PaCa-2 IC ₅₀ (μM)
2 (Breq)			0.020 ± 0.02	5.94		0.98 ± 0.52	7.4 ± 2.3
1		CO ₂ H	0.347 ± 0.072	6.49	0.03	7.40 ± 1.50	18.8 ± 12
23		CO ₂ Me	> 200	6.72	NA	> 100	> 100
25		CO ₂ H	10.2 ± 1.6	4.71	0.28	24.3 ± 14	57.0 ± 13
24		CO ₂ Me	> 200	4.93	NA	54.5 ± 24	55.7 ± 26
27		CO ₂ H	130 ± 52	3.23	0.66	> 100	> 100
18		CO ₂ H	3.70 ± 0.40	5.30	0.13	52.2 ± 23	> 100
17		CO ₂ H	1.60 ± 1.00	5.83	0.03	16.9 ± 6.3	> 100
6		CO ₂ H	124 ± 48	3.87	0.04	> 100	> 100
28		CO ₂ H	0.0721 ± 0.046	5.76	1.38	1.10 ± 1.0	16.2 ± 14
29		CO ₂ Me	> 200	5.98	NA	13.1 ± 5.3	27.9 ± 15

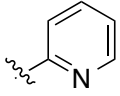
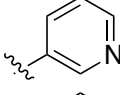
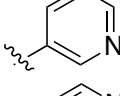
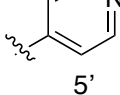
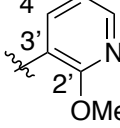
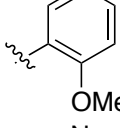
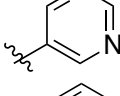
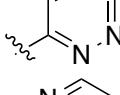
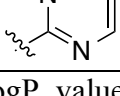
^aData for cLogP values was predicted using ChemBioDraw Professional 16, Lipophilic ligand efficiency (LipE) calculated LipE = pIC₅₀(M) – cLogP.²⁸

Pyridine rings were incorporated at the R₁ to probe for potential interactions with Y38 and T63. Our first goal was to evaluate positional pyridine isomers (Table 3.2). In the DHODH assay, the pyridine analogue **32** is 10- and 6-fold more potent than pyridine analogues **46** and **34**, respectively. This potency difference between **32**, **34**, and **46** suggests a potential interaction

between the pyridine nitrogen of **32** and DHODH. In cells, **32** has a modest effect on cell growth in the HCT-116 line. In contrast, the methyl ester analogue **33** is inactive in the DHODH assay but possesses improved cytotoxicity in cells, which may be a result of improved permeability followed by intracellular hydrolysis to generate **32**. However, this has not been confirmed experimentally. The methoxy electron-donating substituent was added at the 2' position of the pyridine ring to increase the electron density onto the pyridine nitrogen to give **47**, which improves potency in both the DHODH assay and cell-based viability assays. However, this enhancement is greater for phenyl analogue **48**, suggesting that improvements from **32** to **47** are not due to electronic effects alone. In HCT-116 cells, **48** is more potent than **47**, which may be a result of decreased permeability considering the relative cLogP values and modest DHODH potency differences.

Table 3.2. Biological activity of quinolines with R₁ pyridine and pyrimidine moieties.^a



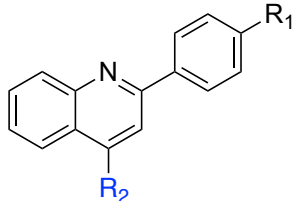
#	R ₁	R ₂	DHODH Assay			MTT Assay	
			IC ₅₀ (μM)	cLogP	LipE	HCT-116 IC ₅₀ (μM)	MIA PaCa-2 IC ₅₀ (μM)
46		CO ₂ H	13.9 ± 4.8	4.47	0.39	> 50	> 50
32		CO ₂ H	0.844 ± 0.12	4.26	1.8	29.4 ± 11	58.6 ± 2.9
33		CO ₂ Me	> 200	4.49	NA	7.20 ± 2.80	8.10 ± 4.0
34		CO ₂ H	9.10 ± 2.00	4.26	0.75	> 50	> 50
47		CO ₂ H	0.284 ± 0.17	4.02	2.53	11.1 ± 2.30	23.4 ± 2.90
48		CO ₂ H	0.179 ± 0.04	5.12	1.63	6.60 ± 2.50	12.8 ± 2.2
49		CO ₂ H	44.0 ± 13.0	2.76	1.60	> 50	> 50
50		CO ₂ H	34.0 ± 39.0	3.24	1.23	> 50	> 50
51		CO ₂ H	> 200	2.97	NA	> 50	> 50

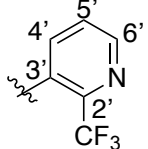
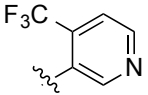
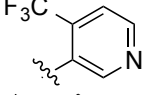
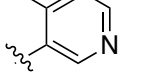
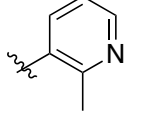
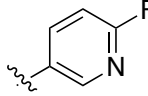
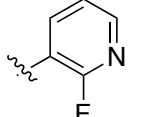
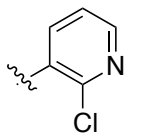
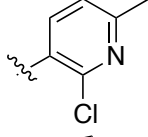
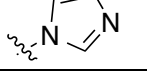
^a cLogP values were calculated using ChemBioDraw Professional 16, Calculated lipophilic ligand efficiency (LipE) = pIC₅₀ (M) – cLogP.²⁸

Replacement of the pyridine ring with pyrimidine **49** resulted in a marked decrease in potency. Incorporation of the additional nitrogen increases tPSA, which may result in a repulsive interaction in a lipophilic pocket as this potency decrease is also observed with pyridazine **50** and

reverse pyrimidine **51**. The electron withdrawing CF₃ substituent was incorporated at the 2' (**52**) and 4' (**53**) positions using the pyridine ring numbering (Table 3.3). Analogue **52** is more potent than **53** in the DHODH assay but shows no significant difference in cells. The same is observed for methyl substituents (**55**, **56**) installed at various positions. Installation of a strongly electron-withdrawing fluoro substituent at the 2' (**58**) and 6' (**57**) positions of the pyridine ring resulted in a marked loss of potency. In fact, compound **58** is 47-fold less potent than **56** and 9-fold less potent than **52** suggesting that steric effects also play an important role. Based on this hypothesis, we incorporated a chlorine to provide **59**. Chlorine has a similar van der Waals radius as a methyl group but different inductive effects. Compound **59** is amongst the most potent analogues synthesized with predicted metabolic stability better than **56**. In cells, compound **59** is more potent in HCT-116 and MIA PaCa-2 than **56**. Further installation of a methyl group at the 6' position (**60**) of the pyridine ring was undertaken to increase binding in a lipophilic pocket. However, this does not improve potency. Neither does replacement of the pyridine with an imidazole (**61**).

Table 3.3. Biological activity of quinolines with R₁ substituted pyridines.^a

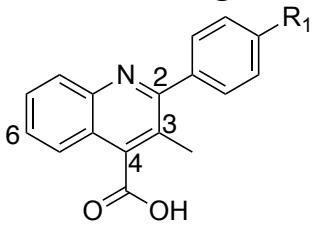


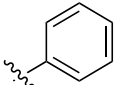
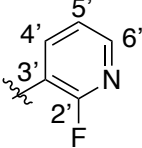
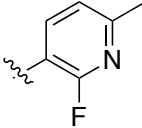
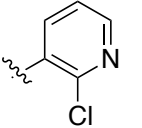
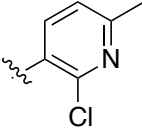
#	R ₁	R ₂	DHODH Assay			MTT Assay	
			IC ₅₀ (μM)	cLogP	LipE	HCT-116 IC ₅₀ (μM)	MIA PaCa-2 IC ₅₀ (μM)
52		CO ₂ H	0.229 ± 0.03	5.14	1.50	9.30 ± 1.70	18.0 ± 2.6
53		CO ₂ H	2.30 ± 1.70	5.14	0.50	7.90 ± 1.60	19.2 ± 1.9
54		CO ₂ Me	> 200	5.37	NA	> 100	> 100
55		CO ₂ H	0.612 ± 0.46	4.46	1.75	22.9 ± 7.0	33.8 ± 6.7
56		CO ₂ H	0.0435 ± 0.031	4.46	2.90	14.7 ± 3.9	24.6 ± 6.3
57		CO ₂ H	17.4 ± 1.9	4.40	0.36	71.0 ± 14.0	>100
58		CO ₂ H	2.01 ± 0.84	4.40	1.30	52.2 ± 4.3	>100
59		CO ₂ H	0.0455 ± 0.025	4.72	2.62	7.3 ± 2.1	11.4 ± 0.44
60		CO ₂ H	0.274 ± 0.025	5.22	1.30	24.0 ± 8.0	39.7 ± 11
61		CO ₂ H	18.1 ± 6.3	3.52	1.22	> 100	> 100

^a cLogP values were calculated using ChemBioDraw Professional 16, Calculated lipophilic ligand efficiency (LipE) = pIC₅₀ (M) – cLogP.²⁸

Altogether, 2'-substituted pyridine analogues (e.g., **56**, **59**) are amongst the most potent of the core quinoline series. Potency differences between 2' position substituents may be a reflection of lipophilicity, inductive, or entropic effects that lower the total number of conformations the pyridine ring can adopt. A comparison between **47** and **52** suggests that inductive effects may not have a significant effect on potency. However, a comparison of analogues **47**, **52**, **56**, **58**, and **59** suggests that substituent size may be a contributing factor. The size of the substituent may factor into undesirable clashes or limit the degrees of conformational freedom. Nonetheless, since analogues **56** and **59** were the most potent analogues synthesized at this stage of the project, the SAR was extended around **59**.

On the basis of SAR developed around the pendant R₁ position (Tables 3.1-3.3), we focused on further incorporating a C3 methyl substituent as is found in brequinar (Figure 3.1). We postulated that this added substituent would further limit conformational freedom around the C2 biaryl bond and hence minimize entropic penalties required for interaction with the nitrogen on the pendant pyridine ring for analogues shown in Tables 3.2 and 3.3. Additionally, the C3 methyl substituent should minimize potential stacking interactions between molecules in solution leading to better aqueous solubility. Synthesized analogues with the C3 methyl were generally more potent than the corresponding C3 desmethyl congeners in the DHODH assay with the notable exceptions of **62** and **65** (Table 3.4). Analogue **62** is less potent than **28** in the DHODH and cell based assays whereas **65** is moderately less potent than **59** in both assays.

Table 3.4. Biological activity of C3 methyl-substituted quinolines.^a

#	R ₁	DHODH Assay			MTT Assay	
		IC ₅₀ (μM)	cLogP	LipE	HCT-116 IC ₅₀ (μM)	MIA PaCa-2 IC ₅₀ (μM)
62		0.131 ± 0.027	5.66	1.23	12.8 ± 2.4	10.9 ± 1.4
63		0.850 ± 0.47	4.30	0.61	71.0 ± 20.0	>100
64		3.93 ± 1.6	4.80	0.61	>100	>100
65		0.0772 ± 0.055	4.62	2.49	23.0 ± 10.0	28.7 ± 16
66		0.274 ± 0.025	5.12	1.44	30.0 ± 6.3	15.7 ± 4.5

^a cLogP values were calculated using ChemBioDraw Professional 16, Calculated lipophilic ligand efficiency (LipE) = pIC₅₀ (M) – cLogP.²⁸

The next iteration of our optimization campaign was to evaluate core modifications of the C6 position of the quinoline ring. In general, the crystal structure (PDB: 1D3G) depicts a small pocket that could be occupied by a suitable C6 substituent (Figure 3.3). Additionally, SMARTCyp, a software for predicting cytochrome P450-mediated metabolism, identified the C6 position of a non-substituted analogue as a site of metabolic liability.³⁹ Thus, incorporation of a C6 substituent may improve potency and decrease metabolic liabilities. The SAR around this position was limited to substituents that could be easily incorporated by our synthetic methodology. The data in Table 3.5 show that C6 –F analogues are more potent than corresponding C6 –Cl or CH₃ congeners. This may be attributed to the size of the substituent,

suggesting that smaller lipophilic functional groups are better tolerated. For analogues with the C6 substituents, **71** ($IC_{50} = 0.0106 \pm 0.0011 \mu\text{M}$) possesses an IC_{50} on par with brequinar ($IC_{50} = 0.020 \pm 0.02 \mu\text{M}$) but with a lower cLogP (4.76 vs 5.94). The lowered cLogP may explain the potency differences in the HCT-116 cell line. Despite similar potency in the DHODH assay, **71** is less potent than brequinar in HCT-116 ($IC_{50} = 7.30 \pm 2.0 \mu\text{M}$ vs. $IC_{50} = 0.98 \pm 0.52 \mu\text{M}$, respectively). This may be due to analogue **71** being less cell permeable than brequinar. Nonetheless, compound **71** is our most potent analogue in the DHODH assay within the quinoline series.

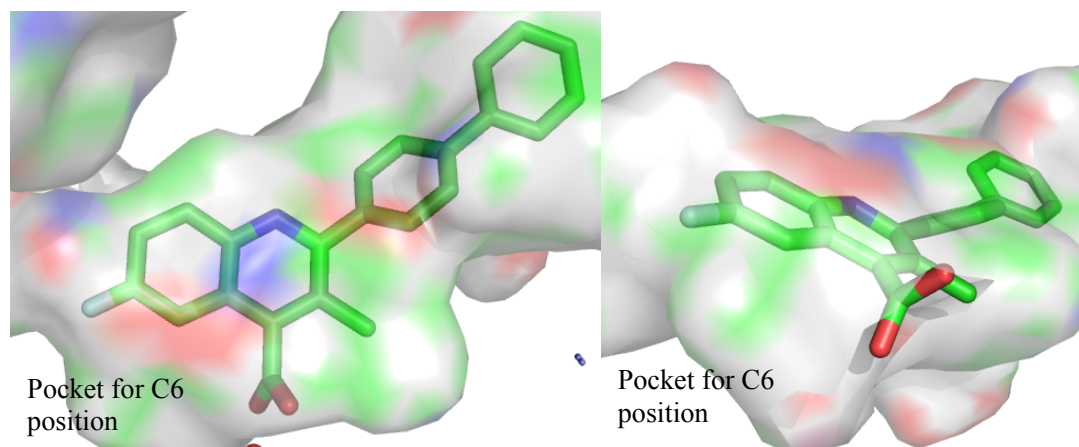
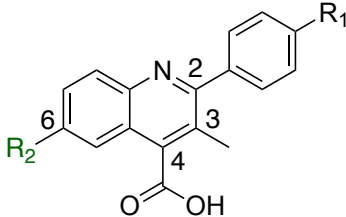
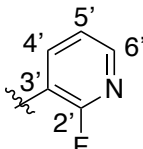
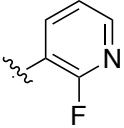
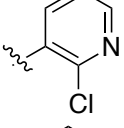
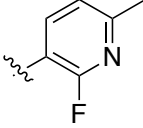
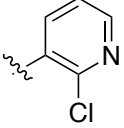
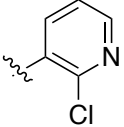
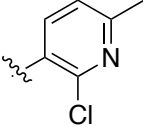
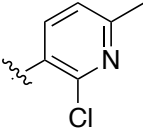


Figure 3.3. Depicted binding cavity of a brequinar analogue. The pocket for a C6 substituent is depicted from PDB file 1D3G.

Table 3.5. Biological activity of C6 / R₁ substituted quinolines.^a

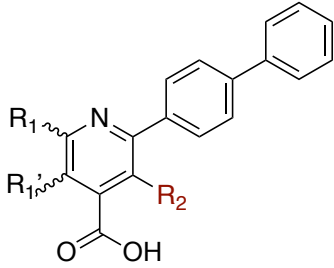


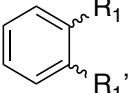
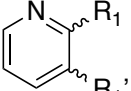
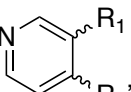
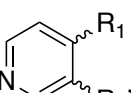
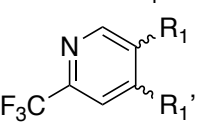
#	R ₁	R ₂	DHODH Assay		MTT Assay		
			IC ₅₀ (μM)	cLogP	LipE	HCT-116 IC ₅₀ (μM)	MIA PaCa-2 IC ₅₀ (μM)
67		F	0.173 ± 0.2	4.45	2.31	15.0 ± 5.0	53.1 ± 44
68		Cl	0.246 ± 0.03	5.02	1.60	25.0 ± 19.0	26.0 ± 13
69		Me	0.0593 ± 0.020	5.12	2.11	24.0 ± 3.2	>100
70		F	5.67 ± 0.63	4.95	0.30	>100	>100
71		F	0.0106 ± 0.0011	4.76	3.21	7.30 ± 2.0	23.3 ± 22
72		Cl	0.0437 ± 0.0086	5.34	2.02	9.40 ± 1.6	>100
73		F	0.0329 ± 0.046	5.27	2.21	6.10 ± 0.70	13.0 ± 0.71
74		Cl	0.107 ± 0.02	5.84	1.13	9.47 ± 4.2	31.4 ± 25

^a cLogP values were calculated using ChemBioDraw Professional 16, Calculated lipophilic ligand efficiency (LipE) = pIC₅₀ (M) – cLogP.²⁸

To form potential interactions with Y356, a scaffold hop was made from the quinoline to naphthyridine core (Table 3.6). The SAR highlights that 1,7-naphthyridines are the most potent within the broad series synthesized and support our hypothesis of the importance of H-bonding interactions with Y356. Both the 1,6- and 1,8- naphthyridines (**77** and **75**) are less potent than the quinoline (**62**) and suggest that these nitrogen placements generate unfavorable interactions. In contrast, the 1,7-naphthyridine (**76**) displays greater potency than the quinoline congener ($IC_{50} = 0.0539 \pm 0.017 \mu\text{M}$ vs. $IC_{50} = 0.131 \pm 0.027 \mu\text{M}$, respectively).

Table 3.6. Biological activity of naphthyridines.^a



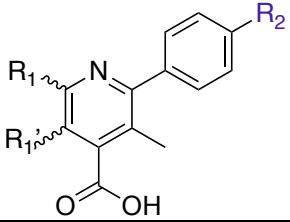
#	R ₁	R ₂	DHODH Assay			MTT Assay	
			IC ₅₀ (μM)	cLogP	LipE	HCT-116 IC ₅₀ (μM)	MIA PaCa-2 IC ₅₀ (μM)
62		Me	0.131 ± 0.027	5.66		12.8 ± 2.4	10.9 ± 1.4
75		Me	4.18 ± 0.61	4.16	1.22	> 100	> 100
76		Me	0.0539 ± 0.017	4.16	3.11	24.0 ± 8.0	41.8 ± 36
77		Me	3.75 ± 2.70	4.16	1.27	>100	>100
78		Me	0.0257 ± 0.0062	5.04	2.56	3.21 ± 2.6	17.7 ± 14

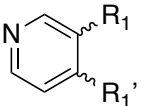
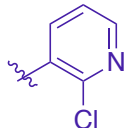
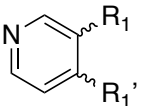
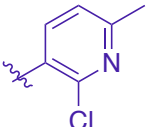
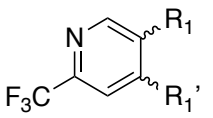
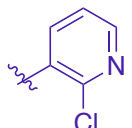
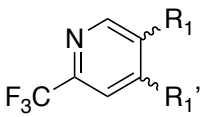
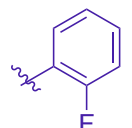
^a cLogP values were calculated using ChemBioDraw Professional 16, Calculated lipophilic ligand efficiency (LipE) = $pIC_{50} (M) - cLogP$.²⁸

Our focus then shifted to C6 substituted 1,7-naphthyridines. For the quinoline series, analogues possessing a C6 substitution are far more potent than their non-substituted analogues

(**65** vs **71**, **66** vs **73**). We postulated that a C6 substituted 1,7-naphthyridine would be more potent than the corresponding C6 substituted quinolines and possess a lower cLogP. The data (Table 3.6) suggest that C6 substituents on the 1,7-naphthyridine result in a more potent series as **78** is 2-fold more potent than **76**. Based on this observation, we sought to incorporate the terminal 2-chloro-3-pyridine moiety onto the core 1,7-naphthyridine scaffold.

Unfortunately, 1,7-naphthyridines analogues with a pyridine terminal attachment (**79-81**) (Table 3.7) are not as potent as the naphthyridines with a terminal phenyl group (**76**, **78**) or corresponding analogues within the quinoline series (**71**, **73**). This may be due to an induced fit binding. If the naphthyridine forces an induced fit to interact with Y356, then the distance between the pyridine nitrogen and Y38 and T63 may be too large to form an interaction and result in an unfavorable clashing with hydrophobic residues. Furthermore, while these analogues possess modest activity in the DHODH assay, they are not active in HCT-116 cells. In fact, analogues with a cLogP lower than 4 (**79**, **80**) do not adversely affect cell growth below 100 μ M. In contrast, analogue **82**, containing the terminal fluorophenyl like brequinar, is potent in both the DHODH and MTT assays. Collectively, the potency of the 1,7-naphthyridines in the DHODH assay suggests potential interactions are being formed with DHODH, possibly via Y356.

Table 3.7. Biological activity of R₂ pyridine-substituted naphthyridines.^a


#	R ₁	R ₂	DHODH Assay			MTT Assay	
			IC ₅₀ (μM)	cLogP	LipE	HCT-116 IC ₅₀ (μM)	MIA PaCa-2 IC ₅₀ (μM)
79			0.353 ± 0.05	3.13	3.32	>100	>100
80			10.2 ± 3.6	3.63	1.36	>100	>100
81			0.226 ± 0.110	4.01	2.64	54.5 ± 17	>100
82			0.0125 ± 0.0011	5.19	2.71	1.01 ± 0.27	38.0 ± 41.0

^a cLogP values were calculated using ChemBioDraw Professional 16, Calculated lipophilic ligand efficiency (LipE) = pIC₅₀ (M) – cLogP.²⁸

3.5 Crystallography

The structures of DHODH co-crystallized with **73** and **76** were solved to 1.46 Å and 2.70 Å resolution, respectively. DHODH:**73** was solved with two molecules in the asymmetric unit, while DHODH:**76** contained only one. Their overall structures are similar in that the single chain of DHODH:**76** aligns with RMSD values of 0.734 Å and 0.732 Å to the A and B chains of DHODH:**73**, respectively. The structures also adopt the same fold as other brequinar analogues bound to DHODH reported in the literature.^{24, 40, 41}

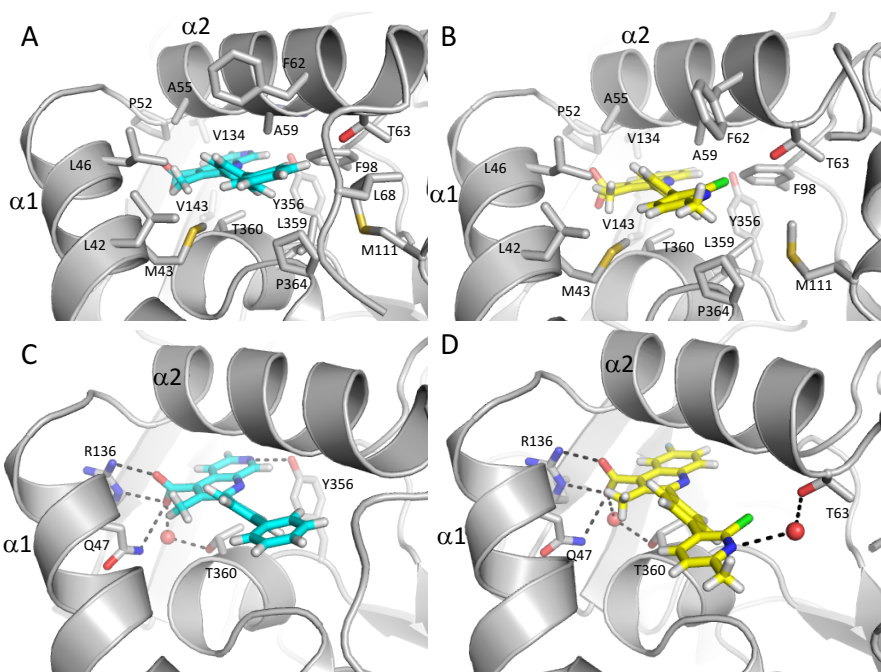


Figure 3.4. Interactions between DHODH and analogues 76 and 73. Noncovalent interactions of DHODH with **76** (cyan) and **73** (yellow). (A) and (B) outline hydrophobic interactions and (C) and (D) demonstrate hydrogen-bonding (dashed lines). **73** shown modeled in predominant conformation. Nitrogen is shown in blue, oxygen (red), sulfur (yellow), chlorine (green), and fluorine (light blue), hydrogens (white).

Consistent with previous structures of DHODH bound to brequinar analogs,^{24, 40, 41} inhibitors **73** and **76** occupy the proposed ubiquinone binding site, a hydrophobic channel formed by $\alpha 1$ and $\alpha 2$ helices directed toward the proximal redox site with the 4-carboxylic acid quinoline ring system oriented toward the active site. Both compounds are stabilized by a substantial number of hydrophobic interactions with the side chains of DHODH residues lining the pocket (L42, M43, L46, P52, A55, A59, F62, and T63) (Figure 3.4, A and B). The more deeply buried quinoline ring of **73** and naphthyridine ring of **76** form van der Waals contacts with a series of hydrophobic residues near the redox site including F96, V134, V143, T360, Y356, L359, and P364 (Figure 3.4, A and B). The C7-fluorine substituent of **73** is directed toward the FMN cofactor as in previous structures with other brequinar analogs,^{24, 41} and the C4 carboxylate of both inhibitors form salt bridges with R136 and participate in H-bonding with Q47 and T360 through a water molecule (Figure 3.4, C and D).

In contrast to previous structures, the additional nitrogen incorporated into the 1,7-naphthyridine ring of **76** is within 2.9 Å of the Y356 hydroxyl group, allowing this inhibitor to participate in an additional H-bonding interaction within the binding site (Figure 3.4C).

In place of the unsubstituted phenyl ring of **76** and the 2-fluorophenyl ring of brequinar, **73** features a 2-chloro-6-methyl pyridine ring that can adopt two different orientations. Based on the ligand omit map density, the chlorine substituent can be directed toward the α 1 helix, but this orientation has low occupancy, likely in part due to steric clashes with the hydrophobic residues lining the binding pocket. The higher occupancy orientation of the pyridine ring directs the chlorine toward F98. In this orientation, the pyridine nitrogen is directed toward space usually occupied by the disordered 68-72 loop. In one molecule of the asymmetric unit, density corresponding to a water lies within 3.2 Å of the pyridine nitrogen and mediates a H-bond with the side chain of T63 (Figure 3.4D). The 6-methyl substituent is also directed toward space usually occupied by the loop connecting the two domains; steric clashes with this highly flexible loop might contribute to the intrinsic disorder of this loop and explain why density corresponding to residues 68-70 is absent in the structure with **73** in contrast to the DHODH:**76**, in which these residues were able to be modeled.

There is additional density near the solvent-exposed entrance to the channel occupied by the inhibitor. The extra electron density in this site has been reported in previous structures of DHODH with brequinar analogs.^{24, 41} Liu and colleagues modeled a detergent, DDAO, in this site.²⁴ In our structures of DHODH:**73** and DHODH:**76**, we modeled the aliphatic chain in common to the two detergents, Anzergent 3-10 and HEGA-8, used for crystallization. The aliphatic chain forms van der Waals interactions with the side chains of F62 and P69 as well as the backbone of residues 67-69. Additionally, the detergent makes contact with the phenyl group of **76**. In the DHODH:**73** structure, the aliphatic chain does not interact with the loop, but forms van der Waals interactions with the side chains of F62, L46, L42 and F37 along with the terminal substituted pyridine of **73**. Although the detergent is not physiologically relevant, it is likely that this face of the protein and the bound inhibitor make contacts with aliphatic chains of phospholipids comprising the membrane.²⁴

3.6 Pharmacokinetic evaluation and thermodynamic solubility

We deemed compound **71** to possess an overall profile that merited pharmacokinetic evaluation in mice (Table 3.8). When **71** was administered either orally or intravenously, a similar elimination half-life of 2.73-2.78 hours was observed. Oral bioavailability for **71** is 56%, which is suitable for DHODH inhibition considering its potency. For PO dosing, the C_{\max} was 5313 ng/mL and was reached in 0.25 h. The low C_{\max} of **71** may be an indication of poor intestinal membrane permeability. This may be improved through development of formulations or pro-drug approaches. However, the clearance rate and volume of distribution are favorable for continuous inhibition, suggesting that **71** is well suited for further investigation.

Analogue **76** is more soluble in aqueous solutions than compounds of the quinoline series. In comparison to brequinar, compound **76** is 2.5 – 3x more soluble in PBS at pH 7.4 (Table 3.9). The nitrogen of the naphthyridine core significantly increases the aqueous solubility in comparison to the quinoline core. However, a comparison between **71** and brequinar highlights that despite a lower cLogP, **71**'s aqueous solubility is not significantly different from that of brequinar. The large chlorine group may limit the total solvent exposure of **71**'s pyridine moiety, which minimizes its effect on aqueous solubility. Nonetheless, compound **76** is endowed with better drug-like properties compared to brequinar, with potent DHODH inhibition and improved aqueous solubility.

Table 3.8. Pharmacokinetic parameters of analogue 71.^a

Route	Dose	C_0/C_{\max}	T_{\max}	AUC (0- TLDC)	AUC (0- INF)	$t_{1/2}$	CL	CL-F	V_{ss}	V_{z_F}	%F
	mg/kg	ng/mL	h	h*ng/mL	h*ng/mL	h	mL/h/kg		mL/kg		%
IV	10	45381	NA	32261	32306	2.73	309	N/A	496	NA	N/A
PO	20	5313	0.25	35896	36035	2.78	N/A	555	NA	2226	56%

^aPK parameters were estimated using non-compartmental analysis with Phoenix/WINONLIN. C_0 = initial concentration, C_{\max} = Maximum observed concentration, T_{\max} = Time to reach C_{\max} , AUC(0-TLDC) = Area under the concentration-time curve from time zero to time of last detectable concentration, AUC(0-inf) = Area under the concentration-time curve from time zero to infinite, CL = Systemic clearance, CL_F = Apparent clearance, V_{ss} = Volume of distribution at steady state, V_{z_F} = Volume of distribution associated with the terminal elimination phase, Terminal elimination half-life ($t_{1/2}$) was calculated based on data points (≥ 3) in the terminal phase with correlation of coefficient > 0.90 , %F = bioavailability.

Table 3.9. Thermodynamic solubility of selected analogues.^a

#	μM	$\mu\text{g/mL}$	Initial dose	pH after assay
			concentration	
			mg/mL	
2 (brequinar)	1085.2	407.4	6.2	7.4
	1048.6	393.6	6.4	7.4
1	43.9	14.5	2.9	7.4
	48.0	15.9	4.9	7.4
71	1000.1	392.8	5.8	7.4
	982.1	385.8	4.9	7.4
76	2628.4	894.6	6.7	7.4
	3096.3	1053.6	8.7	7.4

^aAssay performed using CLND in phosphate buffer saline, pH 7.4. Analyte concentrations were determined via a standard calibration curve.

3.7 Conclusions

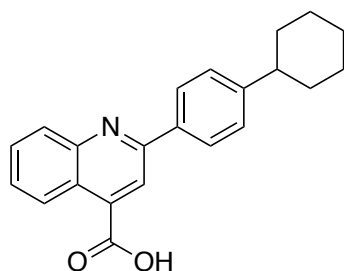
This study reports our efforts towards the development of a novel DHODH inhibitor with improved potency and aqueous solubility. Our efforts toward designing molecular interactions with T63 led to the potent inhibitors **71** (DHODH $\text{IC}_{50} = 0.0106 \pm 0.0011 \mu\text{M}$) and **73** (DHODH $\text{IC}_{50} = 0.0329 \pm 0.046 \mu\text{M}$) both possessing a lower cLogP than brequinar (4.76, 5.27 vs. 5.94 respectively). A co-crystal structure of **73** and DHODH depicts a water-mediated H-bonding interaction with the terminal pyridine and T63 (Figure 3.4D). Efforts to form an interaction with Y365 led to the 1,7-naphthyridine inhibitors; **76** (DHODH $\text{IC}_{50} = 0.0539 \pm 0.017 \mu\text{M}$), **78** (DHODH $\text{IC}_{50} = 0.0257 \pm 0.0062 \mu\text{M}$), and **82** (DHODH $\text{IC}_{50} = 0.0125 \pm 0.0011 \mu\text{M}$). In a co-crystal structure with DHODH, the 7' nitrogen of **76**'s core forms a H-bond with the hydroxyl of Y356 (Figure 3.4C). Furthermore, analogue **76** is significantly more soluble in aqueous solution than brequinar. Pharmacokinetic evaluation of **71** highlights suitable oral bioavailability (%F = 56%) and half-life ($t_{1/2} = 2.78 \text{ h}$), suitable for further investigation. Collectively, these inhibitors depict the potential to enhance binding with DHODH through novel H-bonding interactions. The results of this study delineate the possibility to simultaneously improve potency while lowering the cLogP for inhibitors that occupy a lipophilic binding pocket. The inhibitors disclosed in this study present suitable leads for further inhibitor design and early stage development. Future studies will seek to improve cell permeability by optimizing pro-drug design. Additionally, the

ability of these inhibitors to induce differentiation in acute myeloid leukemia will be evaluated along with *in vivo* efficacy studies.

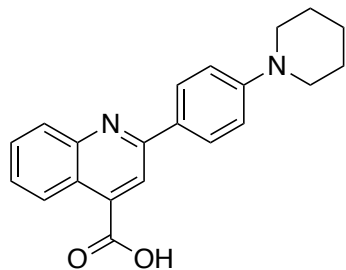
3.8 Experimental

General methods. Reagents and anhydrous solvents were used without further purification and purchased from commercial sources. Cinchophen and brequinar were purchased from commercial sources and utilized without further purification. A Biotage® Initiator+ was used to perform microwave catalyzed reactions in sealed vials. Reaction progress was monitored by UV absorbance using thin-layer chromatography (TLC) on aluminum-backed precoated silica plates from Silicycle (SiliaPlate™, 200 µm thickness, F₂₅₄). Purifications using flash chromatography were performed using Silicycle silica gel (SiliaFlash® F60, 40-63 µm, 230-400 mesh, PN: R10030B) and a small percentage of compounds were purified using a Biotage® Isolera Chromatography system equipped with 10 g and 25 g Ultra-SNAP Cartridge columns (25 µm spherical silica). Glassware for reactions were oven dried in preparation and reactions were performed using nitrogen or argon atmosphere using standard inert conditions. ¹H NMR spectra were obtained using a Bruker (300 or 400 MHz) or a Varian (400 or 500 MHz) instrument. Spectral data are reported using the following abbreviations: (s = singlet, d = doublet, t = triplet, q = quartet, m = multiplet, dd = doublet of doublets), coupling constants are reported in Hz, followed by integration. ¹³C NMR spectra were obtained at 126 MHz on a Varian 500 MHz instrument with a proton decoupled probe. A Shimadzu LCMS 20-20 system was utilized for generating HPLC traces and obtaining mass spectrometry data. The system is equipped with a PDA UV detector and Kinetex® 2.6 µm, XB-C18 100 Å, 75 x 4.6 mm column, which was used at room temperature. HPLC gradient method utilized a 1% to 90% MeCN in H₂O with 0.01% formic acid over 20 minutes with a 0.50 mL/min flow rate. Reverse-phase preparatory purifications were performed on a Shimadzu LC-20 modular HPLC system. This system utilized a PDA detector and a Kinetex® 5 µm XB-C18 100 Å, 150 x 21.2 mm column. Purification methods used a 27-minute gradient from 10% to 90% MeCN in H₂O with 0.02% trifluoroacetic acid. The chemicals *n*-BuLi and TMS-diazomethane present hazards. The chemical *n*-BuLi is pyrophoric and must be utilized under an inert atmosphere. The chemical TMS-diazomethane is toxic and potentially explosive. Caution should be utilized when working with these chemicals.

General protocol A, Pfitzinger synthesis: Isatin (1.0 -1.2 eq) was added to a room temperature solution of KOH (4.0 eq) in an EtOH/H₂O solution and mixed with various *para*-substituted derivatives of acetophenone (1.0 eq). The solution was heated to reflux for 24-48 hours, concentrated *in vacuo*, and re-dissolved in 1 M NaOH/EtOAc. The aqueous layer was washed with EtOAc (3x) and acidified using HCl or glacial acetic acid until precipitant was observed (pH 2-3). The precipitant was filtered over a fritted funnel, washed with 1 M HCl, and washed again with 2-propanol, diethyl ether, or ethanol to yield final compounds (2-81%).

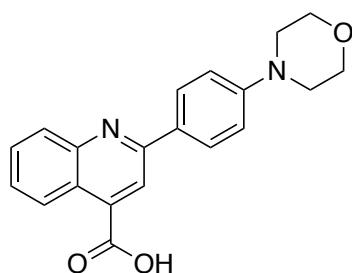


2-(4-Cyclohexylphenyl)quinoline-4-carboxylic acid (1): Isatin (987 mg, 6.71 mmol), 1-(4-cyclohexylphenyl)ethan-1-one (1.00 g, 4.95 mmol), and KOH (1.55 g, 27.6 mmol) were dissolved in 30 mL EtOH and 10 mL H₂O. Following general protocol A, 2-(4-cyclohexylphenyl)quinoline-4-carboxylic acid was recovered as a white powder (374 mg, 1.13 mmol, 23%). ¹H NMR (500 MHz, DMSO-*d*₆) δ 8.64 (d, *J* = 8.6 Hz, 1H), 8.41 (d, *J* = 1.8 Hz, 1H), 8.21 – 8.15 (m, 2H), 8.14 – 8.08 (m, 1H), 7.85 – 7.79 (m, 1H), 7.71 – 7.61 (m, 1H), 7.40 – 7.34 (m, 2H), 2.59 – 2.50 (m, 1H), 1.83 – 1.73 (m, 4H), 1.72 – 1.65 (m, 1H), 1.49 – 1.27 (m, 4H), 1.27 – 1.10 (m, 1H); ¹³C NMR (126 MHz, DMSO-*d*₆) δ 168.09, 156.23, 150.06, 148.86, 138.00, 136.02, 130.55, 130.14, 127.97, 127.72 (2H), 127.64 (2H), 125.85, 123.81, 119.42, 44.03, 34.22 (2H), 26.73 (2H), 26.00; LCMS (ESI) 332.2 [M+H]⁺, 330.2 [M-H]⁻; HPLC Purity at 254 nm, 98.6%.



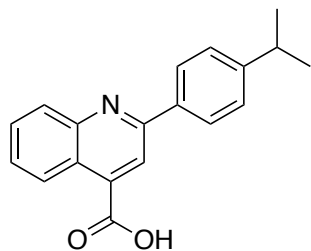
2-(4-(Piperidin-1-yl)phenyl)quinoline-4-carboxylic acid (25):

Isatin (247 mg, 1.68 mmol), 1-(4-(piperidin-1-yl)phenyl)ethan-1-one (200 mg, 0.99 mmol), and KOH (336 mg, 6.00 mmol) were dissolved in 7 mL EtOH and 2 mL H₂O. Following general protocol A, 2-(4-(piperidin-1-yl)phenyl)quinoline-4-carboxylic acid was recovered as a red solid (88 mg, 0.27 mmol, 27%). ¹H NMR (400 MHz, DMSO-*d*₆) δ 8.59 (d, *J* = 8.4 Hz, 1H), 8.37 (s, 1H), 8.18 (d, *J* = 8.6 Hz, 2H), 8.09 (d, *J* = 8.4 Hz, 1H), 7.80 (t, *J* = 8.4, 6.9 Hz, 1H), 7.68 – 7.58 (m, 1H), 7.16 – 7.04 (m, 2H), 3.34 – 3.27 (m, 4H), 1.71 – 1.54 (m, 6H); LCMS (ESI) 333.3 [M+H]⁺, 331.2 [M-H]⁻; HPLC Purity at 254 nm, 99.7%.

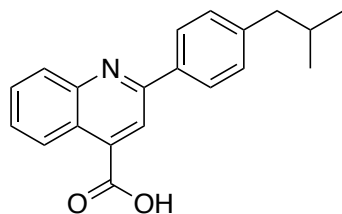


2-(4-Morpholinophenyl)quinoline-4-carboxylic acid (27):

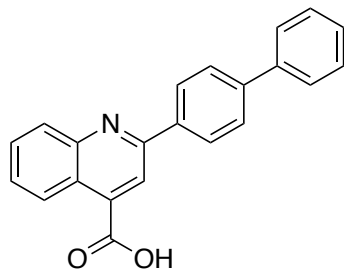
Isatin (247 mg, 1.68 mmol), 1-(4-morpholinophenyl)ethan-1-one (200 mg, 0.98 mmol), and KOH (336 mg, 6.00 mmol) were dissolved in 7 mL EtOH and 1 mL H₂O. Following general protocol A, 2-(4-morpholinophenyl)quinoline-4-carboxylic acid was recovered as a red solid (132 mg, 0.40 mmol, 41%). ¹H NMR (400 MHz, DMSO-*d*₆) δ 8.60 (d, *J* = 8.5 Hz, 1H), 8.39 (s, 1H), 8.21 (d, *J* = 8.7 Hz, 2H), 8.10 (d, *J* = 8.4 Hz, 1H), 7.85 – 7.76 (m, 1H), 7.68 – 7.59 (m, 1H), 7.11 (d, *J* = 8.7 Hz, 2H), 3.77 (t, *J* = 4.8 Hz, 4H), 3.26 (t, *J* = 4.9 Hz, 4H); LCMS (ESI) 335.9 [M+H]⁺, 333.2 [M-H]⁻; HPLC Purity at 254 nm, 98.8%.



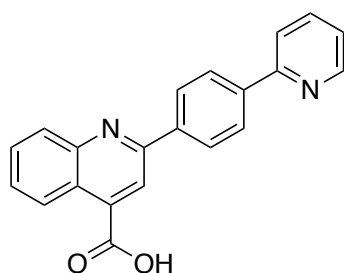
2-(4-Isopropylphenyl)quinoline-4-carboxylic acid (18): Isatin (264 mg, 1.79 mmol), 1-(4-isopropylphenyl)ethan-1-one (0.27 mL, 1.62 mmol), and KOH (275 mg, 4.91 mmol) were dissolved in 7 mL EtOH and 1 mL H₂O. Following general protocol A, 2-(4-isopropylphenyl)quinoline-4-carboxylic acid was recovered as a yellow solid (130 mg, 0.45 mmol, 28%). **¹H NMR** (400 MHz, DMSO-*d*₆) δ 8.65 (d, *J* = 8.3 Hz, 1H), 8.44 (s, 1H), 8.23 (d, *J* = 8.3 Hz, 2H), 8.16 (d, *J* = 8.5 Hz, 1H), 7.89 – 7.81 (m, 1H), 7.75 – 7.67 (m, 1H), 7.46 (d, *J* = 8.3 Hz, 2H), 3.09 – 2.94 (m, 1H), 1.28 (d, *J* = 6.9 Hz, 6H); **LCMS** (ESI) 292.2 [M+H]⁺, 290.2 [M-H]⁻; **HPLC** Purity at 254 nm, 95.8%.



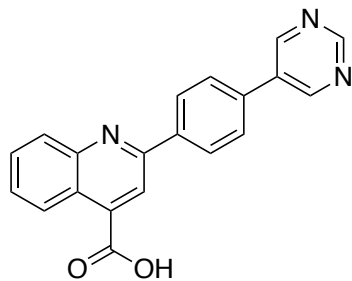
2-(4-Isobutylphenyl)quinoline-4-carboxylic acid (17): Isatin (500 mg, 3.40 mmol), 1-(4-isobutylphenyl)ethan-1-one (0.57 mL, 3.08 mmol), and KOH (1.14 g, 20.4 mmol) were dissolved in 12 mL EtOH + 2 mL H₂O. Following general protocol A, 2-(4-isobutylphenyl)quinoline-4-carboxylic acid was recovered as a pink solid (101 mg, 0.33 mmol, 10% yield). **¹H NMR** (300 MHz, DMSO-*d*₆) δ 8.68 (d, *J* = 8.4 Hz, 1H), 8.14 (d, *J* = 7.9 Hz, 2H), 8.03 – 7.94 (m, 2H), 7.66 (t, *J* = 7.6 Hz, 1H), 7.46 (t, *J* = 7.6 Hz, 1H), 7.33 (d, *J* = 7.9 Hz, 2H), 2.59 – 2.52 (m, 2H), 2.00 – 1.85 (m, 1H), 0.91 (d, *J* = 6.6 Hz, 6H); **LCMS** (ESI) 306.1 [M+H]⁺, 304.2 [M-H]⁻; **HPLC** Purity at 254 nm, 99.9%.



2-([1,1'-Biphenyl]-4-yl)quinoline-4-carboxylic acid (28): Isatin (168 mg, 1.14 mmol), 1-([1,1'-biphenyl]-4-yl)ethan-1-one (200 mg, 1.02 mmol), KOH (230 mg, 4.11 mmol) were dissolved in 3 mL EtOH with 1 mL H₂O. Following general protocol A, 2-([1,1'-biphenyl]-4-yl)quinoline-4-carboxylic acid was recovered as a beige solid (74 mg, 0.23 mmol, 20% yield) after recrystallization from ethanol. ¹H NMR (300 MHz, CD₃OD-*d*₄) δ 8.46 – 8.36 (m, 1H), 8.19 (d, *J* = 8.4 Hz, 2H), 8.14 – 8.02 (m, 2H), 7.83 – 7.63 (m, 5H), 7.56 (ddd, *J* = 8.2, 6.8, 1.2 Hz, 1H), 7.44 (t, *J* = 7.4 Hz, 2H), 7.40 – 7.28 (m, 1H); LCMS (ESI) 326.2 [M+H]⁺, 324.1 [M-H]⁻; HPLC Purity at 254 nm, 98.9%.

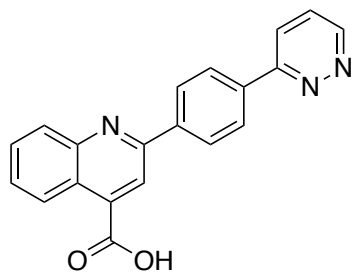


2-(4-(Pyridin-2-yl)phenyl)quinoline-4-carboxylic acid (46): Isatin (82 mg, 0.56 mmol), intermediate **93** (100 mg, 0.51 mmol), and KOH (112 mg, 2.00 mmol) were dissolved 4 mL in EtOH with 1 mL H₂O. Following general protocol A, 2-(4-(pyridin-2-yl)phenyl)quinoline-4-carboxylic acid was recovered as a tan solid (62 mg, 0.19 mmol, 37%). ¹H NMR (300 MHz, CD₃OD-*d*₄) δ 8.71 – 8.64 (m, 1H), 8.46 (d, *J* = 8.4 Hz, 1H), 8.31 (d, *J* = 8.1 Hz, 2H), 8.22 – 8.10 (m, 4H), 8.04 – 7.94 (m, 2H), 7.78 (t, *J* = 7.7 Hz, 1H), 7.61 (t, *J* = 7.7 Hz, 1H), 7.42 (t, *J* = 6.0 Hz, 1H); LCMS (ESI) 326.9 [M+H]⁺, 324.9 [M-H]⁻; HPLC Purity at 254 nm, 99.4%.



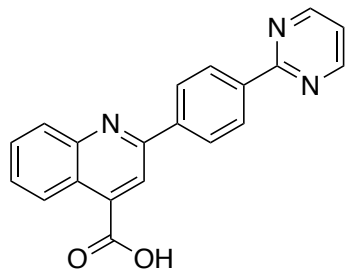
2-(4-(Pyrimidin-5-yl)phenyl)quinoline-4-carboxylic acid (49):

Isatin (56 mg, 0.38 mmol), intermediate **94** (75 mg, 0.38 mmol), and KOH (64 mg, 1.14 mmol) were dissolved in 3 mL EtOH and 1 mL H₂O. Following general protocol A, 2-(4-(pyrimidin-5-yl)phenyl)quinoline-4-carboxylic acid was recovered as a yellow solid (24 mg, 0.07 mmol, 18% yield). ¹H NMR (300 MHz, DMSO-*d*₆) δ 9.31 – 9.21 (m, 3H), 8.66 (d, *J* = 8.5 Hz, 1H), 8.56 (s, 1H), 8.48 (d, *J* = 8.3 Hz, 2H), 8.21 (d, *J* = 8.4 Hz, 1H), 8.05 (d, *J* = 8.4 Hz, 2H), 7.94 – 7.85 (m, 1H), 7.79 – 7.68 (m, 1H); LCMS (ESI) 328.2 [M+H]⁺, 326.9 [M-H]⁻; HPLC Purity at 254 nm, 99.5%.



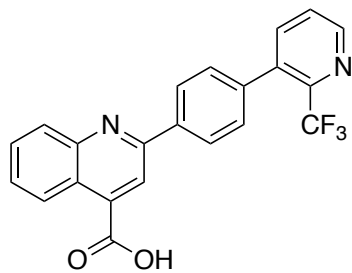
2-(4-(Pyridazin-3-yl)phenyl)quinoline-4-carboxylic acid (50):

(Isatin (203 mg, 1.38 mmol), intermediate **95** (273 mg, 1.38 mmol), and KOH (309 mg, 5.52 mmol) were dissolved in 10 mL EtOH. Following general protocol A, 2-(4-(pyridazin-3-yl)phenyl)quinoline-4-carboxylic acid was recovered as a tan solid (160 mg, 0.49 mmol, 36%). ¹H NMR (400 MHz, DMSO-*d*₆) δ 9.25 (dd, *J* = 4.8, 1.5 Hz, 1H), 8.66 (d, *J* = 8.5 Hz, 1H), 8.56 (s, 1H), 8.50 (d, *J* = 8.3 Hz, 2H), 8.42 – 8.29 (m, 3H), 8.20 (d, *J* = 8.4 Hz, 1H), 7.91 – 7.79 (m, 2H), 7.74-7.70 (m, 1H); LCMS (ESI) 327.9 [M+H]⁺, 325.9 [M-H]⁻; HPLC Purity at 254 nm, 96.7%.



2-(4-(Pyrimidin-2-yl)phenyl)quinoline-4-carboxylic acid (51):

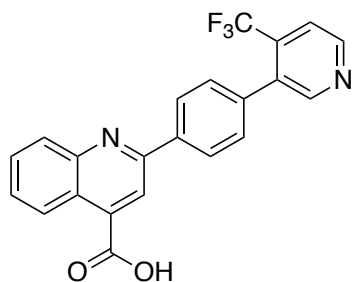
Isatin (67 mg, 0.46 mmol), intermediate **96** (109 mg, 0.55 mmol), KOH (103 mg, 1.84 mmol) were dissolved in 3 mL EtOH and 1 mL H₂O. Following general protocol A, 2-(4-(pyrimidin-2-yl)phenyl)quinoline-4-carboxylic acid was recovered as a tan solid (80 mg, 0.24 mmol, 52%). ¹H NMR (400 MHz, DMSO-*d*₆) δ 8.96 (d, *J* = 4.8 Hz, 2H), 8.67 (d, *J* = 8.2 Hz, 1H), 8.61 – 8.54 (m, 3H), 8.50 – 8.46 (m, 2H), 8.20 (d, *J* = 8.4 Hz, 1H), 7.90 – 7.84 (m, 1H), 7.75 – 7.69 (m, 1H), 7.50 (t, *J* = 4.8 Hz, 1H); LCMS 328.1 [M+H]⁺, 326.1 [M-H]⁻; HPLC Purity at 254 nm, 96.8%



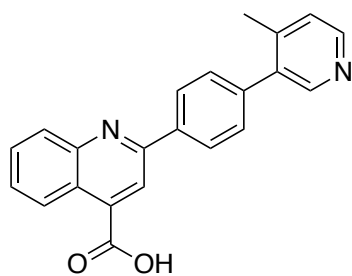
2-(4-(2-(trifluoromethyl)pyridin-3-yl)phenyl)quinoline-4-

carboxylic acid (52): (2-(Trifluoromethyl)pyridin-3-yl)boronic acid (190 mg, 1.12 mmol), 1-(4-bromophenyl)ethan-1-one (200 mg, 1.02 mmol), K₂CO₃ (563 mg, 4.08 mmol), and Pd(PPh₃)₄ (118 mg, 10% mol) were dissolved in dioxane (10 mL) and heated to reflux overnight. The solvent was concentrated and the residue was partitioned between EtOAc and H₂O. Product was extracted with EtOAc (3x), poured over a silica pad, and eluted with additional EtOAc. The elution was concentrated for use in next step. 1-(4-(2-(Trifluoromethyl)pyridin-3-yl)phenyl)ethan-1-one, isatin (160 mg, 1.02 mmol) and KOH (227 mg, 4.06 mmol) were dissolved in 5 mL EtOH and 1 mL H₂O. The mixture was stirred under refluxing conditions for 24 hours and then concentrated. Residue was re-dissolved in 1 M KOH and washed with EtOAc (3x). The aqueous layer was acidified with AcOH until precipitant formation was observed, pH 3-4. The solid was collected and washed with Et₂O and 2-propanol to yield 2-(4-(2-(trifluoromethyl)pyridin-3-yl)phenyl)quinoline-4-carboxylic acid as a tan solid (39 mg, 0.10 mmol, 10% yield over two steps). ¹H NMR (400 MHz, DMSO-*d*₆) δ 8.83 (dd, *J* = 4.7, 1.5 Hz,

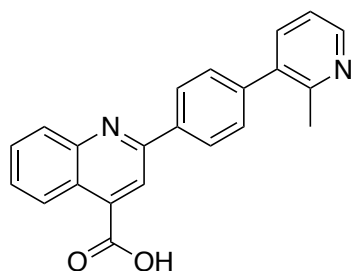
1H), 8.71 – 8.66 (m, 1H), 8.55 (s, 1H), 8.43 (d, $J = 8.4$ Hz, 2H), 8.21 (d, $J = 8.4$ Hz, 1H), 8.05 – 8.02 (m, 1H), 7.92 – 7.82 (m, 2H), 7.77 – 7.71 (m, 1H), 7.59 (d, $J = 8.1$ Hz, 2H); **LCMS** (ESI) 395.1 $[M+H]^+$, 393.1 $[M-H]^-$; **HPLC** Purity at 254 nm, 99.8%.



2-(4-(4-(Trifluoromethyl)pyridin-3-yl)phenyl)quinoline-4-carboxylic acid (53): Isatin (220 mg, 1.50 mmol), intermediate **97** (235 mg, 0.89 mmol), and KOH (300 mg, 5.36 mmol) were dissolved in 10 mL absolute EtOH. Following general protocol A, 2-(4-(4-(trifluoromethyl)pyridin-3-yl)phenyl)quinoline-4-carboxylic acid was recovered as a tan solid (88 mg, 0.22 mmol, 25%). **¹H NMR** (400 MHz, DMSO- d_6) δ 8.97 – 8.90 (m, 1H), 8.80 (s, 1H), 8.69 (d, $J = 8.5$ Hz, 1H), 8.58 – 8.53 (m, 1H), 8.47 – 8.40 (m, 2H), 8.21 (d, $J = 8.4$ Hz, 1H), 7.95 – 7.85 (m, 2H), 7.74 (t, 1H), 7.62 (d, $J = 8.0$ Hz, 2H); **LCMS** (ESI) 394.9 $[M+H]^+$, 392.9 $[M-H]^-$; **HPLC** Purity at 254 nm, 97.1%.

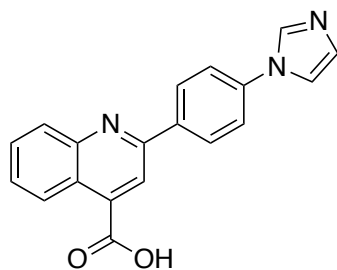


2-(4-(4-Methylpyridin-3-yl)phenyl)quinoline-4-carboxylic acid (55): Isatin (140 mg, 0.95 mmol), intermediate **98** (200 mg, 0.95 mmol), and KOH (320 mg, 5.71 mmol) were dissolved in 4 mL EtOH and 2 mL H₂O. Following general protocol A, 2-(4-(4-Methylpyridin-3-yl)phenyl)quinoline-4-carboxylic acid was recovered as a beige solid (85 mg, 0.25 mmol, 26% yield). **¹H NMR** (300 MHz, DMSO- d_6) δ 8.85 – 8.74 (m, 2H), 8.68 (d, $J = 8.5$ Hz, 1H), 8.56 (s, 1H), 8.48 (d, $J = 8.1$ Hz, 2H), 8.20 (d, $J = 8.4$ Hz, 1H), 7.95 – 7.84 (m, 2H), 7.78 – 7.68 (m, 3H), 2.53 (s, 4H); **LCMS** (ESI) 341.2 $[M+H]^+$, 339.2 $[M-H]^-$; **HPLC** Purity at 254 nm, 99.8%.



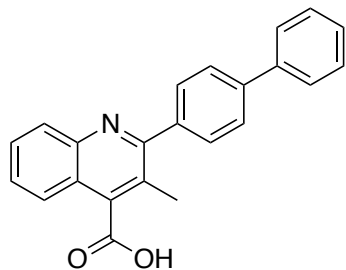
2-(4-(2-Methylpyridin-3-yl)phenyl)quinoline-4-carboxylic acid

(56): Isatin (173 mg, 1.18 mmol), intermediate **99** (249 mg, 1.18 mmol) and KOH (394 mg, 7.04 mmol) were dissolved in 4 mL EtOH and 2 mL H₂O. Following general protocol A, 2-(4-(2-methylpyridin-3-yl)phenyl)quinoline-4-carboxylic acid recovered as a tan solid, (228 mg, 0.67 mmol, 57% yield). ¹H NMR (400 MHz, DMSO-*d*₆) δ 8.75 – 8.68 (m, 1H), 8.50 (dd, *J* = 4.9, 1.7 Hz, 1H), 8.38 – 8.32 (m, 2H), 8.19 (s, 1H), 8.09 – 8.02 (m, 1H), 7.77 – 7.68 (m, 2H), 7.62 – 7.51 (m, 3H), 7.35 (dd, *J* = 7.7, 4.8 Hz, 1H), 2.51 (s, 8H); LCMS (ESI) 341.2 [M+H]⁺, 339.1 [M-H]⁻; HPLC Purity at 254 nm, 99.6 %.



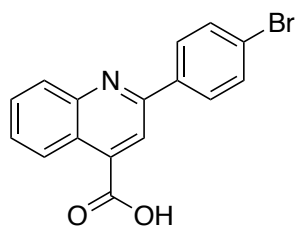
2-(4-(1*H*-Imidazol-1-yl)phenyl)quinoline-4-carboxylic acid (61)

Isatin (265 mg, 1.80 mmol), 1-(4-(1*H*-imidazol-1-yl)phenyl)ethan-1-one (200 mg, 1.08 mmol), and KOH (242 mg, 4.32 mmol) were dissolved in 7 mL EtOH and 1 mL H₂O. Following general protocol A, 2-(4-(1*H*-imidazol-1-yl)phenyl)quinoline-4-carboxylic acid was recovered as a tan solid (116 mg, 0.36 mmol, 33%). ¹H NMR (400 MHz, DMSO-*d*₆) δ 8.64 (dd, *J* = 8.5, 1.4 Hz, 1H), 8.50 (s, 1H), 8.49 – 8.40 (m, 3H), 8.22 – 8.14 (m, 1H), 7.92 – 7.82 (m, 4H), 7.75 – 7.66 (m, 1H), 7.18 (s, 1H); LCMS (ESI) 315.9 [M+H]⁺, 313.9 [M-H]⁻; HPLC Purity at 254 nm, 95.4%.



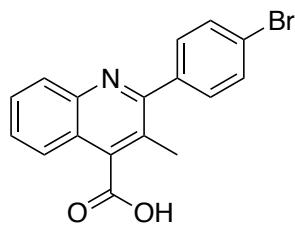
2-([1,1'-Biphenyl]-4-yl)-3-methylquinoline-4-carboxylic acid (62):

Isatin (200 mg, 1.36 mmol), 1-([1,1'-biphenyl]-4-yl)propan-1-one (237 mg, 1.13 mmol), and KOH (266 mg, 4.75 mmol) were dissolved in 5 mL EtOH and 2 mL H₂O. Following general protocol A, 2-([1,1'-biphenyl]-4-yl)-3-methylquinoline-4-carboxylic acid was recovered as a tan solid (8 mg, 0.02 mmol, 2%) after trituration with diethyl ether and 2-propanol and then recrystallization from EtOH. ¹H NMR (300 MHz, DMSO-*d*₆) δ 8.08 (d, *J* = 8.2 Hz, 1H), 7.87 – 7.66 (m, 9H), 7.52 (t, *J* = 7.5 Hz, 2H), 7.42 (t, *J* = 7.3 Hz, 1H), 2.46 (s, 3H); LCMS (ESI) 340.2 [M+H]⁺, 338.1 [M-H]⁻; HPLC Purity at 254 nm, 97.5%.



2-(4-Bromophenyl)quinoline-4-carboxylic acid (83):

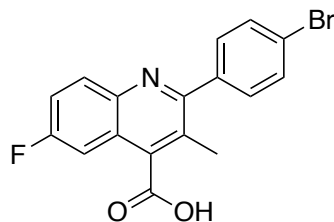
Isatin (5.00 g, 34.0 mmol), 1-(4-bromophenyl)ethan-1-one (6.70 g, 34.0 mmol), KOH (11.4 g, 204 mmol) were dissolved in 55 mL EtOH and 24 mL H₂O. Following general protocol A, 2-(4-bromophenyl)quinoline-4-carboxylic acid was recovered as a yellow solid (9.02 g, 27.7 mmol, 81%). ¹H NMR (300 MHz, DMSO-*d*₆) δ 8.68 (d, *J* = 8.3 Hz, 1H), 8.20 (d, *J* = 8.5 Hz, 2H), 8.08 (s, 1H), 8.02 (d, *J* = 8.4 Hz, 1H), 7.72 (dd, *J* = 12.5, 8.1 Hz, 3H), 7.53 (t, *J* = 7.6 Hz, 1H); MS (ESI) 328.0 [M+H]⁺.



2-(4-Bromophenyl)-3-methylquinoline-4-carboxylic acid (84):

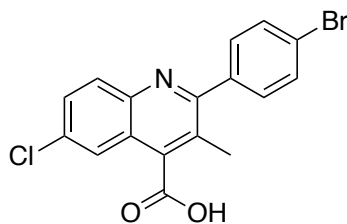
Isatin (5.00 g, 34.0 mmol), 1-(4-bromophenyl)propan-1-one (7.41 g, 34.7 mmol), and KOH (11.4 g, 204 mmol) were dissolved in 55 mL EtOH and 24 mL H₂O. Following general protocol A, 2-(4-

bromophenyl)-3-methylquinoline-4-carboxylic acid was recovered as a white solid (8.73 g, 25.6 mmol, 75%) upon recrystallization in EtOH. $^1\text{H NMR}$ (300 MHz, $\text{DMSO-}d_6$) δ 8.03 (d, $J = 8.5$ Hz, 1H), 7.81 – 7.56 (m, 7H), 2.36 (s, 3H); **MS** (ESI) 342.0, 343.9 $[\text{M}+\text{H}]^+$, 342.0, 340.0 $[\text{M}-\text{H}]^-$.



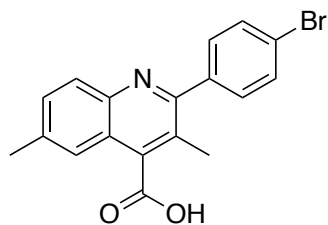
2-(4-Bromophenyl)-6-fluoro-3-methylquinoline-4-carboxylic acid

(85): 5-Fluoroisatin (1.00 g, 6.06 mmol), 1-(4-bromophenyl)propan-1-one (1.29 g, 6.06 mmol), and KOH (1.02 g, 18.2 mmol) were dissolved in 10 mL EtOH and 3 mL H_2O . Following general protocol A, 2-(4-bromophenyl)-6-fluoro-3-methylquinoline-4-carboxylic acid was recovered as a beige solid (853 mg, 2.38 mmol, 39%) $^1\text{H NMR}$ (500 MHz, $\text{DMSO-}d_6$) δ 8.14 – 8.10 (m, 1H), 7.73 – 7.67 (m, 3H), 7.57 (d, $J = 8.1$ Hz, 2H), 7.51 – 7.47 (m, 1H), 2.39 (s, 3H); **MS** (ESI+) 360.0, 361.9 $[\text{M}+\text{H}]^+$ 358.1, 360.2 $[\text{M}-\text{H}]^-$.



2-(4-Bromophenyl)-6-chloro-3-methylquinoline-4-carboxylic acid

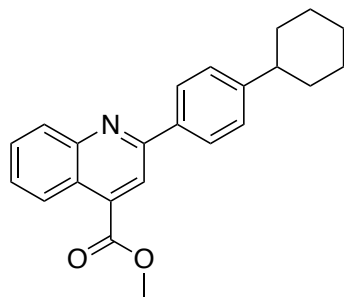
(86): 5-Chloroisatin (1.00 g, 5.49 mmol), 1-(4-bromophenyl)propan-1-one (1.20 g, 5.63 mmol), and KOH (1.23 g, 22.0 mmol) were dissolved in 20 mL EtOH and 10 mL H_2O . Following general protocol A, 2-(4-bromophenyl)-6-chloro-3-methylquinoline-4-carboxylic acid was recovered as a tan solid (1.57 g, 4.18 mmol, 76%) $^1\text{H NMR}$ (400 MHz, $\text{DMSO-}d_6$) δ 8.13 (d, $J = 8.8$ Hz, 1H), 7.88 – 7.81 (m, 2H), 7.79 – 7.75 (m, 2H), 7.68 – 7.62 (m, 2H), 2.47 (s, 3H); **MS** (ESI) 376.0, 377.9 $[\text{M}+\text{H}]^+$.



2-(4-Bromophenyl)-3,6-dimethylquinoline-4-carboxylic acid (87):

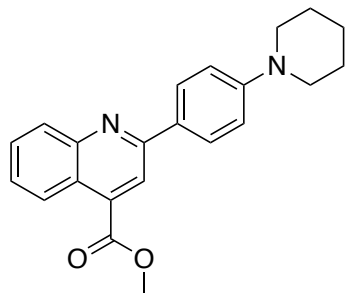
5-Methylisatin (1.00 g, 6.21 mmol), 1-(4-bromophenyl)propan-1-one (1.32 g, 6.20 mmol), and KOH (1.39 g, 24.8 mmol) were dissolved in 10 mL EtOH and 3 mL H₂O. Following general protocol A, 2-(4-bromophenyl)-3,6-dimethylquinoline-4-carboxylic acid was recovered as a tan solid (1.14 g, 3.20 mmol, 52%). ¹H NMR (400 MHz, DMSO-*d*₆) δ 8.07 (d, *J* = 8.6 Hz, 1H), 7.79 – 7.70 (m, 3H), 7.66 – 7.60 (m, 3H), 2.56 (s, 3H), 2.38 (s, 3H); MS (ESI) 356.0 [M+H]⁺.

General protocol B, acid catalyzed esterification: The corresponding carboxylic acid (1.0 eq) was dissolved in solution containing anhydrous MeOH and a catalytic amount of H₂SO₄. The reaction mixture was refluxed overnight before concentrating MeOH. Residue was re-dissolved in H₂O and neutralized before extracting product with EtOAc (3x). The organic layer was dried with MgSO₄, filtered, concentrated, and purified via flash chromatography using a gradient method from 5 to 60% EtOAc in hexane (63-88%).



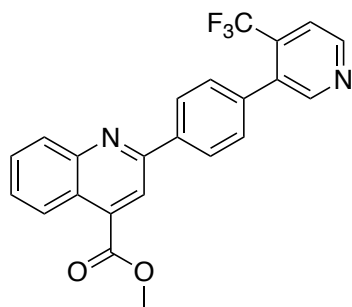
Methyl 2-(4-cyclohexylphenyl)quinoline-4-carboxylate (23):

Compound **1** (25 mg, 0.08 mmol) was dissolved in 2 mL MeOH. H₂SO₄ (16 drops, catalyst) was added to the reaction mixture and the mixture was heated to reflux overnight. Following general protocol B, methyl 2-(4-cyclohexylphenyl)quinoline-4-carboxylate was recovered as an off-white solid (25 mg, 0.07 mmol, 88%) ¹H NMR (300 MHz, CDCl₃-*d*) δ 8.76 (d, *J* = 8.5 Hz, 1H), 8.41 (s, 1H), 8.24 (d, *J* = 8.4 Hz, 1H), 8.15 (d, *J* = 8.0 Hz, 2H), 7.86 – 7.71 (m, 1H), 7.69 – 7.59 (m, 1H), 7.41 (d, *J* = 8.0 Hz, 2H), 4.09 (s, 3H), 2.70 – 2.57 (m, 1H), 2.03 – 1.85 (m, 4H), 1.84 – 1.67 (m, 1H), 1.61 – 1.21 (m, 5H); LCMS (ESI) 346.2 [M+H]⁺; HPLC Purity at 254 nm, 98.7%.



Methyl 2-(4-(piperidin-1-yl)phenyl)quinoline-4-carboxylate (24):

Compound **25** (30 mg, 0.09 mmol) was dissolved in 2 mL MeOH. H₂SO₄ (16 drops, catalyst) was added to the reaction mixture and the mixture was heated to reflux for 12 hours. Following general protocol B, methyl 2-(4-(piperidin-1-yl)phenyl)quinoline-4-carboxylate was recovered as a yellow solid (29 mg, 0.08 mmol, 88%). **¹H NMR** (400 MHz, CDCl₃-*d*) δ 8.71 (dd, *J* = 8.5, 1.4 Hz, 1H), 8.38 (s, 1H), 8.21 – 8.12 (m, 3H), 7.80 – 7.70 (m, 1H), 7.63 – 7.53 (m, 1H), 7.13 – 7.00 (m, 2H), 4.08 (d, *J* = 1.0 Hz, 3H), 3.39 – 3.28 (m, 4H), 1.80 – 1.71 (m, 4H), 1.70 – 1.60 (m, 2H); **LCMS** (ESI) 347.2 [M+H]⁺; **HPLC** Purity at 254 nm, 97.3%.

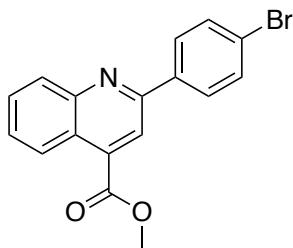


Methyl 2-(4-(4-(trifluoromethyl)pyridin-3-yl)phenyl)quinoline-4-

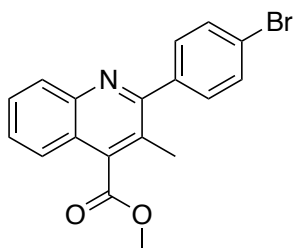
carboxylate (54): Compound **53** (30 mg, 0.08 mmol) was dissolved in anhydrous MeOH with a catalytic amount of H₂SO₄ (30 drops). Following general protocol B, methyl 2-(4-(4-(trifluoromethyl)pyridin-3-yl)phenyl)quinoline-4-carboxylate was recovered as a white solid (19 mg, 0.05 mmol, 63%). **¹H NMR** (400 MHz, CDCl₃-*d*) δ 8.90 – 8.73 (m, 3H), 8.50 (s, 1H), 8.34 (d, *J* = 8.2 Hz, 2H), 8.31 – 8.25 (m, 1H), 7.82 (ddd, *J* = 8.5, 6.8, 1.5 Hz, 1H), 7.71 – 7.65 (m, 2H), 7.56 (d, *J* = 8.0 Hz, 2H), 4.12 (s, 3H); **LCMS** (ESI) 409.1 [M+H]⁺; **HPLC** Purity at 254 nm, 99.9%.

General protocol C, base catalyzed esterification: The corresponding carboxylic acid (1.0 eq), Cs₂CO₃ (1.2 eq), and MeI (2.0 eq) were dissolved in anhydrous DMF. The mixture was stirred at room temperature overnight. Upon completion, the mixture was diluted EtOAc and washed with

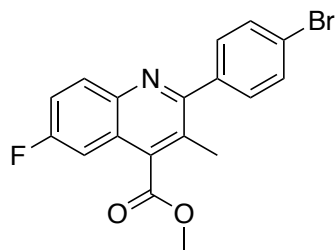
brine (8x). The organic layer was dried with MgSO₄, filtered, concentrated, and purified via flash chromatography using a gradient method from 5 to 60% EtOAc in hexane (43-93%).



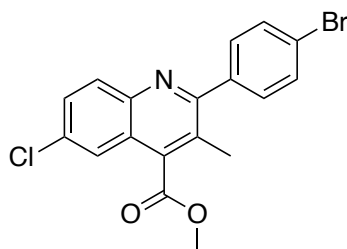
Methyl 2-(4-bromophenyl)quinoline-4-carboxylate (88): Intermediate **83** (9.00 g, 27.4 mmol), Cs₂CO₃ (10.8 g, 33.3 mmol) and MeI (3.48 mL, 55.4 mmol) were stirred at room temperature in 139 mL DMF overnight. Following general protocol C, methyl 2-(4-bromophenyl)quinoline-4-carboxylate (4.07 g, 11.9 mmol, 43%) was recovered as a white solid. ¹H NMR (300 MHz, CDCl₃-*d*) δ 8.79 – 8.71 (m, 1H), 8.36 (s, 1H), 8.25 – 8.17 (m, 1H), 8.14 – 8.06 (m, 2H), 7.83 – 7.74 (m, 1H), 7.71 – 7.61 (m, 3H), 4.09 (s, 3H); **MS** (ESI) 342.0 [M+H]⁺.



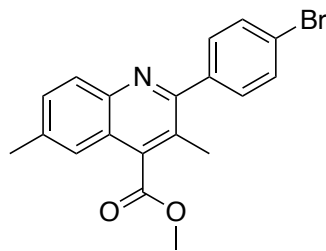
Methyl 2-(4-bromophenyl)-3-methylquinoline-4-carboxylate (89): Intermediate **84** (8.73 g, 25.6 mmol), Cs₂CO₃ (9.98 g, 30.7 mmol) and MeI (3.22 mL, 51.2 mmol) were stirred at room temperature in 140 mL DMF overnight. Following general protocol C, methyl 2-(4-bromophenyl)-3-methylquinoline-4-carboxylate (7.55 g, 21.2 mmol, 83%) was recovered as a white cake-like powder. ¹H NMR (300 MHz, CDCl₃-*d*) δ 8.15 (d, *J* = 8.6 Hz, 1H), 7.78 – 7.69 (m, 2H), 7.70 – 7.57 (m, 3H), 7.47 (d, *J* = 7.5 Hz, 2H), 4.12 (s, 3H), 2.41 (s, 3H); **MS** (ESI) 356.0, 357.9 [M+H]⁺.



Methyl 2-(4-bromophenyl)-6-fluoro-3-methylquinoline-4-carboxylate (90): Intermediate **85** (853 mg, 2.38 mmol), Cs₂CO₃ (928 mg, 2.86 mmol), and MeI (0.3 mL, 4.76 mmol) were stirred at room temperature in 12 mL DMF overnight. Following general protocol C, methyl 2-(4-bromophenyl)-6-fluoro-3-methylquinoline-4-carboxylate recovered (636 mg, 1.71 mmol, 71%) as a solid. ¹H NMR (300 MHz, CDCl₃-*d*) δ 8.13 (dd, *J* = 9.2, 5.4 Hz, 1H), 7.70 – 7.63 (m, 2H), 7.54 – 7.43 (m, 3H), 7.42 – 7.35 (m, 1H), 4.11 (s, 3H), 2.42 (s, 3H); **MS** (ESI) 374.0, 376.0 [M+H]⁺.



Methyl 2-(4-bromophenyl)-6-chloro-3-methylquinoline-4-carboxylate (91): Intermediate **86** (1.57 g, 4.18 mmol), Cs₂CO₃ (1.63 g, 5.02 mmol) and MeI (0.53 mL, 8.36 mmol) were stirred at room temperature in 40 mL DMF overnight. Following general protocol C, methyl 2-(4-bromophenyl)-6-chloro-3-methylquinoline-4-carboxylate (1.21 g, 3.13 mmol, 75%) was recovered as an orange solid. ¹H NMR (300 MHz, CDCl₃-*d*) δ 8.07 (d, *J* = 9.0 Hz, 1H), 7.75 – 7.71 (m, 1H), 7.66 (d, *J* = 8.1 Hz, 3H), 7.49 – 7.42 (m, 2H), 4.13 (s, 2H), 2.42 (s, 3H); **MS** (ESI) 389.9, 392.0 [M+H]⁺.

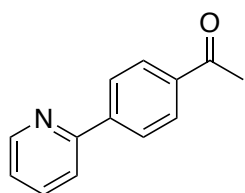


Methyl 2-(4-bromophenyl)-3,6-dimethylquinoline-4-carboxylate (92): Intermediate **87** (1.14 g, 3.08 mmol), Cs₂CO₃ (1.20 g, 3.69 mmol) and MeI (0.38 mL, 6.16 mmol) were stirred at room temperature in 40 mL DMF overnight. Following general protocol C,

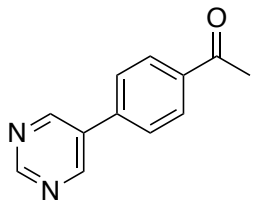
methyl 2-(4-bromophenyl)-3,6-dimethylquinoline-4-carboxylate (1.06 g, 2.87 mmol, 93%) was recovered as an orange solid. $^1\text{H NMR}$ (300 MHz, CDCl_3 -*d*) δ 8.03 (d, $J = 8.6$ Hz, 1H), 7.68 – 7.60 (m, 2H), 7.59 – 7.53 (m, 1H), 7.50 – 7.42 (m, 3H), 4.12 (s, 3H), 2.57 (s, 3H), 2.39 (s, 3H); **MS** (ESI) 370.0, 371.9 $[\text{M}+\text{H}]^+$.

General procedure D, Suzuki coupling Non-microwave protocol: To a degassed round bottom flask containing brominated starting material (1 eq), boronic acid (1.2-1.5 eq), K_2CO_3 (3-4 eq), $\text{Pd}(\text{PPh}_3)_4$ (5-10% mol) was dissolved in dioxane or toluene. The reaction was heated at reflux until loss of starting material was observed via TLC (12-48 hrs). The reaction mixture was concentrated, partitioned between EtOAc/ H_2O , and washed with EtOAc (3x). The organic layer was dried with MgSO_4 and concentrated to a residue, which was then purified by flash silica chromatography using a gradient of 10 to 60% EtOAc in hexane.

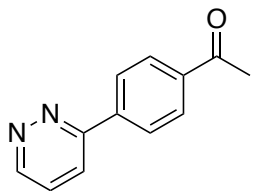
Microwave protocol: Brominated starting material (1 eq), corresponding boronic acid (1.5 eq), base (Na_2CO_3 or K_2HPO_4 , 3-4 eq), and $\text{Pd}(\text{PPh}_3)_4$ ($\approx 5\%$ eq) were dissolved in 2:1 dioxane/ H_2O or toluene/ H_2O in a microwave vial. The vial was capped, purged with argon, and used in a microwave synthesizer. The reaction was heated at 125-130 $^\circ\text{C}$ for 1.5 – 2 hrs and followed the same purification as the non-microwave protocol. Yields for both protocols ranged from 7 – 97%.



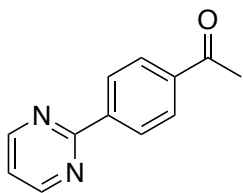
1-(4-(Pyridin-2-yl)phenyl)ethan-1-one (93): (4-Acetylphenyl)boronic acid (1.04 g, 6.34 mmol), 2-iodopyridine (0.52 mL, 4.85 mmol), K_2CO_3 (2.68 g, 19.4 mmol), and $\text{Pd}(\text{PPh}_3)_4$ (280 mg) were dissolved 10 mL dioxane and 1 mL H_2O . The reaction was heated to 100 $^\circ\text{C}$ overnight. Following general protocol D, 1-(4-(pyridin-2-yl)phenyl)ethan-1-one was recovered as a white solid (185 mg, 0.93 mmol, 19%). $^1\text{H NMR}$ (400 MHz, CDCl_3 -*d*) δ 8.78 – 8.74 (m, 1H), 8.15 – 8.06 (m, 4H), 7.84 – 7.80 (m, 2H), 7.34 – 7.29 (m, 1H), 2.67 (s, 3H); **MS** (ESI) 198.0 $[\text{M}+\text{H}]^+$.



1-(4-(Pyrimidin-5-yl)phenyl)ethan-1-one (94): (4-Acetylphenyl)boronic acid (155 mg, 0.94 mmol), 5-bromopyrimidine (100 mg, 0.63 mmol), K_2HPO_3 (219 g, 1.26 mmol), and $Pd(OAc)_2$ (2 mg) were dissolved 10 mL ethylene glycol. The reaction was heated to 80 °C for 4 hours. Following general protocol D, 1-(4-(pyrimidin-5-yl)phenyl)ethan-1-one was recovered as a white solid (104 mg, 0.52 mmol, 55%). 1H NMR (300 MHz, $CDCl_3-d$) δ 9.33 (s, 1H), 9.05 (s, 2H), 8.14 (d, $J = 8.3$ Hz, 2H), 7.72 (d, $J = 8.3$ Hz, 2H), 2.69 (s, 3H); **MS** (ESI) 199.0 $[M+H]^+$.

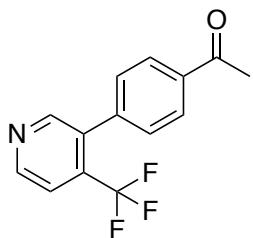


1-(4-(Pyridazin-3-yl)phenyl)ethan-1-one (95): (4-Acetylphenyl)boronic acid (670 mg, 4.08 mmol), 3-bromopyridazine (500 mg, 3.15 mmol), K_2CO_3 (1.74 g, 12.6 mmol), and $Pd(PPh_3)_4$ (182 mg) were dissolved 10 mL dioxane and 1 mL H_2O . The reaction was heated to 100 °C overnight. Following general protocol D, 1-(4-(pyridazin-3-yl)phenyl)ethan-1-one was recovered as a white solid (301 mg, 1.52 mmol, 48%). 1H NMR (400 MHz, $CDCl_3-d$) δ 8.12 – 8.05 (m, 2H), 7.97 – 7.89 (m, 1H), 7.77 – 7.70 (m, 2H), 7.00 – 6.91 (m, 1H), 2.69 (s, 3H); **MS** (ESI) 199.2 $[M+H]^+$.



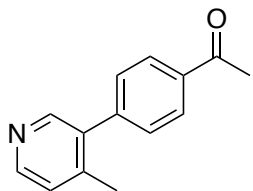
1-(4-(Pyrimidin-2-yl)phenyl)ethan-1-one (96): (4-Acetylphenyl)boronic acid (1.08 g, 6.60 mmol), 3,2-bromopyrimidine (700 mg, 4.40 mmol), K_2CO_3 (2.43 g, 17.6 mmol), and $Pd(PPh_3)_4$ (254 mg) were dissolved 10 mL dioxane. The reaction was heated to 100 °C for 10 hr. Following general protocol D, 1-(4-(pyrimidin-2-yl)phenyl)ethan-1-one was recovered as a white solid (109 mg, 0.55 mmol, 13%). 1H NMR (400 MHz, $CDCl_3-d$) δ 8.87 (d,

$J = 4.8$ Hz, 2H), 8.60 – 8.54 (m, 2H), 8.12 – 8.07 (m, 2H), 7.30 – 7.26 (m, 1H), 2.69 (s, 3H); **MS** (ESI) 199.1 $[M+H]^+$.



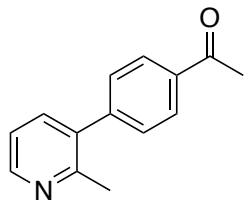
1-(4-(4-(Trifluoromethyl)pyridin-3-yl)phenyl)ethan-1-one (97):

(4-Acetylphenyl)boronic acid (100 mg, 0.44 mmol), 3-bromo-4-(trifluoromethyl)pyridine (109 mg, 0.66 mmol), K_2HPO_4 (230 mg, 1.32 mmol), and $Pd(PPh_3)_4$ (25 mg) were dissolved in 2 mL dioxane and 1 mL H_2O . The mixture was heated to 130 °C for 1.5 hours in a microwave reactor. Following general protocol D, 1-(4-(4-(trifluoromethyl)pyridin-3-yl)phenyl)ethan-1-one was recovered as a clear oil (60 mg, 0.23 mmol, 53%). 1H NMR (300 MHz, $CDCl_3-d$) δ 8.87 – 8.81 (m, 1H), 8.66 (s, 1H), 8.11 – 8.02 (m, 2H), 7.66 (d, $J = 5.1$ Hz, 1H), 7.46 (d, $J = 8.1$ Hz, 2H), 2.67 (s, 3H); **MS** (ESI) 266.0 $[M+H]^+$.



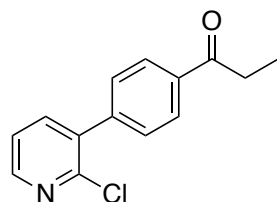
1-(4-(4-Methylpyridin-3-yl)phenyl)ethan-1-one (98):

(4-Acetylphenyl)boronic acid (570 mg, 3.47 mmol), 3-bromo-4-methylpyridine (0.20 mL, 1.79 mmol), Na_2CO_3 (1.47 g, 13.9 mmol), and $Pd(PPh_3)_4$ (200 mg) were dissolved in 10 mL toluene and 1 mL H_2O . The reaction was heated to 120 °C for 10 hr. Following general protocol D, 1-(4-(4-methylpyridin-3-yl)phenyl)ethan-1-one was recovered (368 mg, 1.74 mmol, 97%) as a white solid. 1H NMR (300 MHz, $CDCl_3-d$) δ 8.38 – 8.27 (m, 2H), 7.93 (d, $J = 8.0, 1.6$ Hz, 2H), 7.31 (d, $J = 8.1, 1.6$ Hz, 2H), 7.09 (d, $J = 5.1$ Hz, 1H), 2.52 (s, 3H), 2.17 (s, 3H); **MS** (ESI) 212.1 $[M+H]^+$.



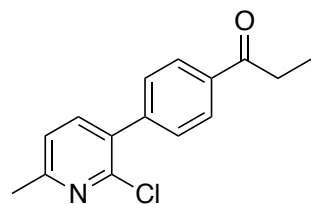
1-(4-(2-Methylpyridin-3-yl)phenyl)ethan-1-one (99):

(4-Acetylphenyl)boronic acid (570 mg, 3.47 mmol), 3-bromo-2-methylpyridine (0.20 mL, 1.73 mmol), Na₂CO₃ (1.47 g, 13.88 mmol), and Pd(PPh₃)₄ (200 mg) were dissolved in 10 mL toluene and 1 mL H₂O. The reaction was heated to 120 °C for 10 hr. Following general protocol D, 1-(4-(2-methylpyridin-3-yl)phenyl)ethan-1-one was recovered as an oil (249 mg, 1.18 mmol, 68%). ¹H NMR (400 MHz, CDCl₃-d) δ 8.57 – 8.54 (m, 1H), 8.09 – 8.04 (m, 2H), 7.58 – 7.53 (m, 1H), 7.47 – 7.42 (m, 2H), 7.27 – 7.22 (m, 1H), 2.68 (s, 3H), 2.54 (s, 3H); MS (ESI) 212.1 [M+H]⁺.



1-(4-(2-Chloropyridin-3-yl)phenyl)propan-1-one (100):

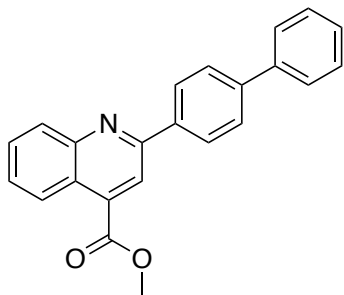
4'-Bromopropiophenone (300 mg, 1.41 mmol), 2-chloropyridine-3-boronic acid (332 mg, 2.11 mmol), K₂HPO₄ (736 mg, 4.23 mmol), and Pd(PPh₃)₄ (81 mg) were added to a microwave vial in 2 mL dioxane and 1 mL H₂O. The mixture was heated to 100 °C for 12 hours. Following general protocol D, 1-(4-(2-chloropyridin-3-yl)phenyl)propan-1-one was recovered as a white solid (134 mg, 0.55 mmol, 39%). ¹H NMR (300 MHz, CDCl₃-d) δ 8.43 (dd, *J* = 4.8, 1.9 Hz, 1H), 8.06 (d, 2H), 7.71 (dd, *J* = 7.5, 1.9 Hz, 1H), 7.56 (d, 2H), 7.41 – 7.34 (m, 1H), 3.06 (q, *J* = 7.2 Hz, 2H), 1.25 (t, *J* = 7.2 Hz, 3H); MS (ESI) 246.0 [M+H]⁺.



1-(4-(2-Chloro-6-methylpyridin-3-yl)phenyl)propan-1-one (101):

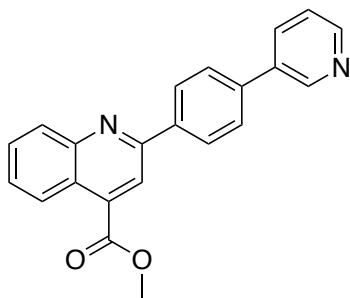
4'-Bromopropiophenone (220 mg, 1.03 mmol), (2-chloro-6-methylpyridin-3-yl)boronic acid (264 mg, 1.54 mmol), K₂HPO₄ (538 mg, 3.09 mmol), and Pd(PPh₃)₄ (60 mg, 5% mmol) were dissolved in 2 mL dioxane and 1 mL H₂O. The mixture was heated to 130 °C for 1.5 hours in a

microwave reactor. Following general protocol D, 1-(4-(2-Chloro-6-methylpyridin-3-yl)phenyl)propan-1-one was recovered as a white solid (137 mg, 0.53 mmol, 51%). ¹H NMR (300 MHz, CDCl₃-*d*) δ 8.07 – 7.99 (m, 2H), 7.59 – 7.49 (m, 3H), 7.19 (d, *J* = 7.7 Hz, 1H), 3.04 (q, *J* = 7.2 Hz, 2H), 2.58 (s, 3H), 1.24 (t, *J* = 7.2 Hz, 3H); MS (ESI) 260.0 [M+H]⁺.



Methyl 2-([1,1'-biphenyl]-4-yl)quinoline-4-carboxylate (29):

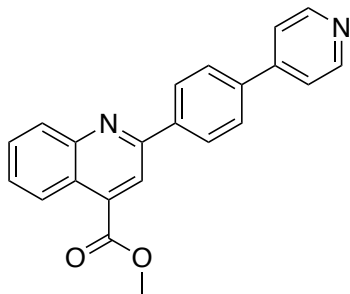
Intermediate **88** (100 mg, 0.29 mmol), phenylboronic acid (53 mg, 0.43 mmol), K₂HPO₄ (151 mg, 0.87 mmol), and Pd(PPh₃)₄ (17 mg, 0.01 mmol) were dissolved in 2 mL dioxane and 1 mL H₂O. The mixture was heated to 130 °C for 1.5 hours in a microwave reactor. Following general protocol D, Methyl 2-([1,1'-biphenyl]-4-yl)quinoline-4-carboxylate was recovered as a white crystal (28 mg, 0.08 mmol, 28%). ¹H NMR (300 MHz, CDCl₃-*d*) δ 8.76 (dd, *J* = 8.6, 1.3 Hz, 1H), 8.46 (s, 1H), 8.35 – 8.20 (m, 3H), 7.85 – 7.73 (m, 3H), 7.74 – 7.58 (m, 3H), 7.49 (t, *J* = 7.4 Hz, 2H), 4.09 (s, 3H); LCMS (ESI) 340.1 [M+H]⁺; HPLC Purity at 254 nm, 99.5%.



Methyl 2-(4-(pyridin-3-yl)phenyl)quinoline-4-carboxylate (33):

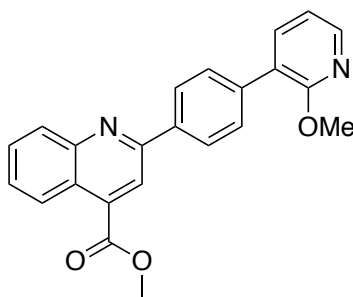
Intermediate **88** (60 mg, 0.18 mmol), pyridin-3-ylboronic acid (23 mg, 0.19 mmol), Pd(PPh₃)₄ (10 mg), and K₂CO₃ (72 mg, 0.53 mmol) were combined in 3 mL toluene and 1 mL H₂O. The mixture was heated at 110 °C overnight. Following general protocol D, methyl 2-(4-(pyridin-3-yl)phenyl)quinoline-4-carboxylate was recovered as a white solid (20 mg, 0.06 mmol, 33%). ¹H NMR (300 MHz, CDCl₃-*d*) δ 8.92 (s, 1H), 8.74 (d, *J* = 8.5 Hz, 1H), 8.62 (d, *J* = 4.8 Hz, 1H), 8.40 (s, 1H), 8.29 (d, *J* = 8.2 Hz, 2H), 8.21 (d, *J* = 8.4 Hz, 1H), 7.91 (dd, *J* = 8.0, 2.0 Hz, 1H),

7.82 – 7.68 (m, 3H), 7.66 – 7.57 (m, 1H), 7.37 (dd, $J = 7.9, 4.8$ Hz, 1H), 4.23 – 3.94 (m, 3H); **LCMS** (ESI) 341.1 $[M+H]^+$; **HPLC** Purity at 254 nm, 99.6%.



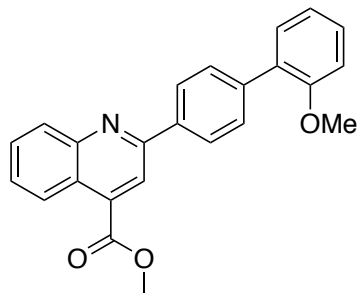
Methyl 2-(4-(pyridin-4-yl)phenyl)quinoline-4-carboxylate (102):

Intermediate **88** (100 mg, 0.29 mmol), 4-pyridineboronic acid pinacol ester (84 mg, 0.41 mmol), $\text{Pd}(\text{PPh}_3)_4$ (17 mg), and K_2CO_3 (151 mg, 0.87 mmol) were dissolved in 2 ml dioxane and 1 mL H_2O . The mixture was heated to 130 °C for 1.5 hours in a microwave reactor. Following general protocol D, methyl 2-(4-(pyridin-4-yl)phenyl)quinoline-4-carboxylate was recovered as an off-white solid (34 mg, 0.10 mmol, 34%). $^1\text{H NMR}$ (300 MHz, CDCl_3-d) δ 8.80 – 8.67 (m, 3H), 8.44 (s, 1H), 8.39 – 8.30 (m, 2H), 8.28 – 8.20 (m, 1H), 7.79 (dd, $J = 8.8, 6.7$ Hz, 3H), 7.70 – 7.55 (m, 3H), 4.09 (s, 3H); **LCMS** (ESI) 341.1 $[M+H]^+$; **HPLC** Purity at 254 nm, 99.6%.

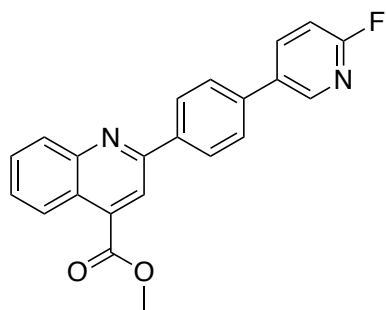


Methyl 2-(4-(2-methoxypyridin-3-yl)phenyl)quinoline-4-

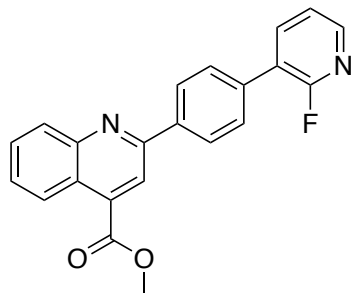
carboxylate (103): Intermediate **88** (200 mg, 0.59 mmol), (2-methoxypyridin-3-yl)boronic acid (108 mg, 0.70 mmol), K_2CO_3 (326 mg, 2.36 mmol), and $\text{Pd}(\text{PPh}_3)_4$ (67 mg) were dissolved in 5 mL toluene and 2 mL H_2O . The mixture was heated to reflux overnight. Following general protocol D, methyl 2-(4-(2-methoxypyridin-3-yl)phenyl)quinoline-4-carboxylate was recovered as an off-white solid (15 mg, 0.04 mmol, 7%). $^1\text{H NMR}$ (300 MHz, CDCl_3-d) δ 8.78 (d, $J = 8.5$ Hz, 1H), 8.48 (s, 1H), 8.34 – 8.19 (m, 4H), 7.86 – 7.61 (m, 5H), 7.08 – 7.00 (m, 1H), 4.11 (s, 3H), 4.03 (s, 3H); **MS** (ESI) 371.1 $[M+H]^+$.



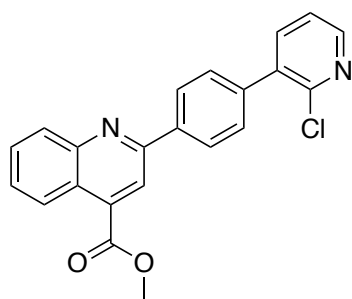
Methyl 2-(2'-methoxy-[1,1'-biphenyl]-4-yl)quinoline-4-carboxylate (104): Intermediate **88** (140 mg, 0.41 mmol), (2-methoxyphenyl)boronic acid (87 mg, 0.57 mmol), K_2CO_3 (250 mg, 1.81 mmol), and $Pd(PPh_3)_4$ (26 mg) were dissolved in 6 mL anhydrous dioxane. The mixture was heated to reflux overnight. Following general protocol D, methyl 2-(2'-methoxy-[1,1'-biphenyl]-4-yl)quinoline-4-carboxylate (14 mg, 0.04 mmol, 10%). 1H NMR (300 MHz, $CDCl_3-d$) δ 8.84 – 8.75 (m, 1H), 8.49 (s, 1H), 8.35 – 8.25 (m, 3H), 7.84 – 7.73 (m, 3H), 7.69 – 7.62 (m, 1H), 7.46 – 7.35 (m, 2H), 7.15 – 7.01 (m, 2H), 4.11 (s, 3H), 3.87 (s, 2H); **MS** (ESI) 370.1 $[M+H]^+$.



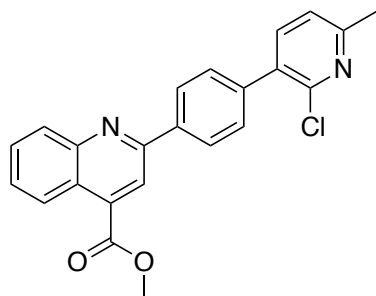
Methyl 2-(4-(6-fluoropyridin-3-yl)phenyl)quinoline-4-carboxylate (105): Intermediate **88** (50 mg, 0.15 mmol), (6-fluoropyridin-3-yl)boronic acid (35 mg, 0.25 mmol), K_2HPO_4 (73 mg, 0.42 mmol) and $Pd(PPh_3)_4$ (8 mg, 7.0×10^{-3} mmol) were dissolved in 1 mL dioxane and 0.5 mL H_2O . The mixture was heated to 130 °C for 1.5 hours in a microwave reactor. Following general protocol D, methyl 2-(4-(6-fluoropyridin-3-yl)phenyl)quinoline-4-carboxylate was recovered as a beige solid (45 mg, 0.13 mmol, 93% yield). 1H NMR (300 MHz, $CDCl_3-d$) δ 8.82 – 8.74 (m, 1H), 8.56 – 8.49 (m, 1H), 8.46 (s, 1H), 8.40 – 8.31 (m, 2H), 8.26 (d, $J = 8.5, 0.9$ Hz, 1H), 8.10 – 8.01 (m, 1H), 7.85 – 7.77 (m, 1H), 7.76 – 7.62 (m, 3H), 7.06 (dd, $J = 8.5, 3.0$ Hz, 1H); **MS** (ESI) 359.0 $[M+H]^+$.



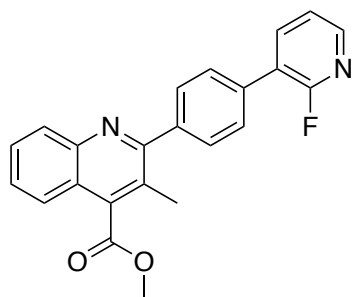
Methyl 2-(4-(2-fluoropyridin-3-yl)phenyl)quinoline-4-carboxylate (106): Intermediate **88** (50 mg, 0.15 mmol), (2-fluoropyridin-3-yl)boronic acid (34 mg, 0.24 mmol), K_2HPO_4 (73 mg, 0.42 mmol) and $Pd(PPh_3)_4$ (8 mg, 7.0×10^{-3} mmol) were dissolved in 1 mL dioxane and 0.5 mL H_2O . The mixture was heated to 130 °C for 1.5 hours in a microwave reactor. Following general protocol D, methyl 2-(4-(2-fluoropyridin-3-yl)phenyl)quinoline-4-carboxylate was recovered as a white solid (45 mg, 0.13 mmol, 93% yield). 1H NMR (300 MHz, $CDCl_3-d$) δ 8.78 (d, $J = 8.6$, 1.3 Hz, 1H), 8.47 (s, 1H), 8.37 – 8.31 (m, 2H), 8.30 – 8.19 (m, 1H), 8.02 – 7.92 (m, 1H), 7.85 – 7.63 (m, 5H), 7.38 – 7.31 (m, 1H); **MS** (ESI) 359.1 $[M+H]^+$



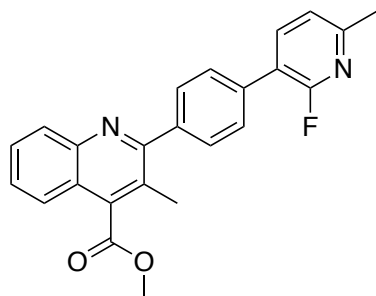
Methyl 2-(4-(2-chloropyridin-3-yl)phenyl)quinoline-4-carboxylate (107): Intermediate **88** (150 mg, 0.44 mmol), (2-chloropyridin-3-yl)boronic acid (110 mg, 0.71 mmol), K_2CO_3 (243 mg, 1.76 mmol), and $Pd(PPh_3)_4$ (25 mg) were dissolved in 5 mL dioxane and 1 mL H_2O . The mixture was heated to reflux overnight. Following general protocol D, methyl 2-(4-(2-chloropyridin-3-yl)phenyl)quinoline-4-carboxylate was recovered as an off-white solid (76 mg, 0.20 mmol, 45%). 1H NMR (300 MHz, $CDCl_3-d$) δ 8.79 (d, $J = 8.5$ Hz, 1H), 8.50 – 8.43 (m, 2H), 8.33 (d, $J = 8.1$ Hz, 2H), 8.27 (d, $J = 8.4$ Hz, 1H), 7.85 – 7.73 (m, 2H), 7.68 (dd, $J = 8.4$, 6.5 Hz, 3H), 7.40 – 7.34 (m, 1H), 4.11 (s, 3H); **MS** (ESI) 375.0 $[M+H]^+$.



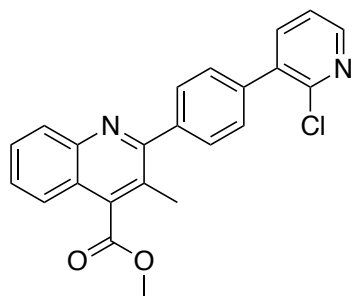
Methyl 2-(4-(2-chloro-6-methylpyridin-3-yl)phenyl)quinoline-4-carboxylate (108): Intermediate **88** (132 mg, 0.39 mmol), (2-chloro-6-methylpyridin-3-yl)boronic acid (100 mg, 0.58 mmol), K_2HPO_4 (204 mg, 1.17 mmol), and $Pd(PPh_3)_4$ (23 mg) were dissolved in 5 mL dioxane and 1 mL H_2O . The mixture was heated to reflux overnight. Following general protocol D, methyl 2-(4-(2-chloro-6-methylpyridin-3-yl)phenyl)quinoline-4-carboxylate (109 mg, 0.29 mmol, 74%). 1H NMR (300 MHz, $CDCl_3-d$) δ 8.83 – 8.74 (m, 1H), 8.47 (s, 1H), 8.35 – 8.22 (m, 3H), 7.86 – 7.77 (m, 1H), 7.72 – 7.61 (m, 4H), 7.21 (d, $J = 7.6$ Hz, 1H), 4.10 (s, 3H), 2.63 (s, 3H); **MS** (ESI) 389.1 $[M+H]^+$.



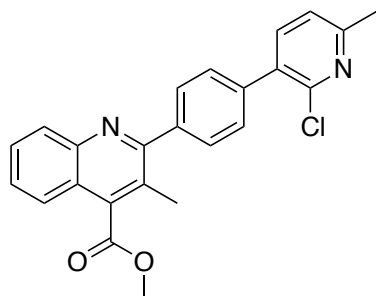
Methyl 2-(4-(2-fluoropyridin-3-yl)phenyl)-3-methylquinoline-4-carboxylate (109): Intermediate **89** (100 mg, 0.28 mmol), (2-fluoropyridin-3-yl)boronic acid (60 mg, 0.42 mmol), K_2HPO_4 (146 mg, 0.84 mmol), and $Pd(PPh_3)_4$ (16 mg, 0.01 mmol) were dissolved in 2 mL dioxane and 1 mL H_2O . The mixture was heated to 130 °C for 1.5 hours in a microwave reactor. Following general protocol D, methyl 2-(4-(2-fluoropyridin-3-yl)phenyl)-3-methylquinoline-4-carboxylate was recovered as a white solid (82 mg, 0.22 mmol, 79%). 1H NMR (300 MHz, $CDCl_3-d$) δ 8.26 – 8.22 (m, 1H), 8.20 – 8.15 (m, 1H), 7.98 – 7.90 (m, 1H), 7.78 – 7.67 (m, 6H), 7.64 – 7.56 (m, 1H), 7.35 – 7.29 (m, 1H), 4.12 (s, 3H), 2.48 (s, 3H); **MS** (ESI) 373.1 $[M+H]^+$.



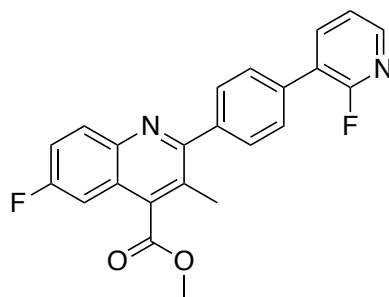
Methyl 2-(4-(2-fluoro-6-methylpyridin-3-yl)phenyl)-3-methylquinoline-4-carboxylate (110): Intermediate **89** (50 mg, 0.13 mmol), (2-fluoro-6-methylpyridin-3-yl)boronic acid (31 mg, 0.20 mmol), K_2HPO_4 (73 mg, 0.42 mmol), and $Pd(PPh_3)_4$ (7 mg, 6.0×10^{-3} mmol) were dissolved in 1 mL dioxane and 0.5 mL H_2O . The mixture was heated to 130 °C for 1.5 hours in a microwave reactor. Following general protocol D, methyl 2-(4-(2-fluoro-6-methylpyridin-3-yl)phenyl)-3-methylquinoline-4-carboxylate was recovered as a white solid (22 mg, 0.06 mmol, 43%). 1H NMR (300 MHz, $CDCl_3-d$) δ 8.17 (d, $J = 8.6$, 1.5 Hz, 1H), 7.89 – 7.79 (m, 1H), 7.78 – 7.66 (m, 6H), 7.60 (t, $J = 7.3$, 6.9, 1.3 Hz, 1H), 7.18 (d, $J = 7.6$, 1.8 Hz, 1H), 4.13 (s, 3H), 2.59 (s, 3H), 2.48 (s, 3H); **MS** (ESI) 387.2 $[M+H]^+$.



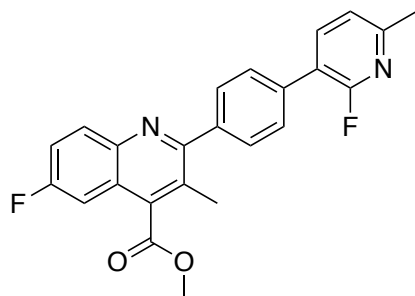
Methyl 2-(4-(2-chloropyridin-3-yl)phenyl)-3-methylquinoline-4-carboxylate (111): Intermediate **89** (50 mg, 0.14 mmol), (2-chloropyridin-3-yl)boronic acid (31 mg, 0.20 mmol), K_2HPO_4 (78 mg, 0.45 mmol), and $Pd(PPh_3)_4$ (8 mg) were dissolved in 2 mL dioxane and 1 mL H_2O . The mixture was heated to 130 °C for 1.5 hours in a microwave reactor. Following general protocol D, methyl 2-(4-(2-chloropyridin-3-yl)phenyl)-3-methylquinoline-4-carboxylate was recovered as a white solid (25 mg, 0.06 mmol, 43%). 1H NMR (300 MHz, $CDCl_3-d$) δ 8.47 – 8.42 (m, 1H), 8.19 (d, $J = 8.5$ Hz, 1H), 7.80 – 7.58 (m, 8H), 7.42 – 7.33 (m, 1H), 4.13 (s, 3H), 2.50 (s, 3H); **MS** (ESI) 389.1 $[M+H]^+$.



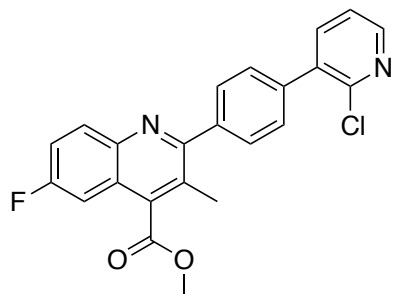
Methyl 2-(4-(2-chloro-6-methylpyridin-3-yl)phenyl)-3-methylquinoline-4-carboxylate (112): Intermediate **89** (100 mg, 0.28 mmol), (2-chloro-6-methylpyridin-3-yl)boronic acid (72 mg, 0.42 mmol), K_2HPO_4 (146 mg, 0.84 mmol), and $Pd(PPh_3)_4$ (16 mg, 0.01 mmol) were dissolved in 2 mL dioxane and 1 mL H_2O . The mixture was heated to 130 °C for 1.5 hours in a microwave reactor. Following general protocol D, methyl 2-(4-(2-chloro-6-methylpyridin-3-yl)phenyl)-3-methylquinoline-4-carboxylate was recovered as a white solid (43 mg, 0.10 mmol, 39%). 1H NMR (300 MHz, $CDCl_3-d$) δ 8.21 – 8.15 (m, 1H), 7.78 – 7.70 (m, 2H), 7.70 – 7.57 (m, 6H), 7.21 (d, $J = 7.7$ Hz, 1H), 4.13 (s, 3H), 2.62 (s, 3H), 2.49 (s, 3H); **MS** (ESI) 403.1 $[M+H]^+$.



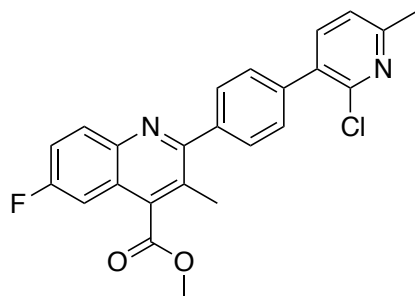
Methyl 6-fluoro-2-(4-(2-fluoropyridin-3-yl)phenyl)-3-methylquinoline-4-carboxylate (113): Intermediate **90** (50 mg, 0.13 mmol), (2-fluoropyridin-3-yl)boronic acid (31 mg, 0.22 mmol), K_2HPO_4 (68 mg, 0.39 mmol) and $Pd(PPh_3)_4$ (7 mg, 6.0×10^{-3} mmol) were dissolved in 1 mL dioxane and 0.5 mL H_2O . The mixture was heated to 130 °C for 1.5 hours in a microwave reactor. Following general protocol D, methyl 6-fluoro-2-(4-(2-fluoropyridin-3-yl)phenyl)-3-methylquinoline-4-carboxylate was recovered as a white solid (34 mg, 0.09 mmol, 69%). 1H NMR (300 MHz, $CDCl_3-d$) δ 8.28 – 8.24 (m, 1H), 8.17 (dd, $J = 9.2, 5.5$ Hz, 1H), 8.01 – 7.91 (m, 1H), 7.78 – 7.66 (m, 4H), 7.56 – 7.46 (m, 1H), 7.44 – 7.32 (m, 2H), 4.13 (s, 3H), 2.49 (s, 3H); **MS** (ESI) 291.1 $[M+H]^+$.



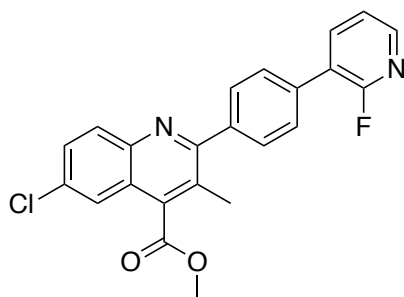
Methyl 6-fluoro-2-(4-(2-fluoro-6-methylpyridin-3-yl)phenyl)-3-methylquinoline-4-carboxylate (114): Intermediate **90** (50 mg, 0.13 mmol), (2-fluoro-6-methylpyridin-3-yl)boronic acid (30 mg, 0.20 mmol), K_2HPO_4 (68 mg, 0.39 mmol), and $Pd(PPh_3)_4$ (7 mg, 6.0×10^{-3} mmol) were dissolved in 1 mL dioxane and 0.5 mL H_2O . The mixture was heated to 130 for 1.5 hours in a microwave reactor. Following general protocol D, methyl 6-fluoro-2-(4-(2-fluoro-6-methylpyridin-3-yl)phenyl)-3-methylquinoline-4-carboxylate was recovered as a white solid. (17 mg, 0.04 mmol, 31%). 1H NMR (300 MHz, $CDCl_3-d$) δ 8.17 (dd, $J = 9.2, 5.5$ Hz, 1H), 7.88 – 7.80 (m, 1H), 7.75 – 7.64 (m, 4H), 7.55 – 7.46 (m, 1H), 7.44 – 7.38 (m, 1H), 7.18 (d, $J = 7.6, 1.8$ Hz, 1H), 4.13 (s, 3H), 2.59 (s, 3H), 2.49 (s, 3H); **MS** (ESI) 405.1 $[M+H]^+$.



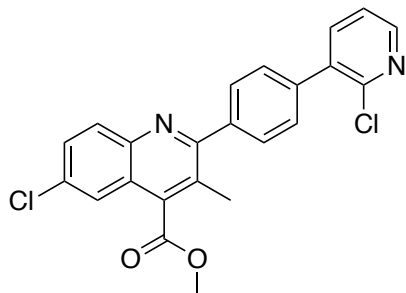
Methyl 2-(4-(2-chloropyridin-3-yl)phenyl)-6-fluoro-3-methylquinoline-4-carboxylate (115): Intermediate **90** (960 mg, 2.67 mmol), (2-chloropyridin-3-yl)boronic acid (503 mg, 3.20 mmol), K_2HPO_4 (1.34 g, 7.70 mmol), and $Pd(PPh_3)_4$ (80 mg) were dissolved in 10 mL dioxane and 4 mL H_2O . The mixture was heated to reflux overnight. Following general protocol D, methyl 2-(4-(2-chloropyridin-3-yl)phenyl)-6-fluoro-3-methylquinoline-4-carboxylate was recovered as a white solid (385 mg, 0.95 mmol, 36%). 1H NMR (300 MHz, $CDCl_3-d$) δ 8.49 – 8.43 (m, 1H), 8.22 – 8.11 (m, 1H), 7.77 – 7.59 (m, 5H), 7.56 – 7.48 (m, 1H), 7.45 – 7.34 (m, 2H), 4.13 (s, 3H), 2.50 (s, 3H); **MS** (ESI) 407.1 $[M+H]^+$.



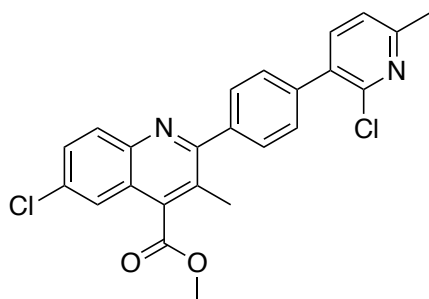
Methyl 2-(4-(2-chloro-6-methylpyridin-3-yl)phenyl)-6-fluoro-3-methylquinoline-4-carboxylate (116): Intermediate **90** (1.00 g, 2.68 mmol), (2-chloro-6-methylpyridin-3-yl)boronic acid (688 mg, 4.02 mmol), K_2HPO_4 (1.40 g, 8.04 mmol), and $Pd(PPh_3)_4$ (155 mg) were dissolved in 11 mL dioxane and 3 mL H_2O . The mixture was heated to reflux overnight. Following general protocol D, methyl 2-(4-(2-chloro-6-methylpyridin-3-yl)phenyl)-6-fluoro-3-methylquinoline-4-carboxylate was recovered as a white solid (474 mg, 1.13 mmol, 42%). 1H NMR (300 MHz, $CDCl_3-d$) δ 8.20 – 8.13 (m, 1H), 7.68 – 7.57 (m, 5H), 7.56 – 7.45 (m, 1H), 7.43 – 7.36 (m, 1H), 7.21 (d, $J = 7.7$ Hz, 1H), 4.12 (s, 3H), 2.61 (s, 3H), 2.49 (s, 3H); **MS** (ESI) 421.1 $[M+H]^+$.



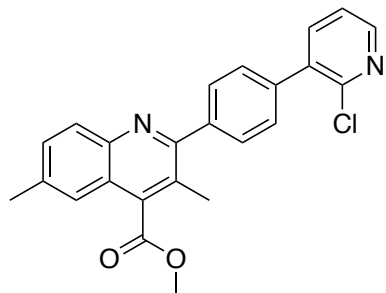
Methyl 6-chloro-2-(4-(2-fluoropyridin-3-yl)phenyl)-3-methylquinoline-4-carboxylate (117): Intermediate **91** (50 mg, 0.13 mmol), (2-fluoropyridin-3-yl)boronic acid (31 mg, 0.22 mmol), K_2HPO_4 (68 mg, 0.39 mmol) and $Pd(PPh_3)_4$ (7 mg, 6.0×10^{-3} mmol) were dissolved in 1 mL dioxane and 0.5 mL H_2O . The mixture was heated to 130 °C for 1.5 hours in a microwave reactor. Following general protocol D, methyl 6-chloro-2-(4-(2-fluoropyridin-3-yl)phenyl)-3-methylquinoline-4-carboxylate was recovered as a yellow solid (19 mg, 0.05 mmol, 38%). 1H NMR (300 MHz, $CDCl_3-d$) δ 8.33 – 8.21 (m, 1H), 8.10 (d, $J = 8.9$ Hz, 1H), 7.96 (t, $J = 8.2$ Hz, 1H), 7.78 – 7.64 (m, 6H), 7.40 – 7.31 (m, 1H), 4.14 (s, 3H), 2.49 (s, 3H); **MS** (ESI) 407.1 $[M+H]^+$.



Methyl 6-chloro-2-(4-(2-chloropyridin-3-yl)phenyl)-3-methylquinoline-4-carboxylate (118): Intermediate **91** (50 mg, 0.13 mmol), (2-chloropyridin-3-yl)boronic acid (34 mg, 0.22 mmol), K_2HPO_4 (68 mg, 0.39 mmol), and $Pd(PPh_3)_4$ (7 mg, 6.0×10^{-3} mmol) were dissolved in 1 mL dioxane and 0.5 mL H_2O . The mixture was heated to 130 °C for 1.5 hours in a microwave reactor. Following general protocol D, methyl 6-chloro-2-(4-(2-chloropyridin-3-yl)phenyl)-3-methylquinoline-4-carboxylate was recovered as a tan solid (4 mg, 0.01 mmol, 8%). 1H NMR (400 MHz, $CDCl_3-d$) δ 8.49 – 8.44 (m, 1H), 8.12 (d, $J = 8.9$, 0.5 Hz, 1H), 7.77 – 7.73 (m, 2H), 7.72 – 7.66 (m, 3H), 7.64 – 7.60 (m, 2H), 7.42 – 7.35 (m, 1H), 4.15 (s, 3H), 2.51 (s, 3H); **MS** (ESI) 423.0 $[M+H]^+$.

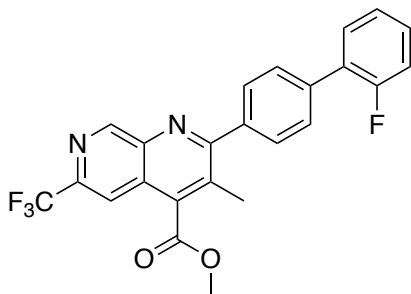


Methyl 6-chloro-2-(4-(2-chloro-6-methylpyridin-3-yl)phenyl)-3-methylquinoline-4-carboxylate (119): Intermediate **91** (50 mg, 0.13 mmol), (2-chloro-6-methylpyridin-3-yl)boronic acid (35 mg, 0.20 mmol), K_2HPO_4 (68 mg, 0.39 mmol), and $Pd(PPh_3)_4$ (7 mg, 6.0×10^{-3} mmol) were dissolved in 1 mL dioxane and 0.5 mL H_2O . The mixture was heated to 130 °C for 1.5 hours in a microwave reactor. Following general protocol D, methyl 6-chloro-2-(4-(2-chloro-6-methylpyridin-3-yl)phenyl)-3-methylquinoline-4-carboxylate was recovered as a solid (28 mg, 0.06 mmol, 46%). 1H NMR (300 MHz, $CDCl_3-d$) δ 8.11 (d, $J = 8.9$ Hz, 1H), 7.75 (d, $J = 2.2$ Hz, 1H), 7.70 – 7.58 (m, 6H), 7.22 (d, $J = 7.7$ Hz, 1H), 4.14 (s, 3H), 2.63 (s, 3H), 2.49 (s, 3H); **MS** (ESI) 437.1, 438.9 $[M+H]^+$.



Methyl 2-(4-(2-chloropyridin-3-yl)phenyl)-3,6-

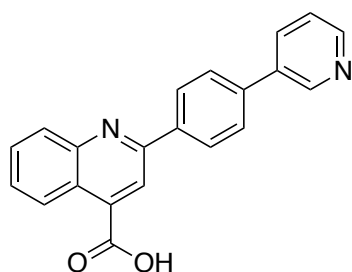
dimethylquinoline-4-carboxylate (120): Intermediate **92** (50 mg, 0.14 mmol), (2-chloropyridin-3-yl)boronic acid (35 mg, 0.23 mmol), K_2HPO_4 (68 mg, 0.39 mmol), and $Pd(PPh_3)_4$ (7 mg, 6.0×10^{-3} mmol) were dissolved in 1 mL dioxane and 0.5 mL H_2O . The mixture was heated to 130 °C for 1.5 hours in a microwave reactor. Following general protocol D, methyl 2-(4-(2-chloropyridin-3-yl)phenyl)-3,6-dimethylquinoline-4-carboxylate was recovered as an off-white solid (9 mg, 0.02 mmol, 16%) upon recrystallization in EtOH. 1H NMR (400 MHz, $CDCl_3-d$) δ 8.45 (dd, $J = 4.8, 1.9$ Hz, 1H), 8.08 (d, $J = 8.6$ Hz, 1H), 7.75 (dd, $J = 7.5, 1.9$ Hz, 1H), 7.71 – 7.68 (m, 2H), 7.64 – 7.56 (m, 3H), 7.51 – 7.48 (m, 1H), 7.37 (dd, $J = 7.6, 4.8$ Hz, 1H), 4.14 (s, 3H), 2.58 (d, $J = 1.0$ Hz, 3H), 2.48 (s, 3H); **MS** (ESI) 403.10 $[M+H]^+$.



Methyl 2-(2'-fluoro-[1,1'-biphenyl]-4-yl)-3-methyl-6-

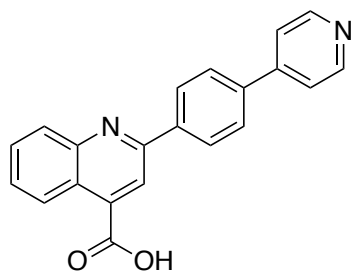
(trifluoromethyl)-1,7-naphthyridine-4-carboxylate (121): Intermediate **132** (14 mg, 0.03 mmol), 2-fluorophenylboronic acid (7 mg, 0.05 mmol), K_2HPO_4 (17 mg, 0.10 mmol), and $Pd(PPh_3)_4$ (1 mg) were dissolved in 1 mL dioxane and 1 mL H_2O . The mixture was heated to 130 °C for 1.5 hours in a microwave reactor. Following general protocol D, methyl 2-(2'-fluoro-[1,1'-biphenyl]-4-yl)-3-methyl-6-(trifluoromethyl)-1,7-naphthyridine-4-carboxylate was recovered (11 mg, 0.02, 66%). 1H NMR (300 MHz, $CDCl_3-d$) δ 9.65 (s, 1H), 8.07 (s, 1H), 7.80 – 7.68 (m, 4H), 7.58 – 7.49 (m, 1H), 7.46 – 7.36 (m, 1H), 7.31 (s, 0H), 7.27 – 7.18 (m, 1H), 4.18 (s, 3H), 2.62 (s, 3H); **MS** (ESI) 441.2 $[M+H]^+$.

General procedure E, basic hydrolysis: Ester derivatives were combined with 1-2 pellets of NaOH (large excess), LiOH, or KOH and dissolved in a 1:1 mixture of THF/H₂O or dioxane/H₂O. The solution was heated to 40 °C until starting material was no longer observed (2-6 hours). Upon completion, solvent was concentrated; residue was re-dissolved in 1 M KOH and washed with EtOAc (3x). The aqueous layer was acidified with HCl until pH 2-3 was reached, chilled overnight at 2-8 °C, then poured over a fritted funnel to collect precipitated product. Product cake was washed with chilled de-ionized H₂O and product was dried under vacuum (15-100%).



2-(4-(Pyridin-3-yl)phenyl)quinoline-4-carboxylic acid (32):

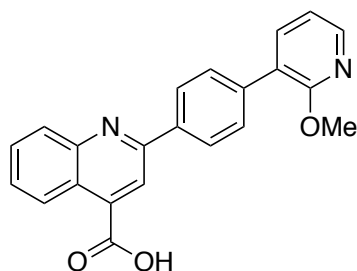
Compound **33** (8 mg, 0.02 mmol) and NaOH (45 mg, 1.13 mmol) was dissolved in a 1 mL THF and 1 mL H₂O. Following general protocol E, a white solid was collected from the vacuum oven to yield 2-(4-(pyridin-3-yl)phenyl)quinoline-4-carboxylic acid (2 mg, 6.13×10^{-3} mmol, 30%). **¹H NMR** (400 MHz, DMSO-*d*₆) δ 9.24 – 9.20 (m, 1H), 8.82 – 8.78 (m, 1H), 8.67 (d, *J* = 8.5, 1.5, 0.6 Hz, 1H), 8.64 – 8.61 (m, 1H), 8.56 (s, 1H), 8.50 (d, *J* = 8.5 Hz, 2H), 8.21 (d, 1H), 8.05 (d, *J* = 8.5 Hz, 2H), 7.93 – 7.85 (m, 2H), 7.78 – 7.71 (m, 1H); **LCMS** (ESI) 326.90 [M+H]⁺, 324.85 [M-H]⁻; **HPLC** Purity at 254 nm, 95.2%.



2-(4-(Pyridin-4-yl)phenyl)quinoline-4-carboxylic acid (34):

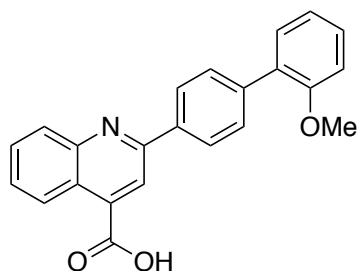
Intermediate **102** (14 mg, 0.04 mmol) and NaOH (62 mg, 1.59 mmol) was dissolved in 1 mL THF and 1 mL H₂O. Following general protocol E, a white solid was collected from the vacuum oven to yield 2-(4-(pyridin-4-yl)phenyl)quinoline-4-carboxylic acid (2 mg, 6.13×10^{-3} mmol,

15%). $^1\text{H NMR}$ (400 MHz, $\text{DMSO-}d_6$) δ 8.72 – 8.66 (m, 3H), 8.39 (d, $J = 8.3$ Hz, 2H), 8.08 (s, 1H), 8.04 – 7.99 (m, 3H), 7.85 – 7.80 (m, 2H), 7.73 – 7.66 (m, 1H), 7.53 – 7.47 (m, 1H); **LCMS** (ESI) 326.85 $[\text{M}+\text{H}]^+$, 324.80 $[\text{M}-\text{H}]^-$; **HPLC** Purity at 254 nm, 95.1%.



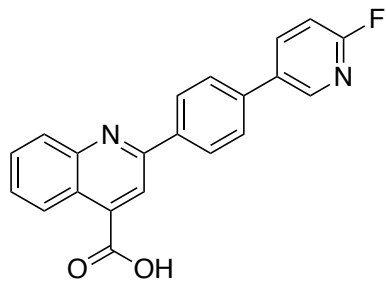
2-(4-(2-Methoxypyridin-3-yl)phenyl)quinoline-4-carboxylic acid

(47): Intermediate **103** (15 mg, 0.04 mmol) and NaOH (63 mg, 1.62 mmol) were dissolved in 1 mL THF and 1 mL H_2O . Following general protocol E, 2-(4-(2-methoxypyridin-3-yl)phenyl)quinoline-4-carboxylic acid was recovered as a beige solid (12 mg, 0.03 mmol, 75%). $^1\text{H NMR}$ (400 MHz, $\text{DMSO-}d_6$) δ 8.65 (d, $J = 8.5$ Hz, 1H), 8.50 (s, 1H), 8.36 (d, $J = 8.0$ Hz, 2H), 8.25 – 8.14 (m, 2H), 7.89 – 7.82 (m, 2H), 7.76 (d, $J = 7.9$ Hz, 2H), 7.70 (t, $J = 7.7$ Hz, 1H), 7.13 (t, $J = 6.2$ Hz, 1H), 3.91 (s, 3H); **LCMS** (ESI) 357.1 $[\text{M}+\text{H}]^+$, 355.1 $[\text{M}-\text{H}]^-$; **HPLC** purity at 254 nm, 99.8%.



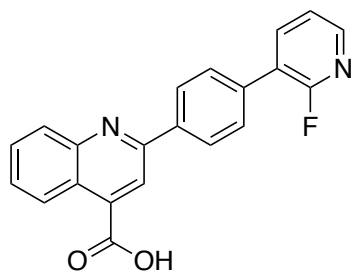
2-(2'-Methoxy-[1,1'-biphenyl]-4-yl)quinoline-4-carboxylic acid

(48): Intermediate **104** (15 mg, 0.04 mmol) and NaOH (68 mg, 1.74 mmol) were dissolved in 1 mL THF and 1 mL H_2O . Following general protocol E, 2-(2'-methoxy-[1,1'-biphenyl]-4-yl)quinoline-4-carboxylic acid was recovered as a beige solid (13 mg, 0.04 mmol, 100%). $^1\text{H NMR}$ (400 MHz, $\text{DMSO-}d_6$) δ 8.69 – 8.61 (m, 1H), 8.49 (s, 1H), 8.37 – 8.27 (m, 2H), 8.17 (d, $J = 8.4$ Hz, 1H), 7.89 – 7.82 (m, 1H), 7.73 – 7.65 (m, 3H), 7.41 – 7.34 (m, 2H), 7.17 – 7.12 (m, 1H), 7.10 – 7.04 (m, 1H), 3.79 (s, 3H); **LCMS** (ESI) 356.2 $[\text{M}+\text{H}]^+$, 354.1 $[\text{M}-\text{H}]^-$; **HPLC** Purity at 254 nm, 98.6%.



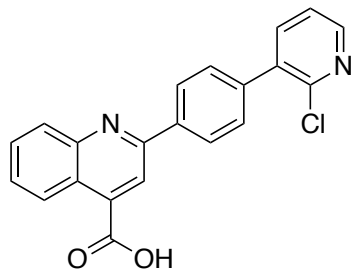
2-(4-(6-Fluoropyridin-3-yl)phenyl)quinoline-4-carboxylic acid

(57): Intermediate **105** (27 mg, 0.08 mmol) and LiOH (45 mg, 1.95 mmol) were dissolved in 1 mL dioxane and 1 mL H₂O. Following general protocol E, 2-(4-(6-fluoropyridin-3-yl)phenyl)quinoline-4-carboxylic acid was recovered as a tan solid (21 mg, 0.06 mmol, 75%). ¹H NMR (300 MHz, CD₃OD-*d*₄) δ 8.63 – 8.56 (m, 1H), 8.46 (d, 1H), 8.38 – 8.27 (m, 3H), 8.19 – 8.08 (m, 2H), 7.91 – 7.83 (m, 2H), 7.78 (t, *J* = 8.5, 6.9, 1.5 Hz, 1H), 7.61 (t, *J* = 8.3, 6.9, 1.3 Hz, 1H), 7.22 (dd, *J* = 8.6, 2.6 Hz, 1H); LCMS (ESI) 345.2 [M+H]⁺, 343.1 [M-H]⁻; HPLC Purity at 254nm, 95.8%.



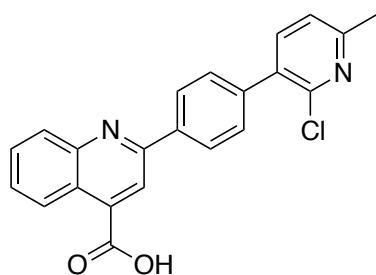
2-(4-(2-Fluoropyridin-3-yl)phenyl)quinoline-4-carboxylic acid

(58): Intermediate **106** (23 mg, 0.06 mmol) and LiOH (45 mg, 1.95 mmol) were dissolved in 1 mL dioxane and 1 mL H₂O. Following general protocol E, 2-(4-(2-fluoropyridin-3-yl)phenyl)quinoline-4-carboxylic acid was recovered as a white solid (17 mg, 0.05 mmol, 72%). ¹H NMR (300 MHz, CD₃OD-*d*₄) δ 8.49 (d, *J* = 8.2 Hz, 1H), 8.30 (d, *J* = 8.4 Hz, 2H), 8.26 – 8.13 (m, 4H), 7.86 – 7.75 (m, 3H), 7.63 (t, *J* = 7.6 Hz, 1H), 7.53 – 7.46 (m, 1H); LCMS (ESI) 345.10 [M+H]⁺, 343.05 [M-H]⁻; HPLC Purity at 254 nm, 99.8%.



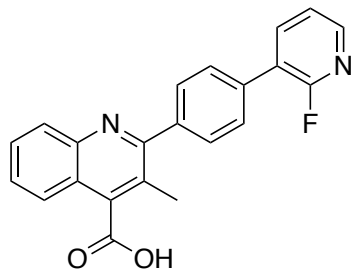
2-(4-(2-Chloropyridin-3-yl)phenyl)quinoline-4-carboxylic acid

(59): Intermediate **107** (76 mg, 0.20 mmol) and 115 mg KOH were dissolved in 2 mL THF and 2 mL H₂O. The mixture was stirred at 35 °C for 1 hour. Following general protocol E, 2-(4-(2-chloropyridin-3-yl)phenyl)quinoline-4-carboxylic acid was recovered as a tan solid (34 mg, 0.09 mmol, 45%). ¹H NMR (400 MHz, DMSO-*d*₆) δ 8.69 – 8.63 (m, 1H), 8.52 (s, 1H), 8.49 – 8.45 (m, 1H), 8.41 (d, *J* = 8.3 Hz, 2H), 8.18 (d, *J* = 8.4 Hz, 1H), 7.99 – 7.95 (m, 1H), 7.90 – 7.83 (m, 1H), 7.74 – 7.66 (m, 3H), 7.59 – 7.53 (m, 1H); LCMS (ESI) 361.05 [M+H]⁺ 359.05 [M-H]⁻; HPLC Purity at 254 nm, 98.6%.

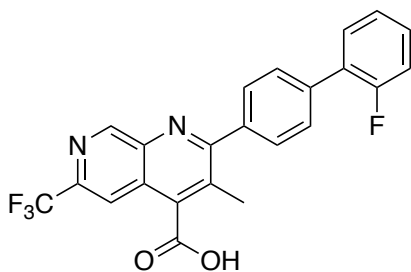


2-(4-(2-Chloro-6-methylpyridin-3-yl)phenyl)quinoline-4-

carboxylic acid (60): Intermediate **108** (70 mg, 0.18 mmol) was dissolved in 3 mL dioxane and 1 mL H₂O with LiOH (86 mg, 1.87 mmol). Following general protocol E, 2-(4-(2-chloro-6-methylpyridin-3-yl)phenyl)quinoline-4-carboxylic acid was recovered as a white solid (22 mg, 33%). ¹H NMR (300 MHz, DMSO-*d*₆) δ 8.67 (d, *J* = 8.5 Hz, 1H), 8.54 (s, 1H), 8.42 (d, *J* = 8.1 Hz, 2H), 8.20 (d, *J* = 8.4 Hz, 1H), 7.93 – 7.84 (m, 2H), 7.79 – 7.66 (m, 3H), 7.43 (d, *J* = 7.6 Hz, 1H), 2.53 (s, 3H); LCMS (ESI) 375.10 [M+H]⁺, 373.05 [M-H]⁻; HPLC Purity at 254 nm, 99.8%.



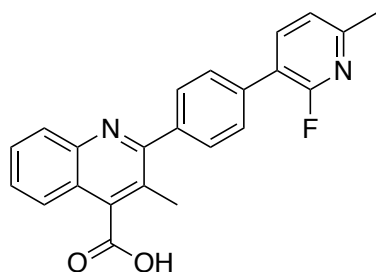
2-(4-(2-Fluoropyridin-3-yl)phenyl)-3-methylquinoline-4-carboxylic acid (63): Intermediate **109** (30 mg, 0.08 mmol) and LiOH (60 mg, 2.50 mmol) were dissolved in a 3 mL dioxane and 3 mL H₂O. The mixture was heated to 100 °C for 1.5 hours. Following general protocol E, 2-(4-(2-fluoropyridin-3-yl)phenyl)-3-methylquinoline-4-carboxylic acid was recovered following purification by preparative reverse-phase chromatography as a white solid (9 mg, 0.03 mmol, 38%). ¹H NMR (300 MHz, DMSO-*d*₆) δ 8.32 – 8.20 (m, 2H), 8.11 – 8.05 (m, 1H), 7.86 – 7.77 (m, 6H), 7.74 – 7.66 (m, 1H), 7.57 – 7.51 (m, 1H), 2.46 (s, 3H); LCMS (ESI) 359.1 [M+H]⁺, 357.2 [M-H]⁻; HPLC Purity at 254 nm, 99.8%.



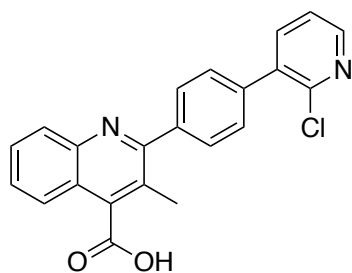
2-(2'-Fluoro-[1,1'-biphenyl]-4-yl)-3-methyl-6-(trifluoromethyl)-1,7-naphthyridine-4-carboxylic acid (82): Intermediate **121** (8 mg, 0.02 mmol) and KOH (61 mg, 1.08 mmol) were dissolved in 0.5 mL THF and 0.5 mL H₂O. The mixture was heated to 50 °C for 4 hours. Following general protocol E, 2-(2'-fluoro-[1,1'-biphenyl]-4-yl)-3-methyl-6-(trifluoromethyl)-1,7-naphthyridine-4-carboxylic acid was recovered following reverse-phase preparatory chromatography (5 mg, 0.01 mmol, 50%). ¹H NMR (300 MHz, CD₃OD-*d*₄) δ 9.48 (s, 1H), 8.29 (s, 1H), 7.78 (s, 4H), 7.66 – 7.57 (m, 1H), 7.44 (q, *J* = 6.3, 5.8 Hz, 1H), 7.37 – 7.21 (m, 2H), 2.63 (s, 3H); LCMS (ESI) 427.1 [M+H]⁺, 425.2 [M-H]⁻; HPLC Purity at 254 nm, 98.4%.

General procedure F, acidic hydrolysis: Ester derivatives were dissolved in anhydrous DCM and 1 M BBr₃ in DCM was added to the solution. The solution was stirred at room temperature

overnight. Upon completion, the solvent was concentrated; residue was re-dissolved in 1 M KOH and washed with EtOAc (3x). The aqueous layer was acidified with HCl until pH 2-3 was reached, chilled overnight at 2-8 °C, then poured over a fritted funnel to collect precipitated product. Product cake was washed with chilled de-ionized H₂O and product was dried under vacuum.

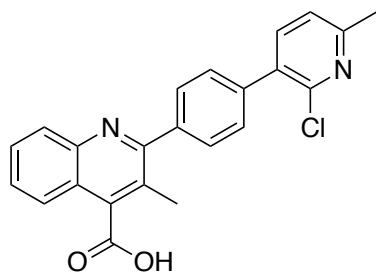


2-(4-(2-Fluoro-6-methylpyridin-3-yl)phenyl)-3-methylquinoline-4-carboxylic acid (64): Intermediate **110** (22 mg, 0.06 mmol) was dissolved in 1 mL DCM and 1 mL 1 M BBr₃ in DCM. Following general protocol F, 2-(4-(2-fluoro-6-methylpyridin-3-yl)phenyl)-3-methylquinoline-4-carboxylic acid was recovered as a white solid (13 mg, 0.03 mmol, 50%) following purification by preparative reverse-phase chromatography. ¹H NMR (300 MHz, CD₃OD-*d*₄) δ 8.12 – 8.06 (m, 1H), 8.06 – 8.00 (m, 2H), 7.82 – 7.68 (m, 5H), 7.65 – 7.58 (m, 1H), 7.38 – 7.32 (m, 1H), 2.56 (s, 3H), 2.47 (s, 3H); LCMS (ESI) 373.15 [M+H]⁺, 371.15 [M-H]⁻; HPLC Purity at 254 nm, 97.5%.

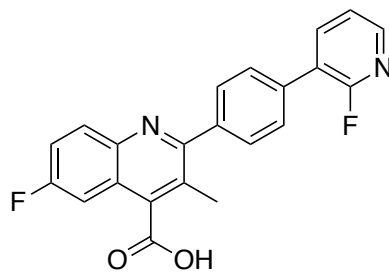


2-(4-(2-Chloropyridin-3-yl)phenyl)-3-methylquinoline-4-carboxylic acid (65): Intermediate **111** (33 mg, 0.09 mmol) was dissolved in 1.5 mL DCM and 1 mL 1 M BBr₃ in DCM. Following general protocol F, 2-(4-(2-chloropyridin-3-yl)phenyl)-3-methylquinoline-4-carboxylic acid was recovered as a white solid (24 mg, 0.06 mmol, 66%) following purification by preparative reverse-phase chromatography. ¹H NMR (300 MHz, DMSO-*d*₆) δ 8.48 (dd, *J* = 4.7, 1.9 Hz, 1H), 8.04 – 7.98 (m, 1H), 7.95 – 7.83 (m, 2H), 7.73 –

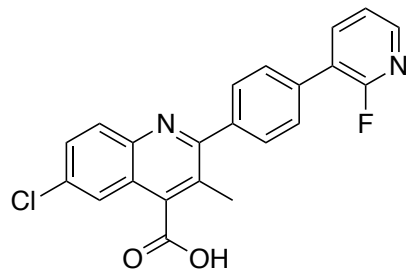
7.55 (m, 6H), 7.53 – 7.45 (m, 1H), 2.35 (s, 3H); **LCMS** (ESI) 375.10 [M+H]⁺, 373.10 [M-H]⁻; **HPLC** Purity at 254 nm, 99.9%.



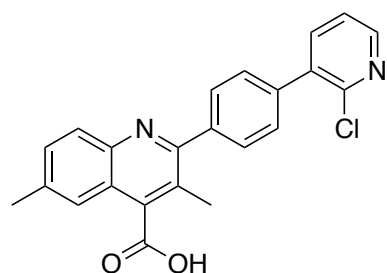
2-(4-(2-Chloro-6-methylpyridin-3-yl)phenyl)-3-methylquinoline-4-carboxylic acid (66): Intermediate **112** (10 mg, 0.02 mmol) was dissolved in 1 mL DCM and 1 mL 1 M BBr₃ in DCM. Following general protocol F, 2-(4-(2-chloro-6-methylpyridin-3-yl)phenyl)-3-methylquinoline-4-carboxylic acid was recovered as a white solid (1 mg, 2.5x10⁻³ mmol, 10%) following purification via preparative reverse-phase chromatography. ¹H NMR (400 MHz, CD₃OD-*d*₄) δ 8.16 (d, *J* = 8.4 Hz, 1H), 8.07 (d, *J* = 8.5 Hz, 1H), 7.95 (t, *J* = 7.5 Hz, 1H), 7.88 – 7.77 (m, 4H), 7.76 – 7.72 (m, 2H), 7.44 – 7.40 (m, 1H), 2.61 (s, 3H), 2.54 (s, 3H); **LCMS** (ESI) 389.15 [M+H]⁺, 387.15 [M-H]⁻; **HPLC** Purity at 254 nm, 99.9%.



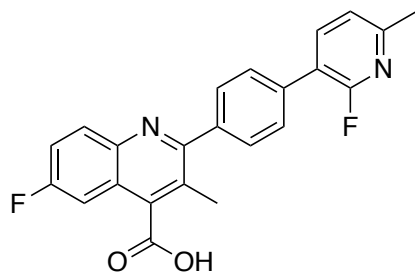
6-Fluoro-2-(4-(2-fluoropyridin-3-yl)phenyl)-3-methylquinoline-4-carboxylic acid (67): Intermediate **113** (34 mg, 0.09 mmol) was dissolved in 1 mL DCM and 1 mL 1 M BBr₃ in DCM. Following general protocol F, 6-fluoro-2-(4-(2-fluoropyridin-3-yl)phenyl)-3-methylquinoline-4-carboxylic acid was recovered as a white solid (15 mg, 0.04 mmol, 44%) following purification by preparative reverse-phase chromatography. ¹H NMR (400 MHz, DMSO-*d*₆) δ 8.29 (d, *J* = 4.8 Hz, 1H), 8.27 – 8.19 (m, 1H), 8.06 – 8.00 (m, 1H), 7.80 – 7.71 (m, 4H), 7.65 – 7.57 (m, 1H), 7.57 – 7.48 (m, 2H), 2.38 (s, 3H); **LCMS** (ESI) 377.15 [M+H]⁺, 375.10 [M-H]⁻; **HPLC** Purity at 254 nm, 98.4%.



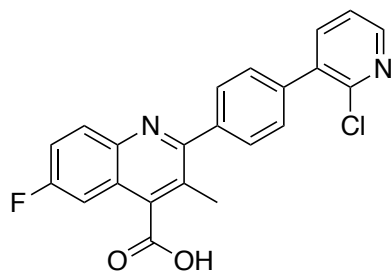
6-Chloro-2-(4-(2-fluoropyridin-3-yl)phenyl)-3-methylquinoline-4-carboxylic acid (68): Intermediate **117** (18 mg, 0.04 mmol) was dissolved in 1 mL DCM and 1 mL 1 M BBr₃ in DCM. Following general protocol F, 6-chloro-2-(4-(2-fluoropyridin-3-yl)phenyl)-3-methylquinoline-4-carboxylic acid was recovered as a white solid (3 mg, 0.01 mmol, 25%) following purification by preparative reverse-phase chromatography. ¹H NMR (300 MHz, CD₃OD-*d*₄) δ 8.27 – 8.16 (m, 2H), 8.04 – 7.97 (m, 2H), 7.85 – 7.78 (m, 2H), 7.75 – 7.66 (m, 3H), 7.52 – 7.45 (m, 1H), 2.48 (s, 3H); LCMS (ESI) 393.10 [M+H]⁺, 391.10 [M-H]⁻; HPLC Purity at 254 nm, 95.5%.



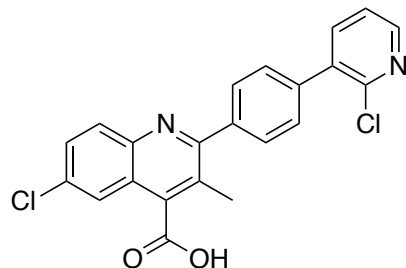
2-(4-(2-Chloropyridin-3-yl)phenyl)-3,6-dimethylquinoline-4-carboxylic acid (69): Intermediate **120** (17 mg, 0.04 mmol) was dissolved in 1 mL DCM and 1 mL 1 M BBr₃ in DCM. Following general protocol F, 2-(4-(2-Chloropyridin-3-yl)phenyl)-3,6-dimethylquinoline-4-carboxylic acid was recovered as a white film (2 mg, 5.15x10⁻³ mmol, 4%) following purification by preparative reverse-phase chromatography. ¹H NMR (300 MHz, CD₃OD-*d*₄) δ 8.05 (t, *J* = 8.6 Hz, 2H), 7.91 – 7.63 (m, 7H), 7.41 (d, *J* = 7.8 Hz, 1H), 2.60 (s, 3H), 2.49 (s, 3H); LCMS (ESI) 389.1 [M+H]⁺, 387.2 [M-H]⁻; HPLC Purity at 254 nm, 98.4%.



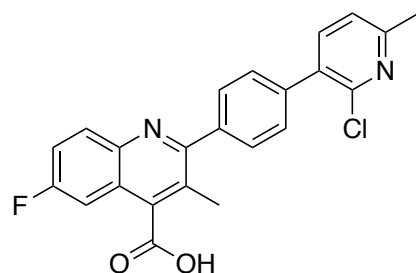
6-Fluoro-2-(4-(2-fluoro-6-methylpyridin-3-yl)phenyl)-3-methylquinoline-4-carboxylic acid (70): Intermediate **114** (17 mg, 0.04 mmol) was dissolved in 1 mL DCM and 1 mL 1 M BBr₃ in DCM. Following general protocol F, 6-Fluoro-2-(4-(2-fluoro-6-methylpyridin-3-yl)phenyl)-3-methylquinoline-4-carboxylic acid was recovered as a white solid (16 mg, 0.04 mmol, 99% yield) upon trituration with ethanol. ¹H NMR (400 MHz, CD₃OD-*d*₄) δ 8.12 – 8.02 (m, 2H), 7.82 – 7.75 (m, 2H), 7.73 – 7.59 (m, 3H), 7.59 – 7.50 (m, 1H), 7.37 – 7.31 (m, 1H), 2.56 (s, 3H), 2.47 (s, 3H); LCMS (ESI) 391.15 [M+H]⁺, 389.15 [M-H]⁻; HPLC Purity at 254 nm, 97.8%.



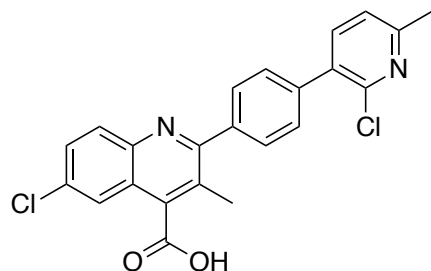
2-(4-(2-Chloropyridin-3-yl)phenyl)-6-fluoro-3-methylquinoline-4-carboxylic acid (71): Intermediate **115** (6 mg, 1.47x10⁻² mmol) was dissolved in 1 mL DCM and 1 mL 1 M BBr₃ in DCM. Following general protocol F, 2-(4-(2-chloropyridin-3-yl)phenyl)-6-fluoro-3-methylquinoline-4-carboxylic acid was recovered as a white film (5 mg, 1.27x10⁻² mmol, 86%) following purification by preparative reverse-phase chromatography. ¹H NMR (400 MHz, DMSO-*d*₆) δ 8.53 – 8.45 (m, 1H), 8.18 – 8.11 (m, 1H), 8.06 – 7.96 (m, 1H), 7.79 – 7.71 (m, 3H), 7.69 – 7.63 (m, 2H), 7.62 – 7.55 (m, 1H), 7.55 – 7.46 (m, 1H), 2.46 (s, 3H); LCMS (ESI) 393.10 [M+H]⁺, 391.10 [M-H]⁻; HPLC Purity at 254 nm, 95.7%.



6-Chloro-2-(4-(2-chloropyridin-3-yl)phenyl)-3-methylquinoline-4-carboxylic acid (72): Intermediate **118** (21 mg, 0.05 mmol) was dissolved in 1 mL DCM and 1 mL 1 M BBr₃ in DCM. Following general protocol F, 6-chloro-2-(4-(2-chloropyridin-3-yl)phenyl)-3-methylquinoline-4-carboxylic acid was recovered as a white solid after purification by preparative reverse-phase chromatography (1 mg, 2.44x10⁻³ mmol, 5%). ¹H NMR (500 MHz, CD₃OD-*d*₄) δ 8.42 (d, *J* = 4.9 Hz, 1H), 8.03 (d, *J* = 9.0 Hz, 1H), 7.98 – 7.94 (m, 2H), 7.76 – 7.66 (m, 5H), 7.53 (dd, *J* = 7.7, 4.8 Hz, 1H), 2.49 (s, 3H); LCMS (ESI) 409.05 [M+H]⁺, 407.10 [M-H]⁻; HPLC Purity at 254 nm, 98.1%.

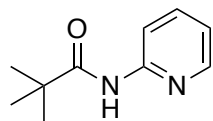


2-(4-(2-Chloro-6-methylpyridin-3-yl)phenyl)-6-fluoro-3-methylquinoline-4-carboxylic acid (73): Intermediate **116** (13 mg, 0.03 mmol) was dissolved in 1 mL DCM and 1 mL 1 M BBr₃ in DCM. Following general protocol F, 2-(4-(2-chloro-6-methylpyridin-3-yl)phenyl)-6-fluoro-3-methylquinoline-4-carboxylic acid was purified via reverse phase preparative chromatography (7 mg, 0.02 mmol, 66%). ¹H NMR (300 MHz, CD₃OD-*d*₄) δ 8.09 – 8.01 (m, 1H), 7.89 – 7.81 (m, 1H), 7.72 – 7.60 (m, 5H), 7.59 – 7.50 (m, 1H), 7.40 (d, *J* = 7.7 Hz, 1H), 2.60 (s, 3H), 2.48 (s, 3H); LCMS (ESI) 407.10 [M+H]⁺, 405.10 [M-H]⁻; HPLC Purity at 254 nm, 95.1%.

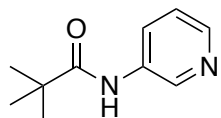


6-Chloro-2-(4-(2-chloro-6-methylpyridin-3-yl)phenyl)-3-methylquinoline-4-carboxylic acid (74): Intermediate **119** (28 mg, 0.06 mmol) was dissolved in 1 mL DCM and 1 mL 1 M BBr₃ in DCM. Following general protocol F, 6-chloro-2-(4-(2-chloro-6-methylpyridin-3-yl)phenyl)-3-methylquinoline-4-carboxylic acid was recovered as a white solid (1 mg, 2.37x10⁻³ mmol, 3%). ¹H NMR (400 MHz, DMSO-*d*₆) δ 8.13 – 8.10 (m, 1H), 7.90 – 7.80 (m, 3H), 7.79 – 7.73 (m, 2H), 7.66 – 7.61 (m, 2H), 7.45 – 7.40 (m, 1H), 2.54 (s, 3H), 2.47 (s, 3H); LCMS (ESI) 424.8 [M+H]⁺, 422.2 [M-H]⁻; HPLC Purity at 254 nm, 95.1%.

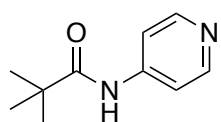
General procedure G, pivaloyl protecting group: The corresponding aminopyridine (1 eq) was added to a round bottom flask containing anhydrous DCM and TEA/DIPEA (1.25 eq). The solution was stirred on an ice bath for 20 minutes before trimethylacetyl chloride (1.1 eq) was added drop-wise. The solution was allowed to warm to room temperature and quenched with H₂O/NaHCO₃. The product was extracted in DCM (3x), dried with MgSO₄, and concentrated *in vacuo*. The solid was recrystallized in hexanes to afford pivaloyl-aminopyridines (53-98%).



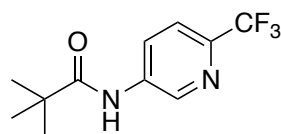
N-(pyridin-2-yl)pivalamide (122): 2-Aminopyridine (1.00 g, 10.6 mmol), triethylamine (1.85 mL, 13.3 mmol), and pivaloyl chloride (1.44 mL, 11.7 mmol) were combined in 18 mL of anhydrous DCM following general protocol G. Product was recrystallized by addition of hexane to generate *N*-(pyridin-2-yl)pivalamide as white needles (1.81 g, 10.2 mmol, 96%). ¹H NMR (400 MHz, CDCl₃-*d*) δ 8.26 – 8.18 (m, 3H), 7.66 (ddd, *J* = 8.6, 7.3, 1.9 Hz, 1H), 7.03 – 6.95 (m, 1H), 1.29 (d, *J* = 1.9 Hz, 9H); MS (ESI) 179.1 [M+H]⁺.



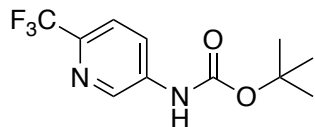
***N*-(pyridin-3-yl)pivalamide (123):** 3-Aminopyridine (1.00 g, 10.6 mmol), triethylamine (1.85 mL, 13.3 mmol), and pivaloyl chloride (1.44 mL, 11.7 mmol) were combined in 18 mL of anhydrous DCM following general protocol G. Product was recrystallized by addition of hexane to generate *N*-(pyridin-3-yl)pivalamide as a tan solid (1.56 g, 10.6 mmol, 83%). ¹H NMR (400 MHz, CDCl₃-*d*) δ 8.57 (d, *J* = 2.6 Hz, 1H), 8.38 – 8.33 (m, 1H), 8.22 – 8.16 (m, 1H), 7.49 (s, 1H), 7.31 – 7.25 (m, 1H), 1.35 (s, 9H); **MS** (ESI) 179.1 [M+H]⁺.



***N*-(pyridin-4-yl)pivalamide (124):** 4-Aminopyridine (1.00 g, 10.6 mmol), triethylamine (1.85 mL, 13.3 mmol), and pivaloyl chloride (1.44 mL, 11.7 mmol) were combined in 18 mL of anhydrous DCM following general protocol G. Product was recrystallized by addition of hexane to generate *N*-(pyridin-4-yl)pivalamide as white needles (991 mg, 5.57 mmol, 53%). ¹H NMR (400 MHz, CDCl₃-*d*) δ 8.57 (d, *J* = 2.6 Hz, 1H), 8.36 (dd, *J* = 4.7, 1.5 Hz, 1H), 8.24 – 8.18 (m, 1H), 7.50 – 7.41 (m, 1H), 7.32 – 7.24 (m, 1H), 1.36 (d, *J* = 1.5 Hz, 9H); **MS** (ESI) 179.1 [M+H]⁺.

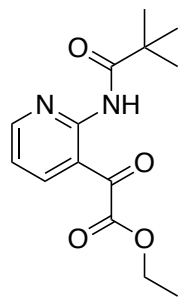


***N*-(6-(trifluoromethyl)pyridin-3-yl)pivalamide (125):** 6-(Trifluoromethyl)pyridin-3-amine (1.00 g, 6.17 mmol), diisopropylethyamine (1.35 mL, 7.71 mmol), and pivaloyl chloride (0.83 mL, 6.78 mmol) were combined in 17 mL of anhydrous DCM following general protocol G. Product was recrystallized by addition of hexane to generate *N*-(6-(trifluoromethyl)pyridin-3-yl)pivalamide as a white powder (1.48 g, 6.04 mmol, 98%). ¹H NMR (300 MHz, CDCl₃-*d*) δ 8.64 – 8.61 (m, 1H), 8.35 (dd, *J* = 8.6, 2.5 Hz, 1H), 7.82 (s, 1H), 7.60 (d, *J* = 8.6 Hz, 1H), 1.31 (s, 9H); **MS** (ESI) 245.2 [M+H]⁺.

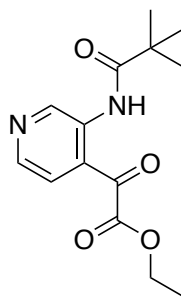


Tert-butyl (6-(trifluoromethyl)pyridin-3-yl)carbamate (126): This protocol was adapted from Hughes *et al.*⁴² 6-(Trifluoromethyl)pyridin-3-amine (4.00 g, 24.7 mmol) and di-*tert*-butyl-dicarbonate (6.73 g, 30.9 mmol) were refluxed in 50 mL anhydrous dioxane. After 24 hours, 1.00 g (4.59 mmol) of additional di-*tert*-butyl-dicarbonate was added and the mixture was stirred at reflux for another 24 hours. After 48 hours, the reaction mixture was quenched by the addition of cold H₂O and extracted with EtOAc. The organic layer was dried with MgSO₄, filtered, and concentrated before purifying via silica chromatography. *Tert*-butyl (6-(trifluoromethyl)pyridin-3-yl)carbamate was recovered as a white powder (2.45 g, 9.35 mmol, 38%). ¹H NMR (300 MHz, CDCl₃-*d*) δ 8.62 (d, *J* = 2.5 Hz, 1H), 8.35 (dd, *J* = 8.6, 2.5 Hz, 1H), 7.82 (s, 1H), 7.60 (d, *J* = 8.6 Hz, 1H), 1.31 (s, 9H); MS (ESI) 263.2 [M+H]⁺.

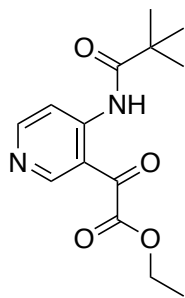
General protocol H, ortho-lithiation: This procedure was adapted from Estel *et al.*⁴³ and Zong *et al.*³⁴ The corresponding pivaloylamino pyridine (1.0 eq) was added to a vacuum purged round bottom flask under argon atmosphere. The solid was dissolved in Et₂O and TMEDA (2.5 eq) then chilled to -78 °C. After 15 minutes, *n*-BuLi (1.6 M in hexanes, 2.5 eq) was added dropwise and the reaction mixture was stirred at -78 °C for 15 minutes and then stirred at -10 °C for 2.5 hours. Afterwards, the temperature was lowered to -78 °C for the addition of diethyl oxalate (3.0 eq) and warmed to room temperature over 1.5 hours. The reaction mixture was quenched with 1.0 M solution of HCl in ice water and extracted with Et₂O (3x). Organic layer was dried, concentrated, and purified via silica chromatography in a gradient from 1% to 10% MeOH in DCM gradient (1–51%).



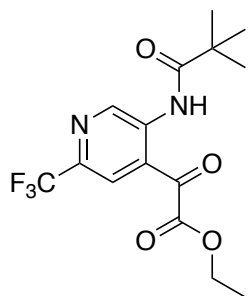
Ethyl 2-oxo-2-(2-pivalamidopyridin-3-yl)acetate (127): Following general protocol H, intermediate **122** (816 mg, 4.58 mmol), TMEDA (1.38 mL, 9.16 mmol), 1.6 M *n*-BuLi (5.73 mL, 9.16 mmol), and diethyl oxalate (1.03 mL, 9.16 mmol) were combined in 12 mL anhydrous diethyl ether. Ethyl 2-oxo-2-(2-pivalamidopyridin-3-yl)acetate was recovered as a yellow oil (136 mg, 0.48 mmol, 10%). ¹H NMR (400 MHz, CDCl₃-*d*) δ 9.86 (s, 1H), 8.59 – 8.48 (m, 1H), 8.03 (dt, *J* = 7.8, 1.6 Hz, 1H), 7.13 (ddd, *J* = 7.9, 4.8, 1.3 Hz, 1H), 4.36 (qd, *J* = 7.2, 1.2 Hz, 2H), 1.37 (td, *J* = 7.1, 1.2 Hz, 3H), 1.29 (s, 9H); MS (ESI) 277.3 [M-H]⁻.



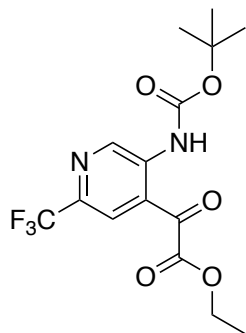
Ethyl 2-oxo-2-(3-pivalamidopyridin-4-yl)acetate (128): Following general protocol H, intermediate **123** (1.00 g, 5.62 mmol), TMEDA (2.10 mL, 14.1 mmol), 1.6 M *n*-BuLi (8.75 mL, 14.1 mmol), and diethyl oxalate (2.29 mL, 16.7 mmol) were combined in 17 mL anhydrous diethyl ether. Ethyl 2-oxo-2-(2-pivalamidopyridin-3-yl)acetate was recovered as an off-white solid (564 mg, 2.39 mmol, 43%). ¹H NMR (400 MHz, CDCl₃-*d*) δ 10.84 (s, 1H), 10.16 (s, 1H), 8.52 (d, *J* = 5.1 Hz, 1H), 7.58 (d, *J* = 5.2 Hz, 1H), 4.50 (q, *J* = 7.1 Hz, 2H), 1.46 (t, *J* = 7.2 Hz, 3H), 1.38 (s, 9H); MS (ESI) 277.2 [M-H]⁻.



Ethyl 2-oxo-2-(4-pivalamidopyridin-3-yl)acetate (129): Following general protocol H, intermediate **124** (1.00 g, 5.62 mmol) and 1.6 M *n*-BuLi (7.4 mL, 11.8 mmol), and diethyl oxalate (2.29 mL, 16.8 mmol) were combined in 16 mL anhydrous diethyl ether. TMEDA was not utilized. Ethyl 2-oxo-2-(4-pivalamidopyridin-3-yl)acetate was recovered as an off-white solid (796 mg, 2.86 mmol, 51%). **¹H NMR** (400 MHz, CDCl₃-*d*) δ 9.78 (s, 1H), 8.37 (d, *J* = 5.8 Hz, 1H), 8.26 (d, *J* = 5.8 Hz, 1H), 8.20 (s, 1H), 4.18 – 4.02 (m, 2H), 1.27 (s, 9H), 1.12 (t, *J* = 7.1 Hz, 3H); **MS** (ESI) 277.2 [M-H]⁻.

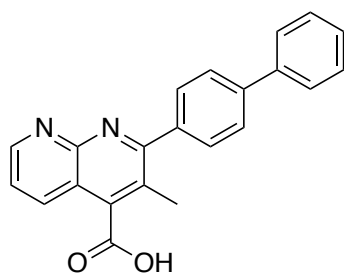


Ethyl 2-oxo-2-(5-pivalamido-2-(trifluoromethyl)pyridin-4-yl)acetate (130): Following general protocol H, intermediate **125** (1.00 g, 4.07 mmol), TMEDA (1.53 mL, 10.2 mmol), 1.6 M *n*-BuLi (6.35 mL, 10.2 mmol) and diethyl oxalate (1.66 mL, 12.2 mmol) were combined in 12 mL anhydrous diethyl ether. Ethyl 2-oxo-2-(5-pivalamido-2-(trifluoromethyl)pyridin-4-yl)acetate was recovered as a yellow oil (188 mg, 0.54 mmol, 13%). **¹H NMR** (300 MHz, CDCl₃-*d*) δ 11.07 (s, 1H), 10.25 (s, 1H), 8.02 (s, 1H), 4.53 (q, *J* = 7.1 Hz, 2H), 1.47 (t, *J* = 7.2 Hz, 3H), 1.38 (s, 9H); **MS** 345.1 [M-H]⁻.



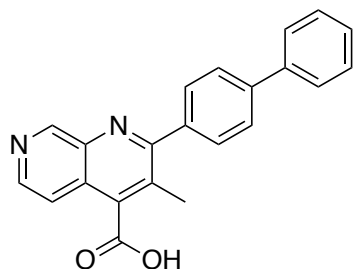
Ethyl 2-(5-((*tert*-butoxycarbonyl)amino)-2-(trifluoromethyl)pyridin-4-yl)-2-oxoacetate (131): Following general protocol H, intermediate **126** (1.00 g, 3.82 mmol), TMEDA (1.20 mL, 8.02 mmol), 1.6 M *n*-BuLi (5.01 mL, 8.02 mmol), and diethyl oxalate (1.55 mL, 11.4 mmol) were dissolved in 13 mL anhydrous diethyl ether. Ethyl 2-(5-((*tert*-butoxycarbonyl)amino)-2-(trifluoromethyl)pyridin-4-yl)-2-oxoacetate was recovered as a yellow oil (44 mg, 0.17 mmol, 1%). ¹H NMR (300 MHz, CDCl₃-*d*) δ 8.51 – 8.47 (m, 1H), 7.65 – 7.58 (m, 1H), 6.98 (s, 1H), 4.35 (q, *J* = 7.1 Hz, 2H), 1.52 (s, 9H), 1.37 (t, *J* = 7.1 Hz, 2H); MS (ESI) 363.2 [M+H]⁺.

General protocol I, generation of naphthyridine core: Corresponding ketone (1.0 eq), α-keto-ester (1.0 eq), and base (KOH or KOtBu, 3-6 eq) were combined in anhydrous EtOH in a sealed vial. The mixture was heated to 100 °C overnight, concentrated to a residue, extracted with 1 M KOH, and washed with EtOAc. The basic layer was acidified by addition of HCl (pH 2-3) and the product was collected via filtration. Product was further purified by reverse-phase preparatory chromatography (3-21%).

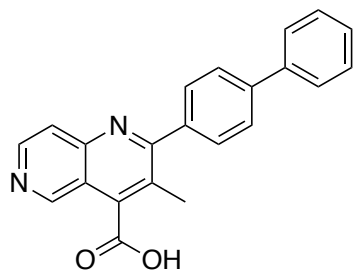


2-([1,1'-Biphenyl]-4-yl)-3-methyl-1,8-naphthyridine-4-carboxylic acid (75): Intermediate **127** (40 mg, 0.14 mmol), 1-([1,1'-biphenyl]-4-yl)propan-1-one (25 mg, 0.12 mmol), and KOtBu (78 mg, 0.7 mmol) were dissolved in 2 mL anhydrous EtOH. Following general protocol I, 2-([1,1'-biphenyl]-4-yl)-3-methyl-1,8-naphthyridine-4-carboxylic acid was recovered as a white solid (9 mg, 0.03 mmol, 21%). ¹H NMR (400 MHz, DMSO-*d*₆) δ 9.14 (s,

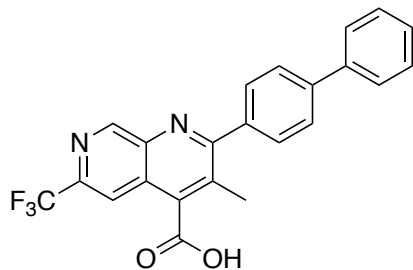
1H), 8.32 (dd, $J = 8.4, 1.9$ Hz, 1H), 7.90 – 7.84 (m, 2H), 7.82 – 7.78 (m, 4H), 7.76 – 7.70 (m, 1H), 7.56 – 7.50 (m, 2H), 7.46 – 7.40 (m, 1H), 2.51 (s, 3H); **LCMS** 341.15 $[M+H]^+$, 339.20 $[M-H]^-$; **HPLC** Purity at 254 nm, 99.3%.



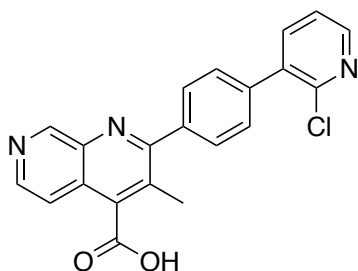
2-([1,1'-Biphenyl]-4-yl)-3-methyl-1,7-naphthyridine-4-carboxylic acid (76): Intermediate **128** (198 mg, 0.71 mmol), 1-([1,1'-biphenyl]-4-yl)propan-1-one (119 mg, 0.57 mmol), and KOH (112, 1.99 mmol) were dissolved in 10 mL anhydrous EtOH. Following general protocol I, 2-([1,1'-biphenyl]-4-yl)-3-methyl-1,7-naphthyridine-4-carboxylic acid was purified as a white solid (26 mg, 0.08 mmol, 11%). **1H NMR** (400 MHz, DMSO- d_6) δ 9.44 (s, 1H), 8.73 – 8.61 (m, 1H), 7.88 – 7.82 (m, 2H), 7.81 – 7.77 (m, 4H), 7.74 (d, $J = 5.7$ Hz, 1H), 7.56 – 7.50 (m, 2H), 7.46 – 7.41 (m, 1H), 2.51 (s, 3H); **LCMS** (ESI) 341.2 $[M+H]^+$, 339.1 $[M-H]^-$; **HPLC** Purity at 254 nm, 97.1%.



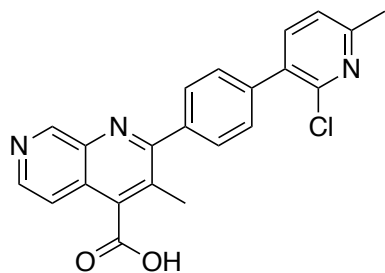
2-([1,1'-Biphenyl]-4-yl)-3-methyl-1,6-naphthyridine-4-carboxylic acid (77): Intermediate **129** (81 mg, 0.29 mmol), 1-([1,1'-biphenyl]-4-yl)propan-1-one (62 mg, 0.29 mmol), and KOH (49 mg, 0.87 mmol) were dissolved in 4 mL anhydrous EtOH. Following general protocol I, 2-([1,1'-biphenyl]-4-yl)-3-methyl-1,6-naphthyridine-4-carboxylic acid was recovered as an amorphous solid (6 mg, 0.02 mmol, 7%). **1H NMR** (400 MHz, CD₃OD- d_4) δ 9.38 (s, 1H), 8.66 (d, $J = 6.0$ Hz, 1H), 7.95 (d, $J = 6.0$ Hz, 1H), 7.88 – 7.82 (m, 2H), 7.79 – 7.68 (m, 4H), 7.55 – 7.47 (m, 2H), 7.46 – 7.36 (m, 1H), 2.53 (s, 3H); **LCMS** (ESI) 341.1 $[M+H]^+$, 339.2 $[M-H]^-$; **HPLC** purity at 254 nm, 96.5%.



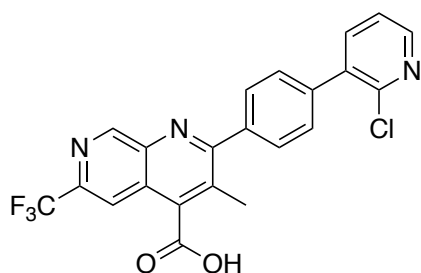
2-([1,1'-Biphenyl]-4-yl)-3-methyl-6-(trifluoromethyl)-1,7-naphthyridine-4-carboxylic acid (78): Intermediate **130** (118 mg, 0.34 mmol), 1-([1,1'-biphenyl]-4-yl)propan-1-one (71 mg, 0.34 mmol), and KOH (76 mg, 1.36 mmol) were dissolved in 5 mL anhydrous EtOH. Following general protocol I, 2-([1,1'-biphenyl]-4-yl)-3-methyl-6-(trifluoromethyl)-1,7-naphthyridine-4-carboxylic acid (4 mg, 0.01 mmol, 3%) was recovered as a clear oil. $^1\text{H NMR}$ (300 MHz, $\text{CD}_3\text{OD}-d_4$) δ 9.42 (s, 1H), 8.29 (s, 1H), 7.84 (d, $J = 8.3$ Hz, 2H), 7.77 – 7.70 (m, 4H), 7.50 (t, $J = 7.6$ Hz, 2H), 7.39 (t, $J = 7.5$ Hz, 1H), 2.57 (s, 3H). **LCMS** (ESI) 409.2 $[\text{M}+\text{H}]^+$, 407.2 $[\text{M}-\text{H}]^-$; **HPLC** Purity at 254 nm, 97.2%.



2-(4-(2-Chloropyridin-3-yl)phenyl)-3-methyl-1,7-naphthyridine-4-carboxylic acid (79): Intermediate **128** (32 mg, 0.12 mmol) intermediate **93** (28 mg, 0.12 mmol), and KOH (60 mg, 1.07 mmol) were dissolved in 2 mL anhydrous EtOH. Following general protocol I, 2-(4-(2-chloropyridin-3-yl)phenyl)-3-methyl-1,7-naphthyridine-4-carboxylic acid (4 mg, 0.03 mmol, 8%) was recovered as a white solid. $^1\text{H NMR}$ (300 MHz, $\text{CD}_3\text{OD}-d_4$) δ 9.34 (s, 1H), 8.57 (d, $J = 5.8$ Hz, 1H), 8.48 – 8.42 (m, 1H), 8.02 – 7.91 (m, 2H), 7.80 – 7.65 (m, 4H), 7.59 – 7.51 (m, 1H), 2.55 (s, 3H); **LCMS** (ESI) 376.1 $[\text{M}+\text{H}]^+$, 374.1 $[\text{M}-\text{H}]^-$; **HPLC** Purity at 254 nm, 96.0%.

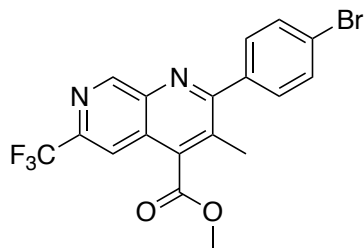


2-(4-(2-Chloro-6-methylpyridin-3-yl)phenyl)-3-methyl-1,7-naphthyridine-4-carboxylic acid (80): Intermediate **128** (66 mg, 0.24 mmol), intermediate **94** (62 mg, 0.24 mmol), and KOH (60 mg, 1.07 mmol) were dissolved in 3 mL anhydrous EtOH. Following general protocol I, 2-(4-(2-chloro-6-methylpyridin-3-yl)phenyl)-3-methyl-1,7-naphthyridine-4-carboxylic acid (2 mg, 0.03 mmol, 4%). **¹H NMR** (300 MHz, CD₃OD-*d*₄) δ 9.88 (s, 1H), 8.80 (d, *J* = 6.5 Hz, 1H), 8.57 (d, *J* = 6.6 Hz, 1H), 7.88 (dd, *J* = 10.8, 7.8 Hz, 3H), 7.72 (d, *J* = 7.9 Hz, 2H), 7.45 (d, *J* = 7.8 Hz, 1H), 2.76 (s, 3H), 2.62 (s, 3H); **LCMS** (ESI) 390.1 [M+H]⁺, 388.1 [M-H]⁻; **HPLC** Purity at 254 nm, 95.0%.



2-(4-(2-Chloropyridin-3-yl)phenyl)-3-methyl-6-(trifluoromethyl)-1,7-naphthyridine-4-carboxylic acid (81): Intermediate **132** (8 mg, 1.9 x 10⁻² mmol) and NaOH (44 mg, 1.15 mmol) were dissolved in dioxane and water then heated to 60 °C overnight. Upon completion, the mixture was concentrated to a residue and the corresponding carboxylic acid was used for the next step without purification. The residue was combined with (2-chloropyridin-3-yl)boronic acid (6 mg, 0.03 mmol), Na₂CO₃ (8 mg, 0.08 mmol), and Pd(PPh₃)₄ (1 mg) and dissolved in 0.5 mL dioxane and 0.5 mL H₂O. The mixture was heated to 110 °C for 3 hours. Upon completion, the mixture was concentrated, re-dissolved in 0.5 M NH₃ in MeOH, and purified via reverse-phase preparatory chromatography to yield 2-(4-(2-chloropyridin-3-yl)phenyl)-3-methyl-6-(trifluoromethyl)-1,7-naphthyridine-4-carboxylic acid as a white film (2 mg, 4.5x10⁻² mmol, 46% over 2 steps). **¹H NMR** (400 MHz, CD₃OD-*d*₄) δ 9.50 (s, 1H), 8.47 – 8.43 (m, 1H), 8.30 (s, 1H), 8.01 – 7.94 (m, 1H), 7.81 (d, *J* = 8.3 Hz, 2H), 7.72 (d,

$J = 8.2$ Hz, 2H), 7.58 – 7.53 (m, 1H), 2.64 (s, 3H); **LCMS** (ESI) 444.2 $[M+H]^+$, 442.2 $[M-H]^-$; **HPLC** Purity at 254 nm, 98.9%.



Methyl 2-(4-bromophenyl)-3-methyl-6-(trifluoromethyl)-1,7-naphthyridine-4-carboxylate (132): Intermediate **131** (1.38 g, 3.82 mmol) was dissolved in 10 mL and 1 mL trifluoroacetic acid. The mixture was stirred at room temperature for 2 hours, before being concentrated to a residue. 1-(4-Bromophenyl)propan-1-one (813 mg, 3.82 mmol), and KOH (856 mg, 15.3 mmol) were added to the residue and the mixture was dissolved in 15 mL anhydrous EtOH. In a sealed vial, the mixture was heated to 100 °C overnight. Upon completion, the mixture was concentration and the residue was re-dissolved in 1 M KOH, washed with EtOAc, and precipitated from aqueous layer by addition of HCl until the pH was 2-3 and precipitant was collected. The dried precipitant was dissolved in 5 mL THF and 1 mL MeOH under an argon atmosphere and chilled to 0 °C. A 2.0 M solution of TMS-diazomethane in THF (0.4 mL, 0.8 mmol) was added to the mixture and the solution was allowed to warm to room temperature over 2 hours. The mixture was quenched by the addition of acetic acid, concentrated, re-dissolved in EtOAc and washed with brine (3x). The organic layer was dried with MgSO₄, filtered, concentrated, and purified by silica chromatography to yield methyl 2-(4-bromophenyl)-3-methyl-6-(trifluoromethyl)-1,7-naphthyridine-4-carboxylate (32 mg, 0.08 mmol, 2% overall yield). **¹H NMR** (300 MHz, CDCl₃-*d*) δ 9.60 (s, 1H), 8.05 (s, 1H), 7.75 – 7.67 (m, 2H), 7.56 – 7.47 (m, 2H), 4.17 (s, 3H), 2.54 (s, 3H); **MS** (ESI) 425.0, 427.0 $[M+H]^+$.

hDHODH expression and purification: hDHODH expression and purification followed the same protocol as described by Madak et al.⁴⁴ The hDHODH construct was kindly provided by the De Brabander lab from UT Southwestern.¹ Briefly, hDHODH was expressed in *E. coli* Rosetta 2 (DE3) in LB medium with ampicillin (100 μ g/mL) and 0.1 mM FMN. Cells were grown at 37 °C to OD₆₀₀ = 0.6, then induced with 1 mM IPTG for 3 hours. Cells were harvested by centrifugation at and the pellet was resuspended in lysis buffer (50 mM Tris-HCl, pH 8.5, 300

mM NaCl, 10% glycerol, 5 mM β -mercaptoethanol, 10 mM imidazole, 2% Triton X-100, 0.5 mM FMN, 200 μ M PMSF, 1 mg/mL lysozyme). The cell suspension was incubated on ice for 2 hours, followed by sonication. The cleared supernatant was incubated with Ni-NTA resin for 1 h at 4 °C, and then loaded onto a column. The column was washed with wash buffer (50 mM Tris-HCl, pH 8.5, 300 mM NaCl, 10% glycerol, 5 mM β -mercaptoethanol, 25 mM imidazole, 0.1 mM FMN) and *h*DHODH was eluted with elution buffer (wash buffer containing 300 mM imidazole). Buffer exchange was carried out using an Amicon concentrator into storage buffer (100 mM HEPES, pH 8.0, 150 mM NaCl, 10% glycerol) and *h*DHODH was stored at -80 °C.

DHODH Inhibition Assay: DHODH activity was monitored as previously described with some modifications.² First, 1 μ L of test compound (50X) or DMSO, 60 nM DHODH, 100 μ M DCIP, and 20 μ M CoQ₁₀ (final concentrations for 50 μ L) in the assay buffer (100 mM HEPES pH 8.0, 150 mM NaCl, 10% glycerol, 0.1% Triton X-100) in a total of 40 μ L were incubated together for 30 min. The assay was started by the addition of 10 μ L of dihydroorotate to a final concentration of 200 μ M. The reduction of DCIP was measured by monitoring the absorbance at 600 nm over 1 hr at room temperature using a microplate reader (BMG Labtech). Data were exported to Microsoft Excel for analysis and IC₅₀ values were determined using GraphPad Prism6.

General protocol for preparation of cells: HCT116 and MiaPaCa cells were grown in RPMI 1640 supplemented with 10% fetal bovine serum (FBS) in the standard conditions of 37 °C and 5% CO₂. Cancer cells were purchased from NCI Developmental Therapeutics Program and ATCC (Manassas, VA).

Biological evaluation in cytotoxicity assay: Cells were seeded in a 96-well plate in 180 μ L cell culture medium and incubated overnight. Compounds were added the following day and were incubated with the cells for 72 h. Post-treatment, thiazolyl blue tetrazolium bromide (MTT) (AMRESCO) was added to a final concentration of 300 μ g/mL and incubated at 37 °C for 3.5 h. The media containing compound and MTT was discarded and 100 μ L DMSO was added to dissolve the insoluble formazan. The plates were shaken at room temperature for 15 min. A microplate reader (Molecular Devices) was then used to obtain the absorbance at 570 nm. Data were evaluated using GraphPad Prism 6 software.

Pharmacokinetic Studies: PK data was generated by the University of Michigan PK core. The study utilized (18) female CD-1 mice with a triple dose design. The drug at 2 mg/mL in PBS containing 20% DMSO and 50% PEG-400 was given by IV injection (10 mg/kg) and oral (PO) 20 mg/kg. At the given time points (0.083 h, 0.167 h, 0.25 h, 0.5 h, 1 h, 2 h, 4 h, 7 h, 16 h and 24 h), blood samples were collected using heparinized calibrated pipettes. Samples were centrifuged at 15,000 rpm for 10 min. Subsequently, blood plasma was collected from the upper layer. The plasma was frozen at -80 °C for later analysis.

Thermodynamic solubility studies: Thermodynamic solubility was evaluated by Analiza (Cleveland, OH) using their standard protocol. In short, solubility was calculated using a CLND detector. Compounds were dissolved in 450 μ L PBS pH 7.4 and shaken overnight at room temperature. The solution was filtered through a 0.45 μ m filter and injected directly into the CLND. Concentrations were determined via calibration curves to assess thermodynamic solubility in solution.

Crystallography:

Cloning, Expression, Purification of DHODH; The gene for N-terminally truncated *h*DHODH (residues 33-396) was subcloned into pMCSG26 LIC site using pET22b-*h*DHODH (residues 30-396) as the template with the following 3' and 5' primers (GTCTCTCCCATGGGAGATGAGCGTTTCTATGCTGAACAC and TGGTGGTGCCCAGCTTCCAGCCTCCGATGATCTGCTCCAATGG).

The C-terminally tagged construct (*h*DHODH-His₆) was transformed into *E. coli* Rosetta 2 (DE3) cells. Transformed cells were grown in Terrific Broth containing 100 μ g/mL ampicillin at 37 °C to an OD₆₀₀ of 0.6. Expression was induced by addition of 0.4 mM IPTG. Cells were incubated at 25 °C overnight, harvested by centrifugation at 6,700 x g and the pellet stored at -80 °C.

Purification of *h*DHODH was performed as published with modifications.⁴⁰ The thawed pellet was resuspended in 160 mL lysis buffer containing 50 mM HEPES pH 8.0, 300 mM NaCl, 10% glycerol, 10 mM imidazole, 0.05% (v/v) THESIT (Sigma Aldrich), 200 μ M phenylmethylsulfoxide, supplemented with a protease inhibitor cocktail (complete EDTA-free,

Sigma Aldrich). Resuspended cells were lysed by sonication and centrifuged at 34,000 x g. The resulting supernatant was added to 10 mL Ni NTA Superflow Resin (Qiagen) pre-equilibrated with lysis buffer. After the lysate was incubated with Ni NTA resin for 1 hour at 4 °C, the resin was washed with lysis buffer containing 20 mM imidazole and the protein eluted with lysis buffer containing 400 mM imidazole. Eluent was loaded onto a HiLoad 16/60 Superdex 75 column (GE Healthcare) pre-equilibrated with 50 mM HEPES pH 7.8, 300 mM NaCl, 10% glycerol, 10 mM DTT, and 40 mM Anzergent 3-10 (Anatrace). Fractions corresponding to *h*DHODH were pooled and 200 mM HEGA-8 (Anatrace) was added before concentrating protein to 18-22 mg/mL.

Crystallization, Data Collection, and Structure Determination

*h*DHODH was incubated with 2 mM L-dihydroorotate and 1 mM inhibitor at 4 °C for two hours and crystallized by sitting drop vapor diffusion at 20 °C. Protein was mixed in a 1:1 ratio with well solution containing 1.7-2.2 M ammonium sulfate, 1.4-1.5 M NaCl, 0.1 M sodium acetate pH 5.3, and 10 mM DTT. Prior to data collection, crystals were cryoprotected in well solution supplemented with 20% ethylene glycol (*h*DHODH:**73**) or silica oil (*h*DHODH:**76**) and flash-cooled in liquid nitrogen. Diffraction data were collected on the Advanced Photon Source LS-CAT beamline 21-ID-G. All data were processed with HKL2000⁴⁵ and both structures were solved by molecular replacement in Phaser⁴⁶ using a previous structure of *h*DHODH (PDB ID: 4IGH) absent its ligands as the search model. Iterative model building and refinement were performed using COOT⁴⁷ and PHENIX⁴⁸, respectively. Ligand restraints were generated in eLBOW.⁴⁹

The structure of *h*DHODH with inhibitor **73** was solved to 1.46 Å in the space group of P1. The structure contained two chains of protein in the asymmetric unit, with an RMSD of 0.329 Å between chains based on SSM superpositioning in COOT. In chain A, residues 33-396 were modeled with the exception of two disordered loop regions corresponding to residues 69-73 and 214-225. Similarly, residues 36-396 of chain B were modeled with the exception of the same two disordered loop regions, which included residues 68-74 and 216-223. In both chains, several peptide residues corresponding to the linker between the protein C-terminal histidine tag were also ordered.

The structure of *h*DHODH with inhibitor **76** was solved to 2.70 Å in the space group P3₂21, with one chain of protein in the asymmetric unit. Residues 34-396 were modeled with the exception of two disordered loop regions 71-73 and 219-223.

Upon comparison with the DHODH:**73** structure (RMSD values of 0.734 for chain A and 0.732 Å chain B), the only significant difference in the protein chains occurs in the residues preceding the first disordered loop region corresponding to residues 65-70. Near this solvent exposed loop in the DHODH:**76** structure, there is electron density for the aliphatic chain in common to both detergents. The density is not ordered as to allow modeling of the full detergent molecule, so we have refined the chain from Anzergent 3-10, which was used during crystallization. The aliphatic chain forms van der Waals interactions with the side chains of F62 and P69 as well as the backbone of residues 67-69. Additionally, the detergent makes contact with the benzyl group of **76**. In the DHODH:**73** structure, the aliphatic chain does not interact with the loop, but forms van der Waals interactions with the side chains of F62, L46, L42 and F37 along with the pyridine group of **73**.

3.9 References

1. Munier-Lehmann, H.; Vidalain, P.-O.; Tangy, F.; Janin, Y. L. On Dihydroorotate Dehydrogenases and Their Inhibitors and Uses. *J. Med. Chem.* **2013**, 56, 3148-3167.
2. Vyas, V. K.; Ghate, M. Recent developments in the medicinal chemistry and therapeutic potential of dihydroorotate dehydrogenase (DHODH) inhibitors. *Mini Rev. Med. Chem.* **2011**, 11, 1039-55.
3. Mohamad Fairus, A. K.; Choudhary, B.; Hosahalli, S.; Kavitha, N.; Shatrah, O. Dihydroorotate dehydrogenase (DHODH) inhibitors affect ATP depletion, endogenous ROS and mediate S-phase arrest in breast cancer cells. *BioChimie* **2017**, 135, 154-163.
4. Brown, K. K.; Spinelli, J. B.; Asara, J. M.; Toker, A. Adaptive Reprogramming of De Novo Pyrimidine Synthesis Is a Metabolic Vulnerability in Triple-Negative Breast Cancer. *Cancer Discov.* **2017**, 7, 391-399.
5. Sharma, A.; Janocha, A. J.; Hill, B. T.; Smith, M. R.; Erzurum, S. C.; Almasan, A. Targeting mTORC1-mediated metabolic addiction overcomes fludarabine resistance in malignant B cells. *Mol. Cancer Res.* **2014**, 12, 1205-15.

6. Dietrich, S.; Kramer, O. H.; Hahn, E.; Schafer, C.; Giese, T.; Hess, M.; Tretter, T.; Rieger, M.; Hullein, J.; Zenz, T.; Ho, A. D.; Dreger, P.; Luft, T. Leflunomide induces apoptosis in fludarabine-resistant and clinically refractory CLL cells. *Clin. Cancer Res.* **2012**, *18*, 417-31.
7. He, T.; Haapa-Paananen, S.; Kaminsky, V. O.; Kohonen, P.; Fey, V.; Zhivotovsky, B.; Kallioniemi, O.; Perala, M. Inhibition of the mitochondrial pyrimidine biosynthesis enzyme dihydroorotate dehydrogenase by doxorubicin and brequinar sensitizes cancer cells to TRAIL-induced apoptosis. *Oncogene* **2014**, *33*, 3538-49.
8. Mathur, D.; Stratikopoulos, E.; Ozturk, S.; Steinbach, N.; Pegno, S.; Schoenfeld, S.; Yong, R.; Murty, V. V.; Asara, J. M.; Cantley, L. C.; Parsons, R. PTEN Regulates Glutamine Flux to Pyrimidine Synthesis and Sensitivity to Dihydroorotate Dehydrogenase Inhibition. *Cancer Discov.* **2017**, *7*, 380-390.
9. White, R. M.; Cech, J.; Ratanasirintra-woot, S.; Lin, C. Y.; Rahl, P. B.; Burke, C. J.; Langdon, E.; Tomlinson, M. L.; Mosher, J.; Kaufman, C.; Chen, F.; Long, H. K.; Kramer, M.; Datta, S.; Neuberg, D.; Granter, S.; Young, R. A.; Morrison, S.; Wheeler, G. N.; Zon, L. I. DHODH modulates transcriptional elongation in the neural crest and melanoma. *Nature* **2011**, *471*, 518-22.
10. Sykes, D. B.; Kfoury, Y. S.; Mercier, F. E.; Wawer, M. J.; Law, J. M.; Haynes, M. K.; Lewis, T. A.; Schajnovitz, A.; Jain, E.; Lee, D.; Meyer, H.; Pierce, K. A.; Tolliday, N. J.; Waller, A.; Ferrara, S. J.; Eheim, A. L.; Stoeckigt, D.; Maxcy, K. L.; Cobert, J. M.; Bachand, J.; Szekely, B. A.; Mukherjee, S.; Sklar, L. A.; Kotz, J. D.; Clish, C. B.; Sadreyev, R. I.; Clemons, P. A.; Janzer, A.; Schreiber, S. L.; Scadden, D. T. Inhibition of Dihydroorotate Dehydrogenase Overcomes Differentiation Blockade in Acute Myeloid Leukemia. *Cell* **2016**, *167*, 171-186 e15.
11. Cody, R.; Stewart, D.; DeForni, M.; Moore, M.; Dallaire, B.; Azarnia, N.; Gyves, J. Multicenter phase II study of brequinar sodium in patients with advanced breast cancer. *Am. J. Clin. Oncol.* **1993**, *16*, 526-8.
12. Dodion, P. F.; Wagener, T.; Stoter, G.; Drozd, A.; Lev, L. M.; Skovsgaard, T.; Renard, J.; Cavalli, F. Phase II trial with Brequinar (DUP-785, NSC 368390) in patients with metastatic colorectal cancer: a study of the Early Clinical Trials Group of the EORTC. *Ann. Oncol.* **1990**, *1*, 79-80.
13. Urba, S.; Doroshow, J.; Cripps, C.; Robert, F.; Velez-Garcia, E.; Dallaire, B.; Adams, D.; Carlson, R.; Grillo-Lopez, A.; Gyves, J. Multicenter phase II trial of brequinar sodium in patients with advanced squamous-cell carcinoma of the head and neck. *Cancer Chemother. Pharmacol.* **1992**, *31*, 167-9.
14. Moore, M.; Maroun, J.; Robert, F.; Natale, R.; Neidhart, J.; Dallaire, B.; Sisk, R.; Gyves, J. Multicenter phase II study of brequinar sodium in patients with advanced gastrointestinal cancer. *Invest. New Drugs* **1993**, *11*, 61-5.

15. Maroun, J.; Ruckdeschel, J.; Natale, R.; Morgan, R.; Dallaire, B.; Sisk, R.; Gyves, J. Multicenter phase II study of brequinar sodium in patients with advanced lung cancer. *Cancer Chemother. Pharmacol.* **1993**, *32*, 64-6.
16. Natale, R.; Wheeler, R.; Moore, M.; Dallaire, B.; Lynch, W.; Carlson, R.; Grillo-Lopez, A.; Gyves, J. Multicenter phase II trial of brequinar sodium in patients with advanced melanoma. *Ann. Oncol.* **1992**, *3*, 659-60.
17. King, S. Y.; Basista, A. M.; Torosian, G. Self-association and solubility behaviors of a novel anticancer agent, brequinar sodium. *J. Pharm. Sci.* **1989**, *78*, 95-100.
18. Joshi, A. S.; King, S. Y.; Zajac, B. A.; Makowka, L.; Sher, L. S.; Kahan, B. D.; Menkis, A. H.; Stiller, C. R.; Schaeffle, B.; Kornhauser, D. M. Phase I safety and pharmacokinetic studies of brequinar sodium after single ascending oral doses in stable renal, hepatic, and cardiac allograft recipients. *J. Clin. Pharmacol.* **1997**, *37*, 1121-8.
19. Fragoso, Y. D.; Brooks, J. B. Leflunomide and teriflunomide: altering the metabolism of pyrimidines for the treatment of autoimmune diseases. *Expert Rev. Clin. Pharmacol.* **2015**, *8*, 315-20.
20. ClinicalTrials.gov [Internet]. Bethesda (MD): National Library of Medicine (US). Identifier NCT02509052, Leflunomide in Treating Patients With Relapsed or Refractory Multiple Myeloma; July 2015, [Cited November 2017]; Available from <https://clinicaltrials.gov/show/NCT02509052>
21. ClinicalTrials.gov [Internet]. Bethesda (MD): National Library of Medicine (US). Identified NCT01611675, Leflunomide + Vemurafenib in V600 Mutant Met. Melanoma; June 2012, [Cited November 2017]; Available from <https://clinicaltrials.gov/show/NCT01611675>
22. Baban, B.; Liu, J. Y.; Mozaffari, M. S. Aryl hydrocarbon receptor agonist, leflunomide, protects the ischemic-reperfused kidney: role of Tregs and stem cells. *Am. J. Physiol. Regul. Integr. Comp. Physiol.* **2012**, *303*, R1136-46.
23. Ramadoss, P.; Marcus, C.; Perdew, G. H. Role of the aryl hydrocarbon receptor in drug metabolism. *Expert Opin. Drug Metab. Toxicol.* **2005**, *1*, 9-21.
24. Liu, S.; Neidhardt, E. A.; Grossman, T. H.; Ocain, T.; Clardy, J. Structures of human dihydroorotate dehydrogenase in complex with antiproliferative agents. *Structure* **2000**, *8*, 25-33.
25. Chen, S. F.; Papp, L. M.; Ardecky, R. J.; Rao, G. V.; Hesson, D. P.; Forbes, M.; Dexter, D. L. Structure-activity relationship of quinoline carboxylic acids. A new class of inhibitors of dihydroorotate dehydrogenase. *BioChem. Pharmacol.* **1990**, *40*, 709-14.
26. Davis, J. P.; Copeland, R. A. Histidine to alanine mutants of human dihydroorotate dehydrogenase. Identification of a brequinar-resistant mutant enzyme. *BioChem. Pharmacol.* **1997**, *54*, 459-65.

27. Bissantz, C.; Kuhn, B.; Stahl, M. A medicinal chemist's guide to molecular interactions. *J. Med. Chem.* **2010**, *53*, 5061-84.
28. Hopkins, A. L.; Keserü, G. M.; Leeson, P. D.; Rees, D. C.; Reynolds, C. H. The role of ligand efficiency metrics in drug discovery. *Nat. Rev. Drug Discov.* **2014**, *13*, 105.
29. Maag, H. Prodrugs of Carboxylic Acids. In *Prodrugs: Challenges and Rewards Part 1*, Stella, V. J.; Borchardt, R. T.; Hageman, M. J.; Oliyai, R.; Maag, H.; Tilley, J. W., Eds. Springer New York: New York, NY, 2007; pp 703-729.
30. Shvekhgeimer, M. G.-A. The Pfitzinger Reaction. (Review). *Chem. Heterocycl. Compd.* **2004**, *40*, 257-294.
31. Sriram, R.; Sessa Sai Pavan Kumar, C. N.; Raghunandan, N.; Ramesh, V.; Sarangapani, M.; Rao, V. J. AlCl₃/PCC-SiO₂-Promoted Oxidation of Azaindoles and Indoles. *Synth. Commun.* **2012**, *42*, 3419-3428.
32. Kumar, C. N. S. S. P.; Devi, C. L.; Rao, V. J.; Palaniappan, S. Use of Pyridinium Chlorochromate and Reusable Polyaniline Salt Catalyst Combination for the Oxidation of Indoles. *Synlett* **2008**, 2008, 2023-2027.
33. Stockmann, V.; Fiksdahl, A. Synthesis of novel 1,7-naphthyridines by Friedländer condensation of pyridine substrates. *J. Heterocycl. Chem.* **2011**, *48*, 1383-1387.
34. Zong, R.; Zhou, H.; Thummel, R. P. Direct access to 4-carboxy-1,8-naphthyridines and related compounds through Pfitzinger-type chemistry. *J. Org. Chem.* **2008**, *73*, 4334-7.
35. Turner, J. A. Regiospecific electrophilic substitution of aminopyridines: ortho lithiation of 2-, 3-, and 4-(pivaloylamino)pyridines. *J. Org. Chem.* **1983**, *48*, 3401-3408.
36. Hewawasam, P.; Meanwell, N. A. A general method for the synthesis of isatins: Preparation of regiospecifically functionalized isatins from anilines. *Tetrahedron Lett.* **1994**, *35*, 7303-7306.
37. Peters, G. J.; Sharma, S. L.; Laurensse, E.; Pinedo, H. M. Inhibition of pyrimidine de novo synthesis by DUP-785 (NSC 368390). *Invest. New Drugs* **1987**, *5*, 235-44.
38. Chen, S. F.; Ruben, R. L.; Dexter, D. L. Mechanism of action of the novel anticancer agent 6-fluoro-2-(2'-fluoro-1,1'-biphenyl-4-yl)-3-methyl-4-quinolinecarboxylic acid sodium salt (NSC 368390): inhibition of de novo pyrimidine nucleotide biosynthesis. *Cancer Res.* **1986**, *46*, 5014-9.
39. Rydberg, P.; Gloriam, D. E.; Zaretski, J.; Breneman, C.; Olsen, L. SMARTCyp: A 2D Method for Prediction of Cytochrome P450-Mediated Drug Metabolism. *ACS Med. Chem. Lett.* **2010**, *1*, 96-100.

40. Das, P.; Deng, X.; Zhang, L.; Roth, M. G.; Fontoura, B. M.; Phillips, M. A.; De Brabander, J. K. SAR Based Optimization of a 4-Quinoline Carboxylic Acid Analog with Potent Anti-Viral Activity. *ACS Med. Chem. Lett.* **2013**, *4*, 517-521.
41. Walse, B.; Dufe, V. T.; Svensson, B.; Fritzson, I.; Dahlberg, L.; Khairoullina, A.; Wellmar, U.; Al-Karadaghi, S. The structures of human dihydroorotate dehydrogenase with and without inhibitor reveal conformational flexibility in the inhibitor and substrate binding sites. *Biochemistry* **2008**, *47*, 8929-36.
42. Hughes, R. O.; Rogier, D. J.; Jacobsen, E. J.; Walker, J. K.; Macinnes, A.; Bond, B. R.; Zhang, L. L.; Yu, Y.; Zheng, Y.; Rumsey, J. M.; Walgren, J. L.; Curtiss, S. W.; Fobian, Y. M.; Heasley, S. E.; Cabbage, J. W.; Moon, J. B.; Brown, D. L.; Acker, B. A.; Maddux, T. M.; Tollefson, M. B.; Mischke, B. V.; Owen, D. R.; Freskos, J. N.; Molyneaux, J. M.; Benson, A. G.; Blevis-Bal, R. M. Design, synthesis, and biological evaluation of 3-[4-(2-hydroxyethyl)piperazin-1-yl]-7-(6-methoxypyridin-3-yl)-1-(2-propoxyethyl) pyrido[3,4-b]pyrazin-2(1H)-one, a potent, orally active, brain penetrant inhibitor of phosphodiesterase 5 (PDE5). *J. Med. Chem.* **2010**, *53*, 2656-60.
43. Estel, L.; Linard, F.; Marsais, F.; Godard, A.; Quéguiner, G. Synthesis of ortho-substituted aminopyridines. Metalation of pivaloylamino derivatives. *J. Heterocycl. Chem.* **1989**, *26*, 105-112.
44. Madak, J. T.; Cuthbertson, C. R.; Chen, W.; Showalter, H. D.; Neamati, N. Design, Synthesis, and Characterization of Brequinar Conjugates as Probes to Study DHODH Inhibition. *Chem. Eur. J.* **2017**, *23*, 13875-13878.
45. Otwinowski, Z.; Minor, W. Processing of X-ray diffraction data collected in oscillation mode. *Methods Enzymol.* **1997**, *276*, 307-26.
46. McCoy, A. J.; Grosse-Kunstleve, R. W.; Adams, P. D.; Winn, M. D.; Storoni, L. C.; Read, R. J. Phaser crystallographic software. *J. Appl. Crystallogr.* **2007**, *40*, 658-674.
47. Emsley, P.; Lohkamp, B.; Scott, W. G.; Cowtan, K. Features and development of Coot. *Acta Crystallogr. D Biol. Crystallogr.* **2010**, *66*, 486-501.
48. Adams, P. D.; Afonine, P. V.; Bunkoczi, G.; Chen, V. B.; Davis, I. W.; Echols, N.; Headd, J. J.; Hung, L. W.; Kapral, G. J.; Grosse-Kunstleve, R. W.; McCoy, A. J.; Moriarty, N. W.; Oeffner, R.; Read, R. J.; Richardson, D. C.; Richardson, J. S.; Terwilliger, T. C.; Zwart, P. H. PHENIX: a comprehensive Python-based system for macromolecular structure solution. *Acta Crystallogr. D Biol. Crystallogr.* **2010**, *66*, 213-21.
49. Moriarty, N. W.; Grosse-Kunstleve, R. W.; Adams, P. D. electronic Ligand Builder and Optimization Workbench (eLBOW): a tool for ligand coordinate and restraint generation. *Acta Crystallogr. D Biol. Crystallogr.* **2009**, *65*, 1074-80.

Chapter 4

Design, Synthesis, and Characterization of Brequinar Conjugates as Probes to Study DHODH Inhibition^d

4.1 Introduction

Over 20 years ago, a potent dihydroorotate dehydrogenase (DHODH) inhibitor, brequinar, was evaluated in multiple cancer clinical trials.^{1, 2} In preclinical studies, brequinar inhibited rapid cellular growth by inducing pyrimidine depletion and suppressed >90% tumor growth in murine studies at 20-40 mg/kg/day.^{3, 4} However, its transition from bench to bedside was disappointing as few patients met their objective response despite the fact that analysis of patient-derived samples showed that DHODH was inhibited and pyrimidine depletion had occurred.⁵ As newer studies emerged suggesting that DHODH may be an effective target,⁶⁻¹⁰ we designed novel molecular probes to better understand its therapeutic relevance in cancer. In this work, we report our convergent syntheses of novel brequinar probes to induce DHODH degradation and improve brequinar's accumulation in the mitochondria. Our approach was to incorporate late-stage functionalization of the brequinar scaffold with molecular "tags" to generate brequinar-based probes.

4.2 Probe design

To induce intracellular DHODH knockdown, we planned to develop a proteolysis-targeting chimera (PROTAC) of brequinar. A bifunctional PROTAC probe can induce intracellular protein degradation by utilizing the cell's ubiquitin proteasome system.^{11, 12} In short, a small molecule with a known target can be attached to an established E3 ligase ligand (tag) and when both moieties are simultaneously bound to their respective target, the E3 ligase may ubiquitinate lysine residues on the target protein.^{13, 14} This ubiquitinated protein is then signaled

^d **Author contributions:** Joseph Madak designed, synthesized, and characterized all compounds. Christine Cuthbertson and Wenmin Chen evaluated compounds in biochemical and cellular assays. Dr. Hollis Showalter and Dr. Nouri Neamati are corresponding authors. This work was previously published as: *Chemistry*, 2017, 23(56):13875-13878. DOI:10.1002/chem.201702999

for degradation by cellular proteasomes. Many examples of this approach have been published.^{11, 12, 15}

Our second probe was designed to direct subcellular localization to the mitochondria by incorporating a membrane permeable delocalized lipophilic cation onto a target compound. The electrochemical gradient required for mitochondrial respiration drives permeable cations across the membrane.^{16, 17} Our plan was to incorporate a large triphenylphosphonium (TPP) cation, which should hinder water solvation and reduce unfavorable interactions with hydrophobic membranes. As a result, these cations are more membrane permeable leading to selective accumulation in the mitochondria. Because DHODH is located within the mitochondria, we propose that improving brequinar's exposure to the target may improve potency in cells.

We postulated that a properly designed PROTAC or TPP probe of brequinar would be more potent in cells than brequinar. To evaluate this hypothesis, we designed probes to optimize the effectiveness of our functional tags without significantly decreasing inhibitory activity for DHODH. The design of the PROTAC probe focused on identifying linker attachment sites on brequinar that would allow for an E3 ligase to be recruited. The brequinar-analogue/DHODH co-crystallized structure (1D3G) shows the presence of multiple lysine residues near the binding pocket (Figure 4.1 (A)).¹⁸ Using this, we targeted probe **133**, shown in Figure 4.1 (B), in which the *para* position of the terminal aromatic ring of brequinar incorporates a linker that should not significantly decrease DHODH potency and permit solvent exposure to the tag. Our second probe, which was aimed at improving mitochondrial accumulation, was designed to ensure an overall positive charge on the probe. Brequinar's carboxylic acid functionality is mostly deprotonated at the pH (7.4) of cellular assays leaving the molecule with an overall negative charge, thus resulting in poor membrane permeability. To successfully transport a charged molecule to the mitochondria, it must possess an overall positive charge and have a high degree of lipophilicity. Toward this end, compound **134** (Figure 4.1, (C)) with the triphenylphosphonium head group became our target probe.

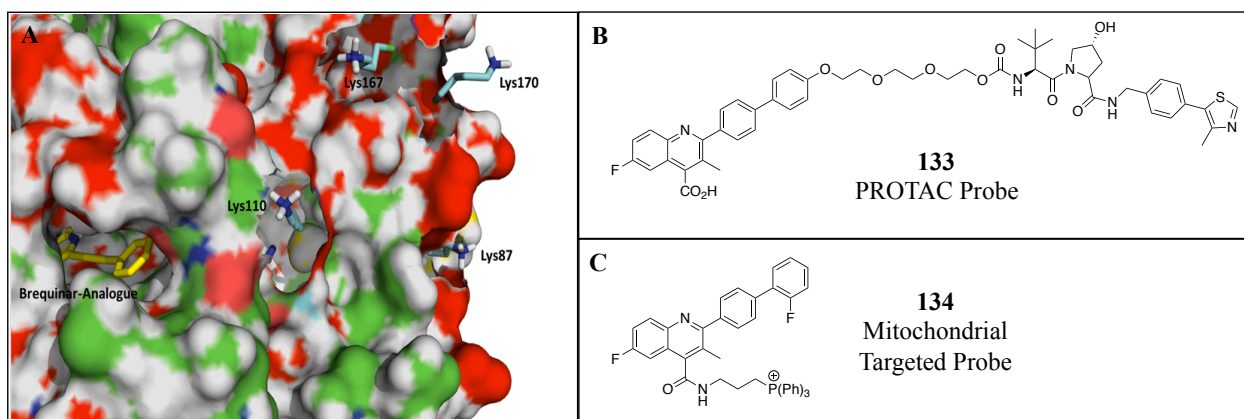
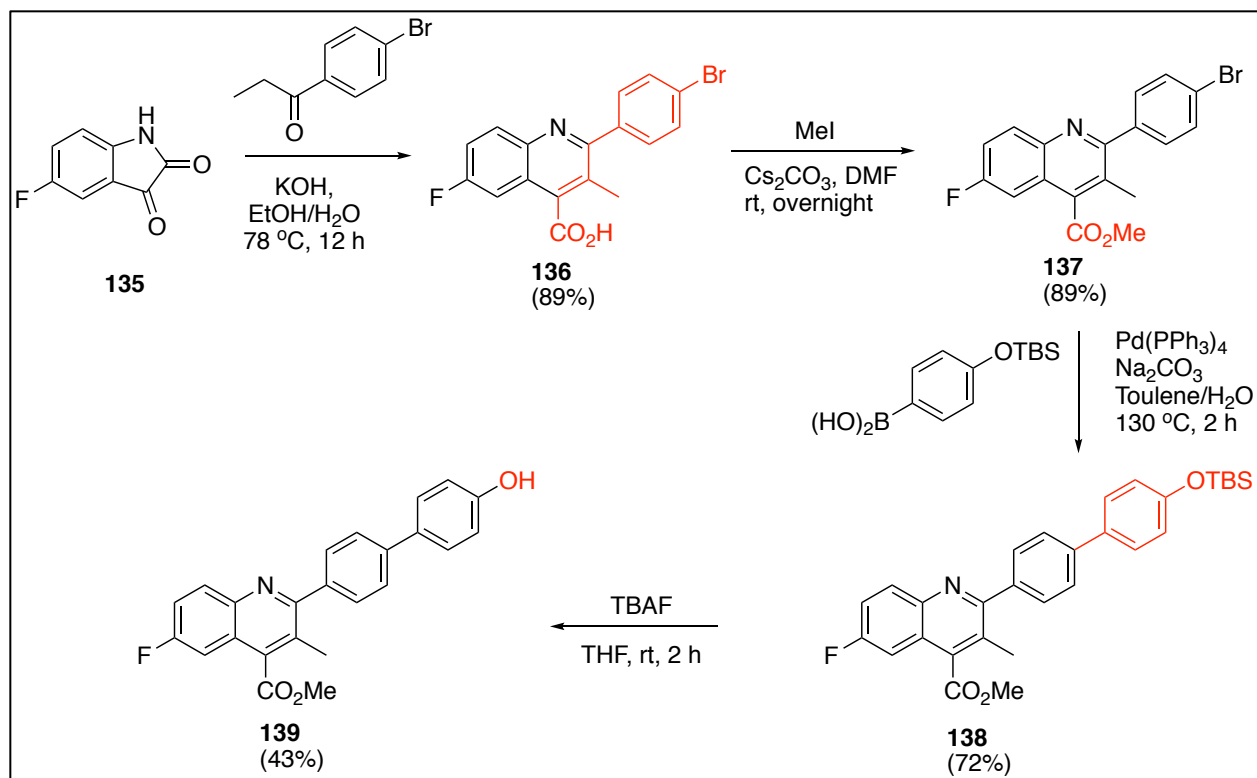


Figure 4.1 Brequinar binding pocket in DHODH and structures of probes. (A) Depiction of the brequinar binding pocket in DHODH and lysine residues with solvent exposure near the binding pocket. (PDB, 1D3G), (B) Structure of PROTAC Probe (**133**) and (C) structure of mitochondrial targeted probe (**134**).

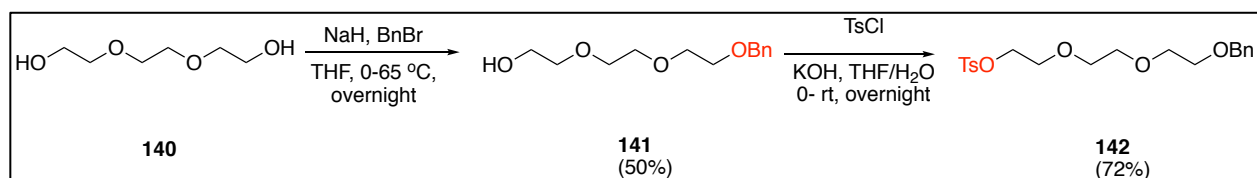
4.3 Synthesis

Our synthetic approach for each probe focused on utilizing a convergent strategy with late-stage incorporation of functional tags. The synthesis of a brequinar-PROTAC probe incorporating an ether attachment at the *para* position of the terminal aromatic ring is outlined in the following schemes. Scheme 4.1 described our initial synthesis of the brequinar moiety. The highly substituted quinoline ring was constructed using the Pfitzinger reaction to make **136**, which was readily esterified to afford **137** in 89% yield upon generation of the cesium salt and exposure to iodomethane.¹⁹ Suzuki coupling of **137** with a suitable phenylboronic acid gave the TBS-protected phenol (**138**) in good yield (72%), which was then treated with TBAF to give **139** in a 25% overall yield from **135**.



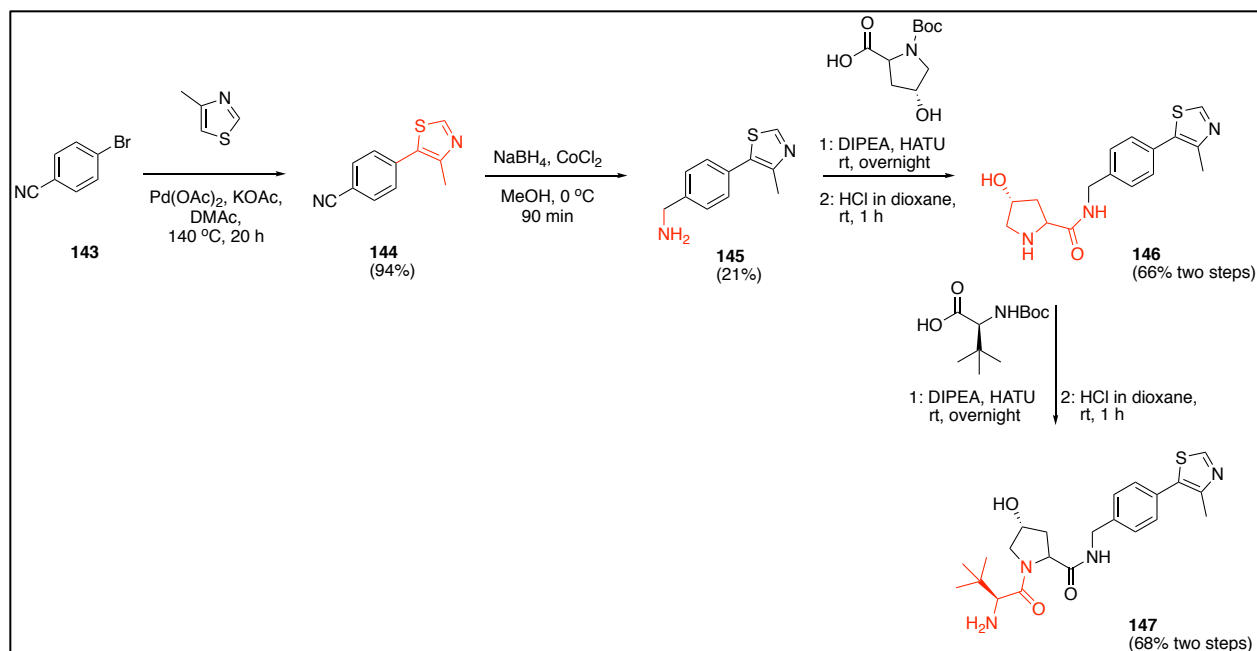
Scheme 4.1: Synthesis of intermediate 139

Intermediate **142**, the linker, was synthesized through 2-steps from triethylene glycol (**140**). A large excess of triethylene glycol in comparison to benzyl bromide was utilized to provide a mono-benzylated product (intermediate **141**, Scheme 4.2). The terminal hydroxyl of **141** was then activated as tosyl leaving group to yield **142**.



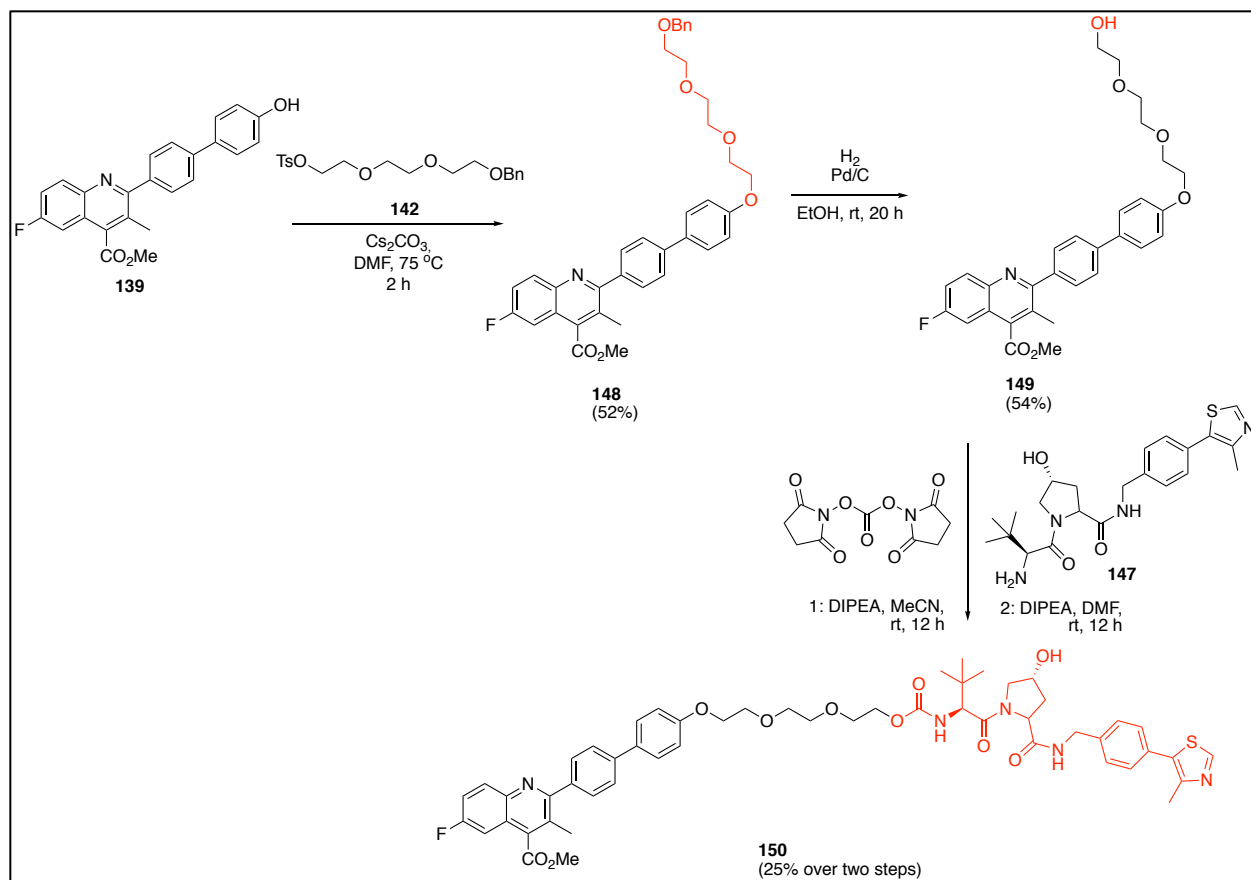
Scheme 4.2: Synthesis of intermediate 142

VHL ligand was synthesized following a previously published 6-step scheme (Scheme 4.3).^{13, 14} Palladium catalyzed coupling of 4-methylthiazole with 4-bromobenzonitrile (**143**) yielded intermediate **144** in 94% yields. Nitrile reduction towards **145** was accomplished using NaBH_4 but was low yielding (21%). Attempts to improve the yield of **145** utilized reductive silylation²⁰ or LiAlH_4 protocols but neither was higher yielding. Amide coupling of **145** to Boc-Hyp-OH and subsequent Boc deprotection yielded **146** in suitable yields (66%). A second two-step amidation/deprotection protocol was utilized to yield VHL ligand **147**.

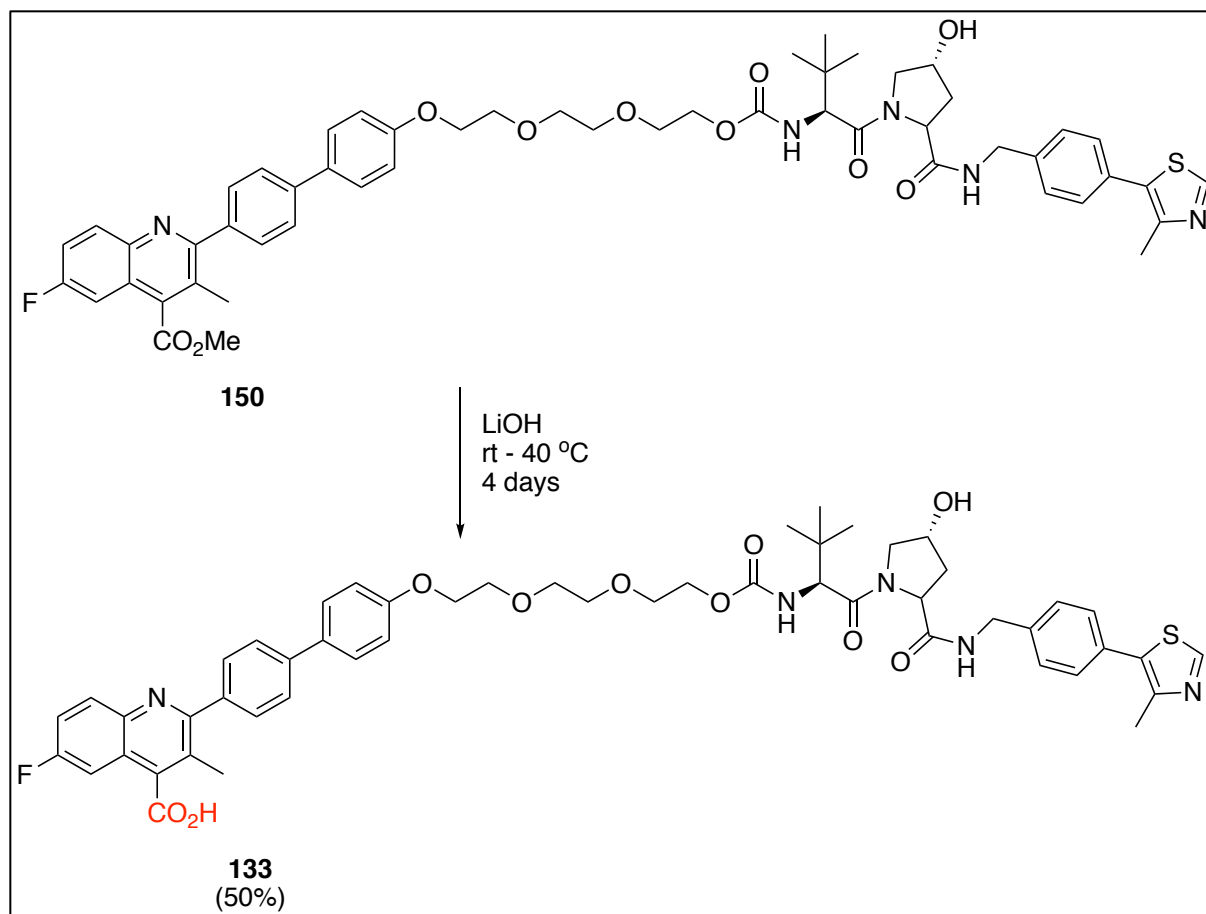


Scheme 4.3: Synthesis of VHL ligand 147.

Condensation of the cesium phenolate salt of **139** with **142**²¹ installed a PEG-linker to give **148**, which was positioned for a second-stage attachment of the VHL ligand (Scheme 4.4). Hydrogenolysis of the benzylated linker of **148** unveiled the terminal alcohol **149** (28% overall yield from **139**), which was then activated with disuccimidyl carbonate. The activated intermediate was reacted under mildly basic conditions with the VHL E3 ligase ligand **147**, to give carbamate **150**. Mild ester hydrolysis of compound **150** was conducted with LiOH to minimize possible epimerization of the *t*-butyl chiral center (Scheme 4.5). Thus, heating of **150** at 40 °C for 5 days resulted in 50% conversion to desired product **133**, which was separated from starting ester **150** by preparative reverse-phase chromatography in a 50% yield and a 1% overall yield from **135**.

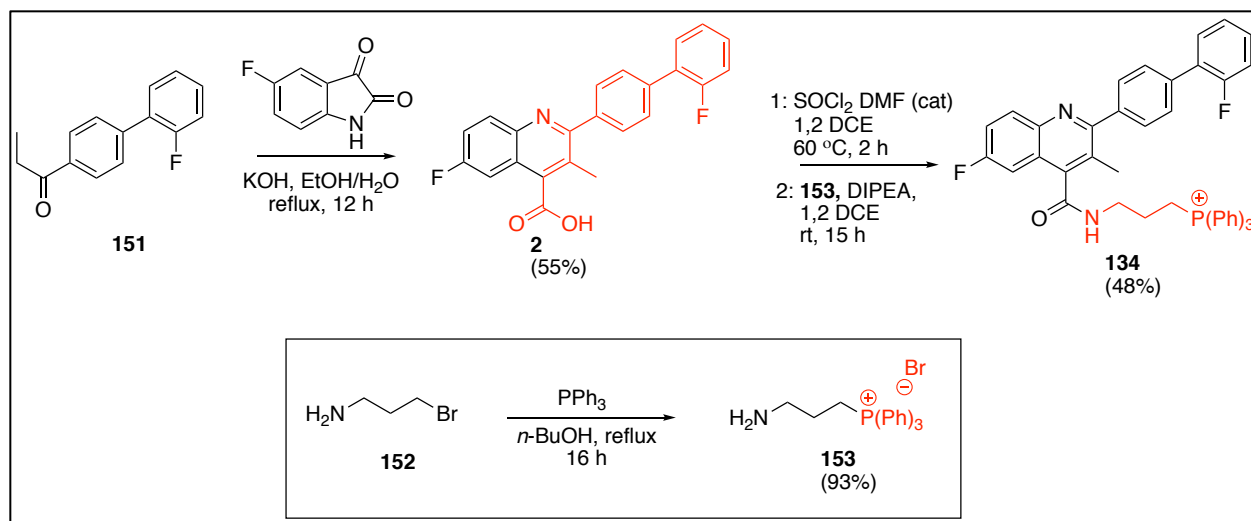


Scheme 4.4: Synthesis of probe 150.



Scheme 4.5: Synthesis of probe 133.

The synthesis of our second probe, **134**, is shown in Scheme 4.6. Brequinar (**2**) was readily synthesized from ketone **151** under classic Pfitzinger conditions.¹⁹ The desired cationic fragment **153** was generated through nucleophilic displacement of bromide **152** with triphenylphosphine. Amide coupling of **153** with **2** required extensive investigation to find conditions that allowed for easy purification of probe **134**. While standard-coupling conditions (HATU, HOBT/EDC) worked well, product purification was best facilitated by simple acid chloride generation of **2** followed by reaction with amine **153**. Probe **134** was generated in 26% overall yield from **151**.



Scheme 4.6 Synthesis of mitochondria-directed probe **134**.

4.4 Biological evaluation of probes

Probe **133** containing the crucial carboxylic acid maintained excellent potency ($IC_{50} = 0.093 \pm 0.04 \mu\text{M}$) in the DHODH assay (Figure 4.2 (C)). However, in cells, **133** did not inhibit cell growth and showed an $IC_{50} > 30 \mu\text{M}$ in HCT-116, a colon cancer cell line that is sensitive to DHODH inhibition, and $> 50 \mu\text{M}$ in MiaPaca-2. Conversely, the methyl ester **150** was more potent in HCT-116 cells ($IC_{50} = 6.8 \pm 2.9 \mu\text{M}$ in HCT-116), which may be a result of superior cellular permeability in comparison to **133**. Ester **150** may be hydrolyzed to the carboxylic acid inside the cell, which may explain its cellular toxicity. This pro-drug approach would significantly improve target exposure and may also explain the difference between **150** and **133**'s cellular activity. Interestingly, HCT-116 dosed with **150** completely blocked colony formation at $2.5 \mu\text{M}$ and fewer colonies formed than were observed at a 4-fold higher dose of brequinar (Figure 4.2, (D)). The results of **150** in the clonogenic assay differed from the MTT, which may have occurred for a few reasons. In the clonogenic assay, cells were treated with **150** for twice as long as they were in the MTT assay, which may be more favorable towards ester hydrolysis to yield **133**. However, **150** hindered new colony formation better than brequinar (**2**) and has inspired us pursue a more in-depth biological characterization of **150**. Unfortunately, protein degradation was not observed with either **150** or **133** via western blot (Figure 4.3). There are several possible explanations for this lack of activity. First, there are currently no published PROTAC probes that induce protein degradation with mitochondrial targets. The protein ubiquitination system within the mitochondria may be significantly different than the cytosol or

utilize a different E3 ligase. Interestingly, Azzu and Brand established that the inner mitochondrial protein UCP2 can be degraded using cytosolic proteasomal machinery, but it is unclear which E3 ligase performs ubiquitination.²² It is possible that a ligand for an E3 ligase that targets mitochondrial proteins is necessary for degradation. Additionally, the linker between brequinar and the VHL ligand could require optimization. We incorporated an ethylene glycol linker to keep the ClogP low. Probe **133** has a predicted ClogP of 8.04 (free acid) with the ethylene glycol linker. If replaced with an aliphatic chain of similar length, the ClogP would be 11.77 (free acid). Finally, other DHODH inhibitors may be better suited for PROTACs. An imatinib-based PROTAC probe did not induce degradation of BCR-ABL despite binding. However, dasatinib and bosutinib-based PROTACs probes did induce BCR-ABL degradation.²³ This suggests that other structurally distinct DHODH inhibitors could induce degradation. Despite this, probe **150** did possess excellent cytotoxicity in HCT-116 that was superior to brequinar in the colony formation assay.

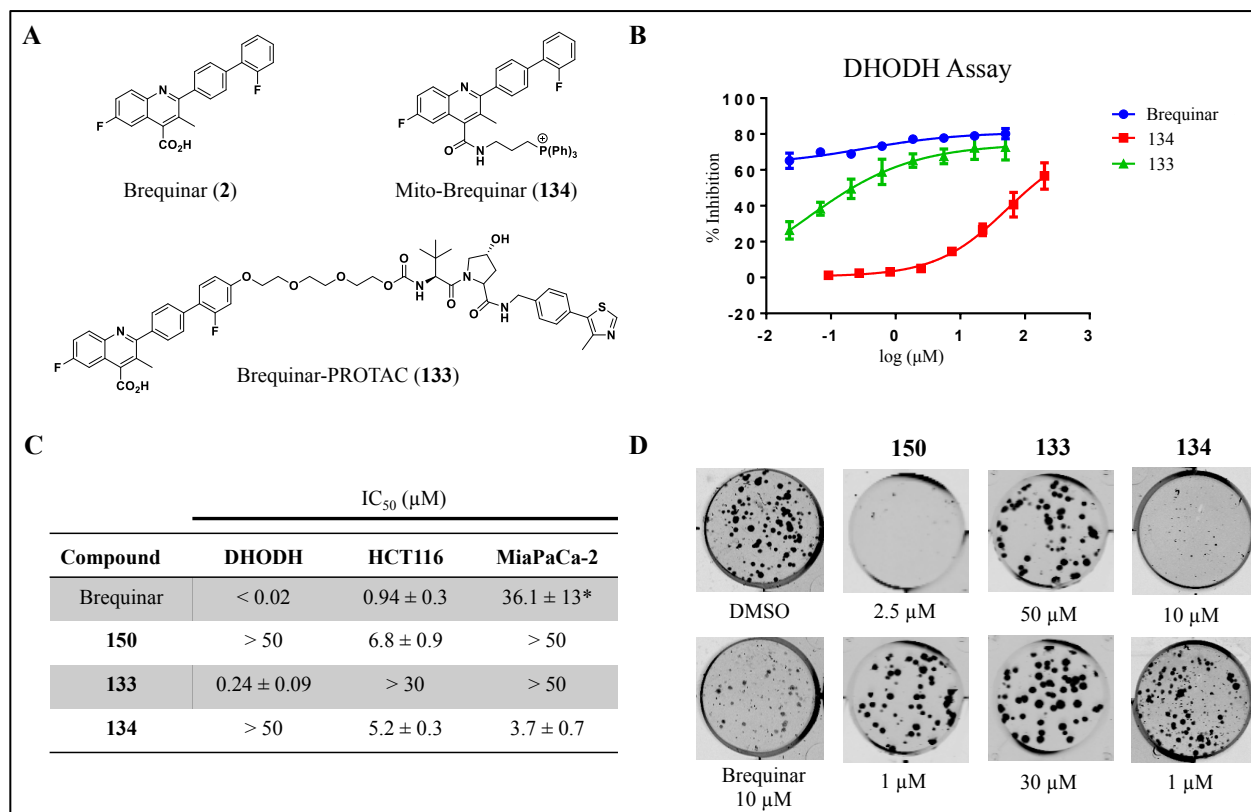


Figure 4.2 Biological evaluation of probes 133, 134, and 150. (A) Structures of brequinar and new probes. (B) Dose response curves from the DHODH assay. (C) IC₅₀ values from brequinar

and new probes tested in DHODH and MTT assay. (D) HCT-116 colonies treated with varying doses of brequinar probes.

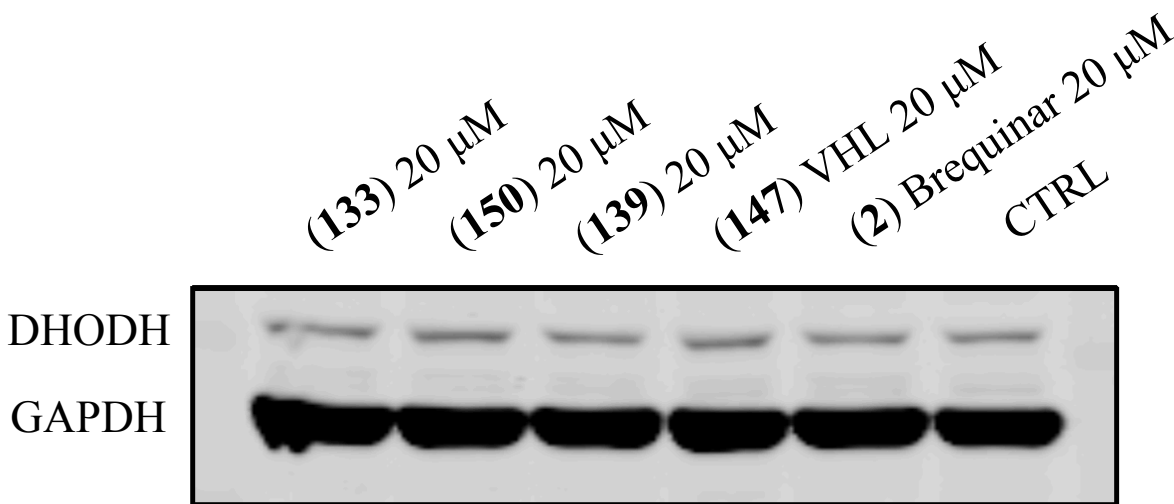


Figure 4.3 Western blot analysis of cells with probes. HCT116 p53^{+/+} cells were treated with compounds and compared to control. No change of DHODH protein expression was observed in HCT116 p53^{+/+} cells after treatment of PROTAC compounds (**133**, **150**), precursor compound **139**, VHL (**147**), or brequinar (**2**) for 12 h.

Probe **134** was not observed to inhibit DHODH at high concentrations ($IC_{50} > 50 \mu\text{M}$), which was expected, but it did display an $IC_{50} = 5.2 \pm 0.3 \mu\text{M}$ in HCT-116 and was the most potent in MiaPaca-2 ($IC_{50} = 3.7 \pm 0.7 \mu\text{M}$). Significant cytotoxicity of **134** in MiaPaca-2, suggested that better mitochondrial accumulation may improve the therapeutic relevance of DHODH inhibition in pancreatic cancer. Probe **134** must be hydrolyzed within the mitochondria to induce cytotoxicity through DHODH inhibition. A $t_{1/2}$ of 277 min was observed for **134** in mouse-liver microsomes, which suggests that active metabolites may be generated during the dosing period. We found the TPP-amide linker **153** did not possess significant cytotoxicity ($IC_{50} > 100 \mu\text{M}$) and that **134** followed similar trends to brequinar (lower IC_{50} value for continuous vs 24 hr treatment). These data support the pro-drug mechanism of action and suggest that further pro-drug analogues are warranted. We acknowledge that an ester attachment may increase the chances of hydrolysis, however our initial efforts to generate an ester analogue of **134** were thwarted by poor compound stability. This proof of concept study has directed us to pursue SAR studies focusing on stable TPP pro-drugs that can be cleaved by mitochondrial esterases.

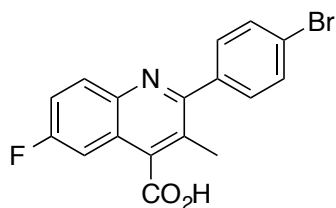
4.5 Conclusions

In summary, we present the synthesis of two new brequinar-based probes to evaluate mechanistic details of DHODH inhibition. We have developed novel synthetic routes to brequinar probes with two different attachment sites off the quinoline scaffold, and have validated that the incorporation of targeting headpieces maintains cytotoxicity in cell lines. Future studies will focus on ligand/linker optimization and further evaluation of these probes.

4.6 Experimental

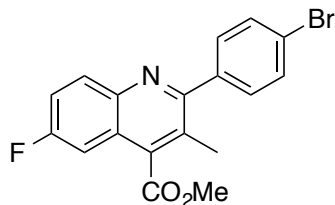
General methods. All reactions were performed under a nitrogen or argon atmosphere using standard inert gas techniques. Glassware for reactions were oven/flame dried in preparation for usage. All reagents and anhydrous solvents were purchased from commercial sources and used without further purification. Microwave catalyzed reactions were performed on a Biotage Initiator+ and sealed vials were purged with argon gas. The progresses of reactions were monitored using analytical thin-layer chromatography (TLC) on aluminum-backed pre-coated silica plates (Silicycle, SiliaPlate 200 μM thickness, F₂₅₄) and visualized by UV absorbance. Flash chromatography purifications were performed using a Biotage® Isolera Chromatography system with 10g and 25g Ultra-SNAP Cartridge columns (25 μm spherical silica). ¹H NMR spectra were obtained using a Bruker (300 or 400 MHz) or a Varian (400 or 500 MHz). Chemical shifts are reported in ppm and calibrated based on known solvent peaks (¹H using CDCl₃ = 7.26 ppm, MeOD = 3.31 ppm, DMSO, 2.50 ppm; ¹³C using CDCl₃ = 77.16 ppm, MeOD = 49.00 ppm, DMSO, 39.52 ppm).²⁴ Spectral data was reported using the following abbreviations: (s = singlet, d = doublet, t = triplet, q = quartet, m = multiplet, dd = doublet of doublets), coupling constants are reported in Hz, followed by integration. ¹³C NMR spectra were obtained at 126 MHz on a Varian 500 MHz instrument with a proton decoupled probe. ¹³C spectra are reported with observed carbon-fluorine splitting and couplings constants are reported with relation to CF bond (J_{CF1} = CF bond, J_{CF2} = *ortho* to CF bond, J_{CF3} = *meta* to CF bond). Data from MS spectrometry and HPLC traces were obtained using a Shimadzu LCMS 20-20 system, which was equipped with photo diode UV detector and a Kinetex® 2.6 μm , XB-C18 100 Å, 75 x 4.6 mm column. HPLC traces were obtained at room temperature using a gradient method from 1% to 90% MeCN in H₂O with 0.01% formic acid over 20 minutes. The flow rate

was 0.50 mL/min. Semi-preparative purifications were performed at room temperature on a Shimadzu LC-20 modular HPLC system, which was equipped with a photo diode UV detector and a Kinetex® 5 µm XB-C18 100 Å, 150 x 21.2 mm column. Semi-preparative purification was performed using a gradient method from 10% to 90% MeCN in H₂O with 0.01% trifluoroacetic acid over 30 minutes.



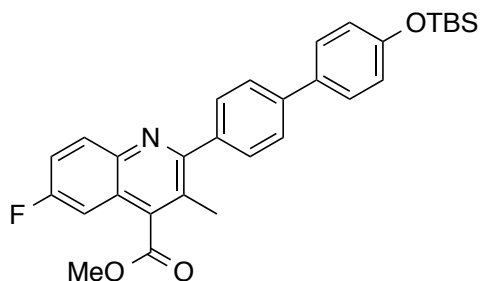
2-(4-Bromophenyl)-6-fluoro-3-methylquinoline-4-carboxylic acid

(136): 5-Fluoroindoline-2,3-dione (1.90 g, 11.5 mmol) and KOH (3.89 g, 69.6 mmol) were dissolved in 19 mL EtOH and the solution was stirred at room temperature. After 15 min, 1-(4-bromophenyl)propan-1-one (2.45 g, 11.5 mmol) was added and the mixture was heated at reflux for 18 h. Upon completion, the mixture was cooled to room temperature and EtOH was removed *in vacuo*. The solution was washed with ethyl acetate (3x) and then acidified with aqueous HCl until pH 2-3 was reached. Product precipitation was observed and the solid was collected over a frit. 2-(4-Bromophenyl)-6-fluoro-3-methylquinoline-4-carboxylic acid was isolated as a tan solid and used without further purification (3.70 g, 10.3 mmol, 89%). **¹H NMR** (500 MHz, DMSO-*d*₆) δ = 8.14 – 8.10 (m, 1H), 7.73 – 7.67 (m, 3H), 7.57 (d, *J* = 8.1 Hz, 2H), 7.51 – 7.47 (m, 1H), 2.39 (s, 3H). **¹³C NMR** (126 MHz, DMSO-*d*₆) δ = 168.70, 160.82 (d, *J*_{CF1} = 247.0 Hz), 159.03, 143.31, 140.91, 139.38, 132.75 (d, *J*_{CF3} = 9.6 Hz), 131.67 (2C), 131.57 (2C), 125.76, 123.70 (d, *J*_{CF3} = 10.2 Hz), 122.53, 120.15 (d, *J*_{CF2} = 25.7 Hz), 108.15 (d, *J*_{CF2} = 23.1 Hz), 18.11. **MS** (ESI+) 360.00, 361.95 [M+H] 358.10, 360.15 [M-H].



Methyl 2-(4-bromophenyl)-6-fluoro-3-methylquinoline-4-

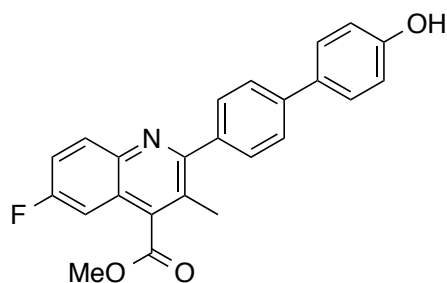
carboxylate (137): 2-(4-Bromophenyl)-6-fluoro-3-methylquinoline-4-carboxylic acid (6.50 g, 18.1 mmol) and Cs_2CO_3 (7.06 g, 21.7 mmol) were dissolved in 90 mL anhydrous DMF and the solution was stirred for 15 min at room temperature under an argon atmosphere. Methyl iodide (2.27 mL, 36.5 mmol) was added drop-wise to the solution and the reaction was stirred at room temperature for an additional 12 hours. The mixture was diluted with brine and product was extracted with EtOAc (3x). The combined EtOAc was washed with brine (6x), dried with magnesium sulfate, and concentrated *in vacuo*. Purification via flash chromatography (2:1 hexane/EtOAc) yielded methyl 2-(4-bromophenyl)-6-fluoro-3-methylquinoline-4-carboxylate as white powder (6.02 g, 16.1 mmol, 89%). $^1\text{H NMR}$ (500 MHz, Chloroform-*d*) δ = 8.11 (dd, J = 9.2, 5.4 Hz, 1H), 7.64 (d, J = 8.3 Hz, 2H), 7.50 – 7.41 (m, 3H), 7.37 (d, J = 9.5, 2.7 Hz, 1H), 4.09 (s, 3H), 2.40 (s, 3H). $^{13}\text{C NMR}$ (126 MHz, Chloroform-*d*) δ 168.01, 161.27 (d, $J_{\text{CF}1}$ = 249.5 Hz), 158.94, 143.53, 139.07, 139.04, 132.44 (d, $J_{\text{CF}3}$ = 9.4 Hz), 131.76 (2C), 130.73 (2C), 126.64, 124.31 (d, $J_{\text{CF}3}$ = 10.3 Hz), 123.13, 119.91 (d, $J_{\text{CF}2}$ = 25.8 Hz), 108.00 (d, $J_{\text{CF}2}$ = 23.4 Hz), 52.95, 18.18. **MS** (ESI+) 373.95, 375.95 [M+H]



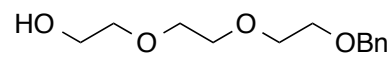
Methyl 2-(4'-((tert-butyldimethylsilyloxy)-[1,1'-

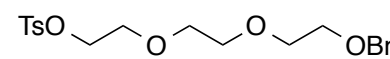
biphenyl]-4-yl)-6-fluoro-3-methylquinoline-4-carboxylate (138): Methyl 2-(4-bromophenyl)-6-fluoro-3-methylquinoline-4-carboxylate (652 mg, 1.75 mmol) and (4-((tert-butyldimethylsilyloxy)phenyl)boronic acid (661 mg, 2.62 mmol) were dissolved in a degassed mixture of 10 mL toluene/5 mL H_2O in a microwave vial. $\text{Pd}(\text{PPh}_3)_4$ (202 mg, 0.17 mmol) and Na_2CO_3 (1.06 g, 10.0 mmol) were added to the mixture, the vial was sealed, and then heated at 130 °C for 2 h. Toluene was removed under reduced pressure and the mixture was extracted with

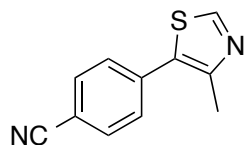
EtOAc (3x), dried with magnesium sulfate, filtered, and concentrated. The residue was loaded onto a silica column and eluted in a gradient of 9:1 hexane/EtOAc to yield methyl 2-(4'-((*tert*-butyldimethylsilyl)oxy)-[1,1'-biphenyl]-4-yl)-6-fluoro-3-methylquinoline-4-carboxylate as a yellow oil (627 mg, 1.25 mmol, 72%). **¹H NMR** (500 MHz, Chloroform-*d*) δ 8.16 (dd, $J = 3.8, 1.1$ Hz, 1H), 7.72 – 7.67 (m, 2H), 7.64 – 7.60 (m, 2H), 7.57 – 7.52 (m, 2H), 7.50 – 7.45 (m, 1H), 7.42 – 7.37 (m, 1H), 6.95 (d, $J = 7.4$ Hz, 2H), 4.11 (s, 3H), 2.48 (s, 3H), 1.03 (s, 9H), 0.26 (s, 6H). **¹³C NMR** (126 MHz, Chloroform-*d*) δ 168.20, 161.15 (d, $J_{\text{CF1}} = 248.9$ Hz), 159.94, 155.70, 143.59, 141.26, 138.87, 138.82, 138.44, 133.76, 132.46 (d, $J_{\text{CF3}} = 9.2$ Hz), 129.44 (2C), 128.25 (2C), 126.95, 126.85 (2C), 124.18 (d, $J_{\text{CF3}} = 10.2$ Hz), 120.55 (2C), 119.65 (d, $J_{\text{CF2}} = 25.7$ Hz), 107.93 (d, $J_{\text{CF2}} = 23.4$ Hz), 52.87, 25.82 (3C), 18.36, -4.24 (2C). **MS** (ESI) 502.25 [M+H]



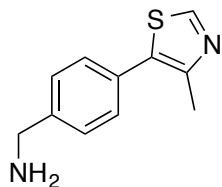
Methyl 6-fluoro-2-(4'-hydroxy-[1,1'-biphenyl]-4-yl)-3-methylquinoline-4-carboxylate (139): Methyl 2-(4'-((*tert*-butyldimethylsilyl)oxy)-[1,1'-biphenyl]-4-yl)-6-fluoro-3-methylquinoline-4-carboxylate (627 mg, 1.25 mmol) was dissolved in 12 mL THF. TBAF (392 mg, 1.50 mmol) was slowly added to the solution and the mixture was stirred at room temperature for 2 hour. Upon completion, the reaction mixture was concentrated, the residue was washed with a saturated solution of aqueous NH_4Cl , and the product was extracted with EtOAc. The organic layer was dried with sodium sulfate, filtered, concentrated, and purified via flash chromatography using 1:1 EtOAc/Hexane to yield methyl 6-fluoro-2-(4'-hydroxy-[1,1'-biphenyl]-4-yl)-3-methylquinoline-4-carboxylate (209 mg, 0.54 mmol, 43%). **¹H NMR** (500 MHz, DMSO-*d*₆) δ 9.63 (s, 1H), 8.16 – 8.12 (m, 1H), 7.75 – 7.68 (m, 2H), 7.68 – 7.64 (m, 2H), 7.61 – 7.53 (m, 3H), 6.89 (d, $J = 8.5, 1.5$ Hz, 2H), 4.07 (s, 3H), 2.41 (s, 3H). **¹³C NMR** (126 MHz, DMSO-*d*₆) δ 167.25, 160.44 (d, $J_{\text{CF1}} = 246.5$ Hz), 159.39, 157.43, 142.92, 140.30, 138.64, 138.60, 137.52, 132.27 (d, $J_{\text{CF3}} = 9.5$ Hz), 129.64 (2C), 127.85 (2C), 126.45, 125.58 (2C), 123.27 (d, $J_{\text{CF3}} = 11.0$ Hz), 119.77 (d, $J_{\text{CF2}} = 25.9$ Hz), 115.82 (2C), 107.82 (d, $J_{\text{CF2}} = 23.2$ Hz), 53.14, 17.84. **MS** (ESI) 388.10 [M+H]


2-(2-(2-(Benzyloxy)ethoxy)ethoxy)ethan-1-ol (141): Compound **141** was prepared following a modified protocol described by Jiang & Yu.²¹ Triethylene glycol (**140**) (3.97 mL, 29.8 mmol) was dissolved in THF (46 mL) and the solution was chilled to 0 °C. After 15 min, NaH (1.20 g, 30.1 mmol) was added and the mixture was stirred for an additional 15 min before adding benzyl bromide (2.10 mL, 17.5 mmol). The reaction mixture was warmed to room temperature overnight. Upon quenching with water, the mixture was concentrated and then extracted with EtOAc. The dried extracts were concentrated to a residue that was purified via flash chromatography eluting with 1:1 hexane/EtOAc to yield 2-(2-(2-(benzyloxy)ethoxy)ethoxy)ethan-1-ol as a clear oil (2.09 g, 8.74 mmol, 50%). ¹H NMR (500 MHz, Chloroform-*d*) δ 7.37 – 7.31 (m, 4H), 7.28 – 7.20 (m, 1H), 4.54 (s, 2H), 3.76 – 3.51 (m, 12H). ¹³C NMR (126 MHz, Chloroform-*d*) δ 138.06, 128.41 (2C), 127.83 (2C), 127.70, 73.28, 72.60, 70.63, 70.57, 70.32, 69.36, 61.67. **MS** (ESI) 241.70 [M+H]

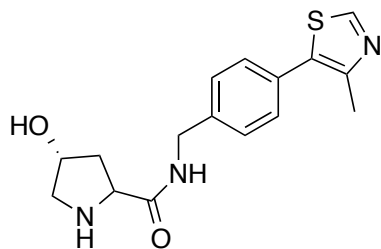

2-(2-(2-(Benzyloxy)ethoxy)ethoxy)ethyl 4-methylbenzenesulfonate (142): 2-(2-(2-(Benzyloxy)ethoxy)ethoxy)ethan-1-ol (**141**) (2.09 g, 8.74 mmol) was dissolved in 60 mL of THF and 20 mL of H₂O. KOH (1.71 g, 30.5 mmol) was added to the mixture, which was stirred at room temperature for 15 min before TsCl (2.00 g, 10.5 mmol) was added and the mixture for stirred overnight. Upon completion, the mixture was poured into a saturated solution of ammonium hydroxide and extracted with dichloromethane (3x). The extract was pooled, dried with magnesium sulfate, filtered, and concentrated to yield 2-(2-(2-(benzyloxy)ethoxy)ethoxy)ethyl 4-methylbenzenesulfonate as a orange oil (2.50 g, 6.33 mmol, 72%), which was used without further purification. ¹H NMR (500 MHz, Chloroform-*d*) δ 7.79 (d, *J* = 8.3 Hz, 2H), 7.38 – 7.21 (m, 7H), 4.55 (s, 2H), 3.71 – 3.57 (m, 12H), 2.43 (s, 3H). ¹³C NMR (126 MHz, Chloroform-*d*) δ 144.91, 138.36, 129.94 (2C), 128.51 (2C), 128.13 (2C), 127.89 (2C), 127.76 (2C), 73.39, 70.93, 70.83, 70.73, 69.55, 69.38, 68.85, 21.78. **MS** (ESI) 395.15 [M+H].



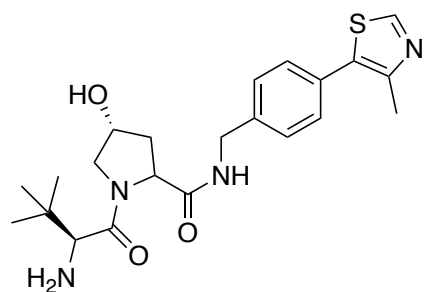
4-(4-Methylthiazol-5-yl)benzonitrile (144): Compound **144** was prepared following a protocol that was reported by Buckley¹⁴ and Galdeno¹³. A mixture containing 4-bromobenzonitrile (5.00 g, 27.5 mmol), 4-methylthiazole (4.98 mL, 54.7 mmol), KOAc (5.40 g, 55.0 mmol), and palladium acetate (62.0 mg, 0.27 mmol) were dissolved in 16 mL DMAc. The mixture was heated to 140 °C overnight, cooled, and then poured into EtOAc. The solution was washed with H₂O (6x), dried with magnesium sulfate, filtered, and concentrated. The resulting oil was crystallized by the addition of hexanes and used without further purification. 4-(4-Methylthiazol-5-yl)benzonitrile was isolated as a yellow solid (5.15 g, 25.8 mmol, 94%) and matched the reported spectral data.¹³ ¹H NMR (400 MHz, Chloroform-*d*) δ 8.76 (s, 1H), 7.75 – 7.71 (m, 2H), 7.60 – 7.55 (m, 2H), 2.59 – 2.56 (m, 3H). **MS** (ESI) 200.90 [M+H].



(4-(4-Methylthiazol-5-yl)phenyl)methanamine (145): Compound **145** was prepared following a protocol reported by Buckley¹⁴ and Galdeno.¹³ Compound **144** (5.15 g, 25.8 mmol) was dissolved in 280 mL anhydrous MeOH. Cobalt chloride hexahydrate (9.90 g, 41.7 mmol) was added and the solution was placed on an ice bath for 30 min. NaBH₄ (5.22 g, 138 mmol) was slowly added over 20 min, bubbling was observed, and the solution turned black. The mixture was stirred for 90 min and quenched with cold H₂O. The quenched solution was poured over a frit to remove insoluble by-products and the filtrate was washed with H₂O then extracted with EtOAc. The organic layer was dried with sodium sulfate, filtered, concentrated, and purified via flash chromatography using a gradient of 1-10% 0.5 M methanolic ammonia in DCM. Compound **13** was isolated (1.12 g, 5.49 mmol, 21%) and matched the reported spectral data.¹⁴ ¹H NMR (400 MHz, Chloroform-*d*) δ 8.65 (s, 1H), 7.41 – 7.35 (m, 4H), 3.90 (s, 2H), 2.50 (s, 3H). **MS** (ESI) 204.90, 187.80 (fragmentation product reported by Galdeno also observed)^{13, 14} [M+H].

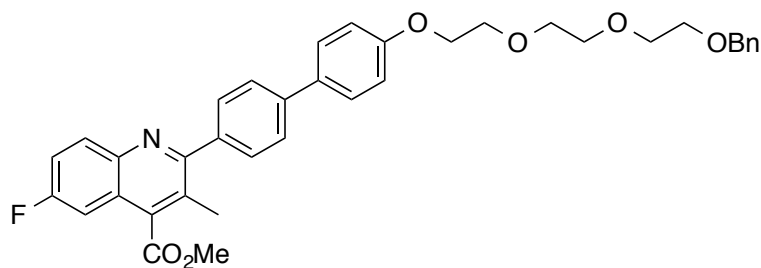


(4R)-4-Hydroxy-N-(4-(4-methylthiazol-5-yl)benzyl)pyrrolidine-2-carboxamide (146): Compound **146** was prepared following a protocol reported by Galdeno¹³. Anhydrous DMF (55 ml) was added to a round-bottom flask containing compound **145** (1.12 g, 5.49 mmol), Boc-Hyp-OH (1.27 g, 5.49 mmol), DIPEA (3.85 mL, 22.0 mmol), and HATU (2.30 g, 6.05 mmol). The mixture was stirred at room temperature overnight. The solution was diluted with H₂O and extracted with EtOAc. The EtOAc layer was washed with brine (6x), dried with magnesium sulfate, and concentrated. The residue was purified via flash chromatography using a gradient from 1-10% 0.5 M methanolic ammonia in DCM. (**MS** (ESI) 418.15 [M+H]). The isolated oil was re-dissolved in 10 mL of 4.0 N HCl in dioxane and stirred at room temperature for 1 h. The solvent was concentrated and used without further purification. Compound **14** was isolated as an oil (1.16 g, 3.66 mmol, 66% two steps) and matched the reported spectral data.¹⁴ **¹H NMR** (300 MHz, Chloroform-*d*) δ 8.69 (s, 1H), 8.28 – 8.04 (m, 1H), 7.45 – 7.32 (m, 4H), 4.52 – 4.44 (m, 3H), 4.10 (t, *J* = 8.4 Hz, 1H), 3.10 – 3.00 (m, 1H), 2.88 – 2.77 (m, 1H), 2.54 (s, 3H), 2.41 – 2.32 (m, 1H), 2.07 – 1.93 (m, 1H). **MS** (ESI) 317.90 [M+H]



(4R)-1-((S)-2-Amino-3,3-dimethylbutanoyl)-4-hydroxy-N-(4-(4-methylthiazol-5-yl)benzyl)pyrrolidine-2-carboxamide (147): A mixture containing compound **146** (1.16 g, 3.29 mmol), Boc-*L*-*tert*-leucine (847 mg, 3.67 mmol), HATU (1.67 g, 4.40 mmol), and DIPEA (2.56 mL, 14.7 mmol) was dissolved in 55 mL DMF. The mixture was stirred at room temperature overnight, diluted with H₂O, and extracted with EtOAc. The EtOAc layer was washed with a saturated NaHCO₃ solution (2x), brine (6x), dried with magnesium sulfate, filtered, and concentrated. (**MS** (ESI) 531.10 [M+H]) Residue containing the

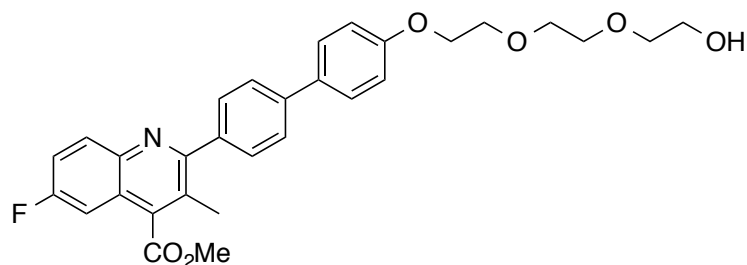
intermediate was dissolved in 10 mL of 4.0 N HCl in dioxane, stirred at room temperature for 1 hour, and followed the workup described by Buckner.¹⁴ The solution was concentrated to an orange oil and matched the reported spectra of (4*R*)-1-((*S*)-2-Amino-3,3-dimethylbutanoyl)-4-hydroxy-*N*-(4-(4-methylthiazol-5-yl)benzyl)pyrrolidine-2-carboxamide (970 mg, 2.25 mmol, 68% yield two steps) and used without further purification. ¹H NMR (300 MHz, Methanol-*d*₄) δ 8.90 (s, 1H), 7.50 – 7.41 (m, 4H), 4.66 – 4.34 (m, 4H), 3.82 – 3.65 (m, 1H), 3.49 (s, 1H), 2.50 (s, 3H), 2.30 – 2.17 (m, 1H), 2.16 – 2.07 (m, 1H), 1.04 (s, 9H). MS (ESI) 431.15 [M+H].



Methyl 2-(4'-(2-(2-(2-

(benzyloxy)ethoxy)ethoxy)ethoxy)-[1,1'-biphenyl]-4-yl)-6-fluoro-3-methylquinoline-4-

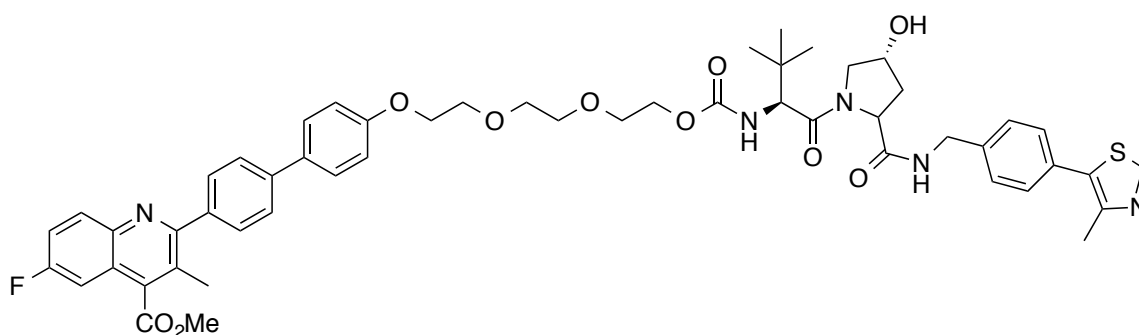
carboxylate (148): Compound **139** (209 mg, 0.54 mmol) was dissolved in 11 mL DMF. Cs₂CO₃ (790 mg, 2.42 mmol) was added to the solution and the mixture was stirred at room temperature for 5 min. 2-(2-(2-(Benzyloxy)ethoxy)ethoxy)ethyl 4-methylbenzenesulfonate (**142**) (255 mg, 0.65 mmol), was slowly added and the mixture was heated at 75 °C for 2 h. The solution was concentrated to an oil, re-dissolved in DCM, washed with brine (6x), dried with magnesium sulfate, and re-concentrated to an oil. The crude was purified by silica chromatography eluting with a gradient from 10% to 40% EtOAc in hexane. Methyl 2-(4'-(2-(2-(2-(benzyloxy)ethoxy)ethoxy)ethoxy)ethyl)-[1,1'-biphenyl]-4-yl)-6-fluoro-3-methylquinoline-4-carboxylate was isolated (173 mg, 0.28 mmol, 52%) and used without further purification. ¹H NMR (500 MHz, Chloroform-*d*) δ 8.20 – 8.15 (m, 1H), 7.71 – 7.66 (m, 2H), 7.61 (d, *J* = 8.3 Hz, 2H), 7.60 – 7.56 (m, 2H), 7.51 – 7.46 (m, 1H), 7.41 – 7.25 (m, 6H), 7.04 – 7.00 (m, 2H), 4.58 (s, 2H), 4.22 – 4.17 (m, 2H), 4.11 (s, 3H), 3.93 – 3.88 (m, 2H), 3.80 – 3.63 (m, 8H), 2.48 (s, 3H). ¹³C NMR (126 MHz, Chloroform-*d*) δ 168.23, 162.20, 161.21 (d, *J*_{CF1} = 249.1 Hz). 159.93, 158.79, 143.53, 141.23, 138.42, 133.39, 132.43 (d, *J*_{CF3} = 9.7 Hz), 129.49 (2C), 128.50 (2C), 128.30 (2C), 127.87 (2C), 127.72, 127.00, 126.88 (2C), 124.23 (d, *J*_{CF3} = 10.1 Hz), 119.76 (d, *J*_{CF2} = 25.7 Hz), 115.17 (2C), 110.14, 107.97 (d, *J*_{CF2} = 23.4 Hz), 73.39, 71.04, 70.87 (2C), 69.91, 69.60, 67.70, 52.94, 18.34. MS (ESI) 610.45 [M+H].



Methyl 6-fluoro-2-(4'-(2-(2-(2-

hydroxyethoxy)ethoxy)ethoxy)-[1,1'-biphenyl]-4-yl)-3-methylquinoline-4-carboxylate (149):

Compound **148** (173 mg, 0.28 mmol) was dissolved in 30 mL anhydrous EtOH and the solution was purged with argon for 30 min. Activated Pd on charcoal (10%) (60 mg) was added to the solution, (excess EtOH was used to submerge all Pd/C) and the mixture was stirred under an H₂ environment overnight. The mixture was filtered over EtOAc washed celite and eluted with EtOAc. Filtrate was concentrated and loaded onto silica column eluting with a gradient of 20 – 66% EtOAc in hexane. Compound **149** was isolated (79 mg, 0.15 mmol, 54%). ¹H NMR (500 MHz, Chloroform-*d*) δ 8.21 (s, 1H), 7.69 (d, *J* = 8.3 Hz, 2H), 7.64 – 7.56 (m, 4H), 7.52 – 7.45 (m, 1H), 7.38 (dd, *J* = 9.5, 2.7 Hz, 1H), 7.07 – 6.99 (m, 2H), 4.24 – 4.18 (m, 2H), 4.11 (s, 3H), 3.94 – 3.88 (m, 2H), 3.79 – 3.69 (m, 6H), 3.69 – 3.61 (m, 2H), 2.48 (s, 3H). ¹³C NMR (126 MHz, Chloroform-*d*) δ 168.16, 161.25 (d, *J*_{CF1} = 249.2 Hz), 159.85, 158.71, 143.29, 141.31, 138.16, 133.47 (2C, overlap), 132.26 (d, *J*_{CF3} = 10.1 Hz), 129.54 (2C), 128.35 (2C), 127.08, 126.90 (2C), 124.28 (d, *J*_{CF3} = 9.9 Hz), 119.90 (d, *J*_{CF2} = 25.5 Hz), 115.17 (2C), 108.00 (d, *J*_{CF2} = 23.7 Hz), 72.64, 71.02, 70.55, 69.91, 67.64, 61.94, 52.98, 18.33. MS (ESI) 520.30 [M+H].



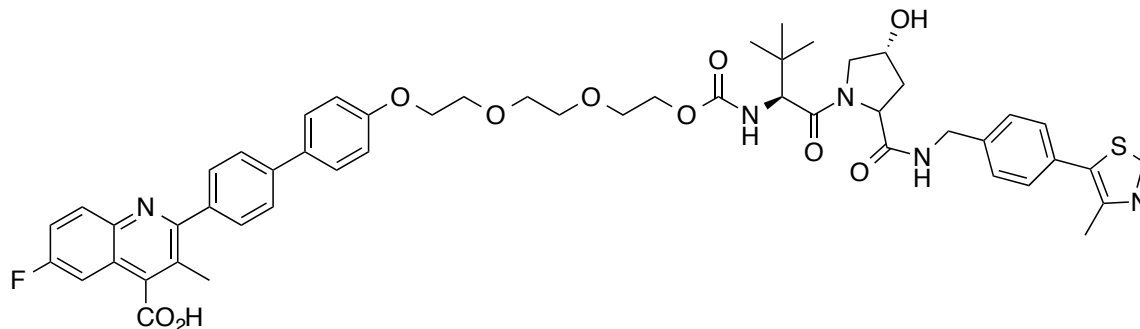
Methyl 6-fluoro-2-(4'-(((12S)-12-((4R)-4-hydroxy-2-((4-(4-methylthiazol-5-

yl)benzyl)carbamoyl)pyrrolidine-1-carbonyl)-13,13-dimethyl-10-oxo-3,6,9-trioxa-11-

azatetradecyl)oxy)-[1,1'-biphenyl]-4-yl)-3-methylquinoline-4-carboxylate (150): Compound

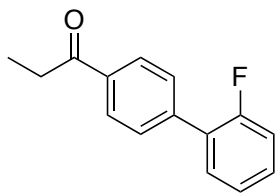
149 (40 mg, 0.08 mmol) was dissolved in 3 mL anhydrous MeCN. DIPEA (0.07 mL, 0.39 mmol)

was added and the mixture was stirred at room temperature for 15 min. *N,N'*-disuccinimidyl carbonate (102 mg, 0.40 mmol) was added and the mixture was stirred at room temperature for 12 hours before being concentrated. The residue was dissolved in DCM and washed with H₂O (3x). The organic layer was dried with magnesium sulfate, filtered, concentrated, and used without further purification. In a separate round-bottom flask, compound **147** (34 mg, 0.08 mmol) was dissolved in DMF (2.0 mL) and DIPEA (0.07 mL, 0.39 mmol). The organic residue containing the succinimidyl intermediate was dissolved in 1.5 mL DMF and the mixture was slowly added to the basic solution containing **147**. The combined solution was stirred at room temperature for 12 hours. Upon completion, the mixture was concentrated to an oil, re-dissolved in EtOAc, and washed with brine (6x). The organic layer was dried with magnesium sulfate, filtered, concentrated, and loaded onto silica column, eluting in a slow gradient towards 90/10 DCM/MeOH with 0.5 M NH₄. Compound **150** was isolated as a clear oil (16 mg, 0.02 mmol, 25% yield, two-steps). ¹H NMR (500 MHz, Methanol-*d*₄) δ 8.83 (s, 1H), 8.10 (dd, *J* = 9.3, 5.4 Hz, 1H), 7.72 (d, *J* = 8.3 Hz, 2H), 7.64 – 7.57 (m, 5H), 7.47 – 7.36 (m, 5H), 7.04 (d, *J* = 8.7 Hz, 2H), 4.58 (t, *J* = 8.3 Hz, 1H), 4.54 – 4.47 (m, 2H), 4.36 – 4.31 (m, 2H), 4.23 – 4.13 (m, 4H), 4.10 (s, 3H), 3.91 – 3.83 (m, 3H), 3.78 (dd, *J* = 10.9, 3.9 Hz, 1H), 3.74 – 3.65 (m, 6H), 2.44 (s, 3H), 2.41 (s, 3H), 2.25 – 2.17 (m, 1H), 2.13 – 2.04 (m, 1H), 1.01 (s, 9H). ¹³C NMR (126 MHz, Methanol-*d*₄) δ 174.40, 172.65, 169.00, 162.55 (d *J*_{CF1} = 244.4 Hz), 161.55, 160.25, 158.57, 152.77, 149.00, 144.32, 142.56, 140.91, 140.21, 139.20, 134.16, 133.38, 132.58 (d, *J*_{CF3} = 9.6 Hz), 131.48, 130.61 (2C), 130.35 (2C), 129.15 (2C), 128.93, 128.46 (2C), 127.47 (2C), 125.51 (d, *J*_{CF3} = 10.1 Hz), 120.94 (d, *J*_{CF2} = 26.2 Hz), 116.16 (2C), 108.98 (d, *J*_{CF2} = 23.9 Hz), 71.78, 71.59, 71.09, 70.90, 70.51, 68.72, 65.44, 60.95, 60.81, 57.99, 53.43, 43.70, 38.90, 36.68, 26.95 (3C), 18.32, 15.83. LCMS (ESI) 976.45 [M+H], 95% purity based on HPLC chromatograph at 254 nm.



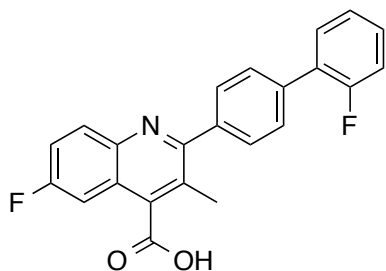
6-Fluoro-2-(4'-(((12*S*)-12-((4*R*)-4-hydroxy-2-((4-(4-methylthiazol-5-yl)benzyl)carbamoyl)pyrrolidine-1-carbonyl)-13,13-dimethyl-10-oxo-3,6,9-trioxa-11-azatetradecyl)oxy)-[1,1'-biphenyl]-4-yl)-3-methylquinoline-4-carboxylic acid (133):

Compound **150** (10 mg, 0.01 mmol) was dissolved in a 1 mL solution of 1:1 THF/H₂O. LiOH (5 mg, 0.21 mmol) was added to the solution and the mixture was stirred at room temperature overnight. LCMS indicated pre-dominantly starting material remained. Additional LiOH (20 mg, 0.83 mmol) was added and the solution was heated to 40 °C for three additional days (reaction progress monitored by LCMS). The mixture was concentrated and purified via reverse phase chromatography eluting with a gradient from 0 to 100 MeCN in H₂O. Compound **1** was isolated as a clear oil (5 mg, 0.01 mmol, 50%). ¹H NMR (300 MHz, Methanol-*d*₄) δ 8.87 (s, 1H), 8.08 – 8.00 (m, 1H), 7.76 (d, *J* = 7.9 Hz, 2H), 7.70 – 7.56 (m, 5H), 7.57 – 7.39 (m, 5H), 7.09 (d, *J* = 8.3 Hz, 2H), 4.65 – 4.49 (m, 3H), 4.41 – 4.33 (m, 2H), 4.26 – 4.13 (m, 4H), 3.96 – 3.84 (m, 3H), 3.84 – 3.62 (m, 7H), 2.52 – 2.38 (m, 6H), 2.30 – 2.06 (m, 1H), 2.06 – 2.02 (m, 1H), 1.04 (s, 9H). ¹³C NMR (126 MHz, Methanol-*d*₄) δ 174.43, 172.66, 161.92 (d, *J*_{CF1} = 247.0 Hz), 161.76, 160.94, 160.16, 158.58, 152.82, 149.02, 144.26, 142.25, 140.23, 140.05, 135.47 (d, *J*_{CF2} = 12.6 Hz), 134.39, 133.41, 131.57, 131.49, 130.50 (2C), 130.37 (2C), 129.15 (2C), 128.94 (2C), 127.39 (2C), 125.78 (d, *J*_{CF3} = 10.0 Hz), 124.87, 120.16 (d, *J*_{CF2} = 26.2 Hz), 116.13 (2C), 110.22 (d, *J*_{CF2} = 22.8 Hz), 71.78, 71.59, 71.10, 70.91, 70.53, 68.71, 65.44, 60.97, 60.82, 57.98, 43.70, 38.92, 36.68, 26.94 (3C), 18.14, 15.81. LCMS (ESI) 962.45. [M+H], 960.35 [M-H], 96% purity based on HPLC chromatograph at 254 nm.



1-(2'-Fluoro-[1,1'-biphenyl]-4-yl)propan-1-one: (151)

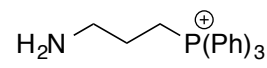
1-(4-Bromophenyl)propan-1-one (2.00 g, 9.39 mmol), (2-fluorophenyl)boronic acid (1.95 g, 14.1 mmol), K_2HPO_4 (3.89 g, 28.2 mmol), and $Pd(PPh_3)_4$ (0.54 g, 0.47 mmol) were added to a microwave vial. 12 mL of dioxane and 2 mL of H_2O were added and the vial was sealed. The reaction was stirred at 130 °C for 1.5 hour and the mixture was concentrated upon completion. The product was purified from the residue via flash chromatography with a gradient of 1% to 60% EtOAc in hexane to yield compound **12** (679 mg, 2.98 mmol, 32% yield). 1H NMR (500 MHz, Chloroform-*d*) δ 8.02 (d, $J = 8.4$ Hz, 2H), 7.62 (dd, $J = 8.4, 1.7$ Hz, 2H), 7.43 (td, $J = 7.8, 1.8$ Hz, 1H), 7.36 – 7.30 (m, 1H), 7.21 (td, $J = 7.6, 1.2$ Hz, 1H), 7.18 – 7.12 (m, 1H), 3.00 (q, $J = 7.2$ Hz, 2H), 1.24 (t, $J = 7.2$ Hz, 3H). MS (ESI) 229.05 [M+H].

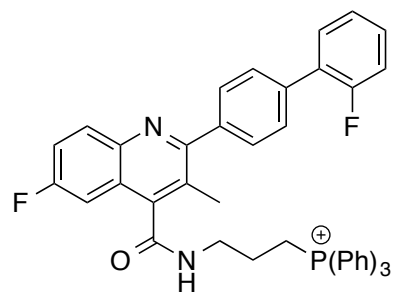


6-Fluoro-2-(2'-fluoro-[1,1'-biphenyl]-4-yl)-3-methylquinoline-

4-carboxylic acid (Brequinar) (2): 5-fluoroisatin (2.17 g, 13.2 mmol) was dissolved in a 35 mL solution of EtOH/ H_2O (2:1 ratio). KOH (2.95 g, 52.6 mmol) were added and the solution was stirred at room temperature for 15 min (solution turns dark when KOH is added). Compound **151** (2.0 g, 8.77 mmol) was added and the mixture was heated at reflux overnight. Upon completion, the mixture was cooled to room temperature, dioxane/EtOH were concentrated *in vacuo*, and the solution was diluted with 1 M KOH. The basic solution was washed with EtOAc (3x) and then acidified to pH 2-3 with HCl (precipitant formation observed). Precipitant was poured over a fritted funnel then triturated with EtOAc and Et_2O , before collection. Compound **20** isolated as a tan solid (1.81 g, 4.82 mmol, 55%). 1H NMR (400 MHz, DMSO-*d*₆) δ 8.15 (dd, $J = 9.2, 5.6$ Hz, 1H), 7.79 – 7.69 (m, 5H), 7.65 (t, $J = 7.8, 1.7$ Hz, 1H), 7.54 – 7.45 (m, 2H), 7.41 – 7.32 (m, 2H), 2.47 (s, 3H). ^{13}C NMR (126 MHz, DMSO-*d*₆) δ 168.38, 160.34 (d, $J_{CF1} = 245.7$ Hz), 160.16, 159.35, 159.28, 158.20, 142.94, 139.26, 135.17, 132.32 (d, $J_{CF3} = 10.0$ Hz), 130.82 (d, $J_{CF4} = 3.3$

Hz), 129.87 (d, $J_{CF3} = 10.1$ Hz), 129.38 (2C), 128.59 (d, $J_{CF4} = 2.9$ Hz), 127.73 (d, $J_{CF3} = 13.9$ Hz), 125.34, 125.07 (d, $J_{CF4} = 3.6$ Hz), 119.67 (d, $J_{CF2} = 25.7$ Hz), 116.21 (d, $J_{CF2} = 22.5$ Hz), 107.72 (d, $J_{CF2} = 23.4$ Hz), 17.77. **MS** (ESI) 375.70 [M+H], 373.65 [M-H].

 **(3-Aminopropyl)triphenylphosphonium (153)**; Compound **153** was prepared following a modified protocol from Zeng *et al.*²⁵ 3-Bromopropan-1-amine (**152**) (1.0 g 4.56 mmol) was dissolved in 20 mL of *n*-BuOH. Triphenylphosphine (1.19 g, 4.56 mmol) was added and the mixture was heated at reflux overnight. The reaction mixture was cooled to RT for 15 min before the addition of 12 mL of hexanes. The mixture was then stirred for 30 min and filtered over a frit. The white solid was washed with another 12 mL hexane (2x) before triturating with a 50/50 solution of *t*-butyl methyl ether and hexane (3x). (3-Aminopropyl)triphenylphosphonium was isolated (1.69 g, 4.24 mmol, 93%) and used without further purification. **¹H NMR** (500 MHz, DMSO-*d*₆) δ 7.94 – 7.73 (m, 15H), 3.98 – 3.86 (m, 2H), 3.10 – 3.02 (m, 2H), 1.97 – 1.82 (m, 2H). **¹³C NMR** (126 MHz, DMSO-*d*₆) δ 135.56 (d, $J_{CP4} = 3.1$ Hz) (3C), 134.06 (d, $J_{CP3} = 10.2$ Hz) (6C), 130.83 (d, $J_{CP2} = 12.5$ Hz) (6C), 118.47 (d, $J_{CP1} = 86.0$ Hz) (3C), 39.24, 20.53, 18.88 (d, $J_{CP1} = 52.8$ Hz). **MS** (ESI) 320.15 [M+H].



(3-(6-Fluoro-2-(2'-fluoro-[1,1'-biphenyl]-4-yl)-3-methylquinoline-4-carboxamido)propyl)triphenylphosphonium (134): Compound **2** (102 mg, 0.27 mmol) was dissolved in 3 mL of anhydrous 1,2 DCE. SOCl₂ (0.11 mL, 1.51 mmol) and 1 drop of DMF were added slowly then the mixture was heated at 60 °C for 2 h. (Acid chloride formation was monitored via TLC; 1 drop of reaction mixture was added to a vial containing TEA and MeOH, then the mixture was checked for the presence of methyl ester). The reaction mixture was cooled to room temperature, concentrated, re-dissolved in 1,2 DCE, and re-concentrated. The acid chloride was re-dissolved in 3 mL 1,2 DCE and slowly added to a separate round bottom flask, which contained a stirring solution of compound **153** (130 mg, 0.33

mmol), DIPEA (0.30 mL, 1.72 mmol), and 2.00 mL of anhydrous 1,2 DCE chilled over an ice bath. (Gas release was observed when the acid chloride was added to the solution). The mixture was stirred overnight. Upon completion, the mixture was concentrated, loaded onto silica column and eluted in a 1-30 % MeOH gradient in DCM with 0.5 M NH₃. Fractions containing desired compound was concentrated, re-dissolved in MeCN and crystallized by the addition of Et₂O/Hexane. The precipitant was poured over a frit and triturated with cold EtOAc, Et₂O, *t*-Butyl methyl ether, and hexane. Compound **134** was isolated as a tan solid with a red tint (89 mg, 0.13 mmol, 48%). ¹H NMR (500 MHz, DMSO-*d*₆) δ 8.88 (t, *J* = 5.6 Hz, 1H), 8.12 (dd, *J* = 9.2, 5.5 Hz, 1H), 7.95 – 7.74 (m, 15H), 7.74 – 7.66 (m, 4H), 7.63 (t, *J* = 8.0 Hz, 1H), 7.50 – 7.42 (m, 1H), 7.40 – 7.33 (m, 3H), 3.72 – 3.54 (m, 4H), 2.32 (s, 3H), 1.94 – 1.81 (m, 2H). ¹³C NMR (126 MHz, DMSO-*d*₆) δ 166.72, 160.67 (d, *J*_{CF1} = 248.2 Hz), 159.62 (d, *J*_{CF1} = 247.0 Hz), 159.57, 143.45, 143.41, 139.79, 135.63, 135.51 (d, *J*_{CP4} = 3.1 Hz) (3C), 134.03 (d, *J*_{CP3} = 10.3 Hz) (6C), 132.62 (d, *J*_{CF3} = 10.0 Hz), 131.25 (d, *J*_{CF4} = 3.3 Hz), 130.81, 130.76 (d, *J*_{CP2} = 12.4 Hz) (6C), 130.35 (d, *J* = 8.1 Hz), 129.74, 129.09 (d, *J* = 3.0 Hz), 128.14 (d, *J*_{CF3} = 13.0 Hz), 125.91, 125.54 (d, *J*_{CF4} = 3.4 Hz), 124.54 (d, *J*_{CF3} = 10.1 Hz), 119.99 (d, *J*_{CF2} = 25.5 Hz), 118.70 (d, *J*_{CP1} = 86.0 Hz) (3C), 116.68 (d, *J*_{CF2} = 22.5 Hz), 108.43, 108.25, 25.94, 22.56, 19.00 (d, *J*_{CP1} = 51.6 Hz), 17.86. LCMS (ESI) 678.15 [M+H], 98% purity based on HPLC chromatograph at 254 nm

hDHODH expression and purification. The *hDHODH* construct was provided by the De Brabander lab at UT Southwestern.²⁶ *hDHODH* was expressed in *E. coli* Rosetta 2 (DE3) in LB medium with ampicillin (100 µg/mL) and 0.1 mM FMN. Cells were grown at 37 °C to OD₆₀₀ = 0.6, then induced with 1 mM IPTG for 3 hours. Cells were harvested by centrifugation at 4,000 x g for 15 min at 4 °C. The pellet was re-suspended in lysis buffer (50 mM Tris-HCl, pH 8.5, 300 mM NaCl, 10% glycerol, 5 mM β-mercaptoethanol, 10 mM imidazole, 2% Triton X-100, 0.5 mM FMN, 200 µM PMSF, 1 mg/mL lysozyme). The cell suspension was incubated on ice for 2 hours, followed by sonication. The lysate was clarified by centrifugation at 35,000 x g for 20 min at 4 °C. After the supernatant was incubated with Ni-NTA resin for 1 h at 4 °C, the resin was loaded onto a column. The column was washed with wash buffer (50 mM Tris-HCl, pH 8.5, 300 mM NaCl, 10% glycerol, 5 mM β-mercaptoethanol, 25 mM imidazole, 0.1 mM FMN) and *hDHODH* was eluted with elution buffer (wash buffer containing 300 mM imidazole). Buffer

exchange was carried out using an Amicon concentrator into storage buffer (100 mM HEPES, pH 8.0, 150 mM NaCl, 10% glycerol) and *h*DHODH was stored at -80 °C.

DHODH activity assay. DHODH activity was monitored as previously described with modifications.²⁷ First, 1 μ L of test compound (50x) or DMSO, 60 nM DHODH, 100 μ M DCIP, and 20 μ M CoQ₁₀ (final concentrations for 50 μ L) in the assay buffer (100 mM HEPES pH 8.0, 150 mM NaCl, 10% glycerol, 0.1% Triton X-100) in a total of 40 μ L were incubated together for 30 min. The assay began with the addition of 10 μ L of dihydroorotate to a final concentration of 200 μ M. The reduction of DCIP was measured by monitoring the absorbance at 600 nm over 1 hr at room temperature using a microplate reader (BMG Labtech). Data were exported to Microsoft Excel for analysis and IC₅₀ values were determined using Prism 6 software.

Microsomal stability studies to determine $t_{1/2}$. Assays to determine microsomal stability and $t_{1/2}$ were performed by the University of Michigan Pharmacokinetics Core. A microsome solution was created, which contained 10 μ L of mouse liver microsome (20 mg/mL) in 330 μ L 0.1 M phosphate buffer (3.3 mM MgCl₂). Aliquots (40 μ L) from stock solutions of test compounds (10 μ M) were added and the mixture was incubated at 37 °C for 3 min. The enzymatic reactions were initiated by addition of 20 μ L NADPH solution (freshly prepared containing 4 mg NADPH in 240 μ L of 0.1M phosphate buffer (3.3 mM MgCl₂)). Aliquots of 40 μ L were removed from reaction solutions and stopped by the addition of chilled acetonitrile, which contained 50 ng/mL of CE302, an internal standard, at the designated time points (0, 5, 10, 15, 30, 45, and 60 min). Verapamil was used as positive control with the same method. The incubated solution was centrifuged at 3500 g for 15 minutes and the supernatant was used for LC/MS/MS analysis. A ratio of the natural log peak area (compound peak area/ internal standard peak area) was plotted against time and used for data extrapolation. Chromatographic conditions utilized a 5 cm x 2.1 mm I.D. 3.5 μ m XBridge column from Waters and utilized a gradient method of 5-95% MeCN in H₂O containing 0.1% formic acid.

Cell culture. HCT116 P53 +/+ and MiaPaca-2 cells were maintained in RPMI-1640 (Gibco) supplemented with 10% heat-inactivated FBS (Gibco). Cells were grown at 37 °C in a humidified atmosphere of 5% CO₂. For subculture and counting, cells were washed with DPBS

(Gibco) without calcium or magnesium, incubated with 0.25% trypsin-EDTA solution (Gibco) for 5 min, neutralized with full medium, centrifuged, re-suspended with culture medium and counted by Countess II FL. All experiments were performed using cells in exponential growth. Cells were routinely checked for Mycoplasma contamination.

Western blot. HCT116 p53^{+/+} cells were seeded into 6-well microtiter plates for 4×10^5 cells per well, and allowed to attach overnight before the addition of the dilution of compound (10X). After 12h treatment, the cells are lysated with RIPA buffer with the presence of protease inhibitors and phosphatase inhibitors. The cells are collected and centrifuged. The pellet was discarded. Protein concentration of whole-cell lysate in the supernatant was determined by BCA protein assay kit (Thermo Scientific). Proteins were resolved in 10% SDS/PAGE and electrotransferred to transfer membrane (Immobilon®-FL). After blocking with TBS blocking buffer (Thermo Scientific), membranes were probed with DHODH primary antibody (Santa Cruz Biotechnology; rabbit; 1:1000) and GAPDH primary antibody (Signaling; rabbit; 1:4000) in 5% BSA (EMD Millipore corporation) in TBST (Tris-buffered saline, 0.1% Tween 20) and then washed and incubated with goat anti-rabbit IgG (H&L) secondary antibody (Dylight 800 4x PEG conjugated; Thermo Scientific; 1:4000). The membrane was imaged by Odyssey® CLx Imaging System.

Clonogenic assay. HCT116 p53^{+/+} cells were seeded 500 cells per well into 24-well plates for or 200 cells per well into 96-well plates, and allowed to attach overnight before the addition of compounds. After 7-day continuous treatment, the medium was removed and crystal violet solution was added to fix and stain the colonies for 20 min. Crystal violet was removed and the colonies were washed with ddH₂O for three times. The colonies were imaged by Odyssey® CLx Imaging System.

Growth inhibition assay. HCT116 p53^{+/+} cells or MiaPaCa-2 cells were seeded 2500-3000 cells per well in 96-well microtiter plates, and allowed to attach overnight before the addition of the serial dilution of compounds (10X). After 72h, cells were incubated with 0.3 mg/mL 3-(4,5-dimethylthiazol-2-yl)-2,5-diphenyltetrazolium bromide (VWR) for an additional 3h at 37 °C. After removal of the supernatant, DMSO was added to the wells, and the absorbance was read at

570 nm. All assays were performed in triplicate. Percentage of cell growth inhibition was expressed as $(1 - A/C) \times 100\%$ (A and C were the absorbance values from experimental and control cells, respectively). IC₅₀ values were determined for each drug from nonlinear regression analysis of log (drug concentration) vs. percentage of cell growth inhibition using Prism 7.0. SD or SEM was calculated based on the IC₅₀ values obtained from at least three independent experiment.

4.7 References:

1. Vyas, V. K.; Ghate, M. Recent developments in the medicinal chemistry and therapeutic potential of dihydroorotate dehydrogenase (DHODH) inhibitors. *Mini Rev Med Chem* **2011**, *11*, 1039-55.
2. Munier-Lehmann, H.; Vidalain, P. O.; Tangy, F.; Janin, Y. L. On dihydroorotate dehydrogenases and their inhibitors and uses. *J Med Chem* **2013**, *56*, 3148-67.
3. Schwartzmann, G.; Peters, G. J.; Laurensse, E.; de Waal, F. C.; Loonen, A. H.; Leyva, A.; Pinedo, H. M. DUP 785 (NSC 368390): schedule-dependency of growth-inhibitory and antiprimidine effects. *Biochem Pharmacol* **1988**, *37*, 3257-66.
4. Dexter, D. L.; Hesson, D. P.; Ardecky, R. J.; Rao, G. V.; Tippett, D. L.; Dusak, B. A.; Paull, K. D.; Plowman, J.; DeLarco, B. M.; Narayanan, V. L.; et al. Activity of a novel 4-quinolinecarboxylic acid, NSC 368390 [6-fluoro-2-(2'-fluoro-1,1'-biphenyl-4-yl)-3-methyl-4-quinolinecarb oxylic acid sodium salt], against experimental tumors. *Cancer Res* **1985**, *45*, 5563-8.
5. Peters, G. J.; Schwartzmann, G.; Nadal, J. C.; Laurensse, E. J.; van Groeningen, C. J.; van der Vijgh, W. J.; Pinedo, H. M. In vivo inhibition of the pyrimidine de novo enzyme dihydroorotic acid dehydrogenase by brequinar sodium (DUP-785; NSC 368390) in mice and patients. *Cancer Res* **1990**, *50*, 4644-9.
6. Sykes, D. B.; Kfoury, Y. S.; Mercier, F. E.; Wawer, M. J.; Law, J. M.; Haynes, M. K.; Lewis, T. A.; Schajnovitz, A.; Jain, E.; Lee, D.; Meyer, H.; Pierce, K. A.; Tolliday, N. J.; Waller, A.; Ferrara, S. J.; Eheim, A. L.; Stoeckigt, D.; Maxcy, K. L.; Cobert, J. M.; Bachand, J.; Szekely, B. A.; Mukherjee, S.; Sklar, L. A.; Kotz, J. D.; Clish, C. B.; Sadreyev, R. I.; Clemons, P. A.; Janzer, A.; Schreiber, S. L.; Scadden, D. T. Inhibition of Dihydroorotate Dehydrogenase Overcomes Differentiation Blockade in Acute Myeloid Leukemia. *Cell* **2016**, *167*, 171-186.e15.
7. He, T.; Haapa-Paananen, S.; Kaminsky, V. O.; Kohonen, P.; Fey, V.; Zhivotovsky, B.; Kallioniemi, O.; Perala, M. Inhibition of the mitochondrial pyrimidine biosynthesis enzyme

dihydroorotate dehydrogenase by doxorubicin and brequinar sensitizes cancer cells to TRAIL-induced apoptosis. *Oncogene* **2014**, 33, 3538-49.

8. Sainas, S.; Pippione, A. C.; Giorgis, M.; Lupino, E.; Goyal, P.; Ramondetti, C.; Buccinna, B.; Piccinini, M.; Braga, R. C.; Andrade, C. H.; Andersson, M.; Moritzer, A. C.; Friemann, R.; Mensa, S.; Al-Kadaraghi, S.; Boschi, D.; Lolli, M. L. Design, synthesis, biological evaluation and X-ray structural studies of potent human dihydroorotate dehydrogenase inhibitors based on hydroxylated azole scaffolds. *Eur J Med Chem* **2017**, 129, 287-302.

9. Mohamad Fairus, A. K.; Choudhary, B.; Hosahalli, S.; Kavitha, N.; Shatrah, O. Dihydroorotate dehydrogenase (DHODH) inhibitors affect ATP depletion, endogenous ROS and mediate S-phase arrest in breast cancer cells. *Biochimie* **2017**, 135, 154-163.

10. Yin, S.; Kabashima, T.; Zhu, Q.; Shibata, T.; Kai, M. Fluorescence assay of dihydroorotate dehydrogenase that may become a cancer biomarker. *Sci Rep* **2017**, 7, 40670.

11. Lai, A. C.; Crews, C. M. Induced protein degradation: an emerging drug discovery paradigm. *Nat Rev Drug Discov* **2017**, 16, 101-114.

12. Toure, M.; Crews, C. M. Small-Molecule PROTACS: New Approaches to Protein Degradation. *Angew Chem Int Ed Engl* **2016**, 55, 1966-73.

13. Galdeano, C.; Gadd, M. S.; Soares, P.; Scaffidi, S.; Van Molle, I.; Birced, I.; Hewitt, S.; Dias, D. M.; Ciulli, A. Structure-guided design and optimization of small molecules targeting the protein-protein interaction between the von Hippel-Lindau (VHL) E3 ubiquitin ligase and the hypoxia inducible factor (HIF) alpha subunit with in vitro nanomolar affinities. *J Med Chem* **2014**, 57, 8657-63.

14. Buckley, D. L.; Gustafson, J. L.; Van Molle, I.; Roth, A. G.; Tae, H. S.; Gareiss, P. C.; Jorgensen, W. L.; Ciulli, A.; Crews, C. M. Small-molecule inhibitors of the interaction between the E3 ligase VHL and HIF1alpha. *Angew Chem Int Ed Engl* **2012**, 51, 11463-7.

15. Buckley, D. L.; Raina, K.; Darricarrere, N.; Hines, J.; Gustafson, J. L.; Smith, I. E.; Miah, A. H.; Harling, J. D.; Crews, C. M. HaloPROTACS: Use of Small Molecule PROTACs to Induce Degradation of HaloTag Fusion Proteins. *ACS Chem Biol* **2015**, 10, 1831-7.

16. Madak, J. T.; Neamati, N. Membrane permeable lipophilic cations as mitochondrial directing groups. *Curr Top Med Chem* **2015**, 15, 745-66.

17. Finichiu, P. G.; James, A. M.; Larsen, L.; Smith, R. A.; Murphy, M. P. Mitochondrial accumulation of a lipophilic cation conjugated to an ionisable group depends on membrane potential, pH gradient and pK(a): implications for the design of mitochondrial probes and therapies. *J Bioenerg Biomembr* **2013**, 45, 165-73.

18. Liu, S.; Neidhardt, E. A.; Grossman, T. H.; Ocain, T.; Clardy, J. Structures of human dihydroorotate dehydrogenase in complex with antiproliferative agents. *Structure* **2000**, *8*, 25-33.
19. Chujo, I.; Masuda, Y.; Fujino, K.; Kato, S.; Ogasa, T.; Mohri, S.; Kasai, M. Synthetic study on novel immunosuppressant KF20444. *Bioorg Med Chem* **2001**, *9*, 3273-86.
20. Gandhamsetty, N.; Jeong, J.; Park, J.; Park, S.; Chang, S. Boron-Catalyzed Silylative Reduction of Nitriles in Accessing Primary Amines and Imines. *J Org Chem* **2015**, *80*, 7281-7.
21. Jiang, Z. X.; Yu, Y. B. The Design and Synthesis of Highly Branched and Spherically Symmetric Fluorinated Macrocyclic Chelators. *Synthesis (Stuttg)* **2008**, 2008, 215-220.
22. Azzu, V.; Brand, M. D. Degradation of an intramitochondrial protein by the cytosolic proteasome. *J Cell Sci* **2010**, *123*, 578-85.
23. Lai, A. C.; Toure, M.; Hellerschmied, D.; Salami, J.; Jaime-Figueroa, S.; Ko, E.; Hines, J.; Crews, C. M. Modular PROTAC Design for the Degradation of Oncogenic BCR-ABL. *Angew Chem Int Ed Engl* **2016**, *55*, 807-10.
24. Gottlieb, H. E.; Kotlyar, V.; Nudelman, A. NMR Chemical Shifts of Common Laboratory Solvents as Trace Impurities. *J Org Chem* **1997**, *62*, 7512-7515.
25. Zeng, Q.; Guo, Q.; Yuan, Y.; Yang, Y.; Zhang, B.; Ren, L.; Zhang, X.; Luo, Q.; Liu, M.; Bouchard, L. S.; Zhou, X. Mitochondria Targeted and Intracellular Biothiol Triggered Hyperpolarized ¹²⁹Xe Magnetofluorescent Biosensor. *Anal Chem* **2017**, *89*, 2288-2295.
26. Das, P.; Deng, X.; Zhang, L.; Roth, M. G.; Fontoura, B. M.; Phillips, M. A.; De Brabander, J. K. SAR Based Optimization of a 4-Quinoline Carboxylic Acid Analog with Potent Anti-Viral Activity. *ACS Med Chem Lett* **2013**, *4*, 517-521.
27. Baldwin, J.; Michnoff, C. H.; Malmquist, N. A.; White, J.; Roth, M. G.; Rathod, P. K.; Phillips, M. A. High-throughput screening for potent and selective inhibitors of Plasmodium falciparum dihydroorotate dehydrogenase. *J Biol Chem* **2005**, *280*, 21847-53.

Chapter 5

Summary and Future Directions

5.1 Summary

Dihydroorotate dehydrogenase (DHODH) remains a viable target for cancer chemotherapy. Inhibition of DHODH is known to induce pyrimidine depletion and halt cell cycle progression at the S phase.¹⁻³ In cells and murine studies, DHODH inhibitors are able to abrogate tumor growth. However, the anticancer properties of DHODH inhibitors, such as brequinar, did not translate well from the bench to bedside. Despite promising preclinical data, brequinar failed to induce an objective response in multiple cancer clinical trials for patients with solid tumors.⁴⁻¹⁰ In fact, no DHODH inhibitor has been FDA approved to date for cancer therapy. Therefore, single agent usage of DHODH inhibitors may not work well for the treatment of solid tumors. However, many studies highlight a promising future for DHODH inhibitors. Multiple studies have demonstrated the ability of DHODH inhibitors to overcome resistance to standard chemotherapy.¹¹⁻¹⁴ For instance, DHODH inhibition has been demonstrated to sensitize triple negative breast cancer cells to genotoxic agents by limiting the supply of nucleotides available for DNA repair.¹⁴ As triple negative breast cancer presents a major public health problem, any enzyme capable of inducing pyrimidine depletion and thus slowing growth is an important target.¹⁵

Beyond sensitizing resistance cell lines, DHODH is vital for cellular differentiation. Inhibition of DHODH has been observed to induce differentiation in acute myeloid leukemia cells (AML).¹⁶ This is not isolated to one study, as DHODH inhibitors have been demonstrated to decrease self-renewal capacities of neural crest cells in zebrafish.¹⁷ These results may have a significant impact on potential therapies in AML or in evaluating the cancer stem cell theory.¹⁸ If the cancer stem cell theory is correct, inducing differentiation may decrease the percentage of pluripotent stem cells and increase the population of differentiated cells that are susceptible to conventional chemotherapy. While the exact mechanism is unknown, this empirical observation strengthens interest in DHODH inhibitors.

Within this dissertation, Chapter 1 (Figure 5.1) highlights the importance of DHODH for cancer. Discussed are the many induced effects by DHODH inhibition and a summary of key studies that will certainly guide the future of DHODH targeted therapy in cancer. In short, shRNA protein knockdown studies demonstrate that DHODH is necessary for cancer cell growth.

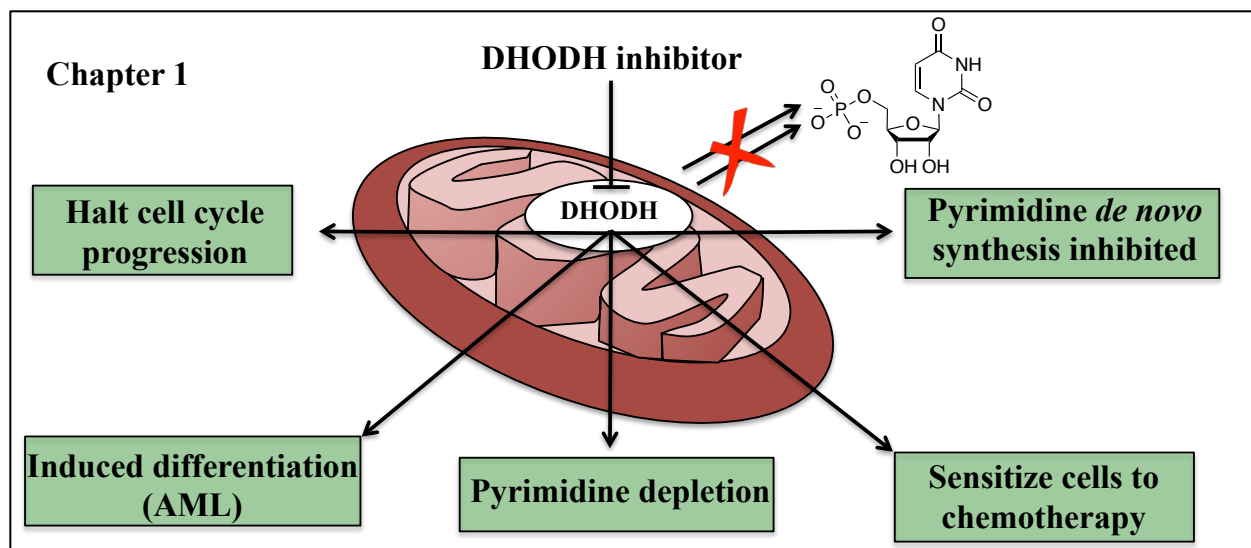


Figure 5.1: Summary of anticancer effects induced by DHODH inhibition.

The enzymatic target of our lead compound was disclosed as DHODH in Chapter 2. This dissertation's focus has always been on anticancer drug discovery. Using a phenotypic cell-based screening approach, a novel inhibitor with an unknown enzymatic target was discovered. Through initial pharmacophore studies, the lead compound presented a remarkably similar structure activity relationship with brequinar, a potent DHODH inhibitor. Cells overexpressing DHODH were found to be most sensitive to lead compound **1** and brequinar. Furthermore, the lead compound was unable to induce greater than 50% cell growth inhibition when treated to uridine-supplemented cells. Uridine-monophosphate is a downstream end product of DHODH's pathway and DHODH inhibition induces cell growth inhibition by halting its production. Finally, when evaluated in the DHODH inhibition assay, lead compound possessed an $IC_{50} = 0.347 \pm 0.072 \mu\text{M}$. These results indicated that DHODH was the target our lead compound and new DHODH inhibitors can be pursued using the DHODH assay.

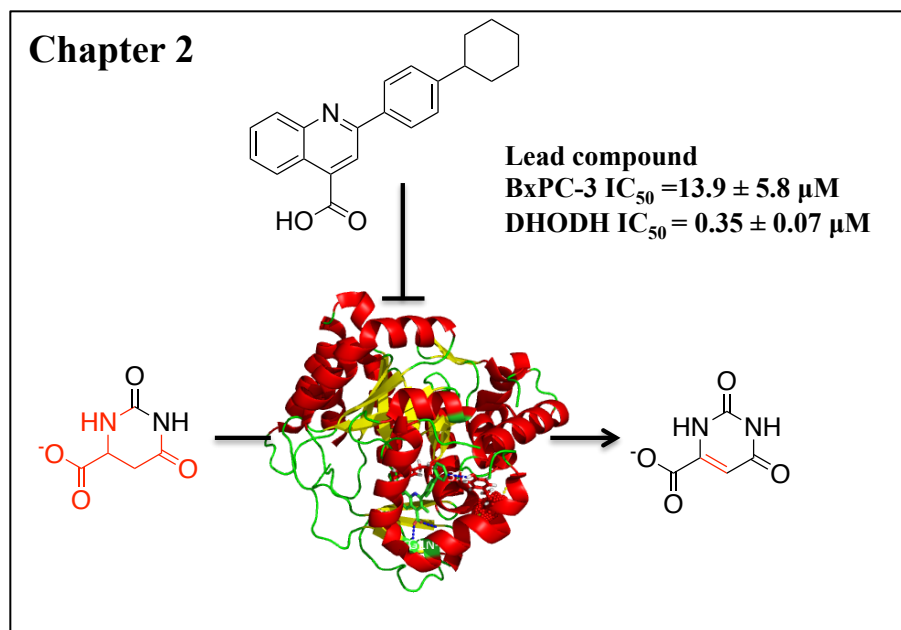


Figure 5.2: Lead compound 1 inhibits DHODH.

In Chapter 3, we pursued a structure-guided approach toward the development of improved dihydroorotate dehydrogenase (DHODH) inhibitors with the goal of forming new interactions between DHODH and the brequinar class of inhibitors. Two potential residues, T63 and Y356, suitable for novel H-bonding interactions were identified in the brequinar-binding pocket. Analogues were designed to maintain the essential pharmacophore and form new electrostatic interactions through strategically positioned H-bond accepting groups. This effort led to the discovery of potent quinoline based analogues **71** (DHODH $IC_{50} = 10.6 \pm 1.1 \text{ nM}$) and **73** (DHODH $IC_{50} = 32.9 \pm 4.6 \text{ nM}$). A co-crystal structure between **73** and DHODH depicts a novel water mediated H-bond interaction with T63. Additional optimization led to the 1,7-naphthyridine **76** (DHODH $IC_{50} = 53.9 \pm 1.7 \text{ nM}$) that forms a novel H-bond with Y356. Importantly, compound **71** possesses significant oral bioavailability ($F = 56\%$) and an elimination $t_{1/2} = 2.78 \text{ hours}$ (PO dosing). In conclusion, the data supports further preclinical studies of our lead compounds toward selection of a candidate for early stage clinical development.

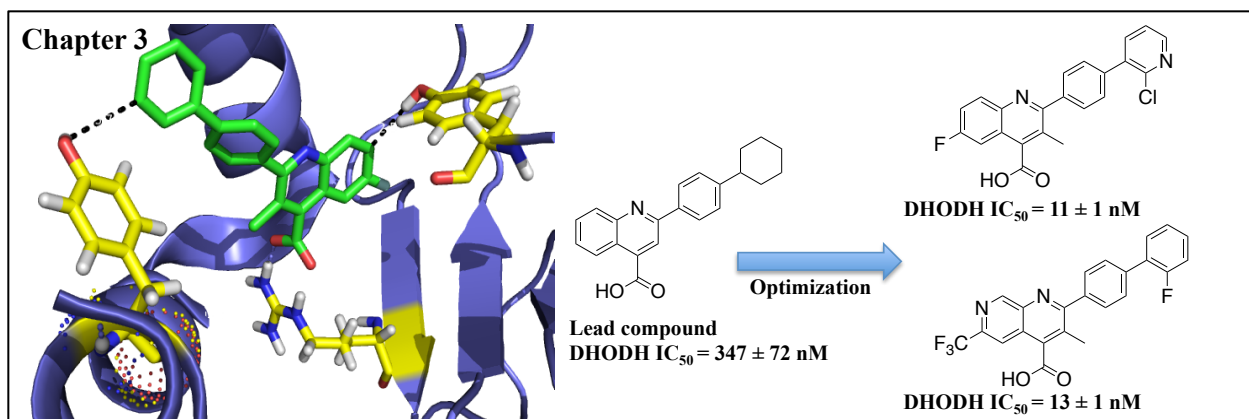


Figure 5.3: Lead optimization of DHODH inhibitors forming new electrostatic interactions

Chapter 4 focuses on the development of brequinar-based probes of DHODH (Figure 5.4). To further understand brequinar-based DHODH inhibition and DHODH's therapeutic relevance in cancer, we have developed novel brequinar-based probes. We disclose a 16-step convergent synthesis of the first brequinar-PROTAC and a 4-step approach towards the first mitochondrial-directed brequinar probe. A PROTAC and mitochondria-directed probe of brequinar both possesses cytotoxicity that is superior to brequinar in a colony formation assay.

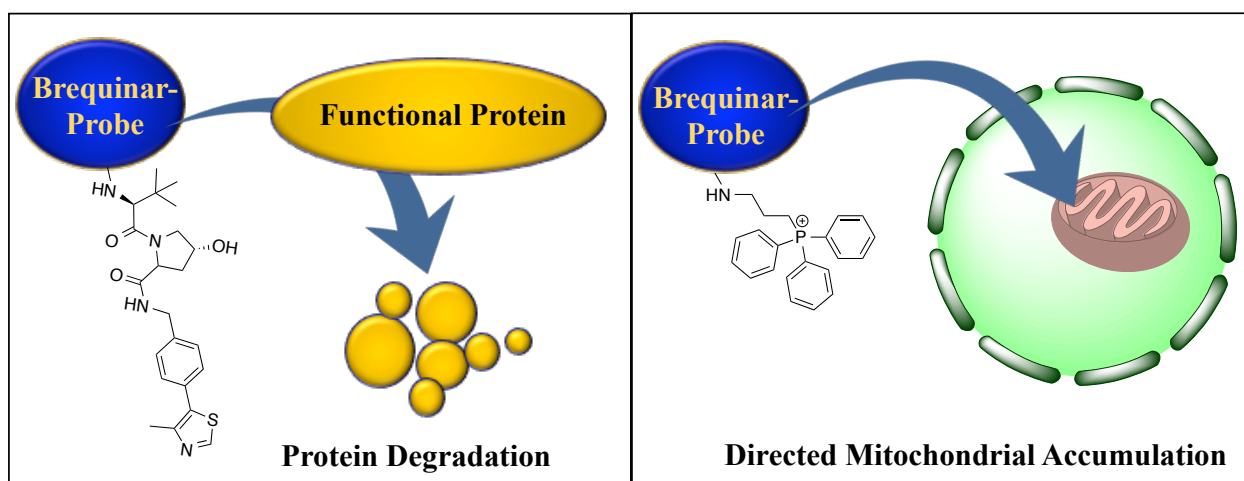


Figure 5.4: Novel probes designed to study DHODH inhibition

5.2 Significance of the study

The work highlights a successful drug discovery project that began with an unknown target and resulted with one of the most potent inhibitors of the DHODH enzyme ever reported. Through rational based drug design and a myriad of medicinal chemistry techniques, an inhibitor with improved water solubility and an $IC_{50} = 0.011 \pm 0.001$ μ M for DHODH was discovered. Additionally, the following contributions to DHODH and cancer have been made:

- First potent inhibitors to incorporate pyridine analogues in lipophilic pocket
- Developed novel synthetic route for generation of naphthyridine analogues and demonstrated a new potential interaction with 1,7 naphthyridines.
- First reported synthesis of a novel C6 substituted 1,7 naphthyridine using ortho-lithiation protocol.
- A total of over 150 final and intermediate compounds were synthesized and characterized
- A 16-step total synthesis was reported for the generation of the first ever brequinar-PROTAC molecule.
- First reported synthesis of novel triphenylphosphonium-brequinar analogue

These findings are of interest to all readers focusing on antimetabolic cancer therapy. Furthermore, this dissertation contributes to the overall understanding of DHODH targeted therapy in cancer. Data that highlights the limitations of DHODH targeted therapy, primarily lack of cellular efficacy and nucleotide salvage pathways are presented. Additionally, the effectiveness of DHODH targeted therapy is discussed; namely the potential for overcoming drug resistance and inducing differentiation. Collectively, this work further elucidates DHODH validity as an enzymatic target for cancer.

5.3 Future directions

5.3.1 Crystallography studies

Next generation DHODH inhibitors for this project will depend upon crystallography studies with a C6 substituted 1,7 naphthyridine. Co-crystal structures with these inhibitors will provide insight into the importance of the C6 position. This task is attainable, as multiple labs have generated co-crystals with human DHODH and this has already been done with two of our compounds.^{19,20} The results from this co-crystal may highlight pockets for additional interactions or sites of solvent exposure that may be utilized to develop additional PROTAC probes.

5.3.2 Non-solid tumor and differentiation assays

The limitations of DHODH-targeted therapy for solid tumors are well known and depicted in this thesis. However, it is possible that DHODH inhibition may be therapeutically relevant for cancers of leukocytes or lymphocytes. During the brequinar clinical trials,

myelosuppression was a commonly observed side effect.^{7, 8, 10, 21-23} In fact, brequinar was briefly pursued as an immunosuppressant for transplantation patients.^{24, 25} Other DHODH inhibitors, e.g., leflunomide/teriflunomide, are FDA approved for autoimmune diseases such as rheumatoid/psoriatic arthritis and multiple sclerosis.^{26, 27} The potential of these inhibitors to suppress the immune system is well documented.²⁷ In cancer chemotherapy studies, DHODH inhibitors were not observed to induce objective responses in solid tumors. However, DHODH inhibitors have never been evaluated in clinical trials for leukemia. The surprising ability of brequinar to induce differentiation in AML may soon signal a change in direction for use of this class. For our inhibitors, cellular activity should be evaluated in leukemia and lymphoma models. Additionally, differentiation assays should be pursued to assess if our DHODH inhibitors possess similar results as brequinar. Furthermore, the combination of brequinar and dipyridamole should be evaluated in differentiation assays.

5.3.3 Combination studies

The future of DHODH inhibitors appears to be in combination therapy. Therefore, studies to identify synergistic pairings should be pursued. Our lab is currently evaluating a combination of DHODH inhibitors with an inhibitor of the nucleotide salvage pathway, dipyridamole.²⁸ For the brequinar clinical trials, the nucleotide salvage pathway was a proposed compensatory mechanism for cells to survive DHODH inhibition. While the combination was previously evaluated *in vitro*, the results were not further pursued *in vivo*.²⁹ However, the *in vitro* results were promising, with brequinar and dipyridamole able to halt cell growth in the presence of 5-10 μM of uridine. The combination was unsuccessful at high concentrations of uridine $>50 \mu\text{M}$ but those concentrations may not be physiologically relevant. Nonetheless, DHODH inhibitors in combination with dipyridamole should be evaluated *in vivo* to assess if intracellular uridine levels may be reached to fuel rapid cellular growth. This represents one of many combinations that should be pursued with a DHODH inhibitor.

Altogether, the work described in this thesis makes a significant contribution to DHODH targeted cancer therapy. Our work discloses a potent human DHODH inhibitor with improved aqueous solubility, the first ever brequinar-PROTAC, and first brequinar-TPP compounds. These inhibitors and probes will significantly advance the understandings of DHODH in cancer. Future

studies with these inhibitors will seek to identify synthetic lethal targets for combination studies. One combination with dipyridamole is already under evaluation *in vivo*.

5.4 References

1. Mohamad Fairus, A. K.; Choudhary, B.; Hosahalli, S.; Kavitha, N.; Shatrah, O. Dihydroorotate dehydrogenase (DHODH) inhibitors affect ATP depletion, endogenous ROS and mediate S-phase arrest in breast cancer cells. *Biochimie* **2017**, 135, 154-163.
2. Munier-Lehmann, H.; Vidalain, P.-O.; Tangy, F.; Janin, Y. L. On Dihydroorotate Dehydrogenases and Their Inhibitors and Uses. *Journal of Medicinal Chemistry* **2013**, 56, 3148-3167.
3. Vyas, V. K.; Ghate, M. Recent developments in the medicinal chemistry and therapeutic potential of dihydroorotate dehydrogenase (DHODH) inhibitors. *Mini Rev Med Chem* **2011**, 11, 1039-55.
4. Bork, E.; Vest, S.; Hansen, H. H. A phase I clinical and pharmacokinetic study of Brequinar sodium, DUP 785 (NSC 368390), using a weekly and a biweekly schedule. *Eur J Cancer Clin Oncol* **1989**, 25, 1403-11.
5. Arteaga, C. L.; Brown, T. D.; Kuhn, J. G.; Shen, H. S.; O'Rourke, T. J.; Beougher, K.; Brentzel, H. J.; Von Hoff, D. D.; Weiss, G. R. Phase I clinical and pharmacokinetic trial of Brequinar sodium (DuP 785; NSC 368390). *Cancer Res* **1989**, 49, 4648-53.
6. Dodion, P. F.; Wagener, T.; Stoter, G.; Drozd, A.; Lev, L. M.; Skovsgaard, T.; Renard, J.; Cavalli, F. Phase II trial with Brequinar (DUP-785, NSC 368390) in patients with metastatic colorectal cancer: a study of the Early Clinical Trials Group of the EORTC. *Ann Oncol* **1990**, 1, 79-80.
7. Cody, R.; Stewart, D.; DeForni, M.; Moore, M.; Dallaire, B.; Azarnia, N.; Gyves, J. Multicenter phase II study of brequinar sodium in patients with advanced breast cancer. *Am J Clin Oncol* **1993**, 16, 526-8.
8. Urba, S.; Doroshov, J.; Cripps, C.; Robert, F.; Velez-Garcia, E.; Dallaire, B.; Adams, D.; Carlson, R.; Grillo-Lopez, A.; Gyves, J. Multicenter phase II trial of brequinar sodium in patients with advanced squamous-cell carcinoma of the head and neck. *Cancer Chemother Pharmacol* **1992**, 31, 167-9.
9. Natale, R.; Wheeler, R.; Moore, M.; Dallaire, B.; Lynch, W.; Carlson, R.; Grillo-Lopez, A.; Gyves, J. Multicenter phase II trial of brequinar sodium in patients with advanced melanoma. *Ann Oncol* **1992**, 3, 659-60.

10. Maroun, J.; Ruckdeschel, J.; Natale, R.; Morgan, R.; Dallaire, B.; Sisk, R.; Gyves, J. Multicenter phase II study of brequinar sodium in patients with advanced lung cancer. *Cancer Chemother Pharmacol* **1993**, *32*, 64-6.
11. Shukla, S. K.; Purohit, V.; Mehla, K.; Gunda, V.; Chaika, N. V.; Vernucci, E.; King, R. J.; Abrego, J.; Goode, G. D.; Dasgupta, A.; Illies, A. L.; Gebregiworgis, T.; Dai, B.; Augustine, J. J.; Murthy, D.; Attri, K. S.; Mashadova, O.; Grandgenett, P. M.; Powers, R.; Ly, Q. P.; Lazenby, A. J.; Grem, J. L.; Yu, F.; Mates, J. M.; Asara, J. M.; Kim, J. W.; Hankins, J. H.; Weekes, C.; Hollingsworth, M. A.; Serkova, N. J.; Sasson, A. R.; Fleming, J. B.; Oliveto, J. M.; Lyssiotis, C. A.; Cantley, L. C.; Berim, L.; Singh, P. K. MUC1 and HIF-1alpha Signaling Crosstalk Induces Anabolic Glucose Metabolism to Impart Gemcitabine Resistance to Pancreatic Cancer. *Cancer Cell* **2017**, *32*, 71-87 e7.
12. Sharma, A.; Janocha, A. J.; Hill, B. T.; Smith, M. R.; Erzurum, S. C.; Almasan, A. Targeting mTORC1-mediated metabolic addiction overcomes fludarabine resistance in malignant B cells. *Mol Cancer Res* **2014**, *12*, 1205-15.
13. Dietrich, S.; Kramer, O. H.; Hahn, E.; Schafer, C.; Giese, T.; Hess, M.; Tretter, T.; Rieger, M.; Hullein, J.; Zenz, T.; Ho, A. D.; Dreger, P.; Luft, T. Leflunomide induces apoptosis in fludarabine-resistant and clinically refractory CLL cells. *Clin Cancer Res* **2012**, *18*, 417-31.
14. Brown, K. K.; Spinelli, J. B.; Asara, J. M.; Toker, A. Adaptive Reprogramming of De Novo Pyrimidine Synthesis Is a Metabolic Vulnerability in Triple-Negative Breast Cancer. *Cancer Discov* **2017**, *7*, 391-399.
15. Bianchini, G.; Balko, J. M.; Mayer, I. A.; Sanders, M. E.; Gianni, L. Triple-negative breast cancer: challenges and opportunities of a heterogeneous disease. *Nature Reviews Clinical Oncology* **2016**, *13*, 674.
16. Sykes, D. B.; Kfoury, Y. S.; Mercier, F. E.; Wawer, M. J.; Law, J. M.; Haynes, M. K.; Lewis, T. A.; Schajnovitz, A.; Jain, E.; Lee, D.; Meyer, H.; Pierce, K. A.; Tolliday, N. J.; Waller, A.; Ferrara, S. J.; Eheim, A. L.; Stoeckigt, D.; Maxcy, K. L.; Cobert, J. M.; Bachand, J.; Szekely, B. A.; Mukherjee, S.; Sklar, L. A.; Kotz, J. D.; Clish, C. B.; Sadreyev, R. I.; Clemons, P. A.; Janzer, A.; Schreiber, S. L.; Scadden, D. T. Inhibition of Dihydroorotate Dehydrogenase Overcomes Differentiation Blockade in Acute Myeloid Leukemia. *Cell* **2016**, *167*, 171-186 e15.
17. White, R. M.; Cech, J.; Ratanasirintraoort, S.; Lin, C. Y.; Rahl, P. B.; Burke, C. J.; Langdon, E.; Tomlinson, M. L.; Mosher, J.; Kaufman, C.; Chen, F.; Long, H. K.; Kramer, M.; Datta, S.; Neuberg, D.; Granter, S.; Young, R. A.; Morrison, S.; Wheeler, G. N.; Zon, L. I. DHODH modulates transcriptional elongation in the neural crest and melanoma. *Nature* **2011**, *471*, 518-22.
18. Fábíán, Á.; Vereb, G.; Szöllösi, J. The hitchhikers guide to cancer stem cell theory: Markers, pathways and therapy. *Cytometry Part A* **2013**, *83A*, 62-71.

19. Liu, S.; Neidhardt, E. A.; Grossman, T. H.; Ocain, T.; Clardy, J. Structures of human dihydroorotate dehydrogenase in complex with antiproliferative agents. *Structure* **2000**, *8*, 25-33.
20. Das, P.; Deng, X.; Zhang, L.; Roth, M. G.; Fontoura, B. M.; Phillips, M. A.; De Brabander, J. K. SAR Based Optimization of a 4-Quinoline Carboxylic Acid Analog with Potent Anti-Viral Activity. *ACS Med Chem Lett* **2013**, *4*, 517-521.
21. King, S. Y.; Agra, A. M.; Shen, H. S.; Chi, C. L.; Adams, D. B.; Currie, V. E.; Bertino, J. R.; Pieniaszek, H. J., Jr.; Quon, C. Y. Protein binding of brequinar in the plasma of healthy donors and cancer patients and analysis of the relationship between protein binding and pharmacokinetics in cancer patients. *Cancer Chemother Pharmacol* **1994**, *35*, 101-8.
22. Moore, M.; Maroun, J.; Robert, F.; Natale, R.; Neidhart, J.; Dallaire, B.; Sisk, R.; Gyves, J. Multicenter phase II study of brequinar sodium in patients with advanced gastrointestinal cancer. *Invest New Drugs* **1993**, *11*, 61-5.
23. de Forni, M.; Chabot, G. G.; Armand, J. P.; Fontana, X.; Recondo, G.; Domenge, C.; Carde, P.; Barbu, M.; Gouyette, A. Phase I and pharmacokinetic study of brequinar (DUP 785; NSC 368390) in cancer patients. *Eur J Cancer* **1993**, *29A*, 983-8.
24. Joshi, A. S.; King, S. Y.; Zajac, B. A.; Makowka, L.; Sher, L. S.; Kahan, B. D.; Menkis, A. H.; Stiller, C. R.; Schaeffle, B.; Kornhauser, D. M. Phase I safety and pharmacokinetic studies of brequinar sodium after single ascending oral doses in stable renal, hepatic, and cardiac allograft recipients. *J Clin Pharmacol* **1997**, *37*, 1121-8.
25. D'Silva, M.; Antoniou, E.; DeRoover, A.; Nishimura, Y.; Howie, A.; McMaster, P. Immunosuppressive effect of brequinar on rat cardiac allograft survival in combination with leflunomide or FK 506. *Transplant Proc* **1996**, *28*, 950-1.
26. Schattenkirchner, M. The use of leflunomide in the treatment of rheumatoid arthritis: an experimental and clinical review. *Immunopharmacology* **2000**, *47*, 291-8.
27. Sanders, S.; Harisdangkul, V. Leflunomide for the treatment of rheumatoid arthritis and autoimmunity. *Am J Med Sci* **2002**, *323*, 190-3.
28. Weber, G.; Jayaram, H. N.; Pillwein, K.; Natsumeda, Y.; Reardon, M. A.; Zhen, Y. S. Salvage pathways as targets of chemotherapy. *Adv Enzyme Regul* **1987**, *26*, 335-52.
29. Peters, G. J.; Kraal, I.; Pinedo, H. M. In vitro and in vivo studies on the combination of Brequinar sodium (DUP-785; NSC 368390) with 5-fluorouracil; effects of uridine. *Br J Cancer* **1992**, *65*, 229-33.